Functional and Structural Characterization of the Vacuolar Anion Channels *At*ALMT9 and *At*ALMT4 in *Arabidopsis thaliana*

Dissertation

zur

Erlangung der naturwissenschaftlichen Doktorwürde

(Dr. sc. nat.)

vorgelegt der

Mathematisch-naturwissenschaftlichen Fakultät

Der Universität Zürich

Von

Jingbo Zhang

aus

Volksrepublik China

Promotionskomitee

Prof. Dr. Enrico Martinoia (Leitung der Dissertation)

Dr. Alexis De Angeli

Prof. Dr. Stefan Hörtensteiner

Prof. Dr. Leo Eberl

Zürich, 2013

Table of Contents

Summary

In higher plants, ALuminum-activated Malate Transporters (ALMTs) form an anion channel family involved in fundamental physiological processes. After an introductory chapter about anion channels I will first present data on the physiological characterizations of one member of this family, *At*ALMT9. We found that *At*ALMT9 is a vacuolar chloride channel mediating chloride accumulation in the vacuole. The chloride currents mediated by *At*ALMT9 are activated by cytosolic malate at physiological concentrations via an increase of the channel open probability. The analysis of *atalmt9* knock-out plants revealed that those plants exhibited an impaired stomatal opening and a decreased wilting in response to drought stress. Our findings demonstrate that *At*ALMT9 is a malate-activated vacuolar chloride channel that is involved in the control of stomata aperture. In the subsequent chapter I will present studies on the structural organization of ALMT channels using *At*ALMT9 as a model. We combined a large-scale mutagenesis scan of conserved residues with a pharmacological approach. This combination allowed us to unravel structural information on *At*ALMT9. We identified two residues linking the first and second putative transmembrane α-helices by forming a salt bridge. Furthermore, we took advantage of the *At*ALMT9 "open channel blocker" citrate to identify a stretch of amino acids that likely constitute the pore forming domain of this anion channel. Moreover, the combination of biophysical and biochemical approaches allowed us to demonstrate that *At*ALMT9 forms an oligomeric complex, probably comprising four subunits that contribute to the formation of the channel's pore. In the third chapter on *At*ALMT9 I investigated the modulation of this channel by cytosolic nucleotides. In this chapter I present evidence that *At*ALMT9-mediated currents are inhibited in a voltage dependent manner by cytosolic nucleotides. The modulation of *At*ALMT9 by nucleotides does not require ATP hydrolysis. Cytosolic nucleotides block *At*ALMT9 currents by competing with the permeating anion and interacting with the permeation pore. Furthermore, I show that permeating anions at the vacuolar side of the channel affect the block by cytosolic nucleotides, further indicating an interaction between nucleotides and permeable anions within the pore. Preliminary results on a second *Arabidopsis* ALMT, *At*ALMT4, are shown in the last result chapter. I demonstrate that *At*ALMT4 is targeted to the vacuolar membrane and is permeable to malate.

Furthermore, *atalmt4* knock-out mutants exhibited a higher sensitivity to drought compared to wild-type plants. These findings suggest that *At*ALMT4 could mediate the efflux of anions from the vacuole being involved in the stomata closure or other physiological processes.

In summary, the research presented in this thesis adds novel insights into the function, the structure and the regulation of vacuolar anion channels. These findings contribute to gain a broader and more integrated understanding of anion transport across the plant cell membranes and the homeostasis of anions in the plant cell.

Zusammenfassung

In höheren Pflanzen bilden die, ALumnium-activated Malate Transporter (ALMT) eine Anionenkanalfamilie, die an grundlegenden physiologischen Prozessen beteiligt ist. Nach einer Einführung in das Gebiet der Anionenkanäle werde ich zuerst Daten zur physiologischen Charakterisierung eines Mitglieds dieser Familie aus *Arabidopsis thaliana*, *At*ALMT9, vorstellen. Wir konnten zeigen, dass *At*ALMT9 ein Chloridkanal ist, welcher die Akkumulation von Chloridionen in die Vakuole ermöglicht. Die durch *At*ALMT9 vermittelten Chloridströme werden durch physiologische Konzentrationen von Malat im Cytosol aktiviert, indem die Öffnungswahrscheinlichkeit des Kanals zunimmt. Eine Analyse der atalmt9 Mutanten zeigte, dass diese Pflanzen die Stomata nicht mehr vollständig öffnen konnten und deshalb auch resistenter gegen Trockenstress waren. Diese Resultate belegten, dass *At*ALMT9 ein malataktivierbarer Chloridkanal ist, der bei der Regulation der Stomataöffnung eine wichtige Rolle spielt. Im nächsten Kapitel beschreibe ich Versuche zur strukturellen Organisation von *At*ALMT9. Dabei haben wir eine breit angelegte Mutagenese an konservierten Aminosäure dieser Transporterfamilie mit einem pharmakologischen Ansatz verbunden. Diese Kombination hat es uns erlaubt, strukturelle Informationen über *At*ALMT9 zu erhalten. Wir haben zwei Aminosäuren in der ersten und zweiten mutmasslichen membranspannenden a-Helix identifiziert, die eine Salzbrücke bilden. Des Weiteren haben wir Citrat als einen „open channel blocker“ benutzt, um Aminosäuren zu identifizieren, welche die Pore dieses Anionenkanals bilden. Es gelang es uns ausserdem mit Hilfe von biophysikalischen und biochemischen Methoden zu zeigen, dass *At*ALMT9 einen Komplex bildet, der wahrscheinlich aus vier gleichen Untereinheiten besteht. Im dritten Kapitel über *At*ALMT9 habe ich die Modulation von *At*ALMT9 durch Nukleotide untersucht. Hier zeige ich, dass die durch *At*ALMT9 verursachten Ströme durch cytosolische Nukleotide in einer spannungsabhängigen Weise gehemmt werden. Diese Modulation ist nicht von der ATP-Hydrolyse abhängig, sondern von der Konkurrenz zwischen Anionen und cytosolischen Nukleotiden in der Pore von *At*ALMT9. Zudem zeige ich, dass Anionen, für die der Kanal durchlässig ist, den Block durch Nukleotide auf der vakuolären Seite beeinflussen. Dies ist ein weiteres Indiz dafür, dass permeable Anionen und Nukleotide innerhalb der Pore interagieren. Schliesslich stelle ich

vorläufige Resultate zu einem weiteren Mitglied der ALMT Familie, *At*ALMT4, vor. Dabei zeige ich, dass *At*ALMT4 auch in der vakuolären Membran lokalisiert ist und für Malat durchlässig ist. Pflanzen, die im *At*ALMT4 Gen mutiert sind, sind empfindlicher gegenüber Trockenheit als die entsprechenden Kontrollpflanzen. Diese Beobachtung deutet darauf hin, dass *At*ALMT4 am Export von Anionen aus der Vakuole beteiligt sein könnte und somit zum Stomataschluss beitragen könnte.

Zusammenfassend hat diese Arbeit neue Einblicke in die Funktion, Struktur und Regulation von vakuolären Kanälen gegeben. Dadurch wurde auch ein umfassenderer Überblick über die Rolle von Anionenkanälen in Pflanzen gewonnen.

1. General Introduction

1.1 Ion Transport Across Biological Membranes

In all cells the intracellular space is physically separated from the external environment by a phospholipidic bilayer, the plasma membrane. The intracellular space of eukaryotic cells, the cytoplasm, is organized by compartmentalization. The organelles, such as endoplasmic reticulum (ER), the Golgi apparatus, lysosomes, vacuoles, mitochondria and chloroplasts, are delimited by intercellular membranes (Alberts et al., 2002). Compartmentalization enables separation of metabolic pathways but also requires exchange of metabolites and information, which is governed by transporters, channels and receptors residing in the corresponding membranes and the electrochemical gradients between different compartments.

Biological membranes are formed by a bilayer of phospholipids in which different types of proteins are embedded. The phospholipid bilayer constitutes a hydrophobic barrier that prevents the free movement of water-soluble molecules (e.g. ions and carbohydrates) between the cytoplasm and the extracellular space. The membrane proteins catalyze the selective transport of molecules, perceive and transduce extra- and intracellular signals and anchor cells to the extracellular matrix. Hence the cellular membranes play multiple roles controlling the exchanges of molecules with the extracellular space or between intracellular compartments and perceiving signals from the extracellular environment (Hille, 2001).

Membrane proteins that mediate the transport of solutes across biological membranes can be divided in two classes based on thermodynamics: passive transporters and active transporters (Gadsby, 2009). Passive transporters permit the fluxes of molecules across membranes along their electrochemical gradient and are dissipative transport systems. A specific category of passive transporters are ion channels that are transmembrane proteins which form selective aqueous pores through which ions selectively diffuse. Ion channels allow the diffusion of solutes with a high rate, about 10^8 ions per second. In addition of allowing fast permeation ion channels can be highly selective for specific ions (like sodium channels, potassium channels; Gouaux and MacKinnon, 2005). The selectivity depends on the specific interaction between the permeating ionic species and the permeation pore of the channel (Zhou et al., 2001; Dutzler et al., 2002; Dutzler et al., 2003; Yamashita et al., 2005). Based on their selectivity characteristics ion channels are traditionally divided into anion channels

and cation channels and further can be grouped into subcategories that reflect their specific selectivity. In order to fulfill their biological function, the activity of ion channels is tightly regulated by different parameters such as the membrane potential, ligands, hormones, light and posttranslational modifications such as protein phosphorylation (Hille, 2001). Another passive transport mechanism is known as facilitated diffusion and mediated by carrier proteins. This ion flux mechanism requires substance binding to the carrier proteins and the subsequent exposure and release of the substance to the other side of the cell membrane. Due to the specific binding of substances, this transport is highly selective but occurs at a much slower rate compared to ion channels. The transport of glucose into red blood cells is catalyzed by this type of carrier proteins (Mueckler, 1994).

Active transporters are transport systems that catalyze the translocation of molecules across cellular membranes uphill their electrochemical gradient. The movement of molecules uphill the electrochemical gradient requires energy input. Dependent on the energy source, active transporters can be classified into primary and secondary active transporters (Gadsby, 2009). Primary active transporters can be energized by ATP hydrolysis, light and redox reactions that are coupled by the protein to the movement of molecules uphill the electrochemical gradient (Lozier et al., 1975; Wikstrom, 2004; Palmgren and Nissen, 2011). Primary active transporters that rely on ATP hydrolysis are called ATP-powered pumps. ATP-powered pumps are for example H^+-ATPase, Na^+/K^+-ATPase and Ca^{2+}-ATPase which transport ions to create electrochemical gradients across the cellular membrane (Post et al., 1972; Gaxiola et al., 2007; Di Leva et al., 2008). Most members of the ABC (ATP-binding cassette) superfamily are ATP-powered pumps, which transport a large variety of substrates, ranging from ions to macromolecules like sugars, amino acids, peptides, or even proteins (Kang et al., 2011). Secondary active transporters use the electrochemical gradient of a chemical species as an energy source and couple the downhill flux of this species to the movement of a second species uphill its electrochemical gradient. Thus, the activity of secondary active transporters is not directly driven by ATP hydrolysis but relies on the presence of electrochemical gradients of solutes across cell membranes that are generated and maintained by primary transporters. Secondary active transporter can be divided into symporters and antiporters. The symporters transport two substrates in

the same direction across the membrane, while the antiporters transport the substrates in opposite directions (Gadsby, 2009).

The transport of ions and protons by pumps establishes and maintains a charge separation across the cellular membrane. The electrochemical gradient generated across membranes by some of these pumps can be used to drive other transport systems such as secondary active transporters. In animal cells, secondary active transporters are often driven by the Na^+ gradients established by the Na^+/K^+-ATPase, which pumps Na^+ ions out of and K^+ ions into the cells across the plasma membrane (Skou and Esmann, 1992; Jorgensen et al., 2003). In higher plant cells, the energy exploited by secondary active transporters is generated by the gradient of protons across cellular membranes. In the plasma membrane, the plasma membrane H^+-ATPases (P-type H^+-ATPase) pump protons out of the cell, whereas the vacuolar H^+-ATPases (V-type H^+-ATPases) and the H^+-pyrophosphatase (H^+-PPase) pump protons into the lumen of the vacuole (Hedrich et al., 1989; Gaxiola et al., 2007; Duby and Boutry, 2009).

1.2 Anion Channels and Transporters in Plant

In higher plants, there are various transport systems that mediate fluxes of ions across cellular membranes. These transport systems, including the anion channels and transporters, are reported to be localized in different membranes of plant cells (Figure 1) e.g. the plasma membrane, tonoplast, endoplasmic reticulum, Golgi, mitochondria and chloroplast (Barbier-Brygoo et al., 2011). In plant cells anion channels and transporters are involved in a multitude of cellular functions, such as intracellular pH regulation, abiotic stress tolerance, stomatal movement, cellular signaling, plant nutrition and cell expansion (Roelfsema and Hedrich, 2005; Kim et al., 2010; Barbier-Brygoo et al., 2011). In this section I will focus on their functions in the control of stomatal movement, nutrient uptake and adaptation to the changing root environment.

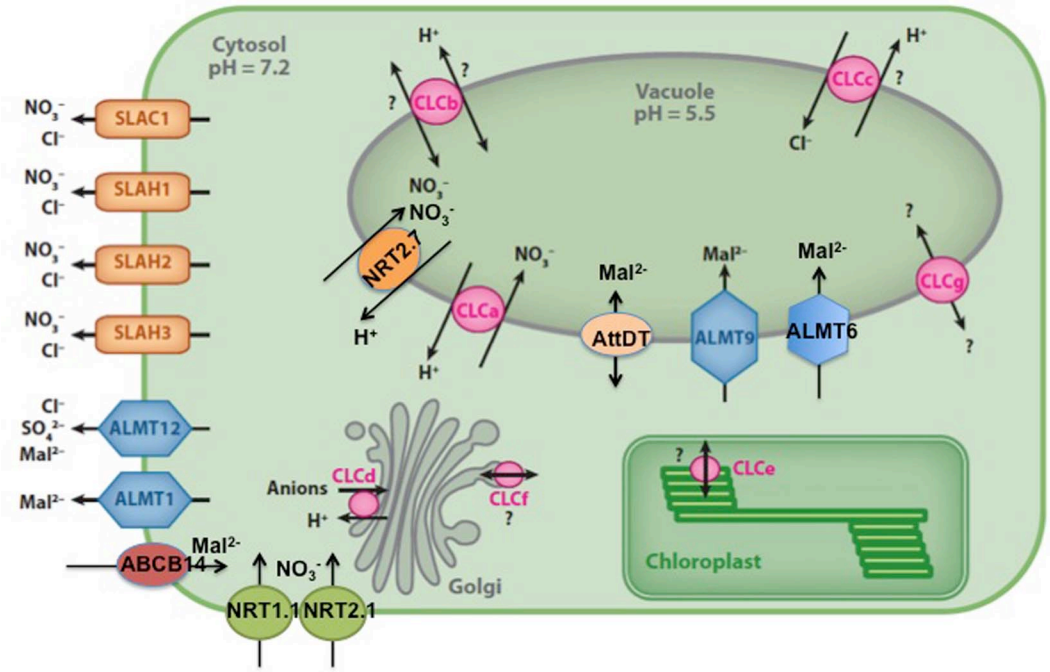

Figure 1. The anion channels and transporters in *Arabidopsis thaliana*.

The members of SLAC (SLow Anion Channel-associated) /SLAH (SLAC homologue) family are targeted to the plasma membrane. Two ALMT members, *At*ALMT1 and *At*ALMT12, have been shown to reside in the plasma membrane, while another two (*At*ALMT6 and *At*ALMT9) are localized in the tonoplast. Two NRTs (Nitrate transporters) (NRT1.1 and NRT 2.1) are present in the plasma membrane, whereas NRT2.7 is localized in the tonoplast. *At*CLC (Chloride channel) family members are located in intracellular membranes: tonoplast (*At*CLCa-c and *At*CLCg), Golgi (*At*CLCd and *At*CLCf), and thylakoid membranes (*At*CLCe). Two other anion transporters, *At*ABC14 and *At*tDT, are present in the plasma membrane and tonoplast, respectively. (Modified from Barbier-Brygoo et al., 2011)

1.2.1 The Roles of Anion Channels and Transporters in Stomata

Stomata are microscopic pores on the surface of the leaves of land plants. Each stomatal pore is surrounded by a pair of specialized epidermal cells named guard cell. Two types of guard cells can be distinguished. The guard cells of dicots and many monocots are kidney shaped with the pore in their center, whereas the guard cells of grasses and few other monocots are shaped like dumbbell with bulbous ends. The pore is a long slit located between two "handles" of the dumbbells. These dumbbell guard cells are associated with special epidermal cells named subsidiary cells which help the guard cells to control the aperture of the stomatal pores (Figure 2). Stomata

regulate gas exchange with the atmosphere to optimally balance CO_2 entry for photosynthesis and water loss, and also participate in temperature regulation (MacRobbie, 1998; Hetherington, 2001; Roelfsema and Hedrich, 2005; Vavasseur and Raghavendra, 2005; Nilson and Assmann, 2007; Kim et al., 2010). To fulfill these tasks, the stomatal aperture is regulated in response to the plant's needs, environmental conditions (light, drought, CO2, relative humidity) (Hetherington, 2001; Schroeder et al., 2001; Shimazaki et al., 2007), and also to biotic factors like pathogens (Gudesblat et al., 2009). The stomatal aperture is regulated by changes in turgor pressure and volume of guard cells. During stomatal opening, guard cells take up and accumulate osmotically active substances, mainly K^+ (Fischer, 1968), and depending on species and time of the day Cl^-, $malate^{2-}$, NO_3^- and other metabolites such as sugars (Poffenroth et al., 1992; Talbort and Zeiger, 1998). This process decreases the water potential in the guard cells, causing water to move into the cells. As water enters the cell, turgor pressure increases, resulting in guard cell swelling. Because of the differential thickening of guard cell cell walls, the swelling and bending of guard cells results in widening the stomatal pore (Blatt, 2000). The opposite process occurs during stomatal closure, a process in which the solutes that are accumulated in the vacuole are released in the apoplast (Ward et al., 1995; MacRobbie, 1998; Pandey et al., 2007). The consequent loss of osmotic potential of the guard cell induces an efflux of water from the cell. This induces a decrease of the cell volume and consequently the closure of the stomata. During stomatal opening and closure the changes in cell volume are sustained by the vacuole plasticity. The guard cell vacuole may occupy 80% - 90% of the total cell in the open state. When the stomata is closed the guard cell vacuole fragments in smaller vacuoles that are able to fuse to generate bigger vacuoles when the stomata opens again (Gao et al., 2005; Gao et al., 2009). Stomata opening requires the movement of large amounts of ions from the cytosol to the vacuole via ion channels and transporters in the vacuolar membrane, and vice versa to regulate the osmotic potential during the stomata closure process (Martinoia et al., 2012).

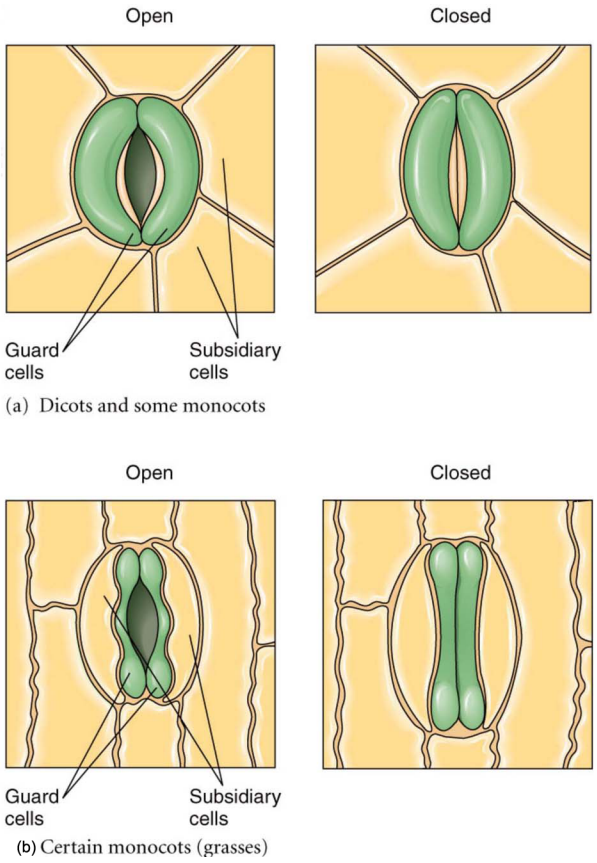

Figure 2. Two types of guard cells.

(a) Guard cells of dicots and many monocots have a kidney shape. The inner wall that faces the pore is much thicker than the outer wall. (b) Guard cells of grasses are dumpbell-shaped, the center of which is narrow and the end is thicker. (Biology, seventh edition. Eldra P. Solomon, Linda R. Berg and Diana W. Martin)

The molecular mechanism of stomatal opening through the uptake of osmotically active solutes is based on the blue light-activation of the plasma membrane H^+-ATPases that cause a hyperpolarization of the plasma membrane potential (Kinoshita and Shimazaki, 1999; Shimazaki et al., 2007). This hyperpolarization activates inward rectifying K^+ channels (KAT1 and KAT2) (Pilot et al., 2001; Lebaudy et al., 2007; Wang and Wu, 2013) that induce the passive influx of K^+ from the apoplast. To balance the positive charges of K^+, also anions including Cl^-, NO_3^- and malate^{2-} (Van Kirk and Raschke, 1978; Guo et al., 2003; Lee et al., 2008) need to be actively taken up through anion transport systems located in the plasma membrane. Furthermore, malate is also synthesized via starch degradation in guard cells to increase the solute load (Vavasseur and Raghavendra, 2005). Because of the unfavorable electrochemical

gradient across the plasma membrane, anions need to be actively taken up by anion/proton symporters (Guo et al., 2003). However, the molecular identity of these symporters is still mostly elusive and only one member of NRT family, *At*NRT1.1/CHL1, has been shown to mediate NO_3^- uptake during stomatal opening (Guo et al., 2003). Furthermore, a member of the ABC transporter family, *At*ABCB14 (Figure 1), has been identified as a malate importer in guard cells, facilitating the accumulation of malate and stomatal opening (Lee et al., 2008).

Stomatal closure is induced by drought stress, darkness, elevated CO_2, low humidity and other factors such as oxidative stress and pathogens (Shimazaki et al., 2007; Gudesblat et al., 2009; Kim et al., 2010). Among these, stomatal closure in response to the water stress hormone ABA is well studied. When water is scarce ABA is released from intracellular stores and is newly synthesized. ABA level can thereby increase up to 50 times in leaves (Acharya and Assmann, 2009). In the cytosol ABA binds to the ABA receptors (PYR/PYL/RCAR proteins). This binding causes a conformational change of ABA receptors that allows the subsequent binding to the PP2C-type protein phosphatases (Miyazono et al., 2009; Nishimura et al., 2009; Santiago et al., 2009; Yin et al., 2009). This interaction subsequently inactivates the activity of the PP2Cs (Ma et al., 2009; Park et al., 2009) that interact with and inhibit the SnRK protein kinases, in particular OST1 (open stomata1), in the absence of ABA (Yoshida et al., 2006). Therefore, as a result of PP2C recruitment to the ABA-bound ABA receptors, SnRK kinases become free to phosphorylate downstream targets, amongst which are phosphorylation-activated anion channels at the plasma membrane (Geiger et al., 2009; Lee et al., 2009; Imes et al., 2013). ABA also leads to a rise in cytosolic free calcium levels that enhance the activity of calcium-dependent protein kinases (CPKs). Subsequently, these CPKs also activate anion channels in the plasma membrane (Geiger et al., 2010; Geiger et al., 2011). The activation of anion channels in the plasma membrane leads to an efflux of anions. The efflux of anions induces a depolarization of the membrane potential, which activates outward-rectifying K^+ channels (GORK in *Arabidopsis*) that mediate potassium ions efflux (Ache et al., 2000; Hosy et al., 2003; Kim et al., 2010). The release of solutes from guard cells reduces their turgor pressure and volume, and finally induces the closure of stomata pore (Pandey et al., 2007; Kim et al., 2010).

In the plasma membrane of guard cells, two types of anion currents have been identified and were suggested to be involved in the efflux of anions during stomatal closure (Schroeder and Hagiwara, 1989; Hedrich et al., 1990; Linder and Raschke, 1992; Schroeder and Keller, 1992). These two types of currents were named Rapid type (R-type) and Slow type (S-type) according to their different kinetics of activation and deactivation (Figure 3) (Roelfsema et al., 2012). The gating of R-type anion channels is accommodated by the membrane potentials within the range of milliseconds (Kolb et al., 1995) and the current-voltage characteristic (I-V) presents a typical bell shape behavior with a steep voltage dependence at negative potentials. Differently, the S-type anion channels exhibit a slow activation kinetic within the range of 10 seconds (Linder and Raschke, 1992) and weak voltage dependence. Recently, genes coding for channels that mediate these two types of anion currents have been identified: *SLAC1* (SLow Anion Channel-associated 1) was the first member coding for a channel mediating the S-type anion currents (Negi et al., 2008; Vahisalu et al., 2008). *At*ALMT12 encodes for one of the channel mediating the R-type anion currents (Meyer et al., 2010b). Both types of anion channel are involved in crucial steps leading to stomatal closure.

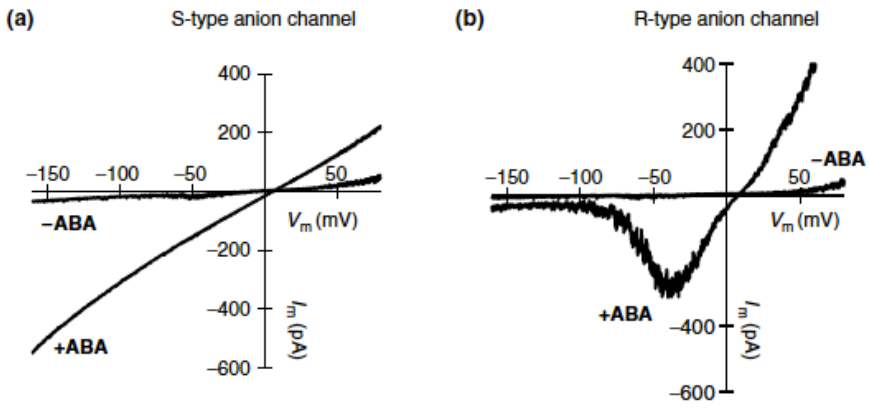

Figure 3. Current-voltage relationships of (a) S-type and (b) R-type anion channels in *Vicia faba* guard cell protoplasts in the absence and presence of ABA. The activities of these two types of anion channels are stimulated by the presence of ABA. The S-type anion channel presents a nearly linear current-voltage relationship, whereas the R-type anion channel shows a strong deactivation at membrane potential more negative than -100 mV (Roelfsema et al., 2012).

1.2.2 The Roles of Anion Channels and Transporters in the Roots

Roots anchor the plant in the soil, facilitate water and nutrient absorption but also take over the function as a storage tissue in many plants. Furthermore, plant roots can release a wide variety of biological compounds to counteract nutrient limitation, detoxify heavy metals and prevent the threat of attack from pathogens (Bais et al., 2006; Badri et al., 2009). Thus, roots participate to the plant adaptation by actively modifying their surrounding environment. Anion channels and transporters in plant roots exhibit an important role in these processes. Therefore, anion channels and transporters in roots have attracted much interest and have been investigated for many years. Here I will present two of their major physiological functions: i) uptake of mineral nutrients such as Cl^- and NO_3^-; ii) extrusion of organic anions to improve plant nutrition (Tomasi et al., 2009), or to chelate heavy metals to protect plants against heavy metal toxicity.

Most plant mineral nutrients such as large part of nitrogen, phosphorus, sulfur and chloride are present as inorganic anions in the soil. The plants take up these anions from the soil solution and transport part of these absorbed nutrients to the xylem vessels for subsequent translocation to the shoot. To reach the xylem vessels, these anions can move via two pathways: the symplastic or the apoplastic pathway (Moon et al., 1986; Steudle, 2000). The symplast is the continuum of cytoplasm, which is connected by plasmodesmata. Anions present in the soil can cross the plasma membrane of root epidermal cells to enter the symplast and travel to the site of release to the xylem vessels without being excreted to the apoplast. In the apoplastic pathway, anions that have been taken up into the root apoplast travel freely along the cell wall compartment through the root cortex until they meet the Casparian strip which is a band of specially modified endodermic cell walls that effectively prevents the entry of water and solutes into the stele via the apoplast (Nagahashi et al., 1974; Moon et al., 1986; Peterson, 1987; Chen et al., 2011). To further enter into the interior of the roots, these anions have to cross at least the plasma membranes of the endodermal cells and therefore need anion channel and transporter systems. In most soils, the concentrations of anions such as Cl^- and NO_3^- are lower than in the plant cell cytosol (Smith et al., 2000; Miller et al., 2007). Together with the highly negative membrane potential in the plasma membrane (Sze et al., 1999; Palmgren, 2001) these are

unfavorable conditions for anion uptake. Therefore anion transporters exploit the proton gradient across the plasma membrane to actively transport anions into root cells (Smith et al., 2000). Uptake systems for HPO_4^{2-}, SO_4^{2-} and NO_3^- have been described in detail and evidence shows that these anions are taken up via specific proton symporters in plants (Rausch and Bucher, 2002; Buchner et al., 2004; Miller et al., 2007). Nitrate uptake, for instance, in the roots includes two types of nitrate transporters, NRT1 and NRT2 (Figure 1), that are denoted as low-affinity and high-affinity nitrate transporters, respectively. In *Arabidopsis*, the NRT1 family comprises 53 members and the first and most extensively studied one is *At*NRT1.1/CHL1 (Tsay et al., 1993). *At*NRT1.1/CHL1 was found to function as a nitrate transporter, but also as a NO_3^- sensor (Ho et al., 2009). Interestingly, *At*NRT1.1 functions as a dual-affinity nitrate transporter that can be switched from the low affinity mode to the high affinity mode by phosphorylation (Liu and Tsay, 2003). The properties of dual-affinity transport and a phosphorylation switch between two modes allow the plasma membrane targeted *At*NRT1.1 to sense a wide range of nitrate concentrations in the soil and to regulate the expression of nitrate-related genes (Ho et al., 2009). In contrast to the NRT1 family in *Arabidopsis*, all seven members of the NRT2 family are suggested to encode only high affinity nitrate transporters (Miller et al., 2007; Tsay et al., 2007). Three nitrate transporters (*At*NRT1.1, *At*NRT2.1 and *At*NRT2.2) are proposed to facilitate high affinity nitrate transport. However, *At*NRT2.1 is believed to predominantly contribute to this process (Li et al., 2007). Moreover, *At*NRT2.1 has to work with *At*NAR2.1 to constitute a two-component nitrate high-affinity transport system that is essential for high affinity nitrate uptake in *Arabidopsis* roots (Okamoto et al., 2006; Orsel et al., 2006).

Organic anions are released into the soil when plants face environmental stresses such as nutrient deficiency (particularly phosphorus) or toxic cations (like Al^{3+}) (Ma, 2000; Ryan et al., 2001). Organic anions can increase P (phosphorus) availability by acidifying the rhizosphere to replenish the pool of soluble P or by replacing inorganic P from insoluble complexes (Ryan et al., 2001; Vance et al., 2003). In addition, organic anions also stimulate microbial activity in the rhizoshere, which could influence the bio-availability of other nutrients (Ryan et al., 2001). When aluminum is present in the toxic form Al^{3+} in acidic soils, the release of organic anions protect the root by chelating and forming non-toxic complexes with Al^{3+} in the rhizosphere (Ma,

2000). So far, exporters for two major organic anions, malate and citrate, have been identified. The excretion of malate at the plasma membrane is catalyzed by ALMT channels in the root, which are activated in response to Al^{3+} (Sasaki et al., 2004; Hoekenga et al., 2006; more detail below/ section 1.3.4). Citrate, on the other hand, is excreted by members of the MATE (Multidrug And Toxic compound Extrusion) transporters. The first two Al-activated citrate transport genes were identified in sorghum (*Sorghum bicolor*) and barley (*Horderm vulgare* L.) in 2007 (Furukawa et al., 2007; Magalhaes et al., 2007). Both proteins are localized in the plasma membrane and their citrate secretion activity is stimulated by aluminum (Furukawa et al., 2007; Magalhaes et al., 2007). In *Arabidopsis*, the MATE family consists of 56 members that are located in different membranes (plasma membrane, tonoplast, chloroplast membrane) (Meyer et al., 2010a). Amongst them, *At*MATE/*At*DTX42 has been identified to be primarily expressed in roots and to modulate the excretion of citrate into the soil in responds to the exposure to Al^{3+} (Liu et al., 2009). Furthermore, an *At*DTX42 homologue, *At*FDR3, excretes citrate into the xylem and is required for long-distance iron transport (Rogers et al., 2002; Green and Rogers, 2004; Durrett et al., 2007; Roschzttardtz et al., 2011).

Because anion channels and transporters exhibit a crucial role for plant, the elucidation of their molecular identity has been subject of intense research. Several gene families of anion channels and transporters have been identified and characterized (Ward et al., 2009; Barbier-Brygoo et al., 2011; Hedrich, 2012; Martinoia et al., 2012). In the next sections, I will present an overview of the anion channel/transporter families of the CLCs (ChLoride Channel), SLACs (SLow Anion Channel-Associated) and *At*tDT (*Arabidopsis thaliana* tonoplast Dicarboxylate Transporter) briefly. Subsequently, I will describe the current knowledge about the ALMT family in detail due to the subject of this thesis.

1.3 The Plant Cell Anion Channel and Transporter Gene Families

1.3.1 The CLC Family

The CLC family is ubiquitously expressed in all living organisms, from bacteria to plants and animals, including humans (Jentsch, 2008). Regarding the name of this family, the CLC proteins were originally found to function as Cl^- channels. Later, several studies revealed that some CLC proteins act as electrogenic anion/proton exchangers (Accardi and Miller, 2004; Picollo and Pusch, 2005; Scheel et al., 2005; De Angeli et al., 2006; Graves et al., 2008; von der Fecht-Bartenbach et al., 2010). In *Arabidopsis thaliana* seven members of the CLC family have been identified (*At*CLCa-*At*CLCg; De Angeli et al., 2009a; Barbier-Brygoo et al., 2011) and, so far, the most thoroughly characterized one is *At*CLCa (De Angeli et al., 2006; Bergsdorf et al., 2009; De Angeli et al., 2009b).

The first study on *At*CLCa showed that the disruption of *AtCLCa* resulted in an approximately 50% reduction of nitrate content compared with wild-type plants (Geelen et al., 2000). Further investigations conducted by De Angeli and coworkers revealed that *At*CLCa is localized in the tonoplast and acts as a proton/nitrate antiporter (De Angeli et al., 2006). *At*CLCa transports two nitrate molecules into the vacuole by releasing one proton into the cytosol. The antiporter behavior of *At*CLCa is determined by two residues: the "gating glutamate" E203 and the "proton glutamate" E207 (Bergsdorf et al., 2009), which are also found in other CLC antiporters like CLC-ec1 in *Escherichia coli* and CLC-5 in human (Accardi et al., 2005; Zdebik et al., 2008). The mutation of the "gating glutamate" E203 of *At*CLCa into an uncharged amino acid alanine abolishes the coupling between NO_3^- and proton, converting *At*CLCa from an antiporter to a channel (Bergsdorf et al., 2009). The mutation of the "proton glutamate" position, E270A, induces a loss of transport function, whereas the double mutation, E203A/E270A, results in a proton uncoupled anion transport activity similar to what of the single mutation E203A (Bergsdorf et al., 2009). Combining these findings with the studies of CLC-ec1 and CLC-5 (Accardi et al.,

2005; Zdebik et al., 2008), the roles of "gating glutamate" and "proton glutamate" for CLC antiporters appear to be conserved.

Despite sharing the same transport mechanism (a ratio of 2 transported anions coupled to 1 transported proton), the nitrate specificity of *At*CLCa is unique compared to other CLC antiporters (e.g. CLC-ec1 and CLC-5) which function as chloride transporter rather than nitrate transporter (Accardi and Miller, 2004; Zifarelli and Pusch, 2009). The ability of *At*CLCa to transport nitrate is determined by a proline residue (P160). When P160 is mutated into a serine, *At*CLCa loses its selectivity for nitrate over chloride but still presents the coupling to protons (Bergsdorf et al., 2009; Wege et al., 2010). Accordingly, in contrast to wild-type *At*CLCa, the introduction of a serine in this position (*At*CLCa $_{P160S}$) fails to rescue reduced nitrate accumulation in *clca* knock-out mutants (Wege et al., 2010).

The fact that *At*CLCa is a anion/proton antipoter rather than an anion channel in the tonoplast provides even stronger support for its physiological function of driving NO_3^- accumulation into the vacuole. The activity of *At*CLCa was found to be regulated by intracellular nucleotides. De Angeli and coworkers demonstrated that cytosolic ATP reversibly inhibited the transport activity of *At*CLCa, whereas AMP and ADP did not (De Angeli et al., 2009b). Competition experiments in this study showed that AMP (but not ADP) competed with ATP at the *At*CLCa binding site to prevent ATP inhibition (De Angeli et al., 2009b). The competition between ATP and AMP appears at the position of D753 in the CBS (cystathionine beta synthase) domain (De Angeli et al., 2009b). Although the physiological relevance of this ATP regulating process is still not clear, the correlation between ATP/AMP ratio and the H^+-ATPase activity may imply that the vacuolar H^+-ATPase could modulate the activity of *At*CLCa to regulate the accumulation of nitrate in the plant cell vacuoles.

Apart from *At*CLCa, all other *Arabidopsis thaliana* CLCs are also localized in intracellular membranes (*At*CLCa-c and g in the tonoplast, *At*CLCe in the chloroplast, *At*CLCd and f in Golgi apparatus; Lv et al., 2009) but have different cellular functions (Barbier-Brygoo et al., 2011). Like *At*CLCa, *At*CLCb is targeted to the vacuolar membrane and functions as an anion/H^+ exchanger. However, the exact coupling ratio between NO_3^- and H^+ has to be determined (Von der Fecht-Bartenbach et al., 2010). In contrast to *At*CLCa, the deletion of *At*CLCb function did not result in a reduced

chloride or nitrate content. Another tonoplast targeted CLC is *At*CLCc which was shown to be involved in the regulation of nitrate levels *in planta* (Harada et al., 2004). However, further studies conducted by Jossier et al. (2010) revealed that *At*CLCc is strongly expressed in guard cells and weakly in the root, playing a role in stomatal movement regulation and salt stress tolerance. These findings indicate that Cl^- may be its principal substrate (Jossier et al., 2010). Since electrophysiological data are lacking, the selectivity of *At*CLCc and its characteristic as being either a channel or a transporter is still unknown.

By contrast to the tonoplast localized CLCs, the physiological characterization of *At*CLCs localized to other intracellular membranes is still preliminary. The chloroplast targeted *At*CLCe was shown to exhibit an interconnected contribution with *At*CLCa to regulate nitrate homeostasis in two different endocellular membranes (Monachello et al., 2009). *At*CLCd co-localizes with V-type ATPases in the trans-Golgi network (TGN) and may have a function in the acidification of the TGN (Gaxiola et al., 1998; Von der Fecht-Bartervach et al., 2007). As for another Golgi membrane targeted CLC, *At*CLCf, the physiological function in the plant cells remains to be explored (Marmagne et al., 2007). Furthermore, the transport activity of these intracellular compartment-localized *At*CLCs has not been characterized, likely because their specific subcellular localization makes it difficult to find a proper expression system for direct studies.

1.3.2 The SLAC Family

As mentioned previously, two types of anion currents (S- and R-type) have been identified to co-exist in the plasma membrane of the guard cells (Schroeder and Hagiwara, 1989; Hedrich et al., 1990; Linder and Raschke, 1992; Schroeder and Keller, 1992). The S-type anion channels are encoded by a small gene family comprised of SLAC1 and four SLAC1-homologos (SLAHs) in *Arabidopsis* (Negi et al., 2008; Vahisalu et al., 2008). The first gene identified and characterized from this family is SLAC1 that plays a role in stomatal closure induced by different stimuli like CO_2, ABA, O_3, darkness, humidity change, Ca^{2+}, H_2O_2, or NO (Negi et al., 2008;

Vahisalu et al., 2008). Very recently, the SLAC1 protein was also reported to be involved in the stomatal opening process by affecting the activity of K^+ uptake channels (Wang et al., 2012; Laanemets et al., 2013). In addition to SLAC1, SLAH3 is also localized in the plasma membrane of guard cells and, together with SLAC1, catalyze the release of chloride and nitrate to regulate the stomatal closure in response to drought stress (Geiger et al., 2011). Electrophysiological studies of SLAC1/SLAH3 in the *Xenopus* oocyte proved that the channel activity of SLAC1/SLAH3 are activated by phosphorylation by the Ca^{2+} -independent protein kinase OST1 (Geiger et al., 2009; Lee et al., 2009), as well as the Ca^{2+} -dependent protein kinases CPKs (Geiger et al., 2010; Geiger et al., 2011; Brandt et al., 2012; Demir et al., 2013). These protein kinases interact with the N-terminal domain of SLAC1/SLAH3 to regulate channel activity (Geiger et al., 2010; Geiger et al., 2011; Brandt et al., 2012). The protein phosphorylation process of SLAC1/SLAH3 is suppressed by the presence of PP2C-type phosphatases like ABI, ABI2 and PP2CA (Geiger et al., 2009; Lee et al., 2009; Geiger et al., 2011; Demir et al., 2013). Together with the identification of the RCAR1/PYR/PYL ABA receptor family which controls the activity of PP2C protein phosphatases when interacting with ABA (Ma et al., 2009; Park et al., 2009), the mechanism of SLAC1/SLAH3 in regulating ABA-induced stomata closure is now well established. ABA stimulates the activity of SLAC1/SLAH3 to induce the efflux of chloride and nitrate, causing depolarization of the plasma membrane. This membrane depolarization activates the activity of outward K^+ channels, leading to the efflux of K^+. The release of solutes from guard cells reduces their turgor pressure and consequently causes stomatal closure.

In 2010, Chen and coworkers determined the crystal structure of the SLAC1 bacterial homolog TehA (Chen et al., 2010). Based on this three-dimensional structure, the putative structural model of SLAC1 was developed. In this model, SLAC1 is a symmetrical trimer, each subunit having ten transmembrane helices and five central transmembrane helices forming a pore (Chen et al., 2010). A phenylalanine residue in TM9 (transmembrane helix 9) of SLAC1, Phe450, which is strictly conserved in the SLAC1 family, is predicted to play a crucial role in gating the SLAC1 anion channel via occluding the anion permeation pathway (Chen et al., 2010). Replacing this Phe450 residue by alanine rendered SLAC1 anion permeability even in the absence of the activating protein kinase OST1 (Chen et al., 2010). Thereby, it is tempting to

speculate that the activation of SLAC1 by OST1 is due to the positional change of Phe450 in the SLAC1 channel pore (Hedrich, 2012).

1.3.3 *At*tDT, a Tonoplast Dicarboxylate Transporter

Malate is an important plant metabolite, playing a central role in plant metabolism. It is an intermediate of the Krebs cycle (Martinoia and Rentsch, 1994; Fernie et al., 2004) and acts as carbon storage in CAM and C_4 plants (Matinoia and Rentsch, 1994; Fernie and Martinoia, 2009). Malate is accumulated in the vacuole as a solute to maintain cellular turgor and regulate intracellular pH (Mathieu et al., 1986; Meyer et al., 2010a). Malate concentrations in the vacuole exhibit diurnal fluctuations in CAM and C_4 plants and can reach up to 350 mM (Matinoia and Rentsch, 1994). The accumulation of malate in the vacuole is a complex process and so far, two different malate transport system have been identified in the vacuolar membrane: a malate transporter and malate channels (Emmerlich et al., 2003; Hafke et al., 2003; Kovermann et al., 2007; Meyer et al., 2011).

*At*tDT is the first and so far the only vacuolar malate transporter identified at the molecular level (Emmerlich et al., 2003). In *Arabidopsis*, *At*tDT is the only homolog of HsNaDC-1, the human sodium dependent dicarboxylate transporter that is targeted to the plasma membrane and energized by sodium (Markovich and Murer, 2004). In contrast to HsNaDC-1, *At*tDT is localized in the tonoplast (Figure 4) and its activity is independent of sodium. It is suggested that this transporter is driven by the difference of membrane potential between cytosol and vacuole (Meyer et al., 2010a). However, the exact transport mechanism remains elusive. Furthermore, physiological results indicate that this transporter acts as both vacuolar importer and exporter (Huth et al., 2005). Deletion of *At*tDT function does not result in any visible phenotype, but strongly reduces the vacuolar malate transport activity, causing lower malate contents in leaves (Emmerlich et al., 2003) and a higher respiratory coefficient (Huth et al., 2005). This indicates that loss of *At*tDT-mediated malate transport into the vacuole results in a higher cytosolic malate consumption, which is required to keep a constant cytosolic malate level. Furthermore, the fact that *At*tDT mutant plants are more sensitive to cytosolic acidification (Huth et al., 2005) indicates that the accumulation

of malate and fumarate in the vacuoles by *At*tDT is crucial for the cytosolic pH regulation in *Arabidopsis*.

There was a long-lasting discussion whether vacuolar malate transport observed by flux analysis and electrophysiology reflected the activity of the same protein (Martinoia et al., 1985; Cheffings et al., 1997; Hafke et al., 2003). The identification of *At*tDT allowed addressing this question. Using *At*tDT mutants it has been shown that malate currents were not affected, while uptake of radioactively labeled malate at low concentrations (0.2 to 1 mM) was reduced by more than 80% (Huth et al., 2005). This observation also indicates that a malate transporter (*At*tDT) and malate channels are present in the tonoplast and exhibit different affinities for malate. These malate channels have been identified to be encoded by ALMTs, an anon channel family that I will describe more details in the next section.

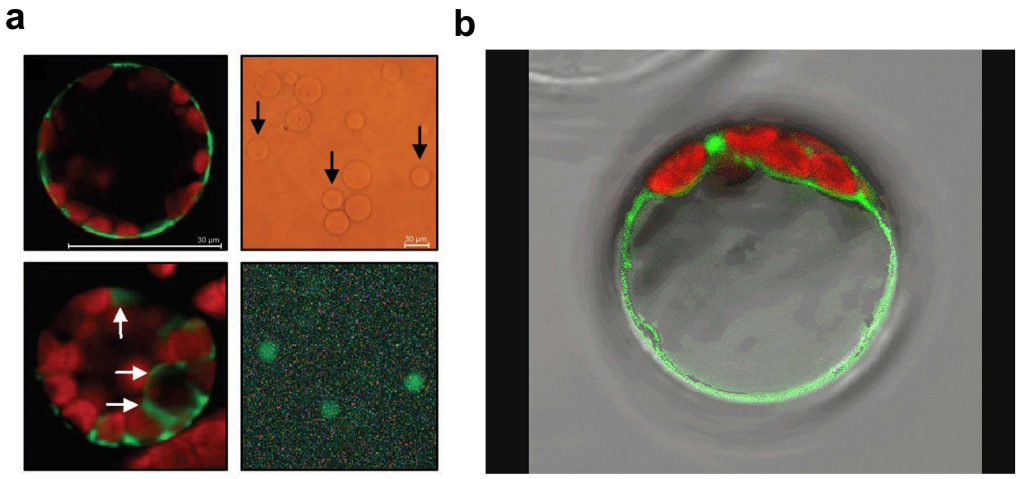

Figure 4. The subcellular localization of *At*tDT-GFP fusion protein in tobacco protoplasts (a). White arrows indicate areas of highest green fluorescence; black arrows highlight the position of single vacuoles exhibiting green fluorescence (From Emmerlich et al., 2003). (b) Transiently transformed *Arabidopsis* protoplasts (own result). The red signal indicates the auto fluorescence of chloroplast and the green signal indicates *At*tDT-GFP fluorescence.

1.3.4 The ALMT Family

In addition to being an important plant metabolite as mentioned previously, malate is also capable of chelating divalent and trivalent cations when present in neutral and slightly acid soil (pK_{a1}=3.5, pK_{a2}=5.1) due to the two deprotonated carboxyl groups (Ryan et al., 2001; Meyer et al., 2010a). Thus the exudation of malate into the soil by roots facilitates the detoxification of heavy metal ions such as Al^{3+} (Ma, 2000; Ryan et al., 2001). In the past decade, the protein families contributing to malate excretion into the soil and vacuole have been identified and characterized. One of these families is the ALMT family. The name of this family is based on the first member which was identified to be involved in aluminum resistance and activated by aluminum (Sasaki et al., 2004). ALMTs are anion channels formed by membrane proteins exclusive to plants. In *Arabidopsis thaliana* the ALMT family consists of 14 members that based on sequence homology can be grouped into three clades (Figure 5, Kovermann et al., 2007). Besides contributing to aluminum tolerance, ALMT proteins have also been found to be implicated in other functions such as loading anions in the vacuole (Kovermann et al. 2007; Meyer et al., 2011) and mediating efflux of anions across the plasma membrane to regulate stomatal movement (Meyer et al., 2010b).

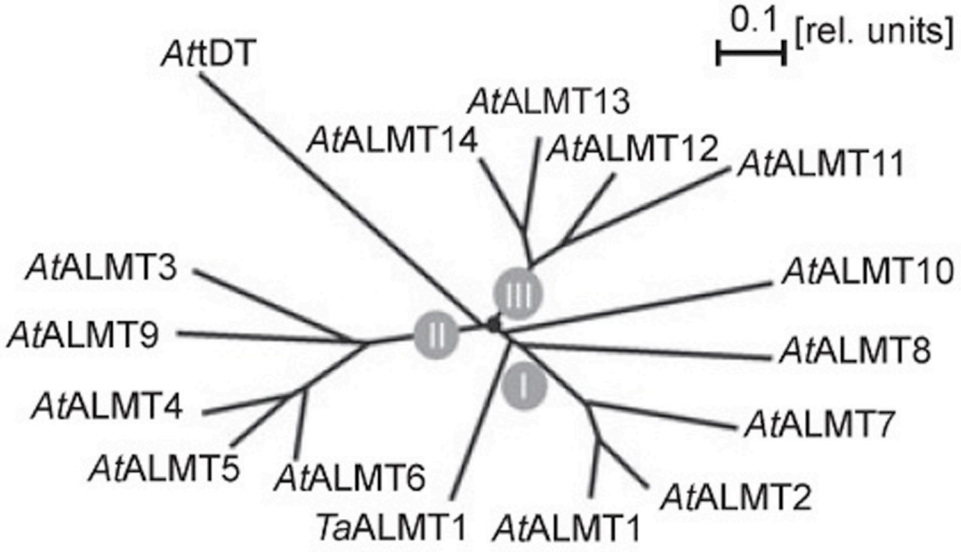

Figure 5. Dendogram analysis of the ALMT protein family.

The Arabidopsis ALMT family consists of 14 members that can be divided into three clades based on the amino acid sequence similarity. *Ta*ALMT1 (*Triticum aestivum*) and *At*ALMT1, both of which are localized in the plasma membrane, share the same clade. (Kovermann et al., 2007)

1.3.4.1 The Plasma Membrane ALMTs

ALMT1 for Aluminum Tolerance

In 1993, Delhaize and coworkers showed that wheat (*Triticum aestivum*) roots extrude malate and that the release of malate is activated by the presence of Al^{3+} (Delhaize et al., 1993a, 1993b). Subsequently, electrophysiological studies conducted on protoplasts isolated from root tips of wheat and maize plants revealed the presence of anion permeable channel(s) located in the plasma membrane which is/are specifically activated by extracellular Al^{3+} (Ryan et al., 1997; Kollmeier et al., 2001; Pineros and Kochian, 2001; Zhang et al., 2001; Pineros et al., 2002). The molecular identity of the wheat representative responsible for this current, *TaALMT1*, was unveiled subsequently (Sasaki et al., 2004). This study showed that i) the expression level of *TaALMT1* in the root apices was higher in Al-tolerant lines compared to the Al-sensitive lines and ii) when heterologously expressed in *Xenopus* oocyte, rice or tobacco cells, *Ta*ALMT1 could mediate an Al^{3+}-activated malate efflux current. Subsequent studies showed that overexpressing *TaALMT1* in transgenic barley (*Hordeum vulgare*) increased its tolerance to Al^{3+} toxicity (Delhaize et al., 2004). By using a green fluorescent protein (GFP) fusion protein, it was shown that *Ta*ALMT1 localized to the plasma membrane (Yamaguchi et al., 2005). These results demonstrated that *TaALMT1* encodes a plasma membrane localized anion channel mediating malate efflux from root cells to the soil. Extracellular Al^{3+} stimulates the activity of *Ta*ALMT1 and enhances the efflux rate of malate which is essential for wheat to cope with Al^{3+} toxicity. Additionally, although exhibits a higher affinity for malate, *Ta*ALMT1 is also permeable to other physiologically relevant anions such as NO_3^-, Cl^- and SO_4^{2-} (Pineros et al., 2008). The activity of *Ta*ALMT1 is regulated not only by extracellular Al^{3+} but also by protein phosphorylation/dephosphorylation of serine (S384) (Ligaba et al., 2009).

In other species homologous genes to *TaALMT1* such as *AtALMT1* in *Arabidopsis* and *BnALMT1, BnALMT2* in *Brassica napus* have been identified to encode plasma membrane localized malate channels exhibiting similar functions in aluminum

toxicity tolerance (Hoekenga et al., 2006; Ligaba et al., 2006; Kobayashi et al., 2007). In contrast, *ZmALMT1*, the homolog of *TaALMT1* in maize (*Zea mays*), has been shown to encode a plasma membrane anion channel with different properties (Pineros et al., 2008). The activity of *Zm*ALMT1 is not regulated by extracellular Al^{3+} and *Zm*ALMT1 is more permeable to inorganic anions such as Cl^- and NO_3^- than to organic anions like malate (Pineros et al., 2008). According to these properties, *Zm*ALMT1 is thought to selectively transport inorganic anions involved in mineral nutrition and ion homeostasis, rather than being involved in aluminum detoxification. Interestingly, ALMT1-type anion channels are not permeable for citrate, which is another major organic anion involved in aluminum detoxification (Magalhaes et al., 2007; Liu et al., 2009).

*At*ALMT12, a Rapid Type (R-Type) Anion Channel in Guard Cells Required for Stomatal Movement

A large number of studies performed over several decades revealed the existence of two types of anion channels, S-types and R-types, which co-exist in the plasma membrane of guard cells (Schroeder and Keller, 1992; Dietrich and Hedrich, 1994). The gating of R-type anion channels is accommodated to the membrane potentials within the range of milliseconds (Kolb et al., 1995) and exhibits a bell shaped current-voltage relationship with a steep voltage dependence (Figure 3). The current-voltage relationship shows that the R-type channels close at negative membrane potentials while a depolarization elicits R-type channel opening. In *Arabidopsis* hypocotyl and guard cells the R-type channel was shown to be regulated by intracellular nucleotides and external anion concentrations (SchulzLessdorf et al., 1996; Thomine et al., 1997; Colcombet et al., 2001). Moreover, it was proposed that intracellular nucleotides constitute a “voltage dependent gate” of the R-type channel acting like open channel blockers (Colcombet et al., 2001). This gating mechanism is similar to what is observed in KIR (potassium inward rectifier) channels from animals which are gated by Mg^{2+} and polyamines (Lopatin et al., 1994; Lu, 2004). Although the first report about these channels was published more than 20 years ago (Schroeder and Keller, 1992), the molecular identify of the first R-type anion channel, *At*ALMT12 (also

named QUAC1 in some studies), was discovered only in 2010 (Meyer et al., 2010b). *At*ALMT12 is a member of the ALMT family in *Arabidopsis* and belongs to clade III (Figure 5) (Kovermann et al., 2007). *AtALMT12* is expressed more than fifty times stronger in guard cells than in the mesophyll of *Arabidopsis* and is localized at the plasma membrane (http://labs.biology.ucsd.edu/schroeder/guardcellchips.html; Meyer et al., 2010b). T-DNA insertion mutants of *AtALMT12* are impaired in stomatal closure in response to darkness, CO_2, ABA and calcium (Meyer et al., 2010b; Sasaki et al., 2010). Electrophysiological studies showed that in presence of malate in the apoplastic-side buffer, the patches performed on guard cell protoplasts isolated from *At*ALMT12 knock-out mutants exhibited a 40% reduction of the R-type anion current compared to those isolated from the corresponding wild-type (Figure 6a) (Meyer et al., 2010b). This indicates that *At*ALMT12 is part of the R-type anion channels in the guard cell plasma membrane. When heterologously expressed in *Xenopus* oocytes in presence of malate in the extracellular solution *At*ALMT12-mediated currents display properties reminiscent of the R-type anion channel and its activity is regulated by extracellular malate (Meyer et al., 2010b). However, in the absence of malate in the extracellular solution *At*ALMT12 mediated only outward currents of inorganic anion such as Cl^- and NO_3^- (Sasaki et al., 2010). Moreover, the results of Meyer et al. (2010b) demonstrate that *At*ALMT12 is part of the plasma membrane R-type anion channels mediating anion efflux from the guard cells during stomatal closure. As *Zm*ALMT1 but in contrast to *At*ALMT1 and *Ta*ALMT1, *At*ALMT12 mediated malate currents are not induced by Al^{3+} (Sasaki et al., 2004; Hoekenga et al., 2006; Pineros et al., 2008; Meyer et al., 2010b).

As the S-type anion channels, *At*ALMT12 is also regulated by protein phosphorylation (Geiger et al., 2009; Lee et al., 2009). Recently, Imes and coworkers (2013) showed that *At*ALMT12 is activated by ABA. This ABA activation is less pronounced in *abi1-1* and *ost1-2* mutants. Considering that OST1 kinase and the protein phosphatase ABI1 are two key components of the ABA signaling pathway, the activity of *At*ALMT12 was suggested to be regulated by a phosphorylation/dephosphorylation process. Furthermore, a bimolecular fluorescence complementation (BiFC) assay confirmed that OST1 and *At*ALMT12 exhibit a direct protein-protein interaction and that the *At*ALMT12 mediated current was activated by OST1 when they were heterologously coexpressed in *Xenopus* oocytes (Figure 6b)

(Imes et al., 2013). This protein-protein interaction results in the OST1-mediated phosphorylation of *At*ALMT12 and activation of *At*ALMT12. Moreover, the deletion of the function of OST1 results in even stronger impairment of stomatal closure phenotypes (Mustilli et al., 2002) than that of the *slac1* or *atalmt12* mutant. This can be explained by the fact that OST1 interacts with and regulates both S- and R-type anion channels in guard cells (Geiger et al., 2009; Lee et al., 2009; Imes et al., 2013) (Figure 6b).

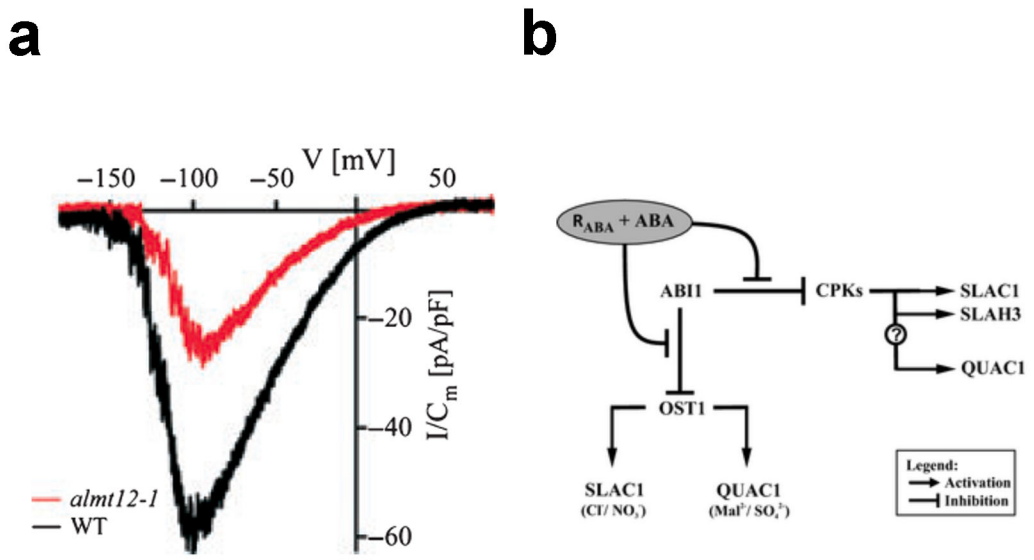

Figure 6. Voltage dependent activation of R-type currents and the model of *At*ALMT12 regulation.

(a) The R-type current density of guard cell protoplasts from WT (black) and *At*ALMT12 knock out plants (red). The current response elicited upon a voltage ramp from +70 to -180 mV, holding potential was set to -180 mV (From Meyer et al., 2010b). (b) Regulation of *At*ALMT12/QUAC1 by ABA signaling pathway components. R_{ABA} is the ABA receptor (From Imes et al., 2013).

1.3.4.2 The Vacuolar Membrane ALMTs: *At*ALMT6 and *At*ALMT9

The first characterized tonoplast targeted ALMT protein is *At*ALMT9 which belongs to clade II (Figure 5, Kovermann et al. 2007). The *AtALMT9* gene is expressed in all organs, however in leaves its cell-type specific expression is detected nearly

exclusively in mesophyll and guard cells (Kovermann et al. 2007). Patch-clamp studies on vacuoles isolated from protoplast extracted from T-DNA insertion lines showed reduced vacuolar malate channel activity. Furthermore, electrophysiological studies using tobacco cells or *Xenopus* oocytes that heterologously over-expressed *At*ALMT9 showed that the channel is conductive for malate and fumatate. These characterizations indicate that *At*ALMT9 may play a role in loading dicarboxylate into the vacuole. However, in this first study the T-DNA insertion mutants of *At*ALMT9 did not present any visible phenotype (Kovermann et al., 2007). As will be presented in the result part of this thesis (result chapter I), the function of *At*ALMT9 goes beyond malate transport in mesophyll vacuoles.

Subsequently, a second vacuolar targeted ALMT of clade II (Figure 5), *At*ALMT6, was characterized (Meyer et al., 2011). *AtALMT6* is predominantly expressed in guard cells and flower tissues in *Arabidopsis.* Patch-clamp studies with vacuoles isolated from *At*ALMT6 over-expressing *Arabidopsis* plants exhibited inward-rectifying currents that demonstrate the influx of malate and fumarate from cytosol into the vacuole (Meyer et al., 2011). Moreover, *At*ALMT6 is regulated by different factors. Firstly, *Arabidopsis* plants overexpressing *At*ALMT6 revealed large malate currents only in the presence of micromolar calcium on the cytosolic side solution. Secondly, the threshold activation of *At*ALMT6 is regulated by vacuolar pH and cytosolic malate. Lowering the cytosolic malate concentrations shifts the activation threshold of inward currents to more negative voltage, while lowering the vacuolar pH shifts it to positive and induce higher outward currents (Meyer et al., 2011). The co-modulation of these two parameters possibly determines the functions of *At*ALMT6 as a malate influx or efflux channel. Although *At*ALMT6 has been identified to be expressed in the guard cells and malate currents of guard cell vacuoles isolated from *atalmt6* knock-out plants were reduced compared to those of wild-type plants, *atalmt6* knock-out plants did not show any stomatal phenotype under standard growth conditions (Meyer et al., 2011). This can be explained either by functional redundancy of vacuolar ALMTs in guard cell vacuoles or by a possible specific function of *At*ALMT6, which would allow observing a phenotype only under conditions which have not been tested so far.

1.3.4.3 The Structure of ALMTs

Many members of the ALMT family have been well characterized with respect to their physiological functions, subcellular localization, substrate selectivity and the channel activity regulation. However, very limited information is available about the structure and the structure-function relationship of ALMTs except for the description of an important phosphorylation site (Ligaba et al., 2009; Furuichi et al., 2010) and studies on the topology (Motoda et al., 2007; Dreyer et al., 2012).

In 2009, Ligaba and coworkers reported that when *Ta*ALMT1 was heterologously expressed in the *Xenopus* oocytes system, the application of protein kinase and phosphatase inhibitors strongly inhibited both basal and Al^{3+} activated malate currents, whereas the malate currents were enhanced by the presence of the protein kinase C activator PMA (phorbol 12-myristate 13-acetate) (Ligaba et al., 2009). These findings indicate that the *Ta*ALMT1 transport activity is modulated by protein phosphorylation/dephosphorylation process. Site-directed mutagenesis was conducted and revealed a key residue serine (S384) which is involved in regulating *Ta*ALMT1 transport activity via direct protein phosphorylation (Ligaba et al., 2009). Subsequently, another study investigated the mechanism of Al^{3+} activation (Furuichi et al., 2010). Three mutations in the C-terminal domain (E274Q, D275N and E284Q) abolished the Al^{3+} activation but kept the basal transport activity of *Ta*ALMT1 (Furuichi et al., 2010). Deletion of the C-terminal domain resulted in a non-functional *Ta*ALMT1, whereby the transport activity can be rescued by fusing the N-terminal region of *Ta*ALMT1 and the C-terminal region of *At*ALMT1 (Furuichi et al., 2010). This study demonstrated that the C-terminal domain is required to keep both basal and Al^{3+} activated *Ta*ALMT1 transport activity and three residues (E274, D275 and E284) in this region are essential for Al^{3+} activation.

In addition to the *in silico* topology analysis of ALMTs provided by Kovermann and coworkers who showed slight differences in the hydropathy pots among different ALMTs (Kovermann et al. 2007), two studies attempted to get more insights in the topology of ALMTs (Motoda et al., 2007; Dreyer et al., 2012). By the combination of computer-prediction and immunocytochemical analyses, Motoda and coworkers generated a secondary structure model of *Ta*ALMT1 (Motoda et al., 2007). In this model, they concluded that the *Ta*ALMT1 protein contains six transmembrane

domains with both C- and N-terminal domains being located on the extracellular side (Figure 7a) (Motoda et al., 2007). By combining sequence alignment and clustering with predicted features of ALMT proteins from 32 plant species, the topological model of ALMTs was updated in 2012 (Dreyer et al., 2012). In addition to the model of Motoda et al. (2007), the C-terminal domain was proposed to span the membrane twice and the large N-terminal part may have another membrane spanning region (Figure 7b). In contrast to the model of Motoda et al. (2007), the C-terminal domain of ALMT proteins in this model is partially extracellular and partially cytosolic. Also in this model the location of the conserved glutamate in the extracellular side would explain how this residue can be involved in external Al^{3+} activation of *At/Ta*ALMT1 (Furuichi et al., 2010), while S384, the key residue involved in the phosphorylation process, resides on the cytosolic side (Ligaba et al., 2009). The proposed models in these studies do not entirely coincide regarding the number of transmembrane spanning domains and the cellular orientation of the N-terminus and the C-terminus (Figure 7). Therefore, the structural organization of ALMTs is still ambiguous and there are still some open questions: i) Which domain determines the different subcellular localizations of ALMTs? ii) What is responsible for the different substrate preference in ALMTs? iii) According to the fact that the channel activity of ALMTs can be stimulated by Al^{3+} (*Ta*ALMT1, *At*ALMT1) and malate (*At*ALMT9), what are the mechanisms and where are the corresponding activation sites? iv) What is the oligomeric organization of ALMTs?

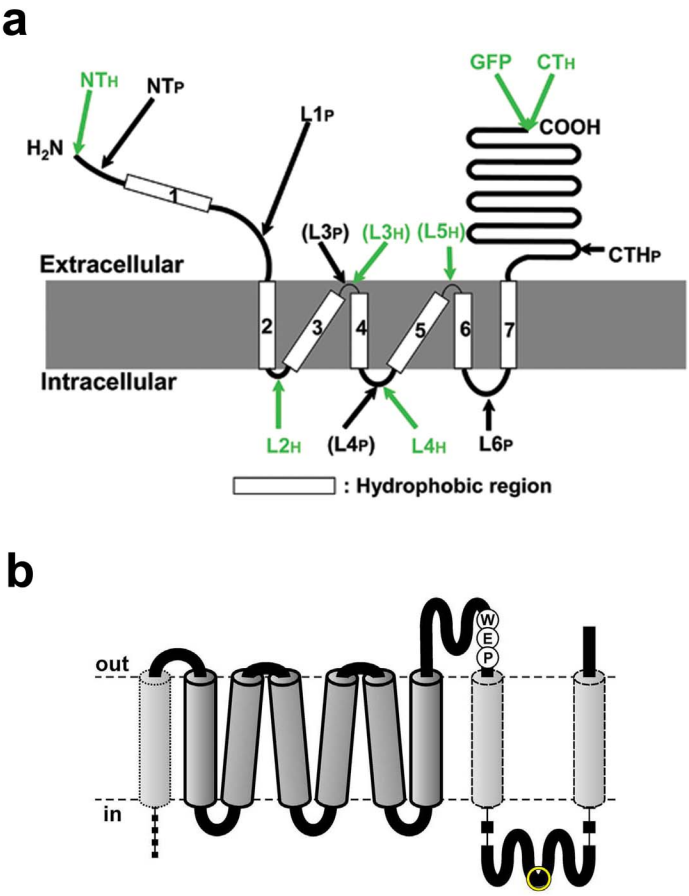

Figure 7. (a) The TaALMT1 topology model proposed by Motoda et al. (2007). In this model, the *Ta*ALMT1 protein contains six transmembrane domains with both C- and N-terminus being located on the extracellular side (From Motoda et al., 2007). (b) The modified topology model for ALMTs updated by Dreyer et al. (2012). In this model the C-terminal half spans twice the membrane and the large N-terminal domain may have another membrane spanning region (dotted). The WEP-motif as well as the position of the phosphorylation site S384 (yellow cycle) of TaALMT1 are indicated (From Dreyer et al., 2012).

2. Aims of the Thesis

As described in the introduction, the aperture of the stomatal pore is regulated by changes in the osmotic potentials of the guard cells. These changes are achieved mainly by the transport of osmotically active solutes, chiefly potassium, chloride, malate and nitrate ions across the plasma and vacuolar membrane. While our knowledge about ions fluxes across the plasma membrane of the guard cells is advanced, much less is known about fluxes across the tonoplast. Although some anion channels and transporters like ALMTs and *At*CLCa have been identified in the vacuolar membrane, to date no genuine chloride ion channel in the tonoplast is known at the molecular level. *At*ALMT9 has been characterized as the first tonoplast targeted ALMT and was found to mediate malate and fumarate fluxes into the vacuolar lumen. However, the physiological role of *At*ALMT9 remains unclear and knock-out plants did not show any significant phenotype under the investigated conditions. The aim of this thesis was therefore to investigate the physiological function, structural organization and regulation of *At*ALMT9 in plant cells. I addressed four main questions:

i) What is the physiological role of the vacuolar membrane localized *At*ALMT9? Based on the previously identified chloride current, is it possible that *At*ALMT9 acts as chloride channel *in vivo*?

ii) Since the structure of ALMTs is still ambiguous, what is the structural organization of *At*ALMT9 and what is the molecular basis underlying the channel functionality?

iii) Why do some ALMTs exhibit a bell-shaped I-V curve but others do not? Are there structural features determining the channel kinetics or is this a regulatory property of the channel that has been investigated under different conditions?

iv) In addition to *At*ALMT6 and *At*ALMT9, other ALMTs (*At*ALMT3, 4, 5) in clad II are also targeted in the vacuolar membrane (Jingbo Zhang, Ulrike Baetz and Cornelia Eisenach, unpublished data). Do these three *At*ALMTs in the vacuolar membrane act as a malate channel as *At*ALMT6 or as a malate activated chloride channel as *At*ALMT9 or do they have additional physiological functions?

3. Result Chapter I

*At*ALMT9 is a Malate-activated Vacuolar Chloride Channel Required for Stomatal Opening in *Arabidopsis*

Alexis De Angeli*, Jingbo Zhang*, Stefan Meyer* and Enrico Martinoia

* These authors contributed equally to this work

Published in *Nature Communications* 2013; 4:1804.

nature COMMUNICATIONS

ARTICLE

Received 7 Aug 2012 | Accepted 27 Mar 2013 | Published 30 Apr 2013

DOI: 10.1038/ncomms2815

OPEN

AtALMT9 is a malate-activated vacuolar chloride channel required for stomatal opening in *Arabidopsis*

Alexis De Angeli[1,2,*], Jingbo Zhang[1,*], Stefan Meyer[1,*,†] & Enrico Martinoia[1]

Water deficit strongly affects crop productivity. Plants control water loss and CO_2 uptake by regulating the aperture of the stomatal pores within the leaf epidermis. Stomata aperture is regulated by the two guard cells forming the pore and changing their size in response to ion uptake and release. While our knowledge about potassium and chloride fluxes across the plasma membrane of guard cells is advanced, little is known about fluxes across the vacuolar membrane. Here we present the molecular identification of the long-sought-after vacuolar chloride channel. AtALMT9 is a chloride channel activated by physiological concentrations of cytosolic malate. Single-channel measurements demonstrate that this activation is due to a malate-dependent increase in the channel open probability. *Arabidopsis thaliana atalmt9* knockout mutants exhibited impaired stomatal opening and wilt more slowly than the wild type. Our findings show that AtALMT9 is a vacuolar chloride channel having a major role in controlling stomata aperture.

[1] Institute of Plant Biology, University of Zurich, Zollikerstrasse 107, CH-8008 Zurich, Switzerland. [2] Institut des Sciences du Végétal, CNRS UPR2355, 1 Avenue de la Terrasse Bat 23, 91198 Gif-sur-Yvette, France. * These authors contributed equally to the work. † Present address: Blood Transfusion Service, SRC, Zurich, Molecular Diagnostics & Cytometry (MOC), Rütistr. 19, 8952-Schlieren, Switzerland. Correspondence and requests for materials should be addressed to A.D.A. (email: deangeli.alexis@gmail.com).

Water availability is critical for crop production. It has been predicted that climate change will bring drought to increasing areas of our arable lands and strategies to produce more drought tolerant plants are critical to future crop improvement (http://ressources.ciheam.org/om/pdf/a80/00800414.pdf). Stomata have a central role in regulating CO_2 uptake required for photosynthesis and water consumption in response to changing environmental conditions[1–5]. The aperture of the stomatal pore is regulated by changes in the osmotic potentials of the guard cells. These changes are mainly achieved by ion transport across cellular membranes[3,4,6–8]. Cells contain organic as well as inorganic anions, both of which are of primary importance for stomatal opening and closure[1,4,6,8,9]. Potassium uptake from the apoplast and its accumulation in the vacuole are crucial during stomatal opening[1,4,7]. This process can only be achieved by a concomitant accumulation of anions, which allow balancing positive charges. The chemical nature of the anions involved in stomatal movements depends on the plant species and the growing conditions[10], however it is generally accepted that chloride, malate and nitrate are the major actors[2,4,11]. Surprisingly, despite the importance of anion transport, until recently the molecular identity of these transporters remained elusive. In the last decade, the CLC[12,13], SLAC[8,9,14] and ALMT[15–20] protein families have been found to be involved in the transport of anions, shedding light on the nature of anion fluxes across plant vacuolar and/or plasma membranes[11]. Despite the fundamental role of the vacuole in accumulating solutes during stomatal movement, none of the mutant plants of the so far identified anion transporters and channels displayed a visible phenotype. *AtCLCc* represents the only exception by exhibiting slightly impaired stomatal movement in epidermal strips[13]. Surprisingly, no genuine vacuolar chloride ion channel has been identified at the molecular level to date and only few reports of chloride channel activity on a functional level exist[21,22].

Among the anion transporter/channel families identified so far, aluminium-activated malate transporters (ALMTs) form a unique family of passive transport systems that are exclusive to plants[15–19]. Plasma membrane-located ALMTs are involved in dicarboxylic acid excretion required for aluminium tolerance and in the efflux of inorganic and organic anions during stomatal closure generating the well-described R-type current[17]. The first characterized ALMT in the tonoplast was AtALMT9, which has been shown to mediate malate and fumarate currents directed into the vacuole of mesophyll cells of *Arabidopsis thaliana*[18]. Subsequently, a second member, AtALMT6, was shown to mediate Ca^{2+}- and pH-dependent malate currents into guard cell vacuoles[19]. Despite the fact that AtALMT6 is expressed nearly exclusively in guard cells, no obvious phenotype was observed. This may be due to the complex regulation of this ALMT. In general, ALMTs present a complex selectivity with a preference for dicarboxylic acids. However, the maize ALMT protein ZmALMT1[23] has been shown to transport exclusively inorganic anions across the plasma membrane of root cells. In contrast, none of the vacuolar ALMTs was unambiguously demonstrated to mediate inorganic anion fluxes[18,19].

The scarce information concerning vacuolar chloride channels prevents the understanding of the physiology of this anion in plants. This is especially true if we consider the impact of the transport of chloride during salt stress tolerance and in mediating stomatal movements[6,8,9,11,24]. Here we show that the major role of AtALMT9 is to act as a malate-induced chloride channel. Chloride currents mediated by AtALMT9 are modulated by cytosolic malate concentrations in the physiological range. *In planta* AtALMT9 is required for proper regulation of stomata opening. Knockout plants for AtALMT9 exhibit a reduced stomata aperture and slower opening kinetics leading to plants with a reduced transpiration level, thus resulting in more drought tolerance than the corresponding wild types.

Results

AtALMT9 is permeable to chloride. To re-evaluate whether AtALMT9 is able to transport chloride, we applied an electrophysiological approach using vacuoles isolated from protoplasts of *Nicotiana benthamiana* transiently overexpressing AtALMT9. To identify the transformed vacuoles, we expressed AtALMT9 fused to GFP at the C-terminus. Whole-vacuole measurements on these tobacco plants displayed a high malate current density[18]. To distinguish anion currents from background cation currents, we designed measuring solutions with the major cation being BisTrisPropane (BTP). BTP is largely impermeable, thus minimizing the cation current contribution in our measurement[12,19]. AtALMT9-mediated currents in the excised out-side-out configuration using symmetrical malate concentrations (100 mM $Malate_{cyt}$/100 mM $Malate_{vac}$) displayed time-dependent relaxations similar to those previously observed for the vacuolar AtALMT9[18] and AtALMT6[19]. Differently from AtALMT6, AtALMT9 is not regulated by cytosolic Ca^{2+} (Supplementary Fig. S1). The mean amplitude of the AtALMT9-mediated currents under these ionic conditions was -1.8 ± 0.6 nA at −120 mV (Fig. 1a,b), the currents displayed an inward rectification (Fig. 1b) and a reversal potential of 0 ± 1 mV. Subsequently, we investigated whether chloride is permeable through AtALMT9. Therefore, we performed experiments in which the cytosolic buffer was exchanged with 100 mM Cl^- (Fig. 1a,b). After this exchange, we could observe a current that was $13.5 \pm 3\%$ of the current measured in presence of malate. The current was inward rectifying and detectable at membrane potentials more negative than −60 mV. Moreover, we found that the chloride currents were characterized by a higher noise compared with those observed for malate (Fig. 1a,b). These data indicate that AtALMT9 is permeable to chloride and mediates its transport from the cytosol to the vacuolar lumen. To ensure that the chloride currents were not due to a background activity, we compared patches from *N. benthamiana* vacuoles expressing AtALMT9-GFP with patches from *N. benthamiana* vacuoles expressing the empty vector using symmetrical chloride buffers (100 mM Cl^-_{cyt}/100 mM Cl^-_{vac}). The patches expressing AtALMT9-GFP displayed time-dependent relaxation and a total current amplitude of -866 ± 150 pA, while empty-vector-transformed patches exhibited no time-dependent relaxation and a total current amplitude of -70 ± 32 pA (Fig. 1c,d). Taken together, these data show that AtALMT9 is not only a malate channel but is also able to transport chloride. Interestingly, chloride fluxes through AtALMT9 are hallmarked by a high level of fluctuations (Fig. 1a,c).

Cytosolic malate is an activator of AtALMT9. Analysing the time course during the exchange in more detail, we observed that during the exchange of the cytosolic buffer from 100 mM malate to 100 mM Cl^-, the fluctuation level of the current raised before it reached a stationary level (Fig. 2a). This behaviour attracted our attention. Indeed, the presence of this marked fluctuation indicated that the current is likely to be mainly mediated by Cl^- ions, although a certain concentration of malate might be still present at the cytosolic side. After an increase in the noise level, the current continued to decline until it reached a steady state when only chloride was present (Fig. 2a). Therefore, we hypothesized that cytosolic malate may not only be a substrate for AtALMT9 but exhibits an additional function. Consequently, we tested whether cytosolic malate was able to modulate AtALMT9-mediated chloride currents. When we exchanged the 100 mM

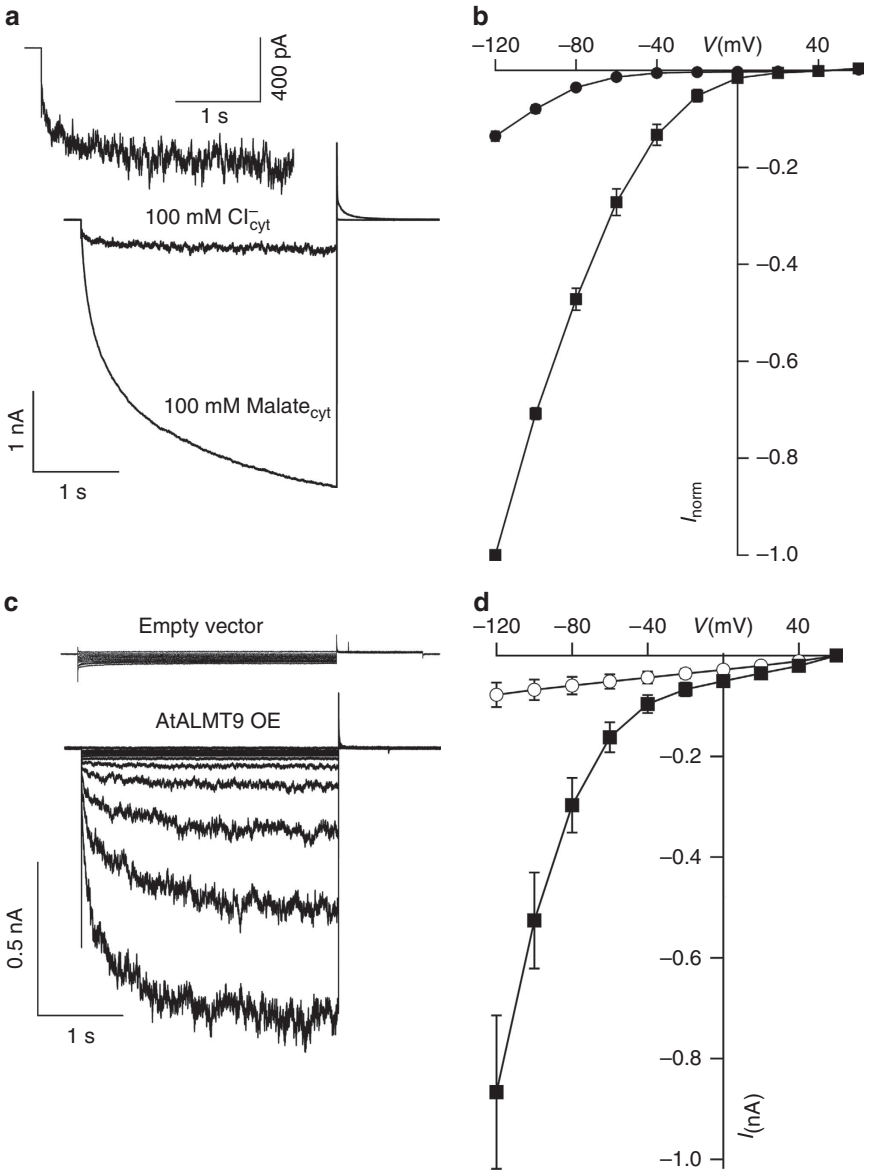

Figure 1 | AtALMT9 mediates chloride transport across the vacuolar membrane. (**a**) Excised cytosolic-side-out patches from *N. benthamiana* display time-dependent currents in symmetrical malate conditions (100 mM $malate_{cyt}$/100 mM $malate_{vac}$; currents evoked in response 3-s pulse at −120 mV followed by a tail pulse at +60 mV, holding potential +60 mV). When cytosolic malate is exchanged with chloride the inward currents decrease and present an increased noise level (upper, curve enlargement of the chloride current). (**b**) Normalized *I*–*V* curves of vacuolar patches from AtALMT9 overexpressing *N. benthamiana* plants in presence of 100 mM malate (squares; $n=8$) or 100 mM chloride (circles; $n=8$) at the cytosolic side (Supplementary Fig. S10; non-normalized *I*–*V* curves). (**c**,**d**) In presence of symmetrical chloride conditions (100 mM Cl^-_{cyt}/100 mM Cl^-_{vac}; −120 mV), only cytosolic-side-out patches from vacuoles isolated from AtALMT9 overexpressing *N. benthamiana* plants present time-dependent relaxation (**c**). Total inward currents were ∼10 times higher in cytosolic-side-out patches from AtALMT9 overexpressing vacuoles than in patches from empty-vector-transformed vacuoles. (**c**) Representative currents measured in vacuolar patches from empty-vector-transformed (upper trace) and from AtALMT9 overexpressing plants (lower trace), currents evoked in response 3-s pulse from +60 mV to −120 mV in −20 mV steps, followed by a tail pulse at +60 mV, holding potential −60 mV. (**d**) *I*–*V* curves measured in vacuolar patches from empty-vector-transformed (open circles; $n=6$) and from AtALMT9 overexpressing *N. benthamiana* plants (square; $n=16$). Error bars represents s.e.m.

Cl^-_{cyt} buffer with a 100 mM Cl^-_{cyt} plus 1 mM $malate_{cyt}$ membrane patches from *N. bethamiana* overexpressing AtALMT9, we observed a stunning increase of the inward currents of 3.7 ± 0.3 times (Fig. 2b). In contrast, in patches from empty-vector-transformed vacuoles, no current increase was observed after the application of 1 mM $malate_{cyt}$ (Supplementary Fig. S2). These results proved that cytosolic malate is able to activate AtALMT9-mediated chloride currents. The currents measured in presence of 1 mM malate exhibited high fluctuations like those in the absence of malate (Fig. 2b). Moreover, the *I*/*V* characteristics showed that the activation triggered by the presence of 1 mM cytosolic malate shifted the threshold of activation from −60 mV to −40 mV (Fig. 2c). This shift of the activation threshold makes AtALMT9-mediated chloride transport physiologically even more relevant, as it occurs at vacuolar membrane potentials in a physiological range[4]. The kinetic analysis of the malate activation demonstrated that malate is an allosteric activator of AtALMT9 (Fig. 2d). The activation was well described by a Hill equation with coefficient

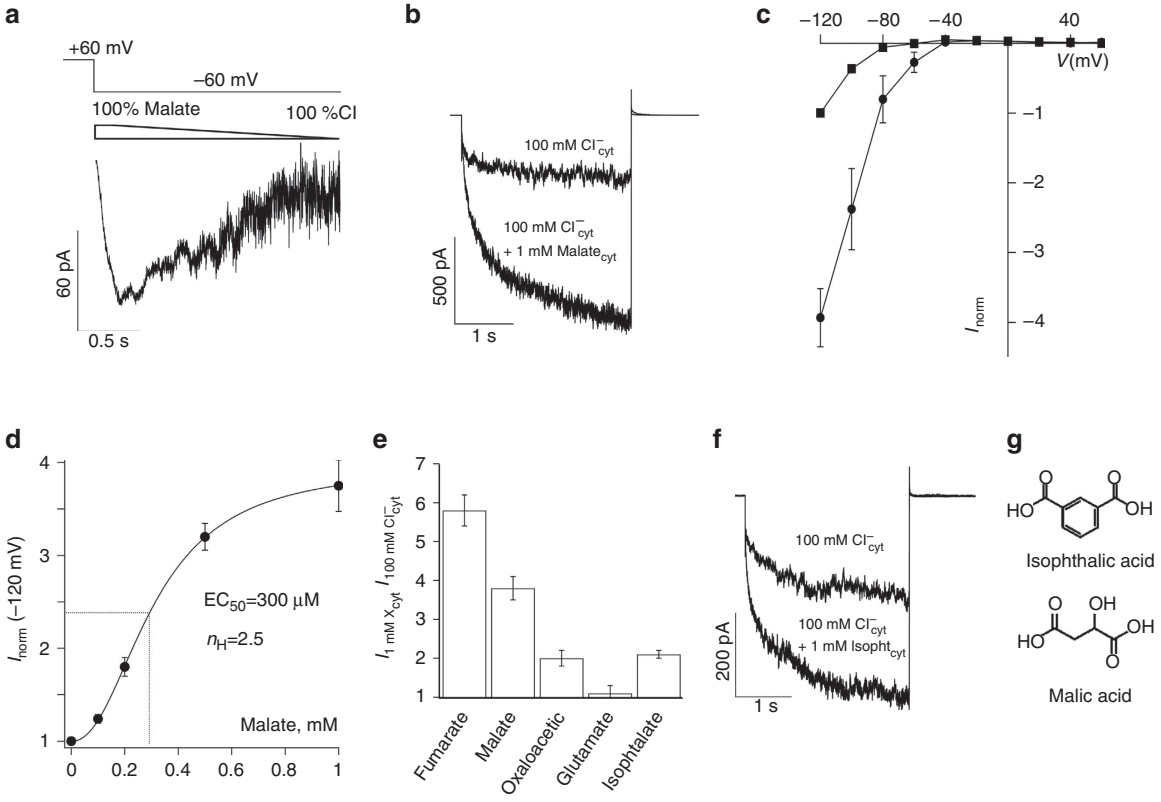

Figure 2 | Cytosolic malate activates AtALMT9-mediated chloride currents. (**a**) During the exchange of the cytosolic solution from 100 mM $malate_{cyt}$ to 100 mM $chloride_{cyt}$, the level of current fluctuation increases before the exchange is complete and the current amplitude reaches a steady state level. (**b**,**c**) In symmetrical chloride conditions (100 mM Cl^-_{cyt}/100 mM Cl^-_{vac}), the AtALMT9-mediated chloride currents increased by a factor of about 4 at −120 mV when 1 mM malate was added on the cytosolic side. Representative currents elicited in an excised cytosolic-side-out patch from an AtALMT9 overexpressing vacuole before (upper trace) and after the perfusion with 1 mM malate (lower trace) (**b**). Normalized *I*–*V* curves of AtALMT9-mediated chloride currents in absence (squares; $n=5$) or in presence of 1 mM $malate_{cyt}$ (circles; $n=5$) (**c**; Supplementary Fig. S10, non-normalized *I*–*V* curves). (**d**) Dose–response curve of the activation of AtALMT9-mediated chloride currents by cytosolic malate at −120 mV. Fitting the data with a Hill equation led to a Hill coefficient (n_H) of 2.5 and an EC_{50} of 300 µM ($n=5$–7). (**e**) Different dicarboxylic acids activate AtALMT9 with different potency while glutamate is not effective; all compounds were tested at a cytosolic concentration of 1 mM ($n=5$–9). (**f**) The interacting site responsible for the activation of AtALMT9 resides at the cytosolic side. Isophthalic acid, a dicarboxylic acid not permeable across AtALMT9 (Supplementary Fig. S4), is able to activate AtALMT9 currents. (**g**) Comparison of the molecular structures of isophtalic acid and malic acid. (**b**,**f**) Currents evoked in response 3-s pulse at −120 mV followed by a tail pulse at +60 mV, holding potential +60 mV. Error bars are s.e.m.

$n_H=2.5$ and an $EC_{50}=300$ µM at −120 mV (Fig. 2d). These data provide two important disclosures: (i) they suggest that AtALMT9 is likely to be a multimeric complex with a number of subunits higher or equal than the Hill coefficient n_H, and (ii) they show that the EC_{50} of the activation by malate is within the physiological range of cytosolic malate concentration, which was reported to be between 400 and 800 µM (refs 25–27). This strongly suggests that AtALMT9 acts as a malate-activated vacuolar chloride channel *in vivo*, as the K_m for malate transport is 27 mM (Supplementary Fig. S3), a value far away from the cytosolic malate concentrations. To test the activation effect of other dicarboxylates, we tested whether fumarate, oxaloacetate and glutamate were able to activate AtALMT9-mediated chloride currents (Fig. 2e). While fumarate and oxaloacetic acid stimulated the chloride fluxes, though at different extents (5.7 ± 0.4 and 2.0 ± 0.2 times, respectively), the amino acid glutamate was ineffective in stimulating chloride transport (Fig. 2e). It indicates that the interaction and the effect of dicarboxylic acids on AtALMT9 activity depend on the structural characteristics of the agonist. This observation is similar to that made for ligand activated channels where different agonists exhibit different degrees of activation[28]. Taken together, our data clearly demonstrate that AtALMT9 is allosterically activated by cytosolic dicarboxylates, especially malate and fumarate. However, it does not answer the question whether the site of interaction is at the cytosolic or at the vacuolar side. Indeed, as effective agonists such as malate and fumarate permeate through AtALMT9, it would be possible that they activate the channel from the vacuolar side. This is a crucial issue due to malate concentrations being in the EC_{50} range in the cytosol but not in the vacuole[25–27]. To address this question, we used a pharmacological approach (Fig. 2f). We tested whether isophtalate, a malate analogue that does not permeate through AtALMT9 (Supplementary Fig. S4) was able to activate chloride currents from the cytosolic side. Indeed, isophtalate was able to trigger the activation of AtALMT9 inducing a 2.1 ± 0.1 fold increase of the chloride current at −120 mV (Fig. 2f). Moreover, cytosolic malate activates the AtALMT9 chloride currents even in presence of 100 mM malate in the vacuolar buffer (Supplementary Fig. S5). These results strongly suggest that the interaction required to induce the activation of AtALMT9 occurs at the cytosolic side.

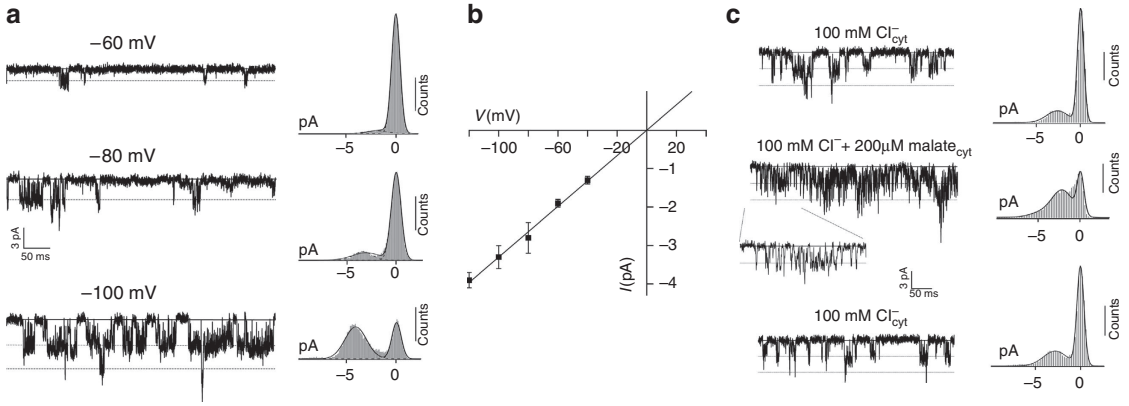

Figure 3 | Single-channel analysis of AtALMT9-mediated chloride currents. (**a**) Representative single-channel recordings at different applied membrane potentials as indicated. Single channels were measured in vacuolar patches from AtALMT9 overexpressing plants in symmetrical chloride conditions (100 mM Cl^-_{cyt}/100 mM Cl^-_{vac}). Corresponding all-point amplitude histograms of the single-channel recordings (right) show that the open probability increases when the applied membrane potential is more negative. (**b**) Single-channel I-V curve obtained from all-point amplitude histograms as in (**a**) shows that AtALMT9 presents a single-channel conductance of 32 pS ($n=3$–5). (**c**) Single channels observed in conditions as in **a** are reversibly activated by 200 µM malate added at the cytosolic side. The activation by cytosolic malate does not alter the single-channel conductance (-2.8 ± 0.4 pA at -80 mV, inset), but increases the open probability as illustrated by the corresponding all-point amplitude histograms (right). In all-point amplitude histograms (**a**,**c**), the continuous line represents the fit with an adequate sum of Gaussian distributions. Data are filtered at 1.5 kHz. Error bars are s.e.m.

Cytosolic malate increases AtALMT9 open probability. The activation of chloride currents by carboxylates can be explained either by an increase of the single-channel conductance and/or the open probability. To answer this question, we performed a single-channel analysis of AtALMT9 (Fig. 3). In excised out-side-out patches from vacuoles overexpressing AtALMT9-GFP, we could identify single-channel transitions with a conductance of 32 ± 2 pS ($n=4$) using conditions identical to those for macroscopic chloride current recordings (Fig. 3a,b). The single-channel amplitude was -3.9 ± 0.2 pA at -120 mV (Fig. 3b), a value corresponding to that determined by non-stationary noise analysis of the macroscopic currents at the same voltage (-3.4 ± 0.8 pA at -120 mV; Supplementary Fig. S6). The reversal potential of the single channels was 0 ± 2 mV, which is very close to the Nernst potential for chloride ($E_{Nernst}(Cl^-)=0$ mV). The open probability of the single-channel transitions was voltage dependent and increased at more negative voltages, which is in agreement with the macroscopic currents measurements (Fig. 1a). Under our experimental conditions, the single channels presented a flickery behaviour characterized by fast transitions between the open and the closed state (Fig. 3a), which explains the characteristic noisy behaviour of the macroscopic chloride currents (Fig. 1). Notably, the characteristics of our single-channel measurements are comparable to the only available measurements of chloride single channels in the vacuolar membrane of higher plants reported so far[21]. This channel also, exhibited a flickery behaviour and a conductance of 34 pS (ref. 21). Next, we tested how the single-channel activity was altered by the addition of malate at the cytosolic side (Fig. 3c). We perfused patches in which single channels could be visualized with the chloride solution including 200 µM malate ($n=4$; Fig. 3c). All-point histograms revealed that 200 µM malate dramatically increased the open probability of AtALMT9 (Fig. 3c). Moreover, all-point histograms could be fitted by a sum of Gaussian functions that were equally spaced indicating that malate activation does not induce a change in the single-channel conductivity (Fig. 3c). This is supported by the observation that single-channel transitions detected in presence of malate displayed the same amplitude (-2.8 ± 0.4 pA at -80 mV) as in the absence of cytosolic malate (-2.7 ± 0.3 pA at -80 mV; Fig. 3c, inset). All together these data show that the single-channel activity observed can be attributed to AtALMT9. In addition, these results are also a final proof that ALMTs are channels and not transporters.

AtALMT9 is a major vacuolar chloride channel. We analysed whether the cytosolic malate activation of the chloride currents was observable also in *A. thaliana* vacuoles. Previously, it has been shown that vacuoles from mesophyll protoplasts display AtALMT9-mediated currents[18], therefore we used this experimental system to test the malate activation in the native system. We designed experiments in which the buffer on the cytosolic side was sequentially exchanged in the following order: (i)100 mM Cl^-_{cyt}; (ii) 100 mM Cl^-_{cyt} + 1 mM $malate_{cyt}$; (iii) 100 mM $malate_{cyt}$, (Fig. 4). In whole-vacuole recordings from Col-0, we could observe a reversible increase of 1.41 ± 0.1 of the chloride currents after the addition of 1 mM malate (Fig. 4a,e,f) and an increase of the noise. The mean current densities at -120 mV in the different conditions were: -5.3 ± 0.6 pA pF^{-1} in 100 mM Cl^-_{cyt}; -7.4 ± 0.9 pA pF^{-1} in 100 mM $Cl^-_{cyt}+1$ mM $malate_{cyt}$; -11.6 ± 2.0 pA pF^{-1} in 100 mM $malate_{cyt}$; (Fig. 4a,e). We performed the same experiments using two AtALMT9 knockout lines, *atalmt9-1* and *atalmt9-2* (Fig. 4). Neither in *atalmt9-1* nor in *atalmt9-2* an increase of the chloride currents was observed (Fig. 4b,c,f). The mean current densities at -120 mV in the knockout lines were: 100 mM Cl^-_{cyt}, *atalmt9-1* -4.4 ± 0.4 pA pF^{-1}, *atalmt9-2* -3.8 ± 0.5 pA pF^{-1}; 100 mM $Cl^-_{cyt}+1$ mM $malate_{cyt}$, *atalmt9-1* -4.5 ± 0.5 pA pF^{-1}, *atalmt9-2* -3.7 ± 0.5 pA pF^{-1}; 100 mM $malate_{cyt}$, *atalmt9-1* -2.1 ± 0.4 pA pF^{-1}, *atalmt9-1* -2.8 ± 0.4 pA pF^{-1}; (Fig. 4b,c,e). The absence of the cytosolic malate activation of the chloride currents in both the knockouts demonstrates that the increase induced by cytosolic malate we observed in Col-0 is due to AtALMT9. Moreover, the absence of the malate activation in *atalmt9-1* and *atalmt9-2* is followed by a dramatic decrease of the current density observed in presence of 100 mM malate in the cytosol.

Despite the fact that we could measure consistent malate activation in wild-type vacuoles, we were puzzled by the smaller extent of the activation compared with that observed in AtALMT9 overexpressing *N. benthamiana* vacuoles. We

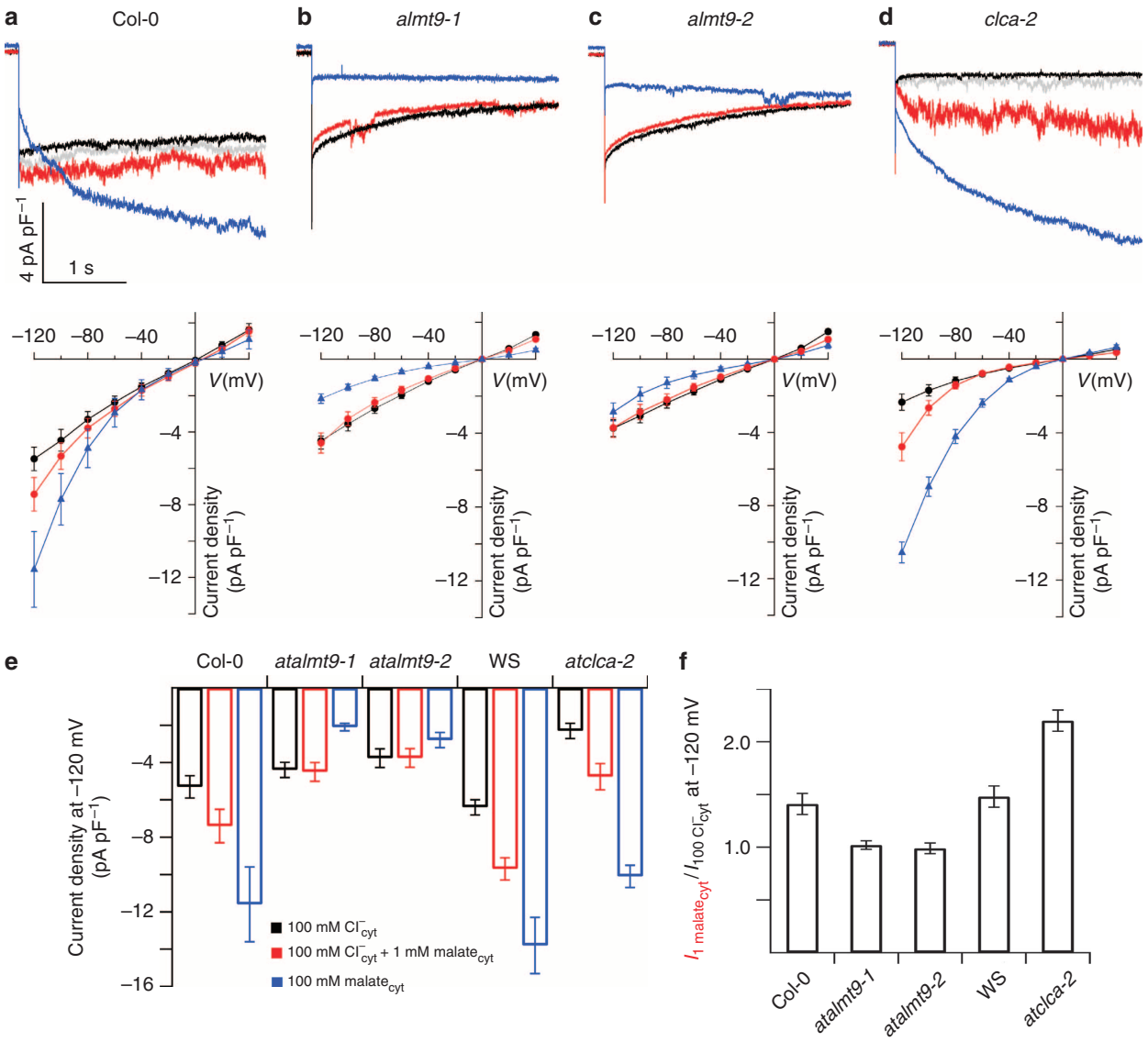

Figure 4 | Cytosolic malate activates chloride currents in *A. thaliana* vacuoles from mesophyll protoplasts. Representative current recordings (upper panel; at −120 mV) and mean *I*-*V* curves normalized to the capacitance (lower panel) obtained in whole-vacuole configuration: (**a**) Col-0 out-crossed wild-type ($n=10$), (**b**) *atalmt9-1* ($n=5$), (**c**) *atalmt9-2* ($n=6$) and (**d**) *atclca-2* ($n=6$) knockout lines during cytosolic solution exchange. Black, 100 mM Cl^-_{cyt}/100 mM Cl^-_{vac}; red, 100 mM Cl^-_{cyt} + 1 mM $malate_{cyt}$/100 mM Cl^-_{vac}; blue, 100 mM $malate_{cyt}$/100 mM $malate_{vac}$; grey, recovery. In the wild-type vacuoles (**a**), the addition of 1 mM $malate_{cyt}$ induces a reversible increase of the chloride currents of 1.43 times at $V_m = -120$ mV while in the *atalmt9-1* (**b**) and *2* (**c**) no activation of the chloride currents is observable. (**d**) the *atclca-2* knockout mutant presents a decreased anionic current background and an increase of the chloride currents in response to 1 mM $malate_{cyt}$ of 2.2 times at −120 mV. (**e**) Mean current density at $V_m = -120$ mV of the different genotypes in the different tested conditions. (**f**) Ratio of the current measured in 100 mM Cl^-_{cyt} + 1 mM $malate_{cyt}$ and the current measured in 100 mM Cl^-_{cyt} for the different genotypes. In **e** and **f**, results from wild-type Wassilewskija (WS; $n=4$) are shown. (**a**–**d**) Currents evoked in response 3-s pulse from +60 mV to −120 mV, holding potential +60 mV. *I*-*V* characteristics were obtained averaging the last 50 ms of the current traces. Error bars are s.e.m.

hypothesized that in our *Arabidopsis*, whole-vacuole measurements there was a background chloride current independent from other vacuolar ALMTs masking the malate activation, which would consequently result in a reduced effect of cytosolic malate. AtCLCa has been shown to mediate the main inorganic anion current across the *Arabidopsis* tonoplast and to be able to transport NO_3^- (ref. 12) but also Cl^- (ref. 29). We found that in the presence of 100 mM Cl^-_{cyt} vacuoles from *atclca-2* exhibited a current density of -2.3 ± 0.4 pA pF^{-1} (Fig. 4d) compared with the -6.4 ± 0.4 pA pF^{-1} observed in the corresponding wild type (WS, Wassilewskija). This result shows that *atclca-2* actually present a strongly diminished background chloride current compared with the wild type (Fig. 4e). When the 100 mM Cl^-_{cyt} + 1 mM $malate_{cyt}$ buffer was applied in *atclca-2*, the current increased by a similar amount as in the wild type. However, as the contribution of AtCLCa was no more present, the activation by malate was increased by a factor of 2.2 ± 0.1 compared with 1.48 ± 0.1 in WS, showing that the reduced background of *atclca-2* resulted in an increased activation effect of $malate_{cyt}$. These results show that the reduced activation of the chloride currents by 1 mM cytosolic malate in wild-type *Arabidopsis* vacuoles (Fig. 4a,e,f) compared with the activation

measured in overexpressing tobacco vacuoles is likely to be due to the higher relative contribution of background chloride currents in *Arabidopsis*.

AtALMT9 controls stomata aperture. As chloride ions are known to have a major role in stomatal movements in *Arabidopsis*, we investigated whether and how AtALMT9 could be involved in this process. Coinciding with *in silico* data (Genevestigator, http://www.genevestigator.ethz.ch), experiments using plants expressing GUS under the control of the *AtALMT9* promoter confirmed that this channel is also expressed in guard cells (Fig. 5a). As the currents mediated by AtALMT9 were strongly inward rectifying, we expected a physiological role of AtALMT9 in the opening process of stomata. Indeed, the closure induced by dark or ABA is not impaired in *atalmt9* mutants (Supplementary Fig. S7). Therefore we performed stomatal opening assays on peeled epidermal strips from two independent *atalmt9* knockout lines using a 30 mM KCl buffer (Fig. 5b). After exposure to light for 2 h, we could detect a 20% and 21%, reduced stomatal aperture in the *atalmt9-1* and *atalmt9-2* mutants, respectively (Fig. 5c). Interestingly, when the same assay was made in presence of 3 mM Cl^- (30 mM K^+, 3 mM Cl^- and 27 mM iminodiacetate), the stomata aperture after the exposure to 2 h light of both wild types and mutants was similar but reduced compared to that of wild type in 30 mM KCl (Fig. 5c). Guard cells accumulate different anions such as malate and Cl^- during stomata opening to balance K^+ charges[4–6]. The relative accumulation of Cl^- and malate in the vacuole depends on the availability of chloride[10,30]. In this context, our data indicate that AtALMT9 is involved in mediating chloride fluxes in the vacuole of guard cells to achieve a complete stomata opening.

Furthermore, we monitored the kinetics of stomatal opening in *Arabidopsis* leaves by measuring changes in the stomatal conductance in response to light (Fig. 5d, Supplementary Fig. S8). Compared with wild-type plants, stomatal conductance was lower after 100 min of light exposure in both *atalmt9* knockout lines and measurements revealed significantly slower opening kinetics in the mutants than in the wild-type plants. To obtain further evidences that loss of AtALMT9 affects also stomatal opening *in planta*, we exposed wild type and knockout plants to drought stress (Fig. 5e). Both knockout lines were more resistant to drought compared with the corresponding wild-type lines. At 8 days after the last watering, wild-type plants had 23% lower water content compared with the corresponding knockout lines (Supplementary Fig. S9). Like in previous studies, no visual

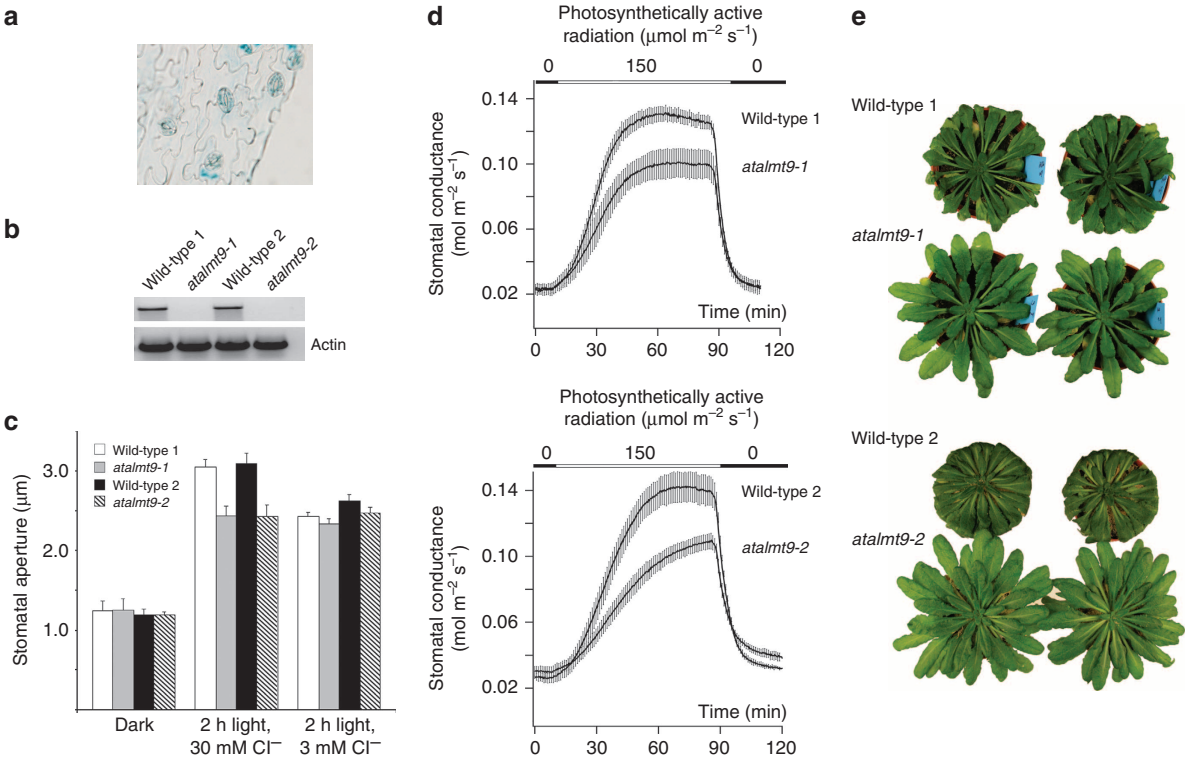

Figure 5 | AtALMT9 is involved in stomatal opening in *A. thaliana*. (**a**) *AtALMT9*-promoter-GUS reporter lines show that AtALMT9 is expressed in guard cells. (**b**) Two independent knockout mutant lines, *atalmt9-1* and *atalmt9-2* (for details see material and methods), were used to determine the role of the AtALMT9 chloride channel in stomatal opening. In both lines, RNA transcripts for AtALMT9 could not be detected. (**c**) Stomatal aperture measurements on stripped epidermis after 2 h of illumination *atalmt9-1* and *atalmt9-2* knockout mutants and wild-type plants. Measurements performed in presence of 30 mM KCl show that the knockout mutants presented a decreased aperture of 20 ± 3% (*atalmt9-1*, $P = 0.004$ *t*-test; $n = 6$) and 21 ± 4% (*atalmt9-2*, $P = 0.003$ *t*-test; $n = 6$) with respect to the corresponding wild types. Measurements performed in presence of 27 mM K-iminodiacetate and 3 mM KCl show that *atalmt9-1* and *atalmt9-2* knockout mutants do not show significant difference in stomatal apertures (*atalmt9-1*, $P = 0.11$ *t*-test; *atalmt9-2*, $P = 0.21$ *t*-test). Each point corresponds to the mean of six experiments, in each experiment at least 60 stomata were analysed. (**d**) Time course of the mean stomatal conductance during light-induced opening. Measurements were performed using a LI-6400; LI-COR gas exchange chamber. It is visible that in both *atalmt9-1* (upper panel; *atalmt9-1*, $n = 6$ plants; wild-type-1, $n = 5$ plants) and *atalmt9-2* (lower panel; *atalmt9-2*, $n = 6$ plants; wild-type-2, $n = 6$ plants) knockouts, the stomatal conductance increase is delayed compared with the corresponding wild-type plants. After 1.5 h, the two knockout lines reach a lower conductance level (*atalmt9-1* 22%; *atalmt9-2* 25%) than the corresponding wild types. (**e**) *atalmt9-1* and *atalmt9-2* are more tolerant to drought, 8 days after stopping watering *atalmt9-1* (upper panel) and *atalmt9-2* (lower panel) are still turgescent, while the corresponding wild types are withered. Error bars are s.e.m.

phenotype on leaves was observed[18]. However, to verify that the drought stress phenotype was not due to a rapid hydropassive water loss, we measured the osmolarity of wild type and knockout mutants. As expected from the similar water content in both lines, the osmolarity of the press sap was also indistinguishable. These results indicate that the increased drought resistance of *atalmt9*-1 and *atalmt9-2* is not due to a less negative water potential in the mutant (Supplementary Fig. S9) but to the impaired stomatal opening (Fig. 5c,d).

Discussion

To guarantee appropriate gas exchanges under changing environmental conditions, ion transport and metabolism have to be integrated processes in guard cells. Anions have to meet the metabolic requirements of the cell as well as to keep the ionic balance and the osmotic potential. Chloride has an important role as an osmoticum and charge balance but is metabolically inactive. In contrast, malate is part of several metabolic pathways and through the action on PEPcase regulates the synthesis of oxaloacetate, its precursor[31]. During stomatal opening concomitantly to potassium uptake, malate and chloride are taken up from the apoplast[1,4,6,32]. Moreover, malate is also synthesized via starch degradation[4,5]. The amount of malate in the apoplast is limited and the synthesis of large amounts of malate through starch breakdown and glycolysis is likely to be slower than the uptake. As the cytosolic volume of guard cells is only about 20–30% of the cellular volume when stomata are closed, small increases of cytosolic malate are sufficient to activate the vacuolar chloride channel and consequently allow a rapid opening reaction via chloride accumulation in the vacuole. Consequently, at least in short terms, malate may not have the role as the main osmolyte during stomatal opening but rather exhibit a so far unexplored signalling function: the regulation of anion fluxes across the plasma and the vacuolar membranes, hence participating in the control of the osmotic pressure of guard cells (Fig. 6). We found that AtALMT9 mediates chloride currents activated by cytosolic malate in a physiological concentration range in both heterologous expression system and under native conditions. In *Arabidopsis*, the relative contribution of AtALMT9 in vacuolar chloride fluxes can be estimated based on our data. We could attribute the relatively weak activation observed in *Arabidopsis* compared with the measurements in *N. benthamiana* overexpressing AtALMT9 to the relative high background currents in *Arabidopsis* vacuoles. However, taking the measured values and deducing the background current by calculating the ratios of $((I_{Cl+mal}^{Col-0} - I_{Cl+mal}^{almt9})/(I_{Cl}^{Col-0} - I_{Cl}^{almt9}))$, an activation of the AtALMT9-mediated chloride current of ~ 3 could be obtained; a value similar to that observed in tobacco.

At -120 mV and in the presence of 100 mM Cl^-, and 1 mM malate the current through AtALMT9 is ~ -3 pA pF^{-1}. We found that beside AtALMT9 the major current under our experimental conditions is generated by AtCLCa with a current density of ~ -3 pA pFA^{-1}. If one takes into account that AtCLCa is a nitrate, chloride/proton antiporter[12,29] and that under our experimental conditions, two protons are exported for each chloride taken up by the vacuole it results that the chloride flux mediated by AtALMT9 is about three times the one mediated by AtCLCa. Nonetheless, it should be mentioned that the relative contributions of AtALMT9 and AtCLCa may differ in function of the given membrane potential and cytosolic chloride concentrations and regulatory factors.

Our results also show that AtALMT9 is required for fast and complete opening of stomata, but has no effect on stomata closure. Mutants of AtALMT9 wilt faster, which is in accordance with the gas exchange data and the measurements made on isolated epidermal strips. AtALMT9 is also expressed in the mesophyll cells[18]. To exclude indirect effect of the mesophyll, we compared water contents and the osmolarity in the leaves of wild-type and mutant plants. Both parameters were displaying no significant differences between wild-type and knockout plants consequently excluding a role of the mesophyll in the observed phenotype. Therefore, the drought-resistant phenotype of the knockout can be attributed to the impaired stomatal opening resulting from a reduced uptake of chloride in guard cell vacuoles. This is in line with the functional properties of AtALMT9 mediating chloride fluxes directed into the vacuole.

Wang and Blatt[33] have recently shown that carboxylates inhibit chloride fluxes across the plasma membrane of *Vicia faba* guard cells, indicating that carboxylates act as important regulatory elements of chloride fluxes across cellular membranes. In our work, we identified AtALMT9 as target of the carboxylate modulation. Whether the inhibition observed by Wang and Blatt[33] is due to an opposite regulatory effect of carboxylates on plasma membrane localized ALMTs or SLACs or whether an inhibition of the plasma membrane chloride efflux was observed due to the activation of the vacuolar chloride currents remains to be established. The discovery that AtALMT9 constitutes a vacuolar chloride channel, which has been sought for over 20 years, assigns a completely novel function to this anion channel. These results may pave the way to get further insights in the regulation of guard cell anion channels and finally to modulate stomatal aperture allowing to produce plants that are more drought tolerant and more productive under certain environmental conditions.

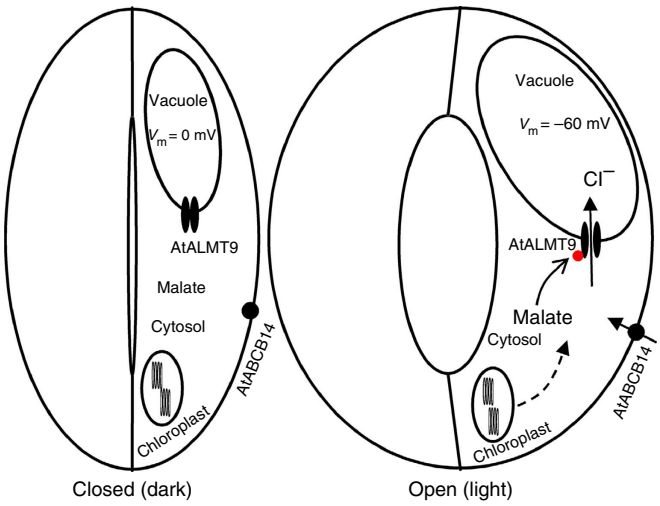

Figure 6 | Model for the role of AtALMT9 in stomatal opening. When stomata are closed (at the end of the dark period), the vacuolar membrane potential is close to 0 mV and cytosolic malate concentrations are low (left panel). In these conditions, AtALMT9 is not active and does mediate anion accumulation into the vacuole. During stomatal opening (right panel), the membrane potential of the vacuole drops to values close to -60 mV. Starch is degraded to malate, which is also taken up from the apoplast inducing a raise of the cytosolic malate concentration. These conditions activate AtALMT9. At the same time, chloride enters into guard cells. To sustain the opening of stomata, solutes have to be accumulated in the vacuole of guard cells to increase the water potential. In this phase, AtALMT9 mediates chloride accumulation in the vacuole.

Methods

Overexpression of AtALMT9-GFP in *Nicotiana benthamiana*. For transient overexpression of AtALMT9-GFP, the complementary DNA was cloned into the pART27 vector as described previously[18].The agrobacterium-mediated infiltration of *N. benthamiana* leaves was perfomed as described[34] with slight modifications.

After agrobacterium-mediated infiltration tobacco plants were grown in greenhouse (16 h light:8 h dark, 25 °C). At 2–3 days after the agrobacterium-mediated infiltration, the transformed leaves were used to extract protoplasts and vacuoles for patch-clamp experiments.

Electrophysiology. Mesophyll protoplasts from tobacco leaves were released by an enzymatic digestion. The enzyme solution contained 0.3% (w/v) cellulase R-10, 0.03% (w/v) pectolyase Y-23, 1 mM $CaCl_2$, 500 mM sorbitol and 10 mM MES, pH 5.3 (550 mOsm). Protoplasts were washed twice and resuspended in the same solution without enzymes. Vacuoles were released from mesophyll protoplast by the addition of 5 mM EDTA and a slight osmotic shock (500 mOsm, see medium below). Vacuoles from transformed protoplasts to be used for patch-clamp experiments were selected using an epifluorescence microscope. Membrane currents from tonoplast patches were recorded using the patch-clamp technique[12,19]. Briefly, currents were recorded with an EPC10 patch-clamp amplifier (HEKA Electronics) using the Patchmaster software (HEKA Electronics). Data were analysed with the FitMaster software (HEKA Electronics). Exchange of the cytosolic-side solution was performed using a gravity-driven perfusion system. In experiments on macroscopic currents recording and whole-vacuole, the pipette resistance was 4–5 MΩ. For single-channel recordings, the pipette resistance was 8–9 MΩ. Only patches presenting a seal resistance higher than 2 GΩ for macroscopic currents and 8–10 GΩ for single-channel recordings were used to perform experiments. In whole-vacuole recordings, to equilibrate the vacuolar lumen with the pipette solution, at least 10 min were waited after the establishment of the whole-vacuole configuration before starting the exchange of the cytosolic-side solution. Current recordings were filtered at 300 Hz for macroscopic currents and 1.5 kHz for single-channel recordings.

The pipette solutions contained: 112 mM malic acid, 5 mM HCl, adjusted with BisTrisPropane, pH 6; 100 mM HCl, adjusted to pH 6 with BisTrisPropane. The osmolarity was adjusted to 550 mOsm with sorbitol. The bath solutions contained: (i) 100 mM malic acid, 3 mM $MgCl_2$, 0.1 mM $CaCl_2$, adjusted to pH 7.5 with BisTrisPropane; (ii) 100 mM HCl, 3 mM $MgCl_2$, 0.1 mM $CaCl_2$, adjusted to pH 7.5 with BisTrisPropane. The osmolarity was adjusted to 500 mOsm with sorbitol. For activation experiments of the chloride currents, the dicarboxylic acids (malic acid, isophtalic acid, fumaric acid, oxaloacetic acid and glutamic acid) were added to the chloride-based bath solution at the concentrations indicated in the text. When needed the pH was adjusted to 7.5 with BisTrisPropane. All chemicals were purchased at Sigma-Aldrich. Liquid junction potentials were measured[35] and corrected when higher that ± 2 mV.

When not stated differently the current–voltage characteristics were obtained by subtracting the current at $t = 0$ from the quasi-stationary currents (averaging the last 50 ms of the current trace) elicited by main voltage pulses.

For the channel activation by malate, the concentration-dependent activation relationship was fitted by the Hill equation in the form of:

$$\frac{I_{act}}{I_{ctrl}} = 1 + \frac{A \cdot [act]^{n_H}}{K_A^{n_H} + [act]^{n_H}}$$

where I_{act} is the current in presence of the activator, I_{ctrl} is the current in absence of the activator. n_H is the Hill coefficient and [act] is the concentration of the activator. K_A is the EC50. A is the maximum current ratio.

Plant material and growth conditions.. All wild type (Col-0) and *atalmt9* mutant plants of *Arabidopsis thaliana* were grown in a plant growth chamber (8 h light 22 °C/16 h dark 18 °C, 55% relative humidity) in potting soil. For drought stress experiments, plants were grown in a defined amount of sieved soil in round pots (6 cm diameter). After 8 weeks of regular irrigation, watering was stopped.

Selection of *atalmt9* knockout lines. Two independent T-DNA insertion lines, *atalmt9-1* (SALK_055490) and *atalmt9-2* (WiscDsLox499H09), were obtained from the Salk Institute Genomic Analysis Laboratory and the Wisconsin *Arabidopsis* T-DNA insertion collection, respectively. Genomic DNA was extracted from 4-week-old plants and mutant plants homozygous for the T-DNA insertion locus were isolated by PCR genotyping using *AtALMT9*-specific primers. To select homozygous lines, we used the *AtALMT9*-specific primer At3g18440-solfor (5′-GATCCTGCAGGCTGGAGAGGATCTTCATAACCTTG-3′) and At3g18440–solrev (5′-GATCGCGGCCGCTTACATCCCAAAACACCTACGAATC-3′) and the T-DNA-specific primer LBb1.3 (5′-ATTTTGCCGATTTCGGAAC-3′) and p745 (5′-AACGTCCGCAATGTGTTATTAAGTTGTC-3′) for *atalmt9-1* and *2*, respectively. The abundance of the *AtALMT9* transcript in homozygous knockout lines and wild-type plants (see below) was assayed by reverse transcriptase–PCR using the *AtALMT9*-specific primers ALMT9-1F (5′-CCTTAAT-TAAATGGCGGCGAAGCAAGGTTCCTTCA-3′) and ALMT9-1794R (5′-TTGGCGCGCCCATCCCAAAACAC CTACGAATCT-3′). As loading control, actin transcript was amplified with the primers 5′-TGGAATCCACGAGACA ACCT-3′ and 5′-TTCTGTGAACGATTCCTGGAC-3′.

Stomatal aperture and gas exchange measurements. Stomatal aperture and conductance were assayed from leaves of 5- to 7-week-old plants. Stomatal conductances of wild-type, *atalmt9-1* and *atalmt9-2* plants were measured using a portable gas exchange system (LI-6400; LI-COR) with an *Arabidopsis* leaf chamber fluorometer (LI-6400-40, LI-COR) and a light source set to 150 µmol m^{-2} s^{-1} (10% blue light). The relative humidity of incoming air was 58% ± 2% and the air flow was set to 300 µmol s^{-1}.

For stomatal aperture measurement, the whole leaf was detached in the dark before start of the light period and glued from the abaxial side onto a coverslip using a non-toxic medical adhesive (Medical Adhesive B Liquid, VM 355-1, Ulrich Swiss). The adaxial epidermis and mesophyll layers were gently removed. The coverslips with the glued abaxial epidermis were placed in a Petri dish containing the opening buffer. The 30 mM Cl^- buffer contains: 30 mM KCl, 5 mM MES, 0.1 mM $CaCl_2$, pH 5.7. The 3 mM Cl^- buffer contains: 3 mM KCl, 13.5 mM K_2 Iminodiacetate,0.1 mM $CaCl_2$, pH 5.7. The epidermis was equilibrated for 30 min in dark ($t = 0$) and then incubated for 2 h in light. Wild-type and knockout leaves were analysed in parallel. Around 20 pictures per leaf and per time point were taken using an inverted microscope (Nikon Eclipse TS100) at a × 40 magnification. Stomatal apertures were measured manually using the ImageJ software. For each time point, more than 60 stomatal apertures were measured.

Tissue-specific expression of AtALMT9 in *Arabidopsis*. For GUS staining, the whole leaf was detached from the same transgenic plants lines as described (1). The abaxial epidermis was peeled and incubated in GUS staining buffer (50 mM $NaHPO_4$ pH 7.2, 0.5% Triton X-100, 1 mM X-Gluc) at 37 °C for 30 h, subsequently the GUS staining buffer was replaced with 70% ethanol. The samples were examined using a Nikon Eclipse TS100 microscope.

References

1. Hetherington, A. M. Guard cell signaling. *Cell* **107,** 711–714 (2001).
2. Kim, T. H., Bohmer, M., Hu, H. H., Nishimura, N. & Schroeder, J. I. Guard cell signal transduction network: advances in understanding abscisic acid, CO_2 and Ca^{2+} signaling. *Annu. Rev. Plant Biol.* **61,** 561–591 (2010).
3. MacRobbie, E. A. C. Signal transduction and ion channels in guard cells. *Phil. Trans. Roy. Soc. Lond.* **1374,** 1475–1488 (1998).
4. Roelfsema, M. R. & Hedrich, R. In the light of stomatal opening: new insights into 'the Watergate'. *New Phytol.* **167,** 665–691 (2005).
5. Vavasseur, A. & Raghavendra, A. S. Guard cell metabolism and CO_2 sensing. *New Phytol.* **165,** 665–682 (2005).
6. Pandey, S., Zhang, W. & Assmann, S. M. Roles of ion channels and transporters in guard cell signal transduction. *FEBS Lett.* **581,** 2325–2336 (2007).
7. Lebaudy, A., Very, A. -A. & Sentenac, H. K^+ channel activity in plants: genes regulations and functions. *FEBS Lett.* **581,** 2357–2366 (2007).
8. Vahisalu, T. *et al.* SLAC1 is required for plant guard cell S-type anion channel function in stomatal signalling. *Nature* **452,** 487–491 (2008).
9. Negi, J. *et al.* CO_2 regulator SLAC1 and its homologues are essential for anion homeostasis in plant cells. *Nature* **452,** 483–486 (2008).
10. Talbott, L. D. & Zeiger, E. Central roles for potassium and sucrose in guard cell osmoregulation. *Plant Physiol.* **111,** 1051–1057 (1996).
11. Barbier-Brygoo, H. *et al.* Anion channels/transporters in plants: from molecular bases to regulatory networks. *Annu. Rev. Plant Biol.* **62,** 25–51 (2011).
12. De Angeli, A. *et al.* The nitrate/proton antiporter AtCLCa mediates nitrate accumulation in plant vacuoles. *Nature* **442,** 939–942 (2006).
13. Jossier, M. *et al.* The Arabidopsis vacuolar anion transporter, AtCLCc, is involved in the regulation of stomatal movements and contributes to salt tolerance. *Plant J.* **64,** 563–576 (2010).
14. Geiger, D. *et al.* Guard cell anion channel SLAC1 is regulated by CDPK protein kinases with distinct Ca^{2+} affinities. *Proc. Natl Acad. Sci. USA* **107,** 8023–8028 (2010).
15. Sasaki, T. *et al.* A wheat gene encoding an aluminum-activated malate transporter. *Plant J.* **37,** 645–653 (2004).
16. Hoekenga, O. A. *et al.* AtALMT1, which encodes a malate transporter, is identified as one of several genes critical for aluminum tolerance in Arabidopsis. *Proc. Natl Acad. Sci. USA* **103,** 9738–9743 (2006).
17. Meyer, S. *et al.* AtALMT12 represents an R-type anion channel required for stomatal movement in Arabidopsis guard cells. *Plant J.* **63,** 1054–1062 (2010).
18. Kovermann, P. *et al.* The *Arabidopsis* vacuolar malate channel is a member of the ALMT family. *Plant J.* **52,** 1169–1180 (2007).
19. Meyer, S. *et al.* Malate transport by the vacuolar AtALMT6 channel in guard cells is subject to multiple regulation. *Plant J.* **67,** 247–257 (2011).
20. Meyer, S., De Angeli, A., Fernie, A. & Martinoia, E. Intra- and extra-cellular excretion of carboxylates from the plant cytosol. *Trends Plant Biol.* **15,** 40–48 (2010).
21. Pei, Z. M., Ward, J. M., Harper, J. F. & Schroeder, J. I. A novel chloride channel in *Vicia faba* guard cell vacuoles activated by the serine/threonine kinase, CDPK. *EMBO J.* **15,** 6564–6574 (1996).

22. Martinoia, E., Meyer, S., De Angeli, A. & Nagy, R. Vacuolar transporters. *Annu. Rev. Plant Biol.* **63,** 183–213 (2012).
23. Pineros, M. A. *et al.* Not all ALMT1-type transporters mediate aluminum-activated organic acid responses: the case of ZmALMT1—an anion-selective transporter. *Plant J.* **53,** 352–367 (2008).
24. Munns, R. & Tester, M. Mechanisms of salinity tolerance. *Annu. Rev. Plant Biol.* **59,** 651–681 (2008).
25. Gerhardt, R. & Heldt, H. W. Measurement of subcellular metabolite levels in leaves by fractionation of freeze-stopped material in nonaqueous media. *Plant Physiol.* **75,** 542–547 (1984).
26. Winter., H., Robinson, D. G. & Heldt, H. W. Subcellular volumes and metabolite concentrations in spinach leaves. *Planta* **193,** 530–535 (1994).
27. Farré, E. M. *et al.* Analysis of the compartmentation of glycolytic intermediates, nucleotides, sugars, organic acids, amino acids, and sugar alcohols in potato tubers using a nonaqueous fractionation method. *Plant Physiol.* **127,** 685–700 (2001).
28. Mayer, M. L. Glutamate receptor ion channels. *Curr. Opin. Neurobiol.* **15,** 282–288 (2005).
29. Wege, S. *et al.* The proline 160 in the selectivity filter of the Arabidopsis NO_3^-/H^+ exchanger AtCLCa is essential for nitrate accumulation in planta. *Plant J.* **63,** 861–869 (2010).
30. Raschke, K. & Schnabl, H. Availability of chloride affects the balance between potassium chloride and potassium malate in guard cells of *Vicia faba* L. *Plant Physiol.* **62,** 84–87 (1978).
31. Cotelle, V., Pierre, J. N. & Vavasseur, A. Potential strong regulation of guard cell phosphoenolpyruvate carboxylase through phosphorylation. *J. Exp. Bot.* **335,** 777–783 (1999).
32. Lee, M. *et al.* The ABC transporter AtABCB14 is a malate importer and modulates stomatal response to CO_2. *Nat. Cell Biol.* **10,** 1217–1223 (2008).
33. Wang, Y. & Blatt, M. R. Anion channel sensitivity to cytosolic organic acids implicates a central role for oxaloacetate in integrating ion flux with metabolism in stomatal guard cells. *Biochem. J.* **439,** 161–170 (2011).
34. Yang, K. Y., Liu, Y. & Zhang, S. Activation of a mitogen-activated protein kinase pathway is involved in disease resistance in tobacco. *Proc. Natl Acad. Sci. USA* **98,** 741–746 (2001).
35. Neher, E. Correction for liquid junction potentials in patch clamp experiments. *Methods Enzymol.* **207,** 123–131 (1992).

Acknowledgements

This work was supported by a long-term EMBO fellowship (A.D.A.), the Chinese Scholarship Council (J.Z.) and the Swiss National Foundation and Ministry of Education and Science and Technology of Korea (K20607000006) (E.M.). We thank D. Bollier for technical support in constructing the patch-clamp devices and U. Baetz for critical reading of the manuscript.

Author contribution

A.D.A., J.Z. and S.M. performed experimental work. A.D.A., S.M. and E.M designed research. A.D.A. and E.M wrote the manuscript.

Additional Information

Supplementary Information accompanies this paper at http://www.nature.com/naturecommunications

Competing financial interests: The authors declare no competing financial interest.

Reprints and permission information is available online at http://npg.nature.com/reprintsandpermissions/

How to cite this article: De Angeli, A. *et al.* AtALMT9 is a malate-activated vacuolar chloride channel required for stomatal opening in *Arabidopsis*. *Nat. Commun.* 3:1804 doi: 10.1038/ncomms2815 (2013).

AtALMT9 is a malate-activated vacuolar chloride channel required for stomatal opening in Arabidopsis

Alexis De Angeli, Jingbo Zhang, Stefan Meyer and Enrico Martinoia

Supplementary Figures

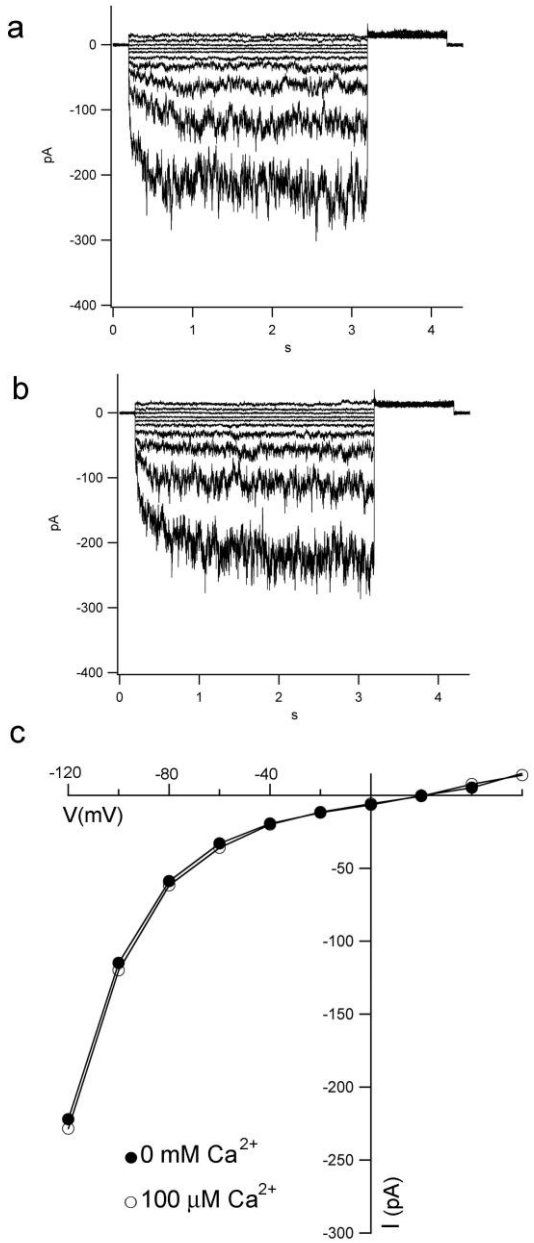

Supplementary Figure S1. Cytosolic Ca^{2+} does not activate AtALMT9 mediated chloride currents. (**a**,**b**) Typical excised cytosolic-side-out patch current form *N. benthamiana* AtALMT9 overexpressing vacuoles in nominal absence of cytosolic calcium (0 mM Ca^{2+}; **a**) and after perfusion with 100 µM cytosolic Ca^{2+} (**b**). (**c**), I/V curves of the total currents from (**a)** and (**b**). The mean ratio is $I_{Ca}/I_{0.1mM\ Ca}$= 1.1 ± 0.1 at -120 mV (n=3). The 0 mM Ca^{2+} *cytosolic solution* contains: 100 mM HCl, 3 mM $MgCl_2$, 5mM EGTA, adjusted to pH 7.5 with BisTrisPropane. The 100 µM Ca^{2+} *cytosolic solution* contains: 100 mM HCl, 3 mM $MgCl_2$, 0.1 mM $CaCl_2$, adjusted to pH 7.5 with BisTrisPropane. *Vacuolar side solution*: 100 mM HCl, adjusted to pH 6 with BisTrisPropane. (**a**,**b**), from a holding potential of 0 mV a series of test voltages from +60 to -120 mV in steps of -20 mV was applied; tail potential -60 mV. Error bars are s.e.m. (**a**, **b**) Currents evoked in response 3s pulse from +60 mV to -120 mV in -20 mV steps, followed by a tail pulse at -60 mV, holding potential +60 mV.

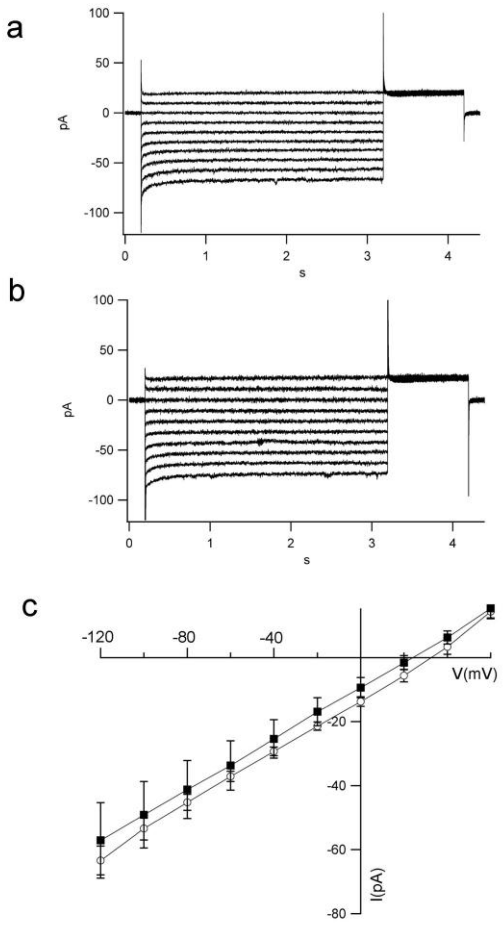

Supplementary Figure S2. Cytosolic malate does not activate chloride currents in excised cytosolic-side-out in patches from empty vector transformed vacuoles. (**a**,**b**) Typical excised cytosolic-side-out patch currents form *N. benthamiana* vacuoles obtained from empty-vector (pART27) transformed protoplasts. (**a**), currents recorded with a 100 mM Cl^-_{cyt} buffer and (**b**) after perfusion with 100 mM Cl^-_{cyt} + 1 mM $malate_{cyt}$ buffer. (**c**), mean I-V curves from currents recorded with a 100 mM Cl^-_{cyt} buffer and after perfusion with 100 mM Cl^-_{cyt} + 1 mM $malate_{cyt}$ buffer (n=6). *Vacuolar side solution*: 100 mM HCl, adjusted to pH 6 with BisTrisPropane. *Cytosolic side buffers*: 100 mM HCl, 3 mM $MgCl_2$, 0.1 mM $CaCl_2$, adjusted to pH 7.5 with BisTrisPropane; 100 mM HCl, 1 mM malic acid, 3 mM $MgCl_2$, 0.1 mM $CaCl_2$, adjusted to pH 7.5 with BisTrisPropane. Error bars are s.e.m. (**a**, **b**)Currents evoked in response 3s pulse from +60 mV to -120 mV in -20 mV steps, followed by a tail pulse at -60 mV, holding potential +60 mV.

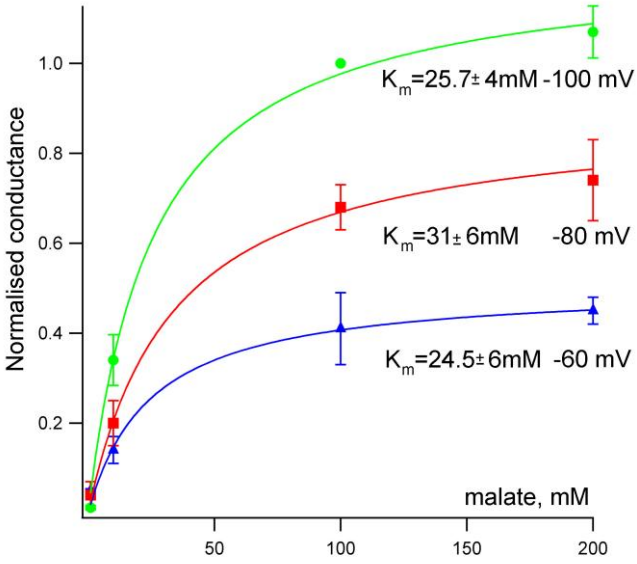

Supplementary Figure S3. Conductance of *At*ALMT9 currents as a function of cytosolic malate concentration measured at different membrane potentials as indicated. The data were normalised to the conductance in 100 mM malate$_{cyt}$ at -100 mV and fitted with a Michaelis-Menten function. The results indicate that the K_m is voltage independent and exhibits a mean value of 27 mM malate.

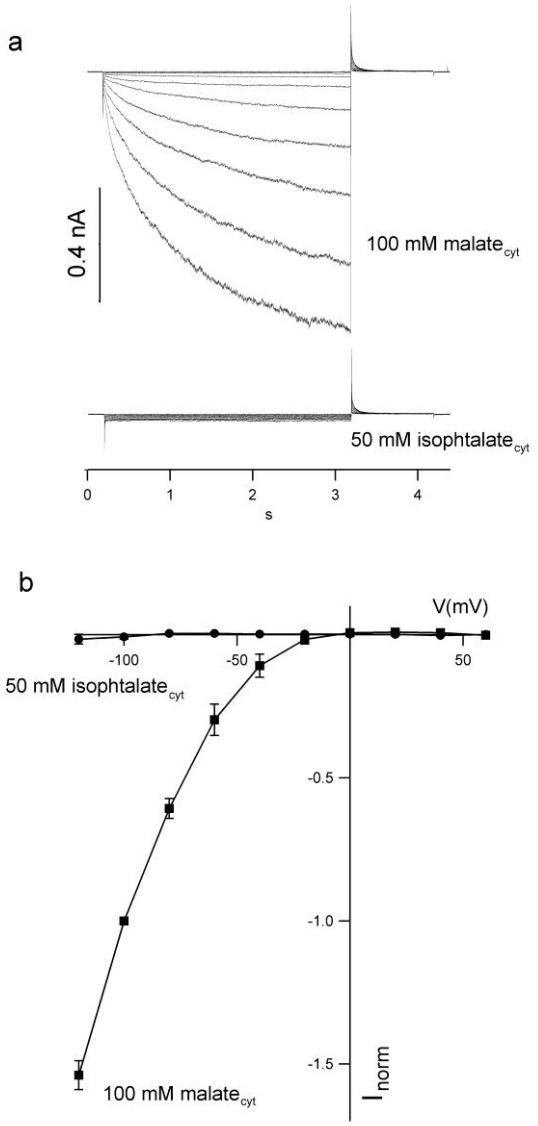

Supplementary Figure S4. Isophtalic acid is not permeable through *At*ALMT9. (a) Representative *At*ALMT9 currents recorded with voltage pulses form 40 to -120 mV in presence of 100 mM malate$_{cyt}$ and 50 mM isophtalate$_{cyt}$. **(b)** Normalised mean IV curves in presence of 100 mM malate$_{cyt}$ and 50 mM isophtalate$_{cyt}$. The currents detected in the presence of isophtalate$_{cyt}$ correspond to 1% at -120 mV of the currents measured in presence of malate. The pipette solutions was: 112 mM malic acid, 5 mM HCl, adjusted with BisTrisPropane to pH 6; the cytosolic solution were: i) 100 mM malic acid, 3 mM $MgCl_2$, 0.1 mM $CaCl_2$, adjusted to pH 7.5 with BisTrisPropane; ii) 50 mM isophtalic acid, 3 mM $MgCl_2$, 0.1 mM $CaCl_2$, adjusted to pH 7.5 with BisTrisPropane. (**a**, **b**) Currents evoked in response 3s pulse from +60 mV to -120 mV in -20 mV steps, followed by a tail pulse at -60 mV, holding potential +60 mV.

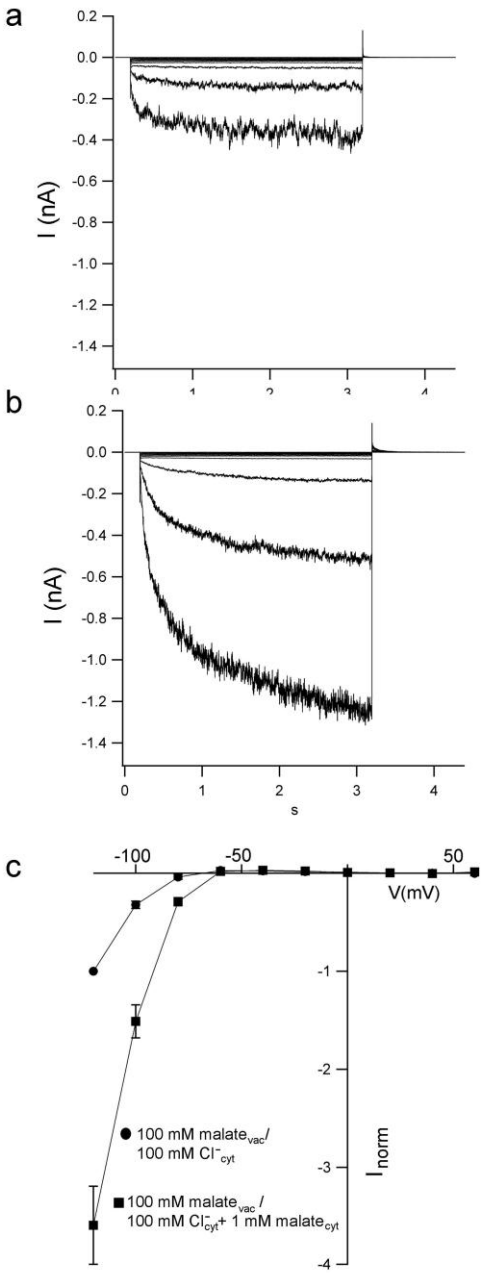

Supplementary Figure S5. Cytosolic malate activates AtALMT9 chloride currents even in presence of 100 mM malate in the vacuolar buffer. (**a**,**b**), Typical excised cytosolic-side-out patch current form *N. benthamiana* AtALMT9 overexpressing vacuoles with 100 mM malate in the vacuolar buffer and 100 mM Cl^-_{cyt} (**a**) and after perfusion with 100 mM Cl^-_{cyt} + 1 mM $malate_{cyt}$ (**b**). (**c**), mean normalised I/V curves of the time dependent currents from (**a)** and (**b**). In presence of 100 mM $malate_{vac}$ the mean ratio $I^{1mal,\ 100\ Cl-}{}_{cyt}/I^{100\ Cl-}{}_{cyt}$= 3.6 ± 0.4 at -120 mV. *Cytosolic side buffers*: 100 mM HCl, 3 mM $MgCl_2$, 0.1 mM $CaCl_2$, adjusted to pH 7.5 with BisTrisPropane; 100 mM HCl, 1 mM malic acid, 3 mM $MgCl_2$, 0.1 mM $CaCl_2$, adjusted to pH 7.5 with BisTrisPropane. *Vacuolar side buffer*: 112 mM malic acid, 5 mM HCl, adjuste with BisTrisPropane, pH 6. (**a**,**b, c**), from a holding potential of -60 mV a series of test voltages from +60 to -120 mV in steps of -20 mV was applied; tail potential -60 mV. Error bars are s.e.m. (**a**, **b**) Currents evoked in response 3s pulse from +60 mV to -120 mV in -20 mV steps, followed by a tail pulse at -60 mV, holding potential +60 mV.

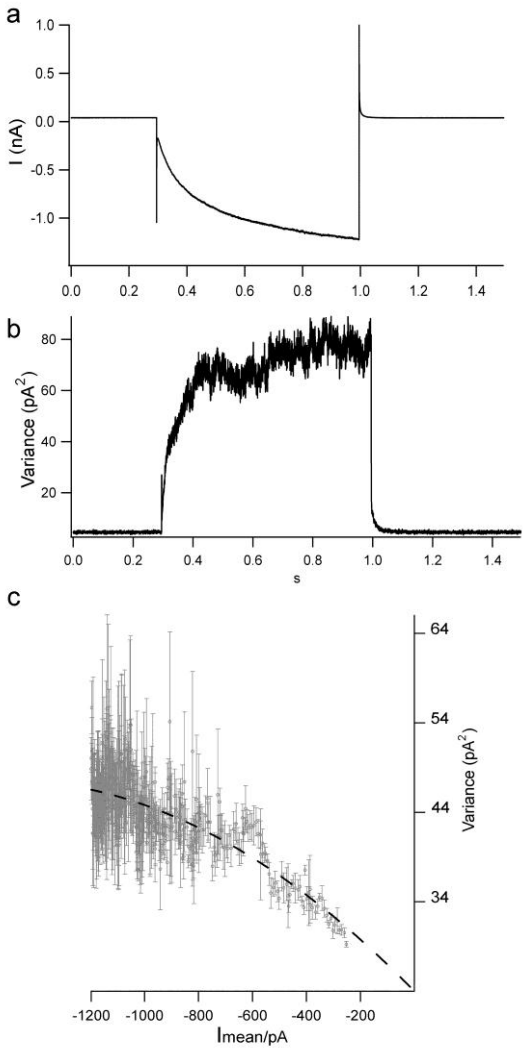

Supplementary Figure S6. Non stationary noise analysis of *At*ALMT9 in excised cytosolic side-out patches. (**a**) Average of 100 macroscopic current recordings and (**b**) corresponding variance from a representative patch recorded at -120 mV. (**c**) Plot of the variance against the corresponding mean current from the same patch as in (**a)**. To estimate the unitary channel current amplitude the variance mean relationship was fitted with the following equation:

$$\sigma^2 = i < I > - \frac{< I >^2}{N}$$

where σ^2 is the variance, i the unitary channel current, <I> is the mean current and N the number of channels in the patch. The mean unitary current amplitude was estimated to be -3.4±0.8 pA at -120 mV (n=3). Data were filtered at 10 kHz and sampled at 5 kHz.

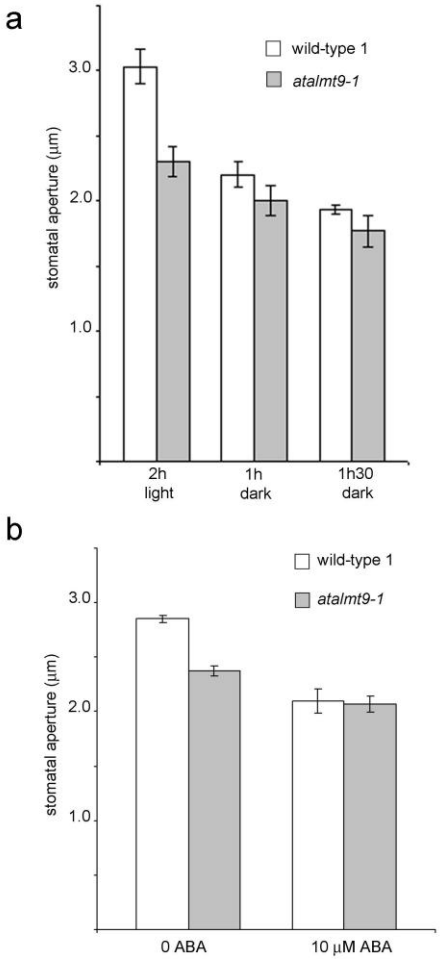

Supplementary Figure S7. AtALMT9 is not involved in triggering stomata closure in response to dark and ABA. (**a**), stomatal aperture were measured after 2h light in 30 mM KCl, after epidermal strips were transferred in the dark and stomatal aperture was measured after 1h and 1h30. In both wild-type (n=4) and *atalmt9-1* knock-out (n=4) the closure was statistically significant (wild-type 1 P=0.03; *atalmt9-1* P=0.01) and close to the same extent. (**b**), stomatal aperture were measured after 2h light in 30 mM KCl, subsequently 10 µM ABA was added and stomata aperture measured after 2h incubation in the light. In both wild-type (n=4) and *atalmt9-1* knock-out (n=4) the closure was statistically significant (wild-type 1 P=0.003; *atalmt9-1* P=0.009) and close to the same extent. In (**a**) and (**b**) the opening buffer was 30 mM KCl, 5 mM MES, 0.1 mM $CaCl_2$, pH 5.7. Error bars are s.e.m.

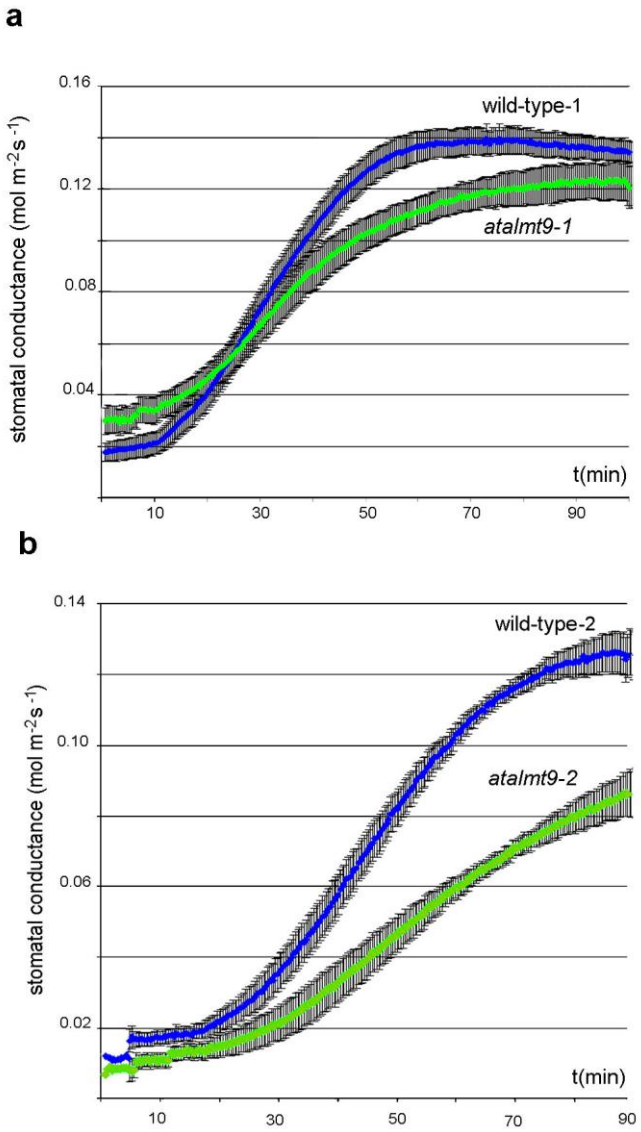

Supplementary Figure S8. Time course of the mean stomata conductance during light-induced opening in a second independent batch of plant. Measurements were performed using a LI-6400; LI-COR gas exchange chamber as in Figure 4d. **(a)** wild-type1 n=9 plants, *atalmt9-1* n=8. **(b)** wild-type n=6, *atalmt9-2* n=8 plants. Error bars represent s.e.m.

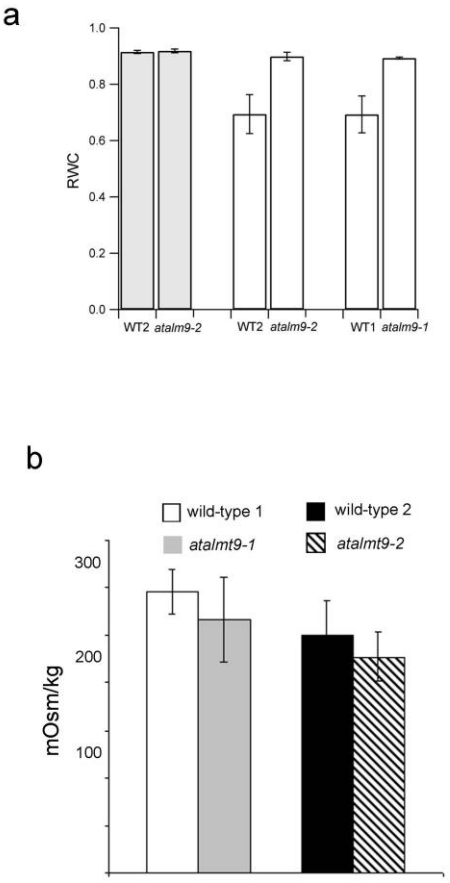

Supplementary Figure S9. (**a**), **Relative water content and osmolarity in wild-type and atalmt9 mutant plants**. Histograms showing the relative water content (RWC) of *atalmt9-1*, *atalmt9-2* and the corresponding wild-type plants before (*atalmt9-2* and corresponding wild-type, grey bars) and 8 days after stopping watering (empty bars). Wild-type plants exhibited a 23% larger water loss compared to the corresponding knockout lines. For each genotype at least 10 different rosettes were used to determine the relative water content. The RWC was calculated with the following equation: RWC=(FW-DW)/FW, FW is fresh weight and DW is dry weight. (**b**), Osmolarity of the leaf sap extracted from *A. thaliana* rosette leaves. Leaves undergo a cycle of freezing/thawing and subsequently were mechanically grinded. After centrifugation the supernatant was collected and used for osmolarity measurements with a micro-osmometer. For each genotype 8 plants were used. No significant difference was observed between wild-types and mutants. Error bars represent s.e.m.

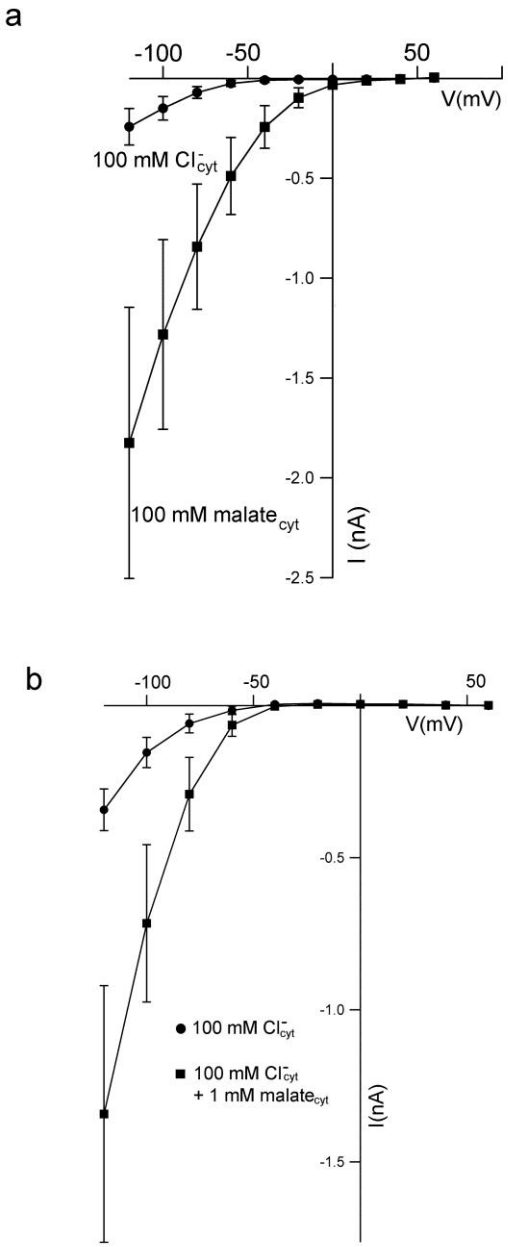

Supplementary Figure S10. (**a**), **Non-normalised I-V curves from Fig 1 b**. *Vacuolar side buffer*: 112 mM malic acid, 5 mM HCl, adjuste with BisTrisPropane, pH 6. *Cytosolic side buffers*: 100 mM HCl, 3 mM $MgCl_2$, 0.1 mM $CaCl_2$, adjusted to pH 7.5 with BisTrisPropane; 100 mM malic acid, 3 mM $MgCl_2$, 0.1 mM $CaCl_2$, adjusted to pH 7.5 with BisTrisPropane. (**b**), **non normalised I-V curves from Fig 1 b**. *Cytosolic side buffers*: 100 mM HCl, 3 mM $MgCl_2$, 0.1 mM $CaCl_2$, adjusted to pH 7.5 with BisTrisPropane; 100 mM HCl, 1 mM malic acid, 3 mM $MgCl_2$, 0.1 mM $CaCl_2$, adjusted to pH 7.5 with BisTrisPropane. *Vacuolar side buffer*: 100 mM HCl, adjusted to pH 6 with BisTrisPropane. Error bars are s.e.m.

4. Result Chapter II

Identification of a Probable Pore Forming Domain in the Multimeric Vacuolar Anion Channel *At*ALMT9

Jingbo Zhang*, Ulrike Baetz*, Undine Krügel, Enrico Martinoia and Alexis De Angeli

* These authors contributed equally to this work

Published in *Plant Physiology* 2013 Oct;163 (2):830-843.

Identification of a Probable Pore-Forming Domain in the Multimeric Vacuolar Anion Channel AtALMT9[1][W][OPEN]

Jingbo Zhang[2], Ulrike Baetz[2], Undine Krügel, Enrico Martinoia, and Alexis De Angeli*

Institute of Plant Biology, University of Zürich, CH–8008 Zurich, Switzerland

Aluminum-**a**ctivated malate transporters (ALMTs) form an important family of anion channels involved in fundamental physiological processes in plants. Because of their importance, the role of ALMTs in plant physiology is studied extensively. In contrast, the structural basis of their functional properties is largely unknown. This lack of information limits the understanding of the functional and physiological differences between ALMTs and their impact on anion transport in plants. This study aimed at investigating the structural organization of the transmembrane domain of the Arabidopsis (*Arabidopsis thaliana*) vacuolar channel AtALMT9. For that purpose, we performed a large-scale mutagenesis analysis and found two residues that form a salt bridge between the first and second putative transmembrane α-helices (TMα1 and TMα2). Furthermore, using a combination of pharmacological and mutagenesis approaches, we identified citrate as an "open channel blocker" of AtALMT9 and used this tool to examine the inhibition sensitivity of different point mutants of highly conserved amino acid residues. By this means, we found a stretch within the cytosolic moiety of the TMα5 that is a probable pore-forming domain. Moreover, using a citrate-insensitive AtALMT9 mutant and biochemical approaches, we could demonstrate that AtALMT9 forms a multimeric complex that is supposedly composed of four subunits. In summary, our data provide, to our knowledge, the first evidence about the structural organization of an ion channel of the ALMT family. We suggest that AtALMT9 is a tetramer and that the TMα5 domains of the subunits contribute to form the pore of this anion channel.

The transport of ions across cellular membranes is mediated by specialized proteins that catalyze the transfer of charged molecules across hydrophobic lipid bilayers. Based on the thermodynamics, two major classes of transport systems can be distinguished: (1) passive transporters such as ion channels, which catalyze the flux of solutes down the electrochemical gradient, and (2) active transporters like pumps and antiporters, which transport molecules against their electrochemical gradient. Independent of the nature of the transport system, the flux of ions across membranes is crucial for a wide range of physiological functions in plants. Among others, ion transport is involved in intracellular pH regulation, metal tolerance, stomatal movement, cellular signaling, plant nutrition, and cell expansion (Roelfsema and Hedrich, 2005; Kim et al., 2010; Barbier-Brygoo et al., 2011). Despite the importance of anion transport in plant physiology, only in the last decade has the molecular identity of anion transport proteins started to be unveiled by identifying the chloride channel (CLC), slow anion channel (SLAC), and aluminum-activated malate transporter (ALMT) families. Their discovery has been a fundamental breakthrough in understanding the molecular mechanisms of anion homeostasis and its roles in various aspects of plant cell physiology (Ward et al., 2009; Barbier-Brygoo et al., 2011; Hedrich, 2012; Martinoia et al., 2012).

The CLC family consists of both anion channels and secondary active transporters, which are ubiquitously expressed in all living organisms. In Arabidopsis (*Arabidopsis thaliana*), the first identified and characterized member of the family was AtCLCa (Hechenberger et al., 1996; Geelen et al., 2000). AtCLCa is targeted to the tonoplast and acts as a $2NO_3^-/H^+$ antiporter (De Angeli et al., 2006). In planta, AtCLCa represents a major vacuolar nitrate transporter driving the accumulation of this anion into the vacuole. Subsequent studies revealed that all other Arabidopsis CLCs are likewise localized in intracellular membranes but feature different cellular functions (Barbier-Brygoo et al., 2011).

The SLAC protein family was identified in the last decade (Negi et al., 2008; Vahisalu et al., 2008). Despite its recent discovery, the characterization of this plant anion transporter family proceeded rapidly (Negi et al., 2008; Vahisalu et al., 2008; Geiger et al., 2009, 2010; Brandt et al., 2012). SLAC1, the first identified member of the family, is involved in slow-type anion currents across the plasma membrane of plant cells (Negi et al., 2008; Vahisalu et al., 2008). This ion channel is expressed in guard cells, where it mediates the efflux of anions into the apoplast, a process that is

[1] This work was supported by the Chinese Scholarship Council (to J.Z.), by a long-term EMBO fellowship (to A.D.A.), and by the Swiss National Foundation (to U.B., E.M., and A.D.A.).

[2] These authors contributed equally to the article.

* Address correspondence to deangeli.alexis@gmail.com.

The author responsible for distribution of materials integral to the findings presented in this article in accordance with the policy described in the Instructions for Authors (www.plantphysiol.org) is: Alexis De Angeli (deangeli.alexis@gmail.com).

[W] The online version of this article contains Web-only data.

[OPEN] Articles can be viewed online without a subscription.

www.plantphysiol.org/cgi/doi/10.1104/pp.113.219832

fundamental for stomata closure. SLAC1 regulates the stomatal aperture in response to different stimuli such as abscisic acid and high CO_2 and ozone concentrations (Negi et al., 2008; Vahisalu et al., 2008). In addition, the activity of SLAC1 is controlled by different kinases (Geiger et al., 2009, 2010) that are part of various signaling pathways. This multiple regulation of SLAC1 suggests that it plays a critical role in the integration of different environmental stimuli.

ALMTs are membrane proteins exclusive to plants. In Arabidopsis, this family consists of 14 members that can be grouped into three clades (Kovermann et al., 2007). The first member of the ALMT family, TaALMT1, was identified in wheat (*Triticum aestivum*) by Sasaki et al. (2004) when screening for genes associated with aluminum resistance. They provided evidence that TaALMT1 as well as AtALMT1, its homolog in Arabidopsis, are channels that catalyze the efflux of malate across the plasma membrane of root cells (Yamaguchi et al., 2005; Hoekenga et al., 2006). This exudation of organic acids into the soil facilitates the detoxification of environmental Al^{3+}. Besides contributing to Al^{3+} tolerance, ALMTs have been found to exhibit other important physiological functions. AtALMT12 has been proposed to mediate rapid anion currents across the plasma membrane of guard cells in order to induce stomata closure (Meyer et al., 2010). AtALMT9 and AtALMT6 have been shown to be channels localized in the tonoplast that mediate the export of malate into the vacuole (Kovermann et al., 2007; Meyer et al., 2011). AtALMT6 is predominantly expressed in guard cells, where its activity is regulated by cytosolic Ca^{2+} and vacuolar pH (Meyer et al., 2011). In contrast, AtALMT9 is widely expressed in several plant tissues, such as the mesophyll and guard cells. Recently, AtALMT9 was shown to play a crucial role in stomata movement, where it functions as a malate-activated chloride channel (De Angeli et al., 2013).

The knowledge about ion channel structures has expanded considerably in the last 20 years. Notably, various three-dimensional structures of such proteins have been solved (Choe, 2002; Jentsch, 2008; Traynelis et al., 2010). This has boosted the research into and the understanding of structure-function relations in transport systems. Among the anion channel families described above, the structure has been determined for CLCs (Dutzler et al., 2002) and SLACs (Chen et al., 2010). Additionally, large structure-function analyses have been conducted, providing detailed knowledge on the molecular basis underlying the ion channel functionality of these families. In contrast, little information was revealed about the structure of ALMTs by describing an important phosphorylation site (Ligaba et al., 2009; Furuichi et al., 2010) and by providing data on the topology (Motoda et al., 2007; Dreyer et al., 2012). However, the proposed models in these studies do not entirely coincide regarding the number of transmembrane-spanning domains, the cellular orientation of the N terminus, and the organization of the C-terminal domain. Therefore, the structural organization of ALMTs is still ambiguous.

In this study, we performed a large-scale mutagenesis analysis of the transmembrane domain (TMD) of Arabidopsis ALMTs using the vacuolar channel AtALMT9 as a model. The aim was to identify regions of the TMD that potentially exhibit functional relevance by forming the pore or the voltage sensor. For that purpose, we took advantage of citrate, which we identified as an open channel blocker of AtALMT9. The use of this blocker allowed elucidation of the structural details of ion channels, such as the quaternary organization and pore-forming domains, when no crystal structure was available (MacKinnon, 1991; Yellen et al., 1991; Ferrer-Montiel and Montal, 1996; Linsdell, 2005). By this means, it is possible to show, for instance, that potassium channels are tetramers and to identify their "selectivity filter" domain (MacKinnon and Yellen, 1990; MacKinnon, 1991). Thus, by using citrate, we pharmacologically investigated structure-function relations in AtALMT9. We identified a region adjacent to and within the fifth putative TMD that is supposedly involved in forming the permeation pathway of AtALMT9. Moreover, we demonstrated that AtALMT9 is a multimeric channel of probably four subunits in which the monomers participate in forming the pore.

RESULTS

Citrate Inhibits AtALMT9-Mediated Malate Currents

Blocking agents represent a common tool as reporter molecules to analyze functional and structural features of ion channels. In an attempt to disclose a blocker of the vacuolar channel AtALMT9, we were guided by a previous finding in which citrate was suggested to competitively inhibit malate uptake across the tonoplast (Rentsch and Martinoia, 1991). In order to test whether citrate is a blocker of AtALMT9, we isolated vacuoles from transiently transformed tobacco (*Nicotiana benthamiana*) protoplasts that overexpressed AtALMT9-GFP (OE AtALMT9). We used the patch-clamp technique to measure macroscopic currents mediated by AtALMT9 in the cytosolic-side-out excised patch configuration (Fig. 1). To avoid rectification due to ion concentration gradients between the two sides of the patched membrane, we performed experiments in symmetric ionic conditions (100 mM $malate_{vac}$/100 mM $malate_{cyt}$). Patches obtained from OE AtALMT9 tobacco vacuoles displayed inward-rectifying malate currents with time-dependent relaxations and a mean amplitude of -1.44 ± 0.51 nA at -120 mV, as reported in previous studies (Fig. 1A; Table I; Kovermann et al., 2007; for convention details regarding the applied voltage, see "Materials and Methods"). Even though citric acid is to 97% a tricarboxylate at pH 7.5 and exhibits similarities to the dicarboxylate malate (Fig. 1B), we could not detect a

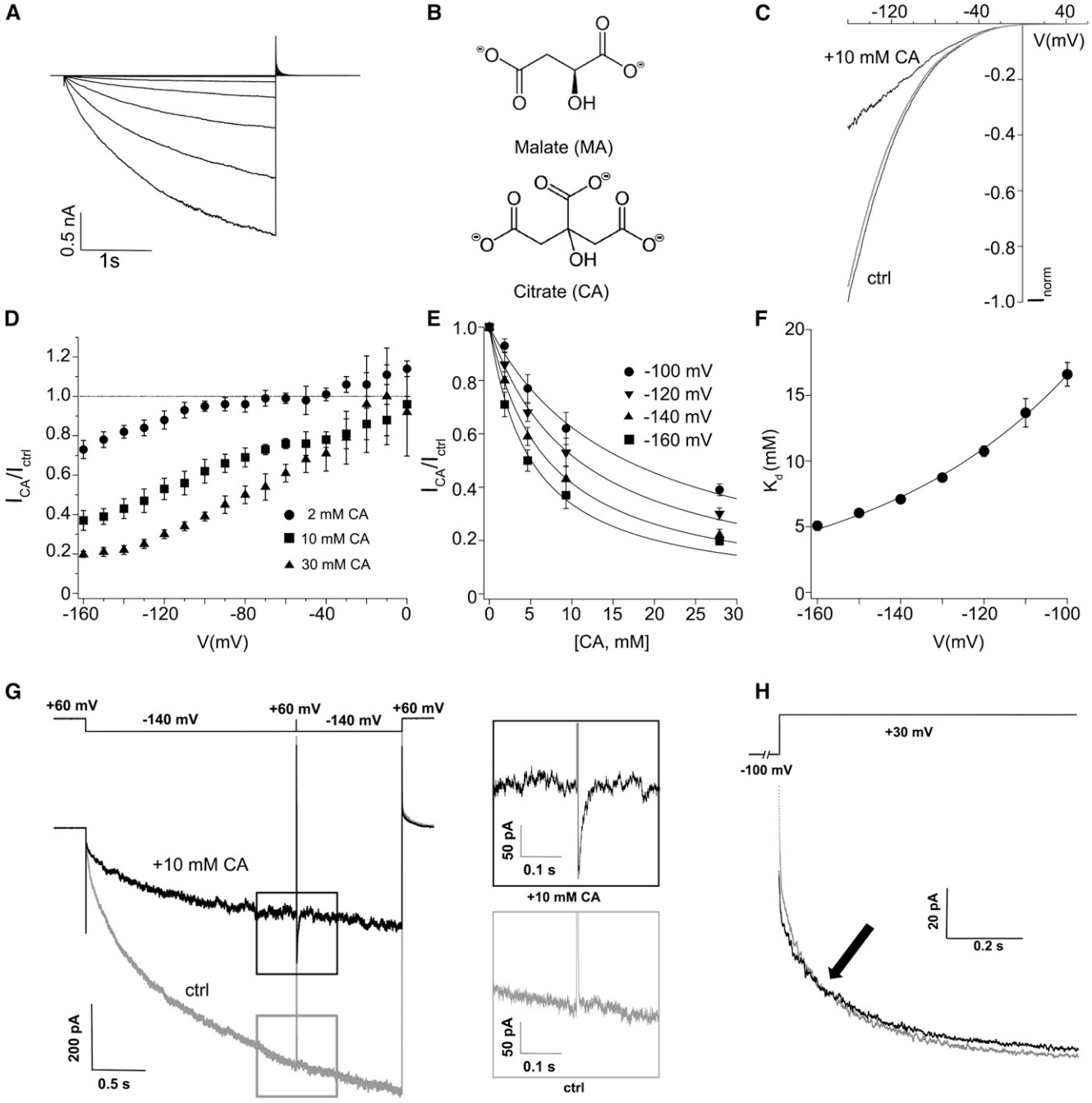

Figure 1. Citrate is a blocker of AtALMT9-mediated malate currents. A, Typical time-dependent currents from excised cytosolic-side-out patches obtained from AtALMT9-overexpressing tobacco vacuoles in symmetric malate conditions (100 mM $malate_{vac}$/100 mM $malate_{cyt}$). Currents were evoked in response to 3-s voltage pulses ranging from +60 mV to −120 mV in 20-mV steps, followed by a tail pulse at +60 mV, with a holding potential at +60 mV. B, Molecular structure of L-malate (MA) and citrate (CA) acids. C, Reversible inhibition of $AtALMT9_{WT}$ currents by 10 mM $citrate_{cyt}$. Normalized current-voltage curves were obtained with a voltage ramp (from +60 to −160 mV in 1.5 s) in cytosolic control solution (ctrl; 100 mM $malate_{cyt}$) and after adding 10 mM $citrate_{cyt}$ (100 mM $malate_{cyt}$ + 10 mM $citrate_{cyt}$). The gray line indicates the recovery in control cytosolic solution. D and E, Ratios between currents recorded in control and $citrate_{cyt}$-containing solutions (I_{CA}/I_{ctrl}) when using different $citrate_{cyt}$ concentrations (n = 4–5). E, Dose-response curves for $citrate_{cyt}$ at different potentials. Solid lines are fits obtained with Equation 1. F, Voltage dependency of the $K_d^{citrate}$. Solid lines correspond to data fitted with Equation 3. G, Representative current recording of a kick-out experiment on AtALMT9-meditated current. The currents were evoked using the voltage pulse protocol shown above the current traces. After the 3-ms pulse at +60 mV, a transient decrease of the current is observable in the presence of 10 mM $citrate_{cyt}$ (black trace inset). In contrast, in cytosolic control solution (gray trace inset), no transient decrease is

Table I. *Properties of wild-type and mutant AtALMT9 channels expressed in tobacco*

Data are presented as means ± SD.

chunK-Sample	I(nA) at −120 mV[a]	No. of Experiments	Conductive	$I_{citrate}/I_{ctrl}$ at −160 mV[b]	$K_d^{citrate}$ at −160 mV[c]	Rectification Rate[d]
					mM	
Untransformed	−0.06 ± 0.03	3	No	–	–	–
$AtALMT9_{WT}$	−1.44 ± 0.51****	11	Yes	0.37 ± 0.05	5.1 ± 0.3	0.19 ± 0.03
K87E	−1.52 ± 0.30**	4	Yes	0.59 ± 0.03****	16.2 ± 2.3	0.22 ± 0.02
K87R	−0.92 ± 0.06***	3	Yes	0.39 ± 0.04	–	–
K93E	−0.11 ± 0.04	5	No	–	–	–
K93A	−0.07 ± 0.03	4	No	–	–	–
K93N	−0.09 ± 0.04	3	No	–	–	–
K93R	−0.80 ± 0.42*	4	Yes	–	–	–
E130A	−0.07 ± 0.01	3	No	–	–	–
E130D	−1.28 ± 0.15****	5	Yes	–	–	–
E130K	−0.13 ± 0.07	4	No	–	–	–
K139E	−1.1 ± 0.15**	3	Yes	0.42 ± 0.04	–	0.16 ± 0.01
R143E	−0.10 ± 0.07	3	No	–	–	–
R143N	−0.09 ± 0.06	3	No	–	–	–
K187E	−0.09 ± 0.08	3	No	–	–	–
K187N	−0.07 ± 0.04	4	No	–	–	–
K193E	−1.46 ± 0.62**	7	Yes	0.99 ± 0.02****	–	0.50 ± 0.09***
K193A	−1.75 ± 0.25****	5	Yes	0.82 ± 0.02****	–	0.24 ± 0.03*
K193N	−0.63 ± 0.14*	3	Yes	0.83 ± 0.03****	–	0.29 ± 0.06*
K193R	−0.94 ± 0.43*	4	Yes	0.39 ± 0.04	–	0.16 ± 0.04
E196A	−0.87 ± 0.26***	6	Yes	0.39 ± 0.06	–	–
R200N	−1.43 ± 0.58**	5	Yes	0.86 ± 0.04****	–	0.18 ± 0.05
R200E	−0.12 ± 0.05	3	No	–	–	–
R200K	−0.62 ± 0.12*	3	Yes	0.38 ± 0.03	–	0.21 ± 0.02
R215E	−0.07 ± 0.03	3	No	–	–	–
R215N	−0.69 ± 0.27*	4	Yes	0.37 ± 0.04	–	0.14 ± 0.01**
R226E	−0.09 ± 0.06	3	No	–	–	–
R226N	−0.14 ± 0.08	4	No	–	–	–
K93E/E130K	−1.30 ± 0.27*	3	Yes	0.37 ± 0.02	–	–

[a]Current measured in 100 mM $malate_{cyt}$/100 mM $malate_{vac}$. Asterisks indicate statistically significant differences from untransformed tobacco (*$P <$ 0.05, **$P < 0.01$, ***$P < 0.001$, ****$P < 0.0001$; two-tailed Student's *t* test). [b]Ratio between the current measured in 100 mM $malate_{cyt}$ + 10 mM $citrate_{cyt}$ and the current measured in 100 mM $malate_{cyt}$. Asterisks indicate statistically significant differences from $AtALMT9_{WT}$ (****$P < 0.0001$; two-tailed Student's *t* test). [c]$K_d^{citrate}$ determined with Equation 1. [d]Rectification rate measured as described in the text. Asterisks indicate statistically significant differences from $AtALMT9_{WT}$ (*$P < 0.05$, **$P < 0.01$, ***$P < 0.001$; two-tailed Student's *t* test).

significant permeation of citrate through AtALMT9 ($I_{citrate}/I_{malate}$ = 5% ± 5%; Supplemental Fig. S1A), as shown for BnALMT1 and BnALMT2 (Ligaba et al., 2006). However, when 10 mM citrate was applied at the cytosolic side (100 mM $malate_{vac}$/100 mM $malate_{cyt}$ + 10 mM $citrate_{cyt}$), AtALMT9 malate currents were reversibly inhibited to residual 37% ± 5% of the original current at −160 mV (Fig. 1C). The inhibition of the ion flux induced by $citrate_{cyt}$ was dose and voltage dependent (Fig. 1, D and E). Notably, the inhibitory effect of $citrate_{cyt}$ on AtALMT9-mediated currents occurred more pronouncedly at more negative membrane potentials (Fig. 1, C and D). However, the inhibition by $citrate_{cyt}$ did not change the voltage dependency of the relative open probability of the channel (Supplemental Fig. S1B). This implies that $citrate_{cyt}$ inhibition does not originate from a shift in channel gating toward more negative membrane potentials. When further analyzing the dose response of $citrate_{cyt}$ inhibition at different applied potentials, we found that the dissociation constant of $citrate_{cyt}$ ($K_d^{citrate}$; 5.1 ± 0.3 mM at −160 mV) was voltage dependent (Fig. 1, E and F). This finding indicates that the inhibiting anion citrate experiences the applied transmembrane electrical field. Consequently, we could estimate that citrate penetrates approximately 17% of the applied transmembrane electrical field (Woodhull, 1973). This, in turn, suggests that the interaction between citrate and the channel occurs within the membrane-spanning domain of AtALMT9 and possibly within the conduction pathway.

Figure 1. (*Continued.*)
observable. H, Crossing of the tail currents at +30 mV in control conditions (gray trace) and in the presence of 10 mM $citrate_{cyt}$ (black trace). AtALMT9 currents were elicited by an activating prepulse at −100 mV for 2 s followed by a tail pulse at +30 mV (1 s), as depicted above the current traces. The holding potential was set to +60 mV. Error bars represent SD.

To obtain direct evidence that citrate acts as an open channel blocker by interacting with the pore of AtALMT9, we investigated whether citrate binds to the activated channel. In a first step, we performed "kick-out experiments" (Becker et al., 1996; Fig. 1G). This approach is based on the reversible dissociation of citrate from its binding site when applying a short voltage pulse to the activated AtALMT9 channel at which $citrate_{cyt}$ was shown to no longer effectively block AtALMT9 (i.e. $V_m \geq 0$ mV; Fig. 1C). The "kick-out pulse" was transient and adjusted in order to not influence the voltage-dependent gating of the channel (Fig. 1G). Consequently, the proportion of channels in an open configuration was stable during and after the kick-out pulse. Therefore, effects on the current after the kick-out pulse did not originate from effects on the channel gating but from reversible pore blocking. During the kick-out experiments, we first activated the channels with a voltage pulse at −140 mV for 2 s. Subsequently, we stepped for 3 ms to a positive membrane potential (+60 mV) and then restored the membrane potential to −140 mV again (Fig. 1G). When this protocol was applied in the presence of the cytosolic control buffer (100 mM $malate_{cyt}$), the 3-ms pulse to +60 mV did not induce any significant channel closure, since the current levels before and immediately after the pulse were indistinguishable (Fig. 1G, gray trace inset). Differently, when applying the same protocol in the presence of 10 mM $citrate_{cyt}$, the 3-ms pulse at +60 mV was followed by a transient increase of the current that relaxed rapidly to the prepulse current amplitude (the time constant of the current relaxation is $\tau = 11.5 \pm 0.4$ ms at −140 mV; Fig. 1G, black trace inset). This fast relaxation after the kick-out pulse reflected the reversible binding kinetic of citrate to the channel. Thus, the results confirmed that citrate is capable of blocking AtALMT9 by binding to the open channel configuration. Concurrently, as expected for channels blocked in the open configuration, deactivating tail currents relaxed more slowly in the presence of $citrate_{cyt}$ than in its absence because of the dissociation of the blocking agent prior to closure of the channel. Hence, the application of an open channel blocker like citrate generates a typical crossover of the tail currents (Clay, 1995; Fig. 1H). Taken together, these data strongly indicate that citrate is an open channel blocker and that its inhibitory effect is likely due to a block of the conduction pathway of AtALMT9.

Effects of Positively and Negatively Charged Amino Acid Residues on Pore Conductivity

Despite the fact that ALMT proteins are known and have been studied for many years, few experimental data are available on the structure-function level (Motoda et al., 2007; Furuichi et al., 2010; Mumm et al., 2013). In particular, no study was conducted to investigate the TMD of ALMTs so far. Based on in silico analyses (http://aramemnon.botanik.uni-koeln.de), AtALMT9 is predicted to consist of a TMD at the N terminus and a soluble C-terminal domain encompassing roughly half of the protein. The TMD is predicted to be formed by six putative transmembrane α-helices, whereby the N terminus exhibits an intracellular orientation (TMα1–TMα6; Fig. 2A). However, other arrangements, such as an inverse inside-outside structure or more α-helices, were also proposed (Motoda et al., 2007; Dreyer et al., 2012). We performed a multiple alignment throughout all members of the ALMT family in Arabidopsis and identified several conserved or partially conserved amino acids within the TMD (Fig. 2B; Supplemental Fig. S2). We focused predominantly on positively charged residues, since they were often found to be relevant for functional elements of ion channels (pore and voltage sensor; Linsdell, 2005; Catterall, 2010). Interestingly, in line with the positive-inside rule (von Heijne and Gavel, 1988), the cytosolic-facing moiety of AtALMT9 exhibits a higher number of positively charged residues compared with the vacuolar moiety. While eight positively charged residues (three Arg and five Lys residues) are located at the cytosolic moiety, only three conserved positive residues face the vacuolar side (Fig. 2, A and B). To analyze the role of these residues in the TMD of AtALMT9, we substituted them by site-directed mutagenesis and monitored the effects of the mutation at a functional level (Fig. 2, D and E; Table I).

We transiently expressed the AtALMT9-GFP mutant channels in tobacco and first analyzed their intracellular localization by confocal laser scanning microscopy to verify whether the introduced point mutations resulted in a mistargeting of the protein. Interestingly, none of the mutations had an effect on the vacuolar targeting of the AtALMT9 channel (Fig. 2C; Supplemental Fig. S3). Subsequently, we analyzed the functionality of the mutated derivatives of AtALMT9 by performing patch-clamp analysis under the same experimental conditions as described above (Fig. 1A). The analysis revealed that the individual residues impacted differently on channel functionality. The removal of the positive charge of conserved Lys and Arg residues and the negative charge of the conserved Glu predicted to be inside the TMDαs (Lys-93, Glu-130, Arg-143, Lys-187, and Arg-226) resulted in a loss of conductivity (Fig. 2, D and E; Table I). On the contrary, substituting other conserved positively and negatively charged residues predicted to be in the loops between the TMDαs (Lys-87, Lys-139, Lys-193, and Glu-196) apparently did not affect the functionality of AtALMT9. In fact, patches from vacuoles transformed with these mutants presented time-dependent inward-rectifying currents with amplitudes that are reminiscent of those observed for $AtALMT9_{WT}$ (Figs. 1A and 2, D and E; Table I). Interestingly, the mutation of the two amino acids Arg-200 and Arg-215, the charge of which is not entirely conserved among the Arabidopsis ALMTs, affected the functionality of AtALMT9 dependent on the introduced residue. When

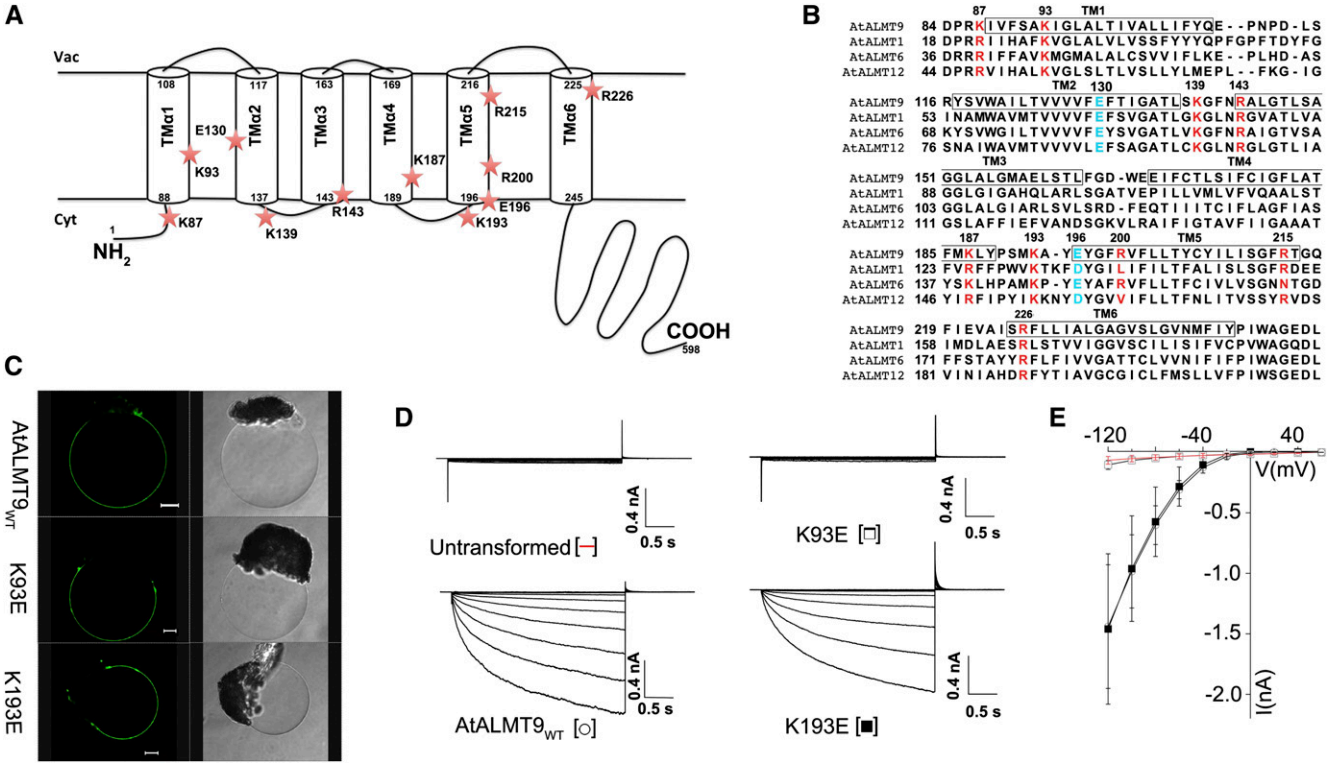

Figure 2. Impact of the mutation of conserved residues on AtALMT9 functionality. A, The TMD of AtALMT9 is predicted to be formed by six putative transmembrane α-helices (TMα1–TMα6) with the N terminus being located in the cytosol. The model illustrates the location of the amino acids targeted by site-directed mutagenesis (red stars). B, Multiple alignment of AtALMT9 with representative AtALMT proteins (AtALMT1, AtALMT6, and AtALMT12). The alignment was conducted with the Jalview software (Waterhouse et al., 2009). The black boxes indicate the predicted TMαs of AtALMT9. The conserved amino acids used for mutagenesis are displayed in red (positively charged residues) and in blue (negatively charged residues). C, Fluorescence and transmission images of vacuoles released from lysed tobacco mesophyll protoplasts transiently overexpressing AtALMT9$_{WT}$-GFP, AtALMT9$_{K93E}$-GFP, and AtALMT9$_{K193E}$-GFP imaged by confocal laser scanning microscopy. Bars = 10 μm. D, Representative current recordings of excised cytosolic-side-out patches of untransformed vacuoles as well as vacuoles overexpressing AtALMT9$_{WT}$, AtALMT9$_{K93E}$, and AtALMT9$_{K193E}$. Currents were evoked in response to 3-s voltage pulses ranging from +60 to −120 mV in 20-mV steps followed by a tail pulse at +60 mV. E, Mean current-voltage curves of untransformed vacuoles (red bars; n = 3), AtALMT9$_{WT}$ (white circles; n = 11), AtALMT9$_{K93E}$ (white squares; n = 5), and AtALMT9$_{K193E}$ (black squares; n = 7). In D and E, AtALMT9 currents were recorded in symmetric ionic conditions (100 mM malate$_{vac}$/100 mM malate$_{cyt}$). The holding potential was set to +60 mV. Error bars denote SD.

Arg-200 and Arg-215 were substituted with an Asn (AtALMT9$_{R200N}$ and AtALMT9$_{R215N}$), we observed time-dependent inward-rectifying currents comparable to AtALMT9$_{WT}$ (Table I; Supplemental Fig. S4, A and C). However, the introduction of a negatively charged residue like Glu (AtALMT9$_{R200E}$ and AtALMT9$_{R215E}$) led to nonfunctional channels (Table I; Supplemental Fig. S4, A and C). In summary, we observed three different effects on AtALMT9 channel functionality when mutating conserved charged residues. Four of the mutations we introduced induced a loss of conductivity, indicating that these residues were essential for the functionality of the channel. Furthermore, mutation of the cytosolic-facing residues did not influence channel functionality, whereas a third set of mutations resulted in a phenotype that was dependent on the introduced charge.

TMα1 and TMα2 Are Connected by a Salt Bridge

The analysis of the primary sequence alignment revealed two conserved charged residues arousing our interest. Lys-93 and Glu-130 are located within TMα1 and TMα2, respectively (Fig. 2, A and B). In the hydrophobic environment of membranes, unitary charges need to be stabilized by an interaction with a solvent and/or with an opposite charge (Perutz, 1978). When Glu-130 was replaced by an Ala or a Lys (AtALMT9$_{E130A}$ or AtALMT9$_{E130K}$), the channel was nonconductive, similar to AtALMT9$_{K93A}$ and AtALMT9$_{K93E}$ (Fig. 3; Table I). However, channels harboring conservative mutations in which the respective charge was kept (AtALMT9$_{K93R}$ and AtALMT9$_{E130D}$) displayed inward currents comparable to AtALMT9$_{WT}$ (Table I). Thus, we hypothesized that the two charged residues

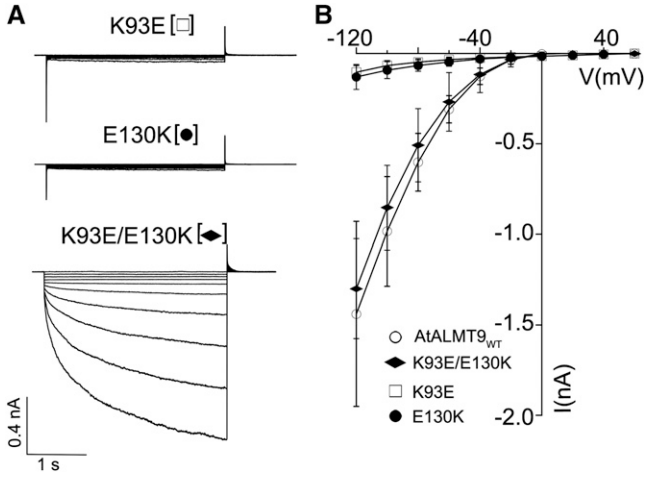

Figure 3. The conserved residues Lys-93 and Glu-130 form a salt bridge within the TMD of AtALMT9. A, Excised cytosolic-side-out current recordings from tobacco vacuoles overexpressing $AtALMT9_{K93E}$, $AtALMT9_{E130K}$, and the double mutant $AtALMT9_{K93E/E130K}$. Currents were evoked in response to 3-s voltage pulses ranging from +60 to −120 mV in 20-mV steps followed by a tail pulse at +60 mV. B, Mean current-voltage curves of malate currents mediated by $AtALMT9_{WT}$ (white circles; $n = 11$), $AtALMT9_{K93E/E130K}$ (black diamonds; $n = 3$), $AtALMT9_{K93E}$ (white squares; $n = 5$), and $AtALMT9_{E130K}$ (black circles; $n = 3$). Currents were recorded in symmetric conditions (100 mM $malate_{vac}$/100 mM $malate_{cyt}$). The holding potential was set to +60 mV. Error bars represent SD.

Lys-93 and Glu-130 could interact to form a salt bridge. To test this assumption, we generated a double mutant, $AtALMT9_{K93E/E130K}$, in which the charges of the amino acids Lys-93 and Glu-130 were exchanged. Astonishingly, the doubly mutated channel was functional and exhibited electrophysiological properties similar to $AtALMT9_{WT}$ (Fig. 3). $AtALMT9_{K93E/E130K}$ mediated currents with time-dependent relaxations and a mean amplitude of −1.30 ± 0.27 nA at −120 mV (Fig. 3B; Table I). Moreover, the double mutant was inhibited by citrate, as demonstrated for the $AtALMT9_{WT}$ channel (Table I; Supplemental Fig. S5). These results indicate that the positively charged Lys-93 and the negatively charged Glu-130 connect TMα1 and TMα2 by a salt bridge that is essential for the functionality of the channel.

Identification of Positively Charged Residues That Are Part of the Ion Conduction Pathway in AtALMT9

To investigate whether the mutated amino acids are possibly involved in forming the interaction site between citrate and the channel, we determined the sensitivity of the conductive AtALMT9 point mutants to citrate. The four charged residues Lys-87, Lys-139, Glu-196, and Arg-215 are located in the cytosolic loops next to TMα1, TMα2, and TMα5 and at the vacuolar-facing moiety of TMα5, respectively (Fig. 2, A and B). The channel derivatives $AtALMT9_{K87E}$, $AtALMT9_{K139E}$, $AtALMT9_{E196A}$, and $AtALMT9_{R215N}$ showed a moderate or no significant decrease in $citrate_{cyt}$ inhibition compared with $AtALMT9_{WT}$ [$(I_{citrate}/I_{ctrl})^{WT}$ = 0.37 ± 0.05, $(I_{citrate}/I_{ctrl})^{K87E}$ = 0.59 ± 0.03, $(I_{citrate}/I_{ctrl})^{K139E}$ = 0.42 ± 0.04, $(I_{citrate}/I_{ctrl})^{E196A}$ = 0.39 ± 0.06, and $(I_{citrate}/I_{ctrl})^{R215N}$ = 0.37 ± 0.04 at −160 mV; Fig. 4C; Table I]. In marked contrast, substitution of the residues Lys-193 and Arg-200, which reside at the cytosolic loop between TMα4 and TMα5 or within TMα5, respectively, reduced the $citrate_{cyt}$ blockade efficiency dramatically [$(I_{citrate}/I_{ctrl})^{K193N}$ = 0.83 ± 0.03 at −160 mV and $(I_{citrate}/I_{ctrl})^{R200N}$ = 0.86 ± 0.04 at −160 mV; Fig. 4; Table I]. Since the substitution R200E resulted in a nonfunctional channel, the effect of a negatively charged residue at this amino acid position could not be investigated. Nevertheless, the mutation K193E, which introduced a Glu, provided a conductive channel but caused a complete loss of $citrate_{cyt}$ inhibition ($I_{citrate}/I_{ctrl}$ = 0.99 ± 0.02 at −160 mV; Fig. 4, A and C). In addition, when performing kick-out experiments with the citrate-insensitive mutants $AtALMT9_{K193E}$ and $AtALMT9_{R200N}$, the kick-out pulse was not followed by fast-relaxing current transients (Supplemental Figs. S1D and S4B). Since the transient current relaxation is due to the rapid dissociation and subsequent binding of $citrate_{cyt}$ to the open channel configuration of $AtALMT9_{WT}$, its absence provided evidence that $citrate_{cyt}$ was not able to interact with the $AtALMT9_{K193E}$ and $AtALMT9_{R200N}$ mutant channels and did not enter the TMD in these mutants. In contrast, the citrate-sensitive channel $AtALMT9_{R215N}$, which possesses a substitution at the vacuolar-facing part of the membrane, exhibited a transient current relaxation comparable to the wild-type channel after applying a kick-out pulse (Supplemental Fig. S4D).

Taken together, these results indicate that the positively charged residues Lys-193 and Arg-200, which are located adjacent to or within TMα5, are involved in mediating the interaction of citrate with AtALMT9. Considering the fact that citrate acts as an open channel blocker, the data suggest that Lys-193 and Arg-200 are part of the ion conduction pathway of AtALMT9. To further confirm the pore-forming feature of the two residues and TMα5, we explored the functional properties of the conductive AtALMT9 mutants by analyzing the "open channel rectification." This parameter directly reflects the properties of the conduction pathway itself, excluding rectification effects based on voltage-dependent gating. To quantify the open channel rectification of $AtALMT9_{WT}$ and its derivatives, we made used of the rectification rate coefficient (Linsdell, 2005). This coefficient is defined as the ratio between the conductance measured at the end of the activation pulse at −120 mV and the conductance measured at the beginning of the tail pulse at +60 mV (for details, see "Materials and Methods"). The rectification ratio of $AtALMT9_{WT}$ was 0.19 ± 0.03, indicating that the conduction pathway of this channel had intrinsic inward rectification properties. Strikingly, we observed that the citrate-insensitive channel

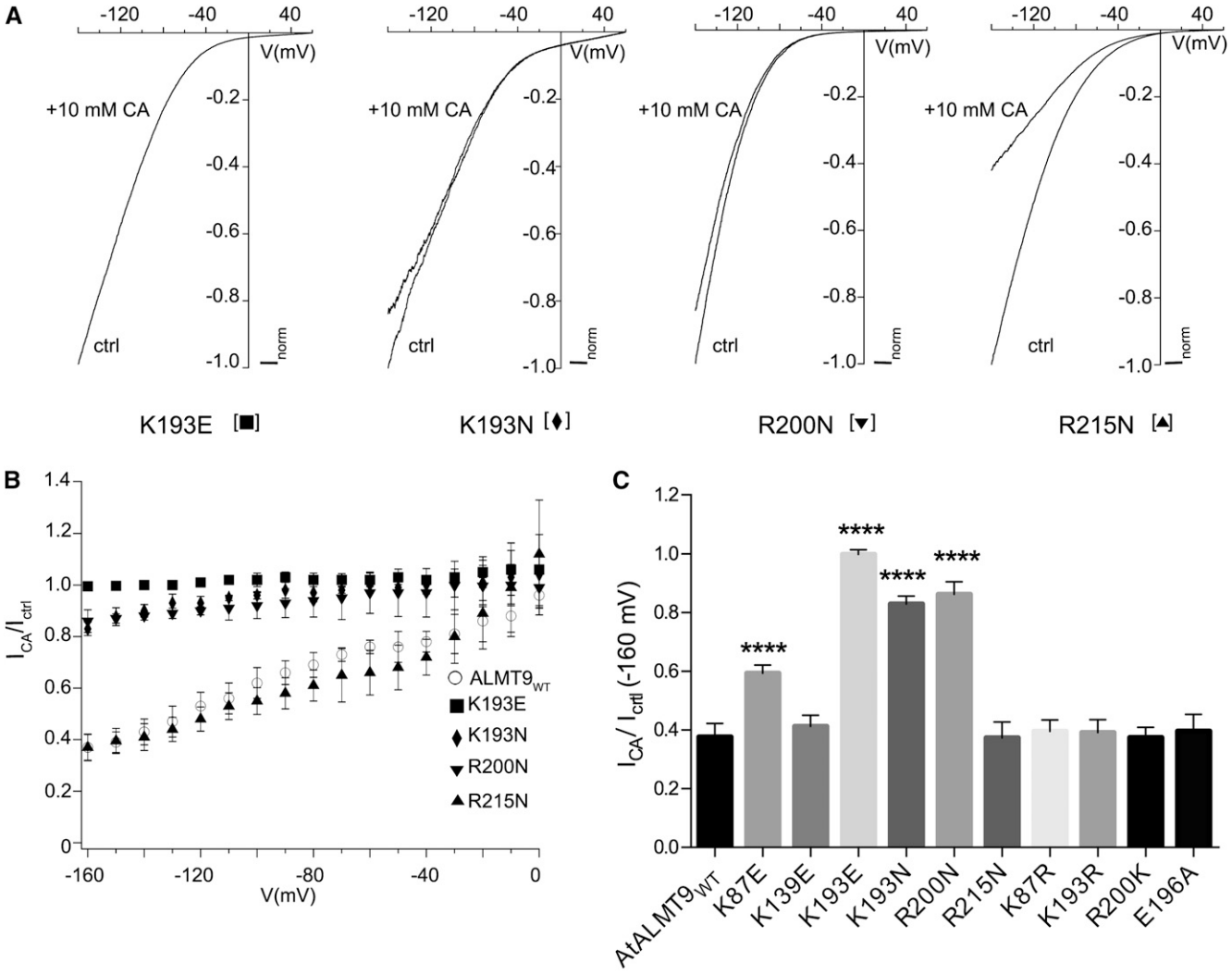

Figure 4. Variable effects of mutations of conserved AtALMT9 residues on citrate blockade. A, Normalized current-voltage curves of the mutants AtALMT9$_{K193E}$, AtALMT9$_{K193N}$, AtALMT9$_{R200N}$, and AtALMT9$_{R215N}$ in control conditions (ctrl) and in the presence of 10 mM citrate$_{cyt}$ (CA) obtained with a voltage ramp (from +60 mV to −160 mV in 1.5 s). B, Ratio between the control currents and the residual currents after inhibition with 10 mM citrate$_{cyt}$ (I_{CA}/I_{ctrl}). Depicted are AtALMT9$_{K193E}$ (squares; $n = 4$), AtALMT9$_{K193N}$ (diamonds; $n = 4$), AtALMT9$_{R200N}$ (inverted triangles; $n = 4$), AtALMT9$_{R215N}$ (triangles; $n = 3$), and AtALMT9$_{WT}$ (circles; $n = 4$). C, Ratios of the currents of different AtALMT9 mutants before and after the application of 10 mM citrate$_{cyt}$ (I_{CA}/I_{ctrl}; $n = 3$–5) at −160 mV. Currents were measured in symmetric conditions (100 mM malate$_{vac}$/100 mM malate$_{cyt}$). Asterisks indicate statistically significant differences from AtALMT9$_{WT}$ (****$P < 0.0001$; two-tailed Student's t test). Error bars denote SD.

AtALMT9$_{K193E}$, which was mutated in an amino acid residue of the pore region, and AtALMT9$_{R215N}$, which harbors a mutation within TMα5, exhibited an altered rectification ratio compared with AtALMT9$_{WT}$ (Table I). AtALMT9$_{K193E}$ showed a markedly increased rectification ratio of 0.50 ± 0.09, whereas AtALMT9$_{R215N}$ exhibited a lower rectification ratio (0.14 ± 0.01). The different rectification rates of AtALMT9$_{K193E}$ and AtALMT9$_{R215N}$ indicate that the mutated residues are involved in conferring rectification characteristics to the pore of AtALMT9. Hence, it is likely that Lys-193 and Arg-215 are involved in forming the conduction pathway. In summary, we could observe alterations in citrate block sensitivity and open channel rectification when analyzing the properties of the conductive mutant channels. We identified three positively charged residues preceding TMα5 or within TMα5 (Lys-193, Arg-200, and Arg-215) that fundamentally contribute to the functionality of the conduction pathway of AtALMT9.

AtALMT9 Is a Multimeric Anion Channel Composed of Four Subunits

The discovery of the mutant channel AtALMT9$_{K193E}$, which is characterized by complete insensitivity to

citrate inhibition, provides the opportunity to investigate whether AtALMT9 is a monomeric or a multimeric channel (MacKinnon, 1991; Kosari et al., 1998). If AtALMT9 is a monomer, a co-overexpression of $AtALMT9_{WT}$ and $AtALMT9_{K193E}$ would not influence the $K_d^{citrate}$. In contrast, in case AtALMT9 functions as a multimeric complex, the heteromultimeric hybrids of $AtALMT9_{WT}$ and $AtALMT9_{K193E}$ would exhibit an altered sensitivity to $citrate_{cyt}$. Therefore, the presence of heteromultimers would result in a shift in $K_d^{citrate}$. We performed experiments in which we coinfiltrated tobacco leaves with a mixture of two *Agrobacterium tumefaciens* strains carrying plasmids with the sequence of either $AtALMT9_{WT}$ or $AtALMT9_{K193E}$ in different ratios (1:1 and 1:4). First, we verified the transcription levels of $AtALMT9_{WT}$ and $AtALMT9_{K193E}$ after coinfiltration. When infiltrating leaves with a 1:1 ratio of the two *A. tumefaciens* strains, we observed that 50.1% ± 9.2% of the *AtALMT9* transcripts were of wild-type origin and 49.9% ± 9.2% were the mutant sequence. Similarly, when coinfiltrating tobacco leaves with the two *A. tumefaciens* strains in a ratio of 1:4, we found that 15% ± 13% of the *AtALMT9* transcripts were the wild-type sequence and 85% ± 13% showed the sequence of $AtALMT9_{K193E}$ (Fig. 5A). Thus, using these *A. tumefaciens* mixtures, we were able to coexpress both AtALMT9 variants in tobacco in a ratio corresponding to that of the infiltration mix. Subsequently, we tested the citrate block sensitivity of vacuoles co-overexpressing $AtALMT9_{WT}$ and $AtALMT9_{K193E}$ in 1:1 and 1:4 ratios. As observed in OE $AtALMT9_{WT}$ patches, the coexpression displayed

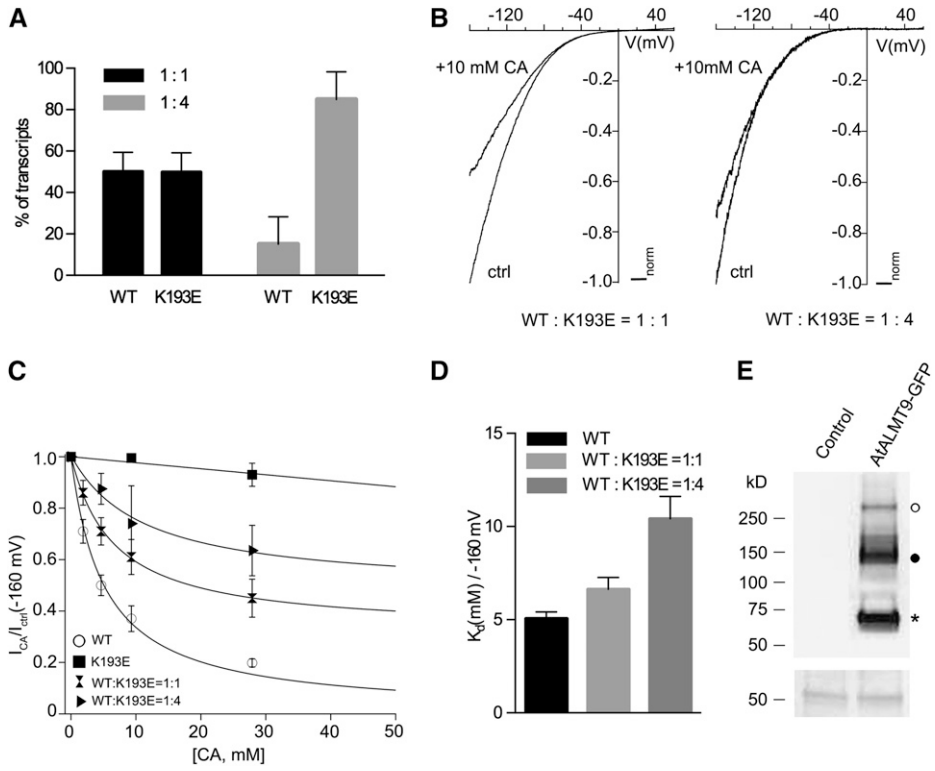

Figure 5. AtALMT9 forms homomultimeric complexes. A, Relative occurrence of $AtALMT9_{WT}$ and $AtALMT9_{K193E}$ transcripts in leaves of tobacco coinfiltrated with a 1:1 and a 1:4 mixture of *A. tumefaciens* strains each carrying plasmids with the sequence of one of the channel variants. Error bars represent SD of four biologically independent replicates (20 transcripts were analyzed for each replicate). B, Representative normalized current-voltage curves obtained with a voltage ramp (from +60 to −160 mV in 1.5 s; the holding potential was +60 mV) measured in excised cytosolic-side-out patches from vacuoles coexpressing $AtALMT9_{WT}$ and $AtALMT9_{K193E}$ at different ratios (left, $AtALMT9_{WT}$:$AtALMT9_{K193E}$ = 1:1; right, $AtALMT9_{WT}$:$AtALMT9_{K193E}$ = 1:4). Currents were recorded in control conditions (ctrl) and in the presence of 10 mM $citrate_{cyt}$ (CA). C, Dose-response curves for $citrate_{cyt}$ from vacuoles overexpressing $AtALMT9_{WT}$ (circles), $AtALMT9_{K193E}$ (squares), $AtALMT9_{WT}$:$AtALMT9_{K193E}$ = 1:4 (triangles), and $AtALMT9_{WT}$:$AtALMT9_{K193E}$ = 1:1 (hourglass; n = 4–7). The data of $AtALMT9_{WT}$ were fitted with Equation 1. Data of the 1:1 and 1:4 ratios were fitted with Equation 2. Error bars denote SD. D, Values of the $K_d^{citrate}$ at V_m = −160 mV derived from C. Currents were recorded in symmetric conditions (100 mM $malate_{vac}$/100 mM $malate_{cyt}$). Error bars display SD. E, Immunoblot analysis of microsomal proteins extracted from untransformed (control) and $AtALMT9_{WT}$-overexpressing (AtALMT9-GFP) leaves of tobacco using an anti-GFP antibody. In the top panel, the lane of protein extracts from AtALMT9-overexpressing leaves displays three bands corresponding to monomeric (star; approximately 70 kD), dimeric (black circle; approximately 140 kD), and tetrameric (white circle; approximately 280 kD) forms of the AtALMT9 protein complex. The bottom panel shows the corresponding Ponceau S staining. WT, Wild type.

malate currents that were blocked by $citrate_{cyt}$ (Fig. 5B). Notwithstanding, the currents in vacuolar patches co-overexpressing both AtALMT9 variants were less sensitive to $citrate_{cyt}$ than currents recorded in vacuoles only expressing $AtALMT9_{WT}$ and showed a shift in $K_d^{citrate}$ (Fig. 5C). The $K_d^{citrate}$ was 6.6 ± 0.6 mM and 10.4 ± 1.2 mM for the 1:1 and 1:4 ratios, respectively, thus representing 1.3- and 2.1-fold increases of $K_d^{citrate}$ compared with $AtALMT9_{WT}$ (Fig. 5D). This increase of $K_d^{citrate}$ in vacuoles simultaneously expressing $AtALMT9_{WT}$ and $AtALMT9_{K193E}$ is in agreement with a model in which both variants assemble to a heteromultimeric channel and citrate interacts with multiple subunits. To further confirm this finding, we performed denaturing PAGE on microsomal proteins extracted from transiently transformed tobacco leaves that overexpressed AtALMT9-GFP (Fig. 5E). Using a GFP-specific antibody, we detected AtALMT9-GFP predominantly as an approximately 70-kD monomer. This band was smaller than predicted based solely on its formula molecular mass (93.5 kD) but was consistent with an apparent reduction in protein size observed under nonreducing conditions (Wittig and Schägger, 2008). We identified two higher order complexes in the absence of reducing agents and without heating up the samples (Fig. 5E). These complexes corresponded in size to an AtALMT9-GFP dimer (approximately 140 kD) and a tetramer (approximately 280 kD; Fig. 5E). Thus, these results provide evidence that AtALMT9-GFP functions as a multimer in which supposedly four subunits form the channel.

DISCUSSION

The usage of blockers and the analysis of their effects on different site-specific mutants have allowed the development of structural models of ion channels when the crystal structures were not solved (MacKinnon, 1991; Yellen et al., 1991; Linsdell, 2005). Due to the absence of detailed data about the structure of ALMTs, the only available information comes from in silico predictions and a few structure-function studies (Motoda et al., 2007; Ligaba et al., 2009; Furuichi et al., 2010; Mumm et al., 2013). Hence, the exact topology of ALMT proteins is not yet unambiguously determined (Motoda et al., 2007; Dreyer et al., 2012). Nonetheless, on the basis of software predictions and the existing data, Arabidopsis ALMT channels are likely to be formed by an N-terminal TMD constituted of six membrane-spanning helices with the N-terminal and the C-terminal domains featuring an intracellular orientation (Fig. 2A; Kovermann et al., 2007; http://aramemnon.botanik.uni-koeln.de). Using in silico analysis, Piñeros et al. (2008) suggested that the TMD is involved in forming the permeation pathway. Nevertheless, the few structure-function studies focused on the C-terminal domain of ALMT proteins (Ligaba et al., 2009; Furuichi et al., 2010; Mumm et al., 2013). Because of the complete lack of experimental data on the N-terminal TMD of ALMTs, we performed a site-directed mutagenesis screen of this region using AtALMT9.

We could identify the three residues Lys-193, Arg-200, and Arg-215 as being important for channel functionality and possibly as being part of the anion conduction pathway. The mutation of Lys-193 and Arg-200, which are localized at the cytosolic face of AtALMT9, strongly impacted on both channel functionality and citrate blockade. The channel variants $AtALMT9_{K193N}$ and $AtALMT9_{K193E}$ display a strong and progressive effect on citrate inhibition sensitivity, resulting in a complete abolition of the open channel blockade in $AtALMT9_{K193E}$. Moreover, $AtALMT9_{K193E}$ features an impaired open channel rectification compared with $AtALMT9_{WT}$. Regarding position Arg-200, the substitution into a Glu results in a nonconductive channel ($AtALMT9_{R200E}$), while the channel variant $AtALMT9_{R200N}$ is functional but has strongly reduced citrate block sensitivity. Differently, mutation of the

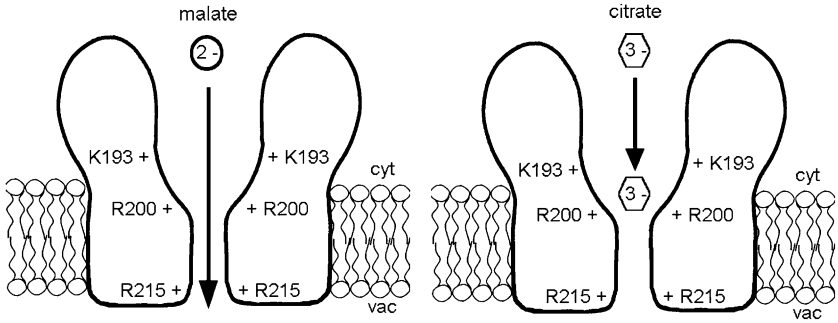

Figure 6. Model illustrating the block of AtALMT9 by cytosolic citrate. Cytosolic citrate inhibits AtALMT9 by acting as an open channel blocker. This indicates that citrate enters the permeation pathway to block AtALMT9 currents. To exert its blocking action, the trivalent anion citrate interacts electrostatically with the two positively charged residues Lys-193 and Arg-200. Lys-193 and Arg-200 are located at the cytosolic side of the channel and are likely to participate in forming the pore entrance. The vacuolar-facing Arg-215 is involved in the anion permeation process through AtALMT9 and, like Lys-193 and Arg-200, is part of the same putative transmembrane helix (TMα5).

residue Arg-215, as expected by its predicted vacuolar-side localization, does not modify citrate inhibition. However, $AtALMT9_{R215N}$ is impaired in its rectification ratio, suggesting that the mutated residue is involved in the permeation process. Again, an exchange of the electrical charge of the residue (R215E) results in a nonconductive channel. Interestingly, the charge conservative mutant channels of these three positions ($AtALMT9_{K193R}$, $AtALMT9_{R200K}$, and $AtALMT9_{R215K}$) maintained the channel properties indistinguishable from $AtALMT9_{WT}$ (Fig. 4C). Therefore, the interaction of citrate with AtALMT9 is mainly electrostatic, and Lys-193 and Arg-200 are key residues in forming the citrate-binding site. When inhibiting AtALMT9 currents, citrate enters the TMD and penetrates 17% of the applied electrical field. Thus, combining this information with the predicted location of Lys-193 and Arg-200, it is likely that the binding site for citrate is placed at the cytosolic entrance of the conduction pathway of AtALMT9 (Fig. 6).

In addition, the results provided information about the topology of the AtALMT9 TMD. Our experimental data point toward an opposite orientation of ALMT proteins compared with the models proposed by Motoda et al. (2007) and Dreyer et al. (2012). Indeed, the fact that the mutation of the cytosolic-facing residues Lys-87, Lys-193, and Arg-200 impairs citrate block (Fig. 4; Supplemental Fig. S4) while the mutation of the vacuolar-facing Arg-215 does not is in agreement with the computer-based prediction of the topology of AtALMT9, with an intracellular localization of the N terminus and an orientation of the protein as depicted in Figure 2. Moreover, this study demonstrates that three residues (Lys-193, Arg-200, and Arg-215) that are important in the anion permeation process reside within TMα5 or in the short loop preceding it. TMα5 is predicted to span the entire membrane, whereby Lys-193 and Arg-200 are located on the opposite side of TMα5 than Arg-215 (Fig. 2). Hence, it is tempting to speculate that TMα5 lines the whole permeation pathway of AtALMT9, similar to what has been previously observed in other ion channels (Hilf and Dutzler, 2009; Hibbs and Gouaux, 2011).

Several introduced mutations of residues in the TMD result in major defects on AtALMT9 conductivity regardless of the chemical properties of the substitution (Table I). This nonfunctionality prevents further investigations but suggests an essential structural role of these residues. Nonetheless, we have identified the distinct structural role of the residue Lys-93. Lys-93 is located within TMα1 and is strictly conserved among different ALMTs (Supplemental Fig. S2). We have demonstrated that Lys-93 forms a salt bridge with another strictly conserved residue in TMα2, Glu-130. This proves that TMα1 and TMα2 are connected by a salt bridge that is crucial for channel functionality. Similar observations of a restored wild-type channel function when exchanging the residues of a salt bridge have been made in the cystic fibrosis transmembrane conductance regulators (Cotten and Welsh, 1999; Cui et al., 2013).

The concomitant finding of the pore blocker citrate and the mutant channel $AtALMT9_{K193E}$ that features abolished block sensitivity allowed investigation of the oligomeric state of AtALMT9 (MacKinnon, 1991). This is an intriguing opportunity, since, to our knowledge, it is not known whether ALMTs present a monomeric or multimeric architecture. To distinguish between these two possibilities, we coexpressed $AtALMT9_{WT}$ and $AtALMT9_{K193E}$ and found that the sensitivity to citrate was decreased and the $K_d^{citrate}$ was shifted. These results are consistent with a model in which AtALMT9 channels form a multimeric complex and citrate interacts with multiples of those subunits. Moreover, since citrate is an open channel blocker interacting with the pore-forming region, our data suggest that several AtALMT9 polypeptides participate in forming the anion conduction pathway. This type of multimeric organization is shared with several other families of ion channels like potassium channels (MacKinnon, 1991), Glu receptors (Rosenmund et al., 1998; Robert et al., 2001), and acid-sensing channels (Kosari et al., 1998, 2006; Snyder et al., 1998). However, due to the low affinity of citrate, it is not possible to apply saturating blocker concentrations that would have allowed determination of the exact stoichiometry of AtALMT9 complexes. Therefore, we used a biochemical approach to provide evidence that AtALMT9 features a multimeric organization. Our data suggest that AtALMT9 forms presumably tetrameric complexes, similar to what has been found for potassium channels (Daram et al., 1997; Doyle et al., 1998). These results are in line with recent findings on AtALMT9, where the induction of chloride conductance by malate was shown to exhibit a Hill coefficient of 2.5, indicating that more than two subunits are required to form a functional channel (De Angeli et al., 2013).

One question that arises from this ensemble of results is whether the structural characteristics we described for AtALMT9 are extendible to other members of the ALMT family. We predominantly investigated residues that are conserved among the family at least in their electrical charge. Moreover, based on secondary structure prediction, the N-terminal TMD has a remarkably conserved topology. Thus, it is probable that the results concerning the structure found for one ALMT are also valid for other members.

In conclusion, our work provides new molecular, biochemical, and biophysical details about the TMD of a member of the ALMT family. We identified a probable pore-forming region of ALMT anion channels and revealed that AtALMT9, and presumably also other ALMTs, are multimeric complexes formed by four subunits in which multiple subunits participate in the formation of the conduction pathway.

MATERIALS AND METHODS

Site-Directed Mutagenesis

Arabidopsis (*Arabidopsis thaliana*) AtALMT9 complementary DNA was cloned into the expression vector pART27 as described previously (Kovermann

et al., 2007). The site-directed mutants were generated following the manufacturer's instructions of the Quikchange Site-Directed Mutagenesis Kit (Agilent Technologies) with slight modifications. All point mutations were verified by sequencing.

Overexpression of AtALMT9-GFP in Tobacco

Agrobacterium tumefaciens (GV3101) was transformed with plasmids containing the sequences of the $AtALMT9_{WT}$ channel and its point-mutated derivatives by electroporation. The *A. tumefaciens*-mediated infiltration of 4-week-old tobacco (*Nicotiana benthamiana*) leaves was performed as described previously with slight modifications (Yang et al., 2001). After transient transformation, tobacco plants were grown in the greenhouse (16 h of light/8 h of dark, 25°C/23°C, 100–200 μmol photons m^{-2} s^{-1}, 60% relative humidity) for another 2 to 3 d and then used to isolate protoplasts for confocal laser scanning microscopy and patch-clamp experiments.

Verification of $AtALMT9_{WT}$ and $AtALMT9_{K193E}$ Coexpression in Tobacco

A. tumefaciens strains harboring plasmids with either the sequence of $AtALMT9_{WT}$ or $AtALMT9_{K193E}$ were coinfiltrated into tobacco in a bacteria ratio of 1:1 and 1:4 after defining the optical density at 600 nm. Whole-leaf RNA was extracted 2 to 3 d after transient transformation, and complementary DNA was subsequently synthesized. We amplified *AtALMT9* via PCR using a 20-μL reaction volume and the Phusion High-Fidelity DNA Polymerase (Thermo Scientific). PCR conditions were set as follows: 98°C for 2 min in the first cycle; subsequently, 30 amplification cycles consisting of 10 s at 98°C, 20 s at 58°C, and 1.20 min at 72°C; the final extension was 5 min at 72°C. Subsequently, we cloned the PCR product into the pJet1.2/blunt cloning vector (CloneJet PCR Cloning Kit; Thermo Scientific) and determined the amount of $AtALMT9_{WT}$ and $AtALMT9_{K193E}$ transcripts by sequencing.

Microscopy

Intracellular localization of AtALMT9-GFP mutants was determined by performing a lysis to release vacuoles of tobacco protoplasts overexpressing the appropriate mutant channel construct. Microscopy was conducted using a Leica DMIRE2 www.leica-microsystems.com laser scanning microscope that was equipped with a 63× glycerol objective. GFP fluorescence signal was imaged at an excitation wavelength of 488 nm, and the emission was detected between 500 and 530 nm. The appropriate Leica confocal software has been used for image acquisition. The images in Supplemental Figure S3 were obtained with an epifluorescence microscope (Nikon Eclipse TS100) and acquired with a digital camera (Nikon DS-Fi1).

Electrophysiology

Mesophyll protoplasts from AtALMT9-GFP-overexpressing tobacco leaves were isolated by enzymatic digestion. The enzyme solution contained 0.3% (w/v) cellulase R-10, 0.03% (w/v) pectolyase Y-23, 1 mM $CaCl_2$, 500 mM sorbitol, and 10 mM MES, pH 5.3, 550 mosmol. Protoplasts were washed twice and resuspended in the same solution without enzymes. Vacuoles were released from mesophyll protoplast by the addition of 5 mM EDTA and a slight osmotic shock (500 mosmol; see medium below). Transformed vacuoles exhibiting an AtALMT9-GFP signal were selected using an epifluorescence microscope. Membrane currents from patches of the tonoplast were recorded using the excised cytosolic-side-out patch-clamp technique as described elsewhere (De Angeli et al., 2013). Briefly, currents were recorded with an EPC10 patch-clamp amplifier (HEKA Electronics) using Patchmaster software (HEKA Electronics). Data were analyzed with FitMaster software (HEKA Electronics). In experiments on macroscopic current recordings, the pipette resistance was 4 to 5 MΩ. Only patches presenting a seal resistance higher than 2 GΩ were used to perform experiments. Macroscopic current recordings were filtered at 300 Hz.

The pipette solution contained 112 mM malic acid and 5 mM HCl and was adjusted with BisTrisPropane (BTP) to pH 6. The osmolarity was adjusted with sorbitol to 550 mosmol. The bath solution contained (1) 100 mM malic acid, 3 mM $MgCl_2$, and 0.1 mM $CaCl_2$, adjusted to pH 7.5 with BTP; (2) 100 mM malic acid, citric acid (2, 5, 10, or 30 mM), 3 mM $MgCl_2$, and 0.1 mM $CaCl_2$, adjusted to pH 7.5 with BTP; and (3) 100 mM citric acid, 3 mM $MgCl_2$, and 0.1 mM $CaCl_2$, adjusted to pH 7.5 with BTP. The osmolarity was adjusted to 500 mosmol using sorbitol. All chemicals were purchased from Sigma-Aldrich. Liquid junction potentials were measured and corrected when higher than ±2 mV (Neher, 1992). Current-voltage characteristics were obtained by subtracting the current at time zero from the quasistationary currents (averaging the last 50 ms of the current trace) elicited by main voltage pulses. In all patch-clamp experiments, the applied membrane potential (V_m) is presented according to the convention for intracellular organelles of Bertl et al. (1992), namely $V_m = V_{cyt} - V_{vac}$, where V_{cyt} and V_{vac} are the cytosolic and vacuolar potentials, respectively.

The dose response for the $citrate_{cyt}$ inhibition of $AtALMT9_{WT}$ currents (Figs. 1 and 5; Supplemental Fig. S4) was fitted and analyzed with the Langmuir isotherm in the following form:

$$\frac{I}{I_0} = 1 - \frac{1}{1 + \frac{K_d^{CA}}{[CA]_{cyt}}} \quad (1)$$

where I is the AtALMT9 current amplitude in the presence of $citrate_{cyt}$, I_0 is the AtALMT9 current under control solution, $[CA]_{cyt}$ is the cytosolic citrate concentration, and K_d^{CA} is the dissociation constant of citrate.

The dose response for the $citrate_{cyt}$ inhibition of the co-overexpression of $AtALMT9_{WT}$ and $AtALMT9_{K193E}$ in 1:1 and 1:4 ratios (Fig. 5) was fitted with the Langmuir isotherm in the following form:

$$\frac{I}{I_0} = 1 - \frac{I_{inh}}{1 + \frac{K_d^{CA}}{[CA]_{cyt}}} \quad (2)$$

where I is the current amplitude in the presence of $citrate_{cyt}$, I_0 is the current amplitude under control solution, $[CA]_{cyt}$ is the cytosolic citrate concentration, K_d^{CA} is the dissociation constant of citrate, and I_{inh} is the maximum fraction of current inhibited by $citrate_{cyt}$.

To estimate the fraction of the electrical field that citrate traverses to reach its binding site, the voltage-dependent dissociation constant relationship was fitted with the equation described by Woodhull (1973):

$$K_d^{CA}(V_m) = K_d^{CA}(0) \cdot e^{\frac{z\delta FV}{RT}} \quad (3)$$

in which $K_d^{CA}(V_m)$ is the voltage-dependent dissociation constant of citrate, $K_d^{CA}(0)$ is the dissociation constant of citrate at 0 mV, V_m is the transmembrane potential, z is the valence of the blocker, δ is the fraction of the electrical membrane field traversed by the blocker, and F, R, and T are the Faraday constant, gas constant, and absolute temperature, respectively. Experiments were performed at room temperature (22°C–25°C).

For all calculations, the actual $citrate^{3-}$ concentration was determined with the Henderson-Hasselbach equation. The $citrate^{3-}$ concentration was estimated to be 93% of the different citric acid forms at pH 7.5.

The rectification rate coefficient was obtained by calculating the ratio between the conductance at the end of the activating pulse (V_m = −120 mV) and the conductance at the very beginning of the deactivating pulse (V_m = +60 mV). The conductance at the end of the activating pulse was estimated by using the ratio between the average current amplitude of the last 5 ms of the activation pulse and the applied activating potential. To calculate the conductance at the beginning of the deactivating pulse, the initial current was extrapolated from a monoexponential fit of the tail currents and divided by the applied deactivating potential of +60 mV.

Microsomal Protein Extraction and Protein Gel-Blot Analysis

Leaf material from unfiltrated (or empty vector-expressing) tobacco plants (data not shown) and AtALMT9-GFP-expressing tobacco plants was homogenized by cryogenic grinding with mortar and pestle and mixed with 4°C ice-cold homogenization buffer (250 mM Tris-HCl, pH 8.5, 25 mM EDTA, 30% Suc, 5 mM dithiothreitol, and protease inhibitor cocktail tablet [Roche]). The debris was sedimented by centrifugation at 5,000 rpm in a table-top centrifuge (Biofuge fresco; Heraeus) for 10 min at 4°C. Afterward, the supernatant fraction was passed through Miracloth (Calbiochem), transferred into ultracentrifugation tubes, and spun down at 35,000 rpm in an ultracentrifuge for 45 min at 4°C (Beckman Optima, SW41Ti). The membranes were solubilized in 100 μL of solubilization buffer (15 mM MOPS, pH 7.0, 1 mM EDTA, 30% glycerol [v/v], 0.5% *n*-dodecyl-β-D-maltoside, and protease inhibitor cocktail tablet [Roche]) for 30 min on ice. Equal protein amounts (Quick Start Bradford

Protein Assay; Bio-Rad) were loaded on SDS-PAGE gels (4%–20% Mini PROTEAN TGX precast gradient gel; Bio-Rad) in the absence of dithiothreitol. Proteins were blotted on polyvinylidene difluoride membranes (0.45 μm; Millipore) using the tank approach (Mini Trans-Blot Electrophoretic Transfer Cell; Bio-Rad), and an anti-GFP antibody (Clontech; 1:1,000) was used for immunodetection.

Sequence data from this article can be found in the GenBank/EMBL data libraries under accession numbers NP_188473.1.

Supplemental Data

The following materials are available in the online version of this article.

Supplemental Figure S1. $AtALMT9_{WT}$ and $AtALMT9_{K193E}$ are poorly permeable for citrate.

Supplemental Figure S2. Multiple alignment of the ALMT protein family of Arabidopsis.

Supplemental Figure S3. Intracellular localization of the different mutant channels of AtALMT9-GFP.

Supplemental Figure S4. AtALMT9 point mutants display different channel conductivity and sensitivity to citrate inhibition.

Supplemental Figure S5. The double mutant $AtALMT9_{K93E/E130K}$ is inhibited by intracellular citrate like $AtALMT9_{WT}$.

Received April 16, 2013; accepted August 5, 2013; published August 5, 2013.

LITERATURE CITED

Barbier-Brygoo H, De Angeli A, Filleur S, Frachisse JM, Gambale F, Thomine S, Wege S (2011) Anion channels/transporters in plants: from molecular bases to regulatory networks. Annu Rev Plant Biol **62:** 25–51

Becker D, Dreyer I, Hoth S, Reid JD, Busch H, Lehnen M, Palme K, Hedrich R (1996) Changes in voltage activation, Cs^+ sensitivity, and ion permeability in H5 mutants of the plant K^+ channel KAT1. Proc Natl Acad Sci USA **93:** 8123–8128

Bertl A, Blumwald E, Coronado R, Eisenberg R, Findlay G, Gradmann D, Hille B, Köhler K, Kolb HA, MacRobbie E, et al (1992) Electrical measurements on endomembranes. Science **258:** 873–874

Brandt B, Brodsky DE, Xue S, Negi J, Iba K, Kangasjärvi J, Ghassemian M, Stephan AB, Hu H, Schroeder JI (2012) Reconstitution of abscisic acid activation of SLAC1 anion channel by CPK6 and OST1 kinases and branched ABI1 PP2C phosphatase action. Proc Natl Acad Sci USA **109:** 10593–10598

Catterall WA (2010) Ion channel voltage sensors: structure, function, and pathophysiology. Neuron **67:** 915–928

Chen YH, Hu L, Punta M, Bruni R, Hillerich B, Kloss B, Rost B, Love J, Siegelbaum SA, Hendrickson WA (2010) Homologue structure of the SLAC1 anion channel for closing stomata in leaves. Nature **467:** 1074–1080

Choe S (2002) Potassium channel structures. Nat Rev Neurosci **3:** 115–121

Clay JR (1995) Quaternary ammonium ion blockade of IK in nerve axons revisited: open channel block vs. state independent block. J Membr Biol **147:** 23–34

Cotten JF, Welsh MJ (1999) Cystic fibrosis-associated mutations at arginine 347 alter the pore architecture of CFTR: evidence for disruption of a salt bridge. J Biol Chem **274:** 5429–5435

Cui G, Freeman CS, Knotts T, Prince CZ, Kuang C, McCarty NA (2013) Two salt bridges differentially contribute to the maintenance of cystic fibrosis transmembrane conductance regulator (CFTR) channel function. J Biol Chem**288:** 20758–20767

Daram P, Urbach S, Gaymard F, Sentenac H, Chérel I (1997) Tetramerization of the AKT1 plant potassium channel involves its C-terminal cytoplasmic domain. EMBO J **16:** 3455–3463

De Angeli A, Monachello D, Ephritikhine G, Frachisse JM, Thomine S, Gambale F, Barbier-Brygoo H (2006) The nitrate/proton antiporter AtCLCa mediates nitrate accumulation in plant vacuoles. Nature **442:** 939–942

De Angeli A, Zhang J, Meyer S, Martinoia E (2013) AtALMT9 is a malate-activated vacuolar chloride channel required for stomatal opening in Arabidopsis. Nat Commun **4:** 1804

Doyle DA, Morais Cabral J, Pfuetzner RA, Kuo A, Gulbis JM, Cohen SL, Chait BT, MacKinnon R (1998) The structure of the potassium channel: molecular basis of K^+ conduction and selectivity. Science **280:** 69–77

Dreyer I, Gomez-Porras JL, Riaño-Pachón DM, Hedrich R, Geiger D (2012) Molecular evolution of slow and quick anion channels (SLACs and QUACs/ALMTs). Front Plant Sci **3:** 263

Dutzler R, Campbell EB, Cadene M, Chait BT, MacKinnon R (2002) X-ray structure of a ClC chloride channel at 3.0 A reveals the molecular basis of anion selectivity. Nature **415:** 287–294

Ferrer-Montiel AV, Montal M (1996) Pentameric subunit stoichiometry of a neuronal glutamate receptor. Proc Natl Acad Sci USA **93:** 2741–2744

Furuichi T, Sasaki T, Tsuchiya Y, Ryan PR, Delhaize E, Yamamoto Y (2010) An extracellular hydrophilic carboxy-terminal domain regulates the activity of TaALMT1, the aluminum-activated malate transport protein of wheat. Plant J **64:** 47–55

Geelen D, Lurin C, Bouchez D, Frachisse JM, Lelièvre F, Courtial B, Barbier-Brygoo H, Maurel C (2000) Disruption of putative anion channel gene AtCLC-a in Arabidopsis suggests a role in the regulation of nitrate content. Plant J **21:** 259–267

Geiger D, Scherzer S, Mumm P, Marten I, Ache P, Matschi S, Liese A, Wellmann C, Al-Rasheid KAS, Grill E, et al (2010) Guard cell anion channel SLAC1 is regulated by CDPK protein kinases with distinct Ca^{2+} affinities. Proc Natl Acad Sci USA **107:** 8023–8028

Geiger D, Scherzer S, Mumm P, Stange A, Marten I, Bauer H, Ache P, Matschi S, Liese A, Al-Rasheid KA, et al (2009) Activity of guard cell anion channel SLAC1 is controlled by drought-stress signaling kinase-phosphatase pair. Proc Natl Acad Sci USA **106:** 21425–21430

Hechenberger M, Schwappach B, Fischer WN, Frommer WB, Jentsch TJ, Steinmeyer K (1996) A family of putative chloride channels from Arabidopsis and functional complementation of a yeast strain with a CLC gene disruption. J Biol Chem **271:** 33632–33638

Hedrich R (2012) Ion channels in plants. Physiol Rev **92:** 1777–1811

Hibbs RE, Gouaux E (2011) Principles of activation and permeation in an anion-selective Cys-loop receptor. Nature **474:** 54–60

Hilf RJ, Dutzler R (2009) Structure of a potentially open state of a proton-activated pentameric ligand-gated ion channel. Nature **457:** 115–118

Hoekenga OA, Maron LG, Piñeros MA, Cançado GMA, Shaff J, Kobayashi Y, Ryan PR, Dong B, Delhaize E, Sasaki T, et al (2006) AtALMT1, which encodes a malate transporter, is identified as one of several genes critical for aluminum tolerance in Arabidopsis. Proc Natl Acad Sci USA **103:** 9738–9743

Jentsch TJ (2008) CLC chloride channels and transporters: from genes to protein structure, pathology and physiology. Crit Rev Biochem Mol Biol **43:** 3–36

Kim TH, Böhmer M, Hu H, Nishimura N, Schroeder JI (2010) Guard cell signal transduction network: advances in understanding abscisic acid, CO_2, and Ca^{2+} signaling. Annu Rev Plant Biol **61:** 561–591

Kosari F, Sheng S, Kleyman TR (2006) Biophysical approach to determine the subunit stoichiometry of the epithelial sodium channel using the Xenopus laevis oocyte expression system. Methods Mol Biol **337:** 53–63

Kosari F, Sheng S, Li J, Mak DO, Foskett JK, Kleyman TR (1998) Subunit stoichiometry of the epithelial sodium channel. J Biol Chem **273:** 13469–13474

Kovermann P, Meyer S, Hörtensteiner S, Picco C, Scholz-Starke J, Ravera S, Lee Y, Martinoia E (2007) The Arabidopsis vacuolar malate channel is a member of the ALMT family. Plant J **52:** 1169–1180

Ligaba A, Katsuhara M, Ryan PR, Shibasaka M, Matsumoto H (2006) The *BnALMT1* and *BnALMT2* genes from rape encode aluminum-activated malate transporters that enhance the aluminum resistance of plant cells. Plant Physiol **142:** 1294–1303

Ligaba A, Kochian L, Piñeros M (2009) Phosphorylation at S384 regulates the activity of the TaALMT1 malate transporter that underlies aluminum resistance in wheat. Plant J **60:** 411–423

Linsdell P (2005) Location of a common inhibitor binding site in the cytoplasmic vestibule of the cystic fibrosis transmembrane conductance regulator chloride channel pore. J Biol Chem **280:** 8945–8950

MacKinnon R (1991) Determination of the subunit stoichiometry of a voltage-activated potassium channel. Nature **350:** 232–235

MacKinnon R, Yellen G (1990) Mutations affecting TEA blockade and ion permeation in voltage-activated K^+ channels. Science **250:** 276–279

Martinoia E, Meyer S, De Angeli A, Nagy R (2012) Vacuolar transporters in their physiological context. Annu Rev Plant Biol **63:** 183–213

Meyer S, Mumm P, Imes D, Endler A, Weder B, Al-Rasheid KAS, Geiger D, Marten I, Martinoia E, Hedrich R (2010) AtALMT12 represents an R-type anion channel required for stomatal movement in Arabidopsis guard cells. Plant J **63:** 1054–1062

Meyer S, Scholz-Starke J, De Angeli A, Kovermann P, Burla B, Gambale F, Martinoia E (2011) Malate transport by the vacuolar AtALMT6 channel in guard cells is subject to multiple regulation. Plant J **67:** 247–257

Motoda H, Sasaki T, Kano Y, Ryan PR, Delhaize E, Matsumoto H, Yamamoto Y (2007) The membrane topology of ALMT1, an aluminum-activated malate transport protein in wheat (Triticum aestivum). Plant Signal Behav **2:** 467–472

Mumm P, Imes D, Martinoia E, Al-Rasheid KA, Geiger D, Marten I, Hedrich R (January 12, 2013) C-terminus mediated voltage gating of Arabidopsis guard cell anion channel QUAC1. Mol Plant http://dx.doi.org/10.1093/mp/sst008

Negi J, Matsuda O, Nagasawa T, Oba Y, Takahashi H, Kawai-Yamada M, Uchimiya H, Hashimoto M, Iba K (2008) CO_2 regulator SLAC1 and its homologues are essential for anion homeostasis in plant cells. Nature **452:** 483–486

Neher E (1992) Correction for liquid junction potentials in patch clamp experiments. Methods Enzymol **207:** 123–131

Perutz MF (1978) Electrostatic effects in proteins. Science **201:** 1187–1191

Piñeros MA, Cançado GMA, Kochian LV (2008) Novel properties of the wheat aluminum tolerance organic acid transporter (TaALMT1) revealed by electrophysiological characterization in *Xenopus* oocytes: functional and structural implications. Plant Physiol **147:** 2131–2146

Rentsch D, Martinoia E (1991) Citrate transport into barley mesophyll vacuoles: comparison with malate-uptake activity. Planta **184:** 532–537

Robert A, Irizarry SN, Hughes TE, Howe JR (2001) Subunit interactions and AMPA receptor desensitization. J Neurosci **21:** 5574–5586

Roelfsema MRG, Hedrich R (2005) In the light of stomatal opening: new insights into 'the Watergate'. New Phytol **167:** 665–691

Rosenmund C, Stern-Bach Y, Stevens CF (1998) The tetrameric structure of a glutamate receptor channel. Science **280:** 1596–1599

Sasaki T, Yamamoto Y, Ezaki B, Katsuhara M, Ahn SJ, Ryan PR, Delhaize E, Matsumoto H (2004) A wheat gene encoding an aluminum-activated malate transporter. Plant J **37:** 645–653

Snyder PM, Cheng C, Prince LS, Rogers JC, Welsh MJ (1998) Electrophysiological and biochemical evidence that DEG/ENaC cation channels are composed of nine subunits. J Biol Chem **273:** 681–684

Traynelis SF, Wollmuth LP, McBain CJ, Menniti FS, Vance KM, Ogden KK, Hansen KB, Yuan H, Myers SJ, Dingledine R (2010) Glutamate receptor ion channels: structure, regulation, and function. Pharmacol Rev **62:** 405–496

Vahisalu T, Kollist H, Wang YF, Nishimura N, Chan WY, Valerio G, Lamminmäki A, Brosché M, Moldau H, Desikan R, et al (2008) SLAC1 is required for plant guard cell S-type anion channel function in stomatal signalling. Nature **452:** 487–491

von Heijne G, Gavel Y (1988) Topogenic signals in integral membrane proteins. Eur J Biochem **174:** 671–678

Ward JM, Mäser P, Schroeder JI (2009) Plant ion channels: gene families, physiology, and functional genomics analyses. Annu Rev Physiol **71:** 59–82

Waterhouse AM, Procter JB, Martin DM, Clamp M, Barton GJ (2009) Jalview version 2: a multiple sequence alignment editor and analysis workbench. Bioinformatics **25:** 1189–1191

Wittig I, Schägger H (2008) Features and applications of blue-native and clear-native electrophoresis. Proteomics **8:** 3974–3990

Woodhull AM (1973) Ionic blockage of sodium channels in nerve. J Gen Physiol **61:** 687–708

Yamaguchi M, Sasaki T, Sivaguru M, Yamamoto Y, Osawa H, Ahn SJ, Matsumoto H (2005) Evidence for the plasma membrane localization of Al-activated malate transporter (ALMT1). Plant Cell Physiol **46:** 812–816

Yang KY, Liu YD, Zhang SQ (2001) Activation of a mitogen-activated protein kinase pathway is involved in disease resistance in tobacco. Proc Natl Acad Sci USA **98:** 741–746

Yellen G, Jurman ME, Abramson T, MacKinnon R (1991) Mutations affecting internal TEA blockade identify the probable pore-forming region of a K^+ channel. Science **251:** 939–942

Identification of a probable pore forming domain in the multimeric vacuolar anion channel AtALMT9

Jingbo Zhang, Ulrike Baetz, Undine Krügel, Enrico Martinoia and Alexis De Angeli

Supplementary Figures

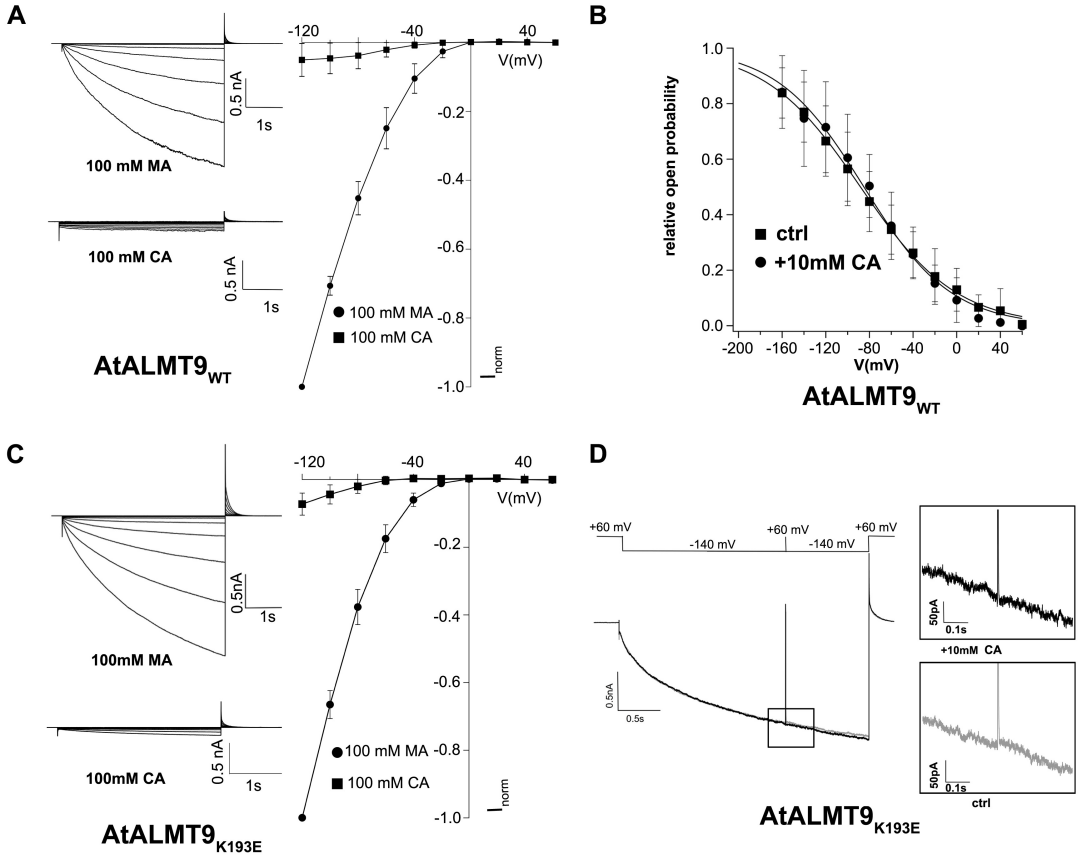

Supplemental Figure S1. AtALMT9$_{WT}$ and AtALMT9$_{K193E}$ are poorly permeable for citrate.

(A, C) Representative traces and normalized mean I-V curves of excised cytosolic-side out patches from *N. benthamiana* vacuoles overexpressing AtALMT9$_{WT}$ (A;

upper traces) and AtALMT9$_{K193E}$ (C; upper traces) displayed time dependent malate currents in symmetric ionic conditions (circles; 100 mM malate$_{vac}$/ 100 mM malate$_{cyt}$). When the cytosolic solution was replaced with 100 mM CA$_{cyt}$ (squares; 100 mM malate$_{vac}$/ 100 mM CA$_{cyt}$) the inward currents decreased and displayed only weak time dependent currents (A, C; lower traces). The current ratios I_{CA}/I_{Malate}(AtALMT9$_{WT}$) = 5 ± 5% and I_{CA}/I_{Malate}(AtALMT9$_{K193E}$) = 7 ± 3% show that CA is poorly permeable compared to malate. Currents were evoked in response to 3 s voltage pulses ranging from +60 mV to -120 mV in -20 mV steps followed by a tail pulse at +60 mV. The holding potential was set +60 mV. Error bars represent sd. Each data point corresponds to 4-11 patches. (B) Voltage dependency of the relative open probability of AtALMT9$_{WT}$ in control conditions (ctrl; 100 mM malate$_{vac}$/ 100 mM malate$_{cyt}$; circles) and in presence of 10 mM CA$_{cyt}$ (100 mM malate$_{vac}$/ 100 mM malate$_{cyt}$+10 mM CA$_{cyt}$; diamonds). The relative open probability was estimated from the initial current amplitude of the tail currents (derived from a mono-exponential fit of the current decay) which followed an activating pulse of various potentials. We were unable to reach the full activation of AtALMT9 channels as it is likely to occur at voltages more negatives than -160 mV, a value at which the vacuolar membrane becomes unstable. Therefore the data (n=8-10) was normalized to the I_{max} value that was obtained by fitting each data set with the Boltzmann equation.

The solid lines represent the best fits of the mean relative open probability in control and in presence of 10 mM CA$_{cyt}$ with a Boltzmann equation in the following form:

$$P_O^{rel} = 1/(1 + e^{\left(\frac{zF(V-V_h)}{RT}\right)})$$

in which P_O^{rel} is the relative open probability, z the gating charge, F the Faraday constant, R the universal gas constant, T the absolute temperature and V_h the voltage of half activation. The fit shows that the presence of 10 mM CA$_{cyt}$ does not change significantly the voltage dependent gating of the channel since V_h = -81 ± 1 mV and z = 0.6 ± 2 under control conditions and V_h = -76 ± 3 mV and z = 0.7 ± 1 with 10 mM CA$_{cyt}$. (D) "Kick-out experiment" performed on the mutant AtALMT9$_{K193E}$. Grey traces were obtained under 100 mM malate$_{vac}$/ 100 mM malate$_{cyt}$ conditions and black traces in the presence of 10 mM CA$_{cyt}$ (100 mM malate$_{vac}$/ 100 mM malate$_{cyt}$+10 mM CA$_{cyt}$). The currents evoked in response to a 2 s voltage pulse at -140 mV. Subsequently, the membrane potential was transiently stepped for 3 ms to +60 mV and then restored to -140 mV for 1 s which was followed by a tail pulse at +60 mV. The holding potential was set to +60 mV. Error bars display sd.

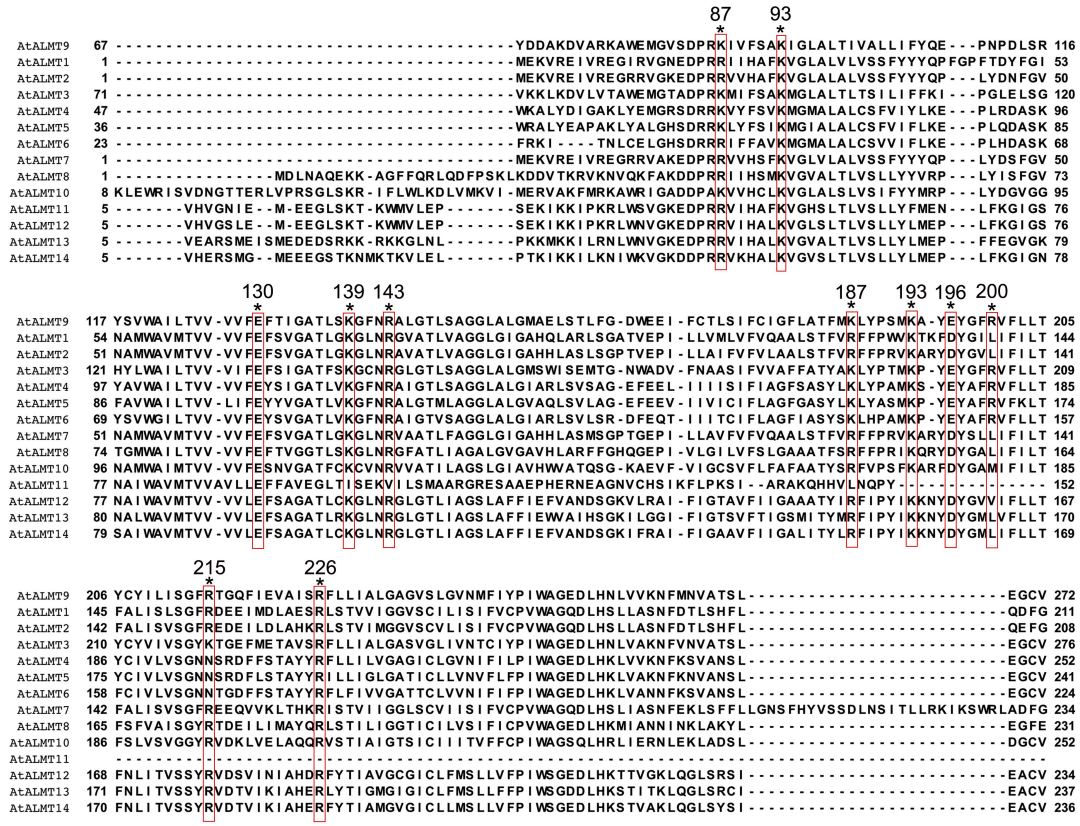

Supplemental Figure S2. Multiple alignment of the ALMT protein family of *Arabidopsis thaliana*.

The alignment was conducted with the Jalview software (Waterhouse *et al.,* 2009). Asterisks and red boxes indicate the residues that were targeted by site-directed mutagenesis in the present study.

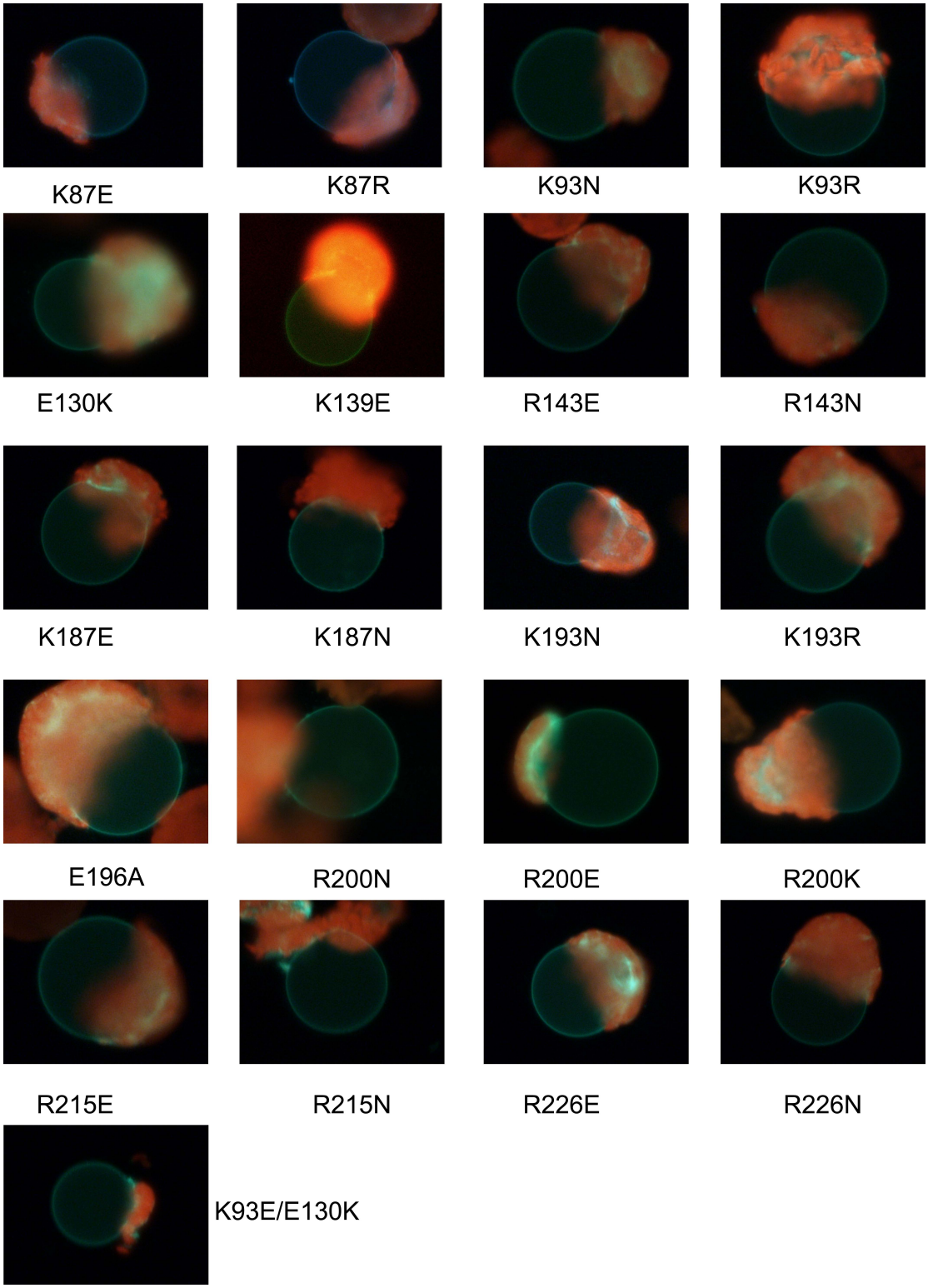

Supplemental Figure S3. Intracellular localization of the different mutant channels of AtALMT9-GFP.

Fluorescence images of vacuoles extracted from *N. benthamiana* protoplasts expressing the different AtALMT9-GFP mutants. None of the introduced mutations altered the tonoplastic localization of AtALMT9. The pictures were obtained with an

epifluorescence microscope (Nikon Eclipse TS100) and acquired with a digital camera (Nikon DS-Fi1).

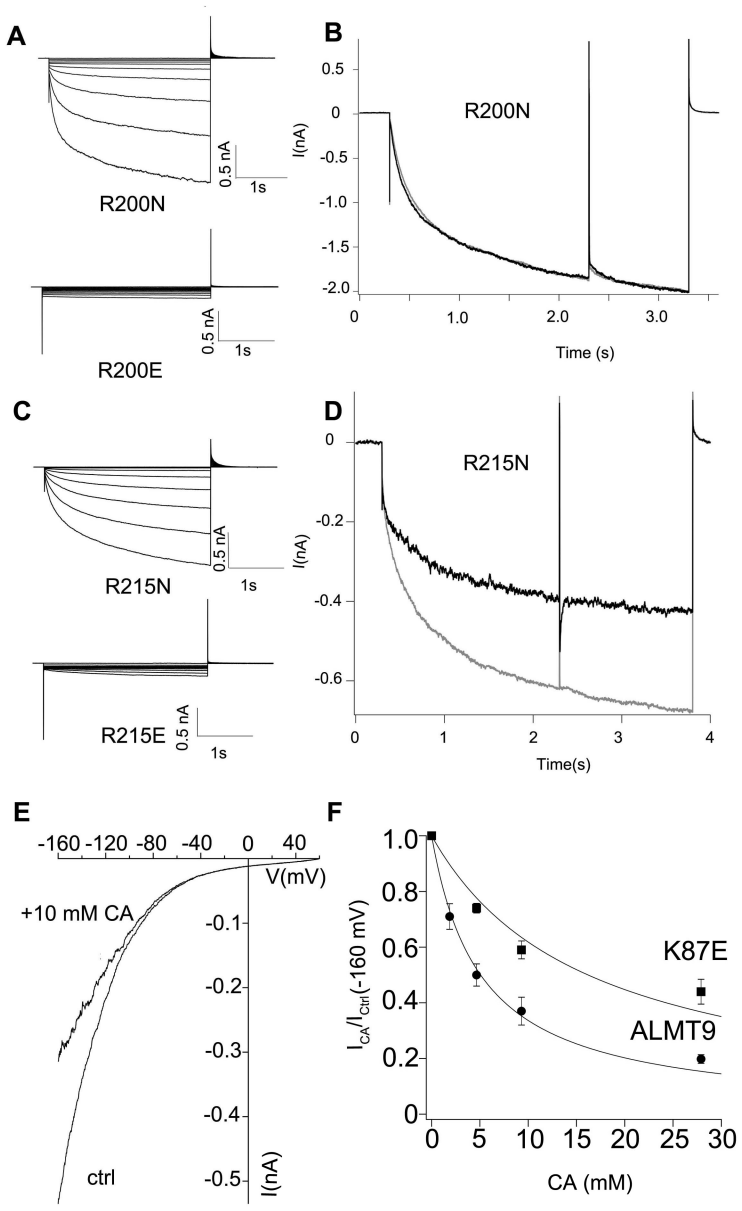

Supplemental Figure S4. AtALMT9 point mutants display different channel conductivity and sensitivity to citrate inhibition

Representative traces of current recordings from vacuoles overexpressing AtALMT9$_{R200N}$ and AtALMT9$_{R200E}$ (A), AtALMT9$_{R215N}$ and AtALMT9$_{R215E}$ (C) in symmetric malate conditions (100 mM malate$_{vac}$/ 100 mM malate$_{cyt}$). Currents were evoked in response to 3 s voltage pulses ranging from +60 mV to -120 mV in -20 mV steps followed by a tail pulse at +60 mV. The holding potential was +60 mV. "Kick-out experiments" were performed with the mutants AtALMT9$_{R200N}$ (B) and AtALMT9$_{R215N}$ (D). Grey traces were obtained in 100 mM malate$_{vac}$/ 100 mM malate$_{cyt}$ conditions and black traces in the presence of 10 mM CA$_{cyt}$ (100 mM

$malate_{vac}$/ 100 mM $malate_{cyt}$ + 10 mM CA_{cyt}). The currents evoked in response to a 2 s voltage pulse at -140 mV. Subsequently the membrane potential was transiently stepped for 3 ms to +60 mV and then restored to -140 mV for 1s which was followed by a tail pulse at +60 mV. The holding potential was set to +60 mV. (E) Representative I-V curves obtained with a voltage ramp (from +60 mV to -160 mV in 1.5 s; holding potential +60 mV) measured in excised cytosolic-side out patches from vacuoles expressing $AtALMT9_{K87E}$ in control conditions (ctrl) and in presence of 10 mM CA_{cyt}. (F) Dose-response of CA_{cyt} concentration-dependent ratio of $AtALMT9_{WT}$ and $AtALMT9_{K87E}$ at -160 mV. To estimate the dissociation constant K_d^{CA} the data points were fitted with a Langmuir isotherm (equation 1). The resulting K_d^{CA} values were 5.1 ± 0.3 mM and 16.2 ± 2.3 mM for $AtALMT9_{WT}$ and $AtALMT9_{K87E}$, respectively. Error bars represent sd.

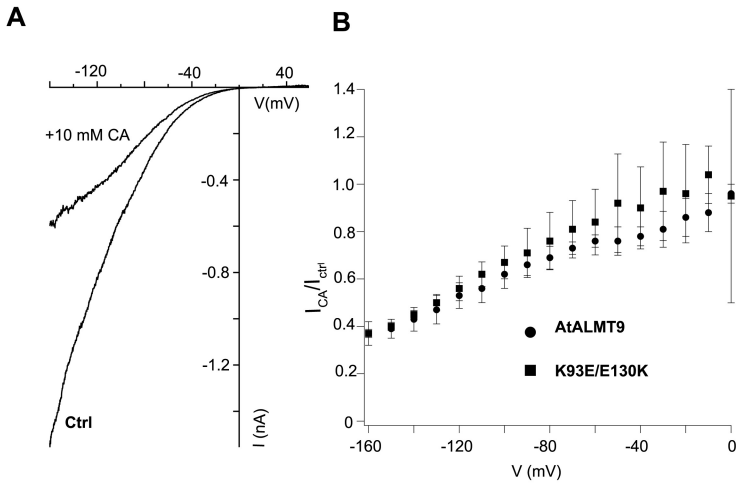

Supplemental Figure S5. The double mutant $AtALMT9_{K93E/E130K}$ is inhibited by intracellular citrate comparable to $AtALMT9_{WT}$.

(A) Representative I-V curves obtained with a voltage ramp (from +60 mV to -160 mV in 1.5 s; holding potential +60 mV) measured in excised cytosolic-side out patches from vacuoles expressing the double mutant $AtALMT9_{K93E/E130K}$ in control conditions (ctrl) and in presence of 10 mM CA_{cyt}. (B) Ratio between currents in presence of 10 mM CA_{cyt} and in control conditions at different membrane potentials. Depicted are $AtALMT9_{WT}$ (circles; n = 4) and $AtALMT9_{K93E/E130K}$ (squares; n = 3). Error bars represent sd

5. Result Chapter III

Block by Intracellular Nucleotides Regulates the Vacuolar Anion Channel *At*ALMT9 of *Arabidopsis*

Jingbo Zhang, Enrico Martinoia and Alexis De Angeli

In preparation for submission.

5.1 Abstract

The ALuminum Activated Malate Transporters (ALMTs) form a membrane protein family exhibiting different important physiological roles in plants, varying from the detoxification of environmental Al^{3+} to the regulation of stomatal movement. In contrast to their functional characterization, the regulation of ALMTs is largely unknown. However, the regulation of anion transporters is of importance to understand their physiological functions. In this study we present the voltage dependent inhibition of *At*ALMT9 by cytosolic nucleotides. The modulation of *At*ALMT9 activity by ATP is based on an 'open channel block mechanism' that gates the channel at negative membrane potentials. Anions present in the vacuolar lumen affect the ATP inhibition behavior and participate in the regulation of *At*ALMT9 mediated currents.

5.2 Introduction

The ALMTs form a membrane protein family exclusive to plants. These proteins have been found to exhibit different important physiological roles in plants, including detoxify the environmental Al^{3+} via extruding organic acids in the soil, transport of anion fluxes through the plasma and vacuolar membrane of guard cells, and due to their expression in guard cells they are involved in the regulation of stomatal movements (Hoekenga et al., 2006; Kovermann et al., 2007; Meyer et al., 2010b; De Angeli et al., 2013). The first gene coding for this type of anion channel, *Ta*ALMT1, was identified in wheat in a screen that aimed at identifying genes associated with aluminum resistance (Sasaki et al., 2004). *Ta*ALMT1 and its homologue in *Arabidopsis thaliana*, *At*ALMT1, have been shown to catalyse the exudation of malate across the plasma membrane of root cells. This release confers tolerance to Al^{3+} (Sasaki et al., 2004; Hoekenga et al., 2006). Another identified plasma membrane targeted ALMT in *Arabidopsis thaliana* is *At*ALMT12, which is a component of the R-type/QUAC channels in guard cells that mediate the efflux of anions in order to reduce stomata closure (Meyer et al., 2010b). *At*ALMT9 was the first vacuolar ALMT identified and characterized in *Arabidopsis thaliana* (Kovermann et al., 2007). It was shown that *At*ALMT9 is able to mediate malate and fumarate currents into the vacuole of *Arabidopsis* mesophyll cells. Recently,

*At*ALMT9 was shown to play a crucial role in guard cells where it functions as a malate-activated chloride channel involved in stomata opening (De Angeli et al., 2013). Moreover, the first information of the structural organization of *At*ALMT9 was obtained (Zhang et al., 2013). In this study we identified a region involved in forming the pore and showed that *At*ALMT9 assembles as multimers/tetramers.

We have been puzzled by the striking differences in the current voltage relationships (i.e. I-V curve) that characterize the different members of the ALMT family. The current voltage relationship is a fundamental characteristic of ion transporters that provides information on their biophysical and physiological properties. *At*ALMT12, which constitutes part of the R-type/QUAC currents in the plasma membrane of guard cells, exhibits a characteristic bell-shaped I-V curve (Meyer et al., 2010b). The bell-shape of the I-V curve results from an abrupt change in the channel conductance from positive to negative at very negative membrane potentials. This indicates that the channels start to close to mediate lower currents after this value (Meyer et al., 2010b). In contrast, the other ALMTs exhibit a monotonic voltage dependent I-V curve with a conductance that remains positive. This fact indicates that the channels stay open at negative membrane potentials (Sasaki et al., 2004; Hoekenga et al., 2006; Kovermann et al., 2007; Meyer et al., 2011; De Angeli et al., 2013). The R-type/QUAC channel of *Arabidopsis* hypocotyl and guard cells was shown to be regulated by cytosolic nucleotides (Hedrich et al., 1990; SchulzLessdorf et al., 1996; Thomine et al., 1997; Colcombet et al., 2001). In hypocotyl protoplasts it was proposed that cytosolic nucleotides are blockers acting as a "voltage dependent gate" of the R-type/QUAC/*At*ALMT12 channel (Colcombet et al., 2001), a gating mode similar to what has been observed in mammalian KIR (potassium inward rectifier) with Mg^{2+} and polyamines (Lopatin et al., 1994; Lu, 2004). However, after the discovery that ALMTs are part of the R-type/QUAC current the effect of intracellular nucleotides on ALMTs has never been investigated.

In the present study we addressed the question of the origin of the different I-V curves behavior of the ALMTs. We used the vacuolar anion channel *At*ALMT9 as a model for ALMT channels with a monotonic I-V curve and found that the cytosolic nucleotides block and regulate *At*ALMT9. The block of *At*ALMT9 by cytosolic nucleotides is voltage dependent and in presence of cytosolic nucleotides the I-V curves becomes bell-shaped similarly to the one of the R-type/QUAC channel.

Moreover, the block by cytosolic nucleotides is modulated by the concentration and the nature of the permeable anion present at the cytosolic and the vacuolar side of the channel. The anions at the vacuolar side affect the block by cytosolic nucleotides indicating that the cytosolic nucleotides and the vacuolar anions interact within the permeation pathway of *At*ALMT9. Our data provide a new insight in the regulation of anion channels in the vacuolar membrane.

5.3 Results

Cytosolic Nucleotides Inhibit *At*ALMT9 Mediated Currents

In order to test the effect of cytosolic nucleotides on *At*ALMT9-mediated currents we performed patch-clamp experiments in excised cytosolic-side-out configuration using vacuoles extracted from *Nicotiana bentamiana* protoplasts that transiently over-expressed *At*ALMT9-GFP. Under control conditions (30 mM $malate_{cyt}$ / 100 mM $malate_{vac}$), voltage pulses starting from a holding potential of +60 mV ranging to -160 mV in -20 mV steps induced the activation of time-dependent inward malate currents (Fig 1A *top panel*; Kovermann et al., 2007; De Angeli et al., 2013; Zhang et al., 2013). When 1 mM free ATP was applied at the cytosolic side of the vacuolar membrane (30 mM $malate_{cyt}$ + 1 mM ATP_{cyt} / 100 mM $malate_{vac}$) *At*ALMT9-mediated currents were reversibly inhibited (Fig. 1A bottom), and similar results were obtained when 1 mM Mg-ATP was applied (Fig. 1C). The presence of 1 mM free ATP in the cytosolic buffer changed the I-V characteristic of *At*ALMT9 from monotonic in control conditions to non-monotonic (i.e. bell-shaped) (Fig 1A, lower panel). Notably, the inhibitory effect of free ATP was significantly higher compared to Mg-ATP (Fig. 1C) indicating that the Mg-ATP form has a lower inhibitory effect and that Mg^{2+} is not required for inhibition. The inhibition by ATP is strongly voltage dependent, being more pronounced at more negative membrane potentials. At -160 mV, the maximum membrane potential we could apply, the currents in the presence of 1 mM free ATP were reduced to 10.5 ± 1.2% of the control currents (30 mM $malate_{cyt}$ + 1 mM ATP_{cyt} / 100 mM $malate_{vac}$) (Fig. 1B, top panel). The voltage dependency of the inhibition could not be adequately described by a standard Boltzmann function at very negative membrane potentials since the inhibition does not reach 100% at any voltage. However, a modified Boltzmann function (Eq. 3 in Method) with an "offset" appropriately described the voltage dependency of the inhibition indicating that at a

given ATP concentration the inhibition never reached 100% at any applied membrane potential (Fig. 1B, top panel). The effect of cytosolic free ATP is dose dependent and also the dissociation constant for ATP (K_d^{ATP}) is a function of the membrane potential with K_d^{ATP} = 90 ± 5 µM at -160 mV (Fig. 1B, lower panel). Using the Woodhull formalism (Woodhull, 1973) to analyze the voltage dependency of K_d^{ATP} we could estimate that ATP transverse ≈ 50% of the applied membrane potential (Fig. 1B, lower panel).

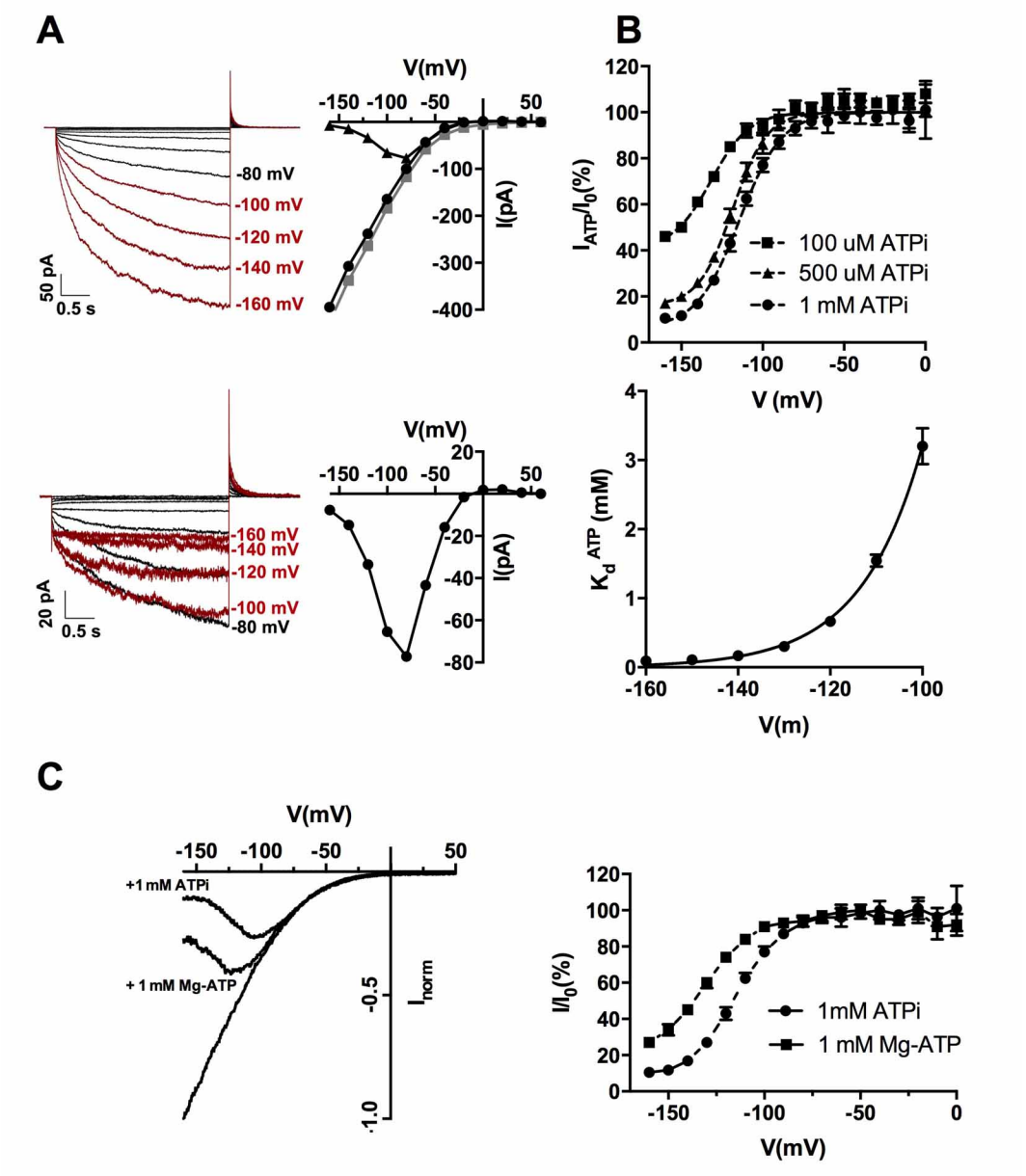

Figure 1. Cytosolic ATP blocks *At*ALMT9 mediated currents in a voltage dependent fashion.

(A) Representative traces and I-V curves of excised cytosolic-side out patches from *N. benthamiana* vacuoles overexpressing *At*ALMT9 in absence or presence of 1 mM free ATP in 30 mM cytosolic malate solution (upper: 30 mM $malate_{cyt}$ / 100 mM $malate_{vac}$, lower: 30 mM $malate_{cyt}$ + 1 mM ATP / 100 mM $malate_{vac}$). Currents were evoked in response to 3 s voltage pulses ranging from +60 mV to -160 mV in -20 mV steps, followed by a tail pulse at +60 mV. The holding potential was set at +60 mV. The grey line indicates the recovery in control cytosolic solution (30 mM $malate_{cyt}$ / 100 mM $malate_{vac}$). (B) Upper: ratio between currents recorded in the absence (I_0) and presence of various concentrations ATP_{cyt} (I_{ATP}) in the cytosolic solution containing 30 mM malate. The dash lines represent the data fitted with a modified Boltzmann equation (Eq. 3; Table 1) (n= 4~7). Lower: Voltage dependency of the dissociation constant for ATP (K_d^{ATP}) in 30 mM malate based solution. Solid line corresponds to data fitted with the Equation described by Woodhull (1973) (Eq. 1). (C) Comparison between the effects of intracellular free ATP and Mg-ATP. Left: Normalized current-voltage curves were obtained with a voltage ramp (from +60 mV to -160 mV in 1.5s) in cytosolic solution as described in A (30 mM $malate_{cyt}$ / 100 mM $malate_{vac}$) and in the presence of 1 mM free ATP (+ 1 mM ATPi) or Mg-ATP (1 mM Mg-ATP). Right: Fraction of current not blocked (I/I_0 ; mean ± SEM, n=3-7) is plotted against applied voltage for 1 mM free ATP or Mg-ATP. The dashed lines indicate the illustration of the tendency but have no theoretical meaning.

Table1. Parameters for the Boltzmann with Offset Analysis

Ionic Conditions			Parameters		
Cytosolic	Vacuolar	ATP_{cyt}/mM	$V_{1/2}$/mV	I_{unh}/%	Location
30 mM malate	100 mM malate	0.1	-131 ± 4	40 ± 7	Fig. 1B
30 mM malate	100 mM malate	0.5	-118 ± 1	16 ± 3	Fig. 1B
30 mM malate	100 mM malate	1	-114 ± 0.8	6 ± 2	Fig. 1B
50 mM malate	100 mM malate	1	-124 ± 8	2 ± 8	Fig. 2B
100 mM malate	100 mM malate	1	-135 ± 2	32 ± 5	Fig. 2B
100 mM Cl^-	100 mM Cl^-	1	- 70 ± 2	27 ± 2	Fig. 3B
100 mM Cl^-	100 mM malate	1	-121 ± 7	32 ± 11	Fig. 3B
100 mM malate	1 mM malate	1	-113 ± 2	39 ± 3	Fig. 4B
100 mM malate	10 mM malate	1	- 122 ± 4	38 ± 6	Fig. 4B
100 mM malate	100 mM Cl^-	1	- 105 ± 13	31 ± 12	Fig. 4B

I_{unh} is the minimum fraction of unblocked current by ATP, $V_{1/2}$ is the potential at which current is half blocked. Data are presented as means ± SD.

The block of *At*ALMT9-mediated currents by ATP depends on the cytosolic concentration of the conductive anion (i.e. malate). Cytosolic ATP inhibits *At*ALMT9 currents more at lower cytosolic malate concentration (Figure 2A, B). Conversely, the K_d^{ATP} is also dependent on the concentration of cytosolic malate. Reducing cytosolic malate concentrations lead to a decreased K_d^{ATP} value (Fig. 2C). The dependency of

the inhibition by cytosolic ATP on the concentration of permeable anion suggests a competition mechanism between cytosolic ATP and malate. To extrapolate whether this modulation happens in the physiological range, a K_d^{ATP} of approximately 50 µM at -160 mV could be determined for malate concentrations in the physiological range (400~ 800 µM) (Gerhardt et al., 1984; Winter et al., 1994; Farre et al., 2001). These results indicate that the modulation observed by free ATP occurs in the physiological range, since free ATP concentrations deduced from cytosolic ATP and Mg^{2+} concentrations are in the range of 30 to 100 µM (Yazaki et al., 1988).

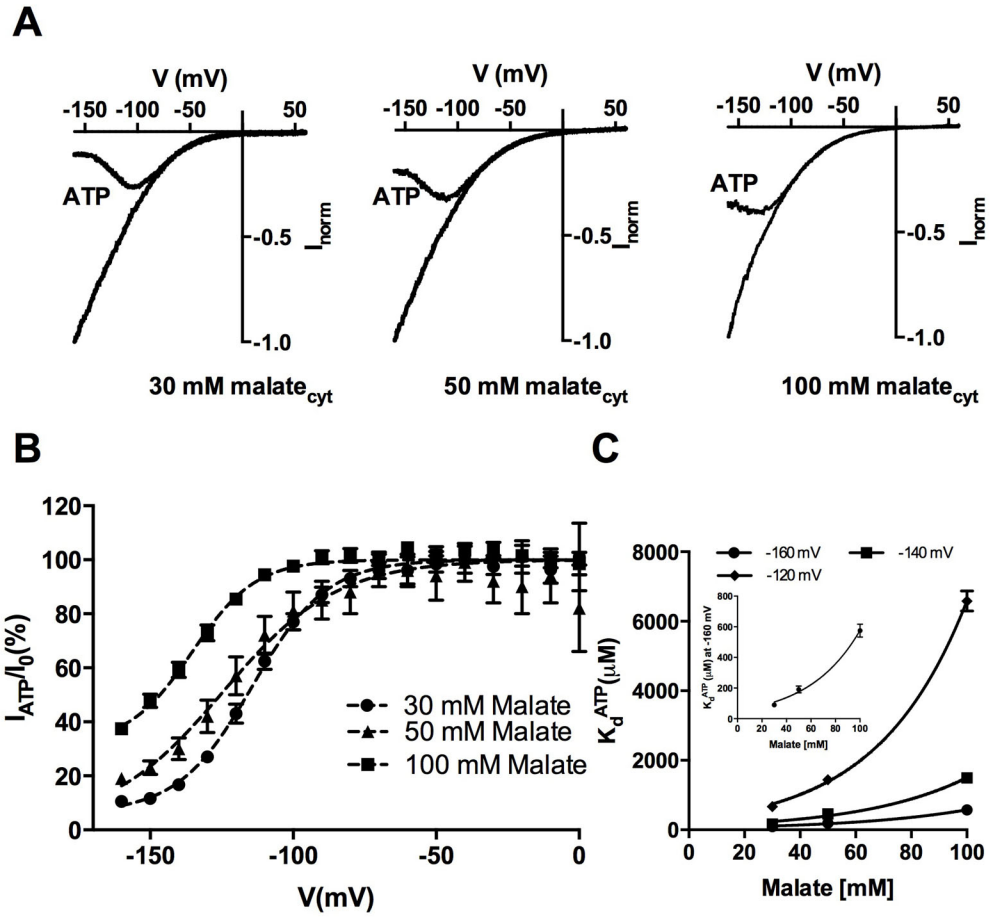

Figure 2. Intracellular ATP blocks *At*ALMT9-mediated currents by competing with cytosolic malate.

Normalized current-voltage curves were obtained with a voltage ramp (from +60 mV to -160 mV in 1.5 s) in cytosolic solution containing various concentrations of malate (30 mM, 50 mM and 100 mM $malate_{cyt}$ / 100 mM $malate_{vac}$) in the presence of 1 mM free ATP (ATP). (B) The fraction of the current that is not blocked (I_{ATP}/I_0 ; mean ± SEM, n=4-7) is plotted against applied voltage for 1 mM free ATP for different malate concentrations. The dashed lines represent the data fitted with a modified Boltzmann equation (Eq. 3; Table 1). (C) The values of K_d^{ATP} at different potentials (-120 mV, -140

mV and -160 mV) are obtained from various cytosolic malate concentrations (30, 50, 100 mM $malate_{cyt}$). Data were fitted with exponential equation (Eq. 2) with no theoretical significance to extrapolate the value of the dissociation at malate concentrations in the physiological range. The inset shows the enlargement of K_d^{ATP} at -160 mV.

The Anions in the Vacuolar Lumen Affect the Inhibition of *At*ALMT9 by Cytosolic Nucleotides

Recently, we have shown that *At*ALMT9 is also permeable to chloride and that it is involved in chloride accumulation in the vacuole (De Angeli et al., 2013). Thus, we tested the effect of free ATP on *At*ALMT9-mediated chloride currents. Similarly to what was observed when malate was the main permeable anion, 1 mM free ATP strongly inhibited *At*ALMT9-mediated chloride currents to 30 ± 4% of the ATP free conditions at -160 mV (100 mM Cl^-_{cyt} + 1mM $malate_{cyt}$ / 100 mM Cl^-_{vac}; Fig. 3). Intriguingly, the I-V curve in chloride conditions inhibited by ATP remained monotonic and did not display a bell-shaped behavior in the investigated voltage range (Fig. 3A, left). However, when chloride was the main permeable anion in the cytosolic solution and 100 mM malate was in the vacuolar buffer (100 mM Cl^-_{cyt} + 1mM $malate_{cyt}$ / 100 mM $malate_{vac}$), the inhibition effect induced by 1 mM free ATP (Fig. 3A, right) resembled the one observed in the malate based cytosolic solution (Fig. 1 and 2). Indeed, under these conditions the inhibitory effect of cytosolic ATP starts abruptly at lower membrane potentials (-60 mV). The analysis of the voltage dependency of the ATP blockade shows that the presence of malate instead of Cl^- in the vacuole shift the effect of cytosolic ATP toward more negative potentials (Fig. 3B). With a Boltzmann function the fitting of the fraction of currents not blocked versus applied voltage yielded a half inhibition voltage ($V_{1/2}$) of -69 ± 2 mV and -121 ± 7 mV with 100 mM Cl^- or 100 mM malate in the vacuole, respectively (Fig. 3B; Table 1). However, the maximal inhibition that could be obtained at hyperpolarized voltages were not dependent on the vacuolar anion, being 27 ± 2% and 32 ± 11% with Cl^- or malate in the vacuole, respectively (Fig. 3B; Table 1).

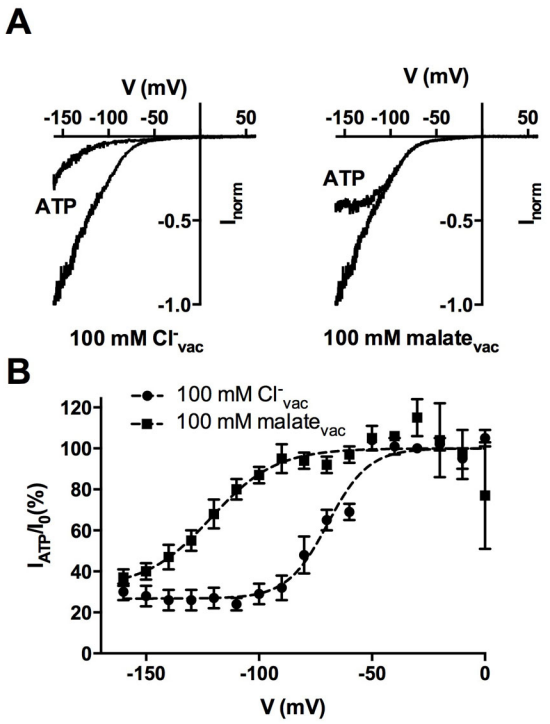

Figure 3. Intracellular ATP blocks *At*ALMT9 mediated chloride currents with different vacuolar solutions.

(A) *At*ALMT9 mediated-currents elicited by a voltage ramp (from +60 mV to -160 mV in 1.5 s, holding potential +60 mV) in cytosolic chloride based solution with the absent or present (ATP) of 1 mM free ATP. The vacuolar solutions contained 100 mM Cl^- (left) (100 mM Cl^- + 1 mM $malate_{cyt}$ / 100 mM Cl^-_{vac}) or malate (right) (100 mM Cl^- + 1 mM $malate_{cyt}$ / 100 mM $malate_{vac}$). (B) Fraction of current which is not blocked (I_{ATP}/I_0 ; mean ± SEM, n=4) is plotted against the applied membrane potential for 100 mM Cl^- or malate in the vacuolar solution. The lines represent the data fitted with a modified Boltzmann equation (Eq. 3; Table 1) yielding $V_{1/2}$ = -69 ± 2 mV (100 mM Cl^-) and $V_{1/2}$ = -121 ± 7 mV (100 mM malate).

In order to evaluate whether the effect of vacuolar malate affect ATP inhibition when malate was present at the cytosolic site we used a cytosolic solution containing 100 mM malate and varied the vacuolar concentration of malate. When the concentration of malate was progressively raised in the vacuolar solution (1 mM $malate_{vac}$ + 99 mM MES_{vac}, 10 mM $malate_{vac}$ + 90 mM MES_{vac}, 100 mM $malate_{vac}$) the ATP block was shifted to more negative membrane potentials (Fig. 4B). Moreover, when the vacuolar malate was completely replaced by Cl^- (100 mM $malate_{cyt}$ / 100 mM Cl^-_{vac}), 1 mM free ATP exhibited a similar inhibition as under cytosolic Cl^- conditions (100 mM Cl^-_{cyt} / 100 mM Cl^-_{vac}). The fit of the I_{ATP}/I_0 versus the applied voltage with a modified Boltzmann function (Eq. 3) provided a $V_{1/2}$ = -113 ± 2 mV, -123 ± 4 mV, -135 ± 2 mV and -105 ± 13 mV with 1mM, 10 mM, 100 mM malate or 100 mM Cl^- in the

vacuole, respectively (Fig. 4B; Table 1). These results show that the permeable anions in the vacuole affect the inhibition behavior of cytosolic ATP on *At*ALMT9. Thus, this suggests that cytosolic ATP and vacuolar malate interact within the conduction pathway of *At*ALMT9 at the cytosolic side.

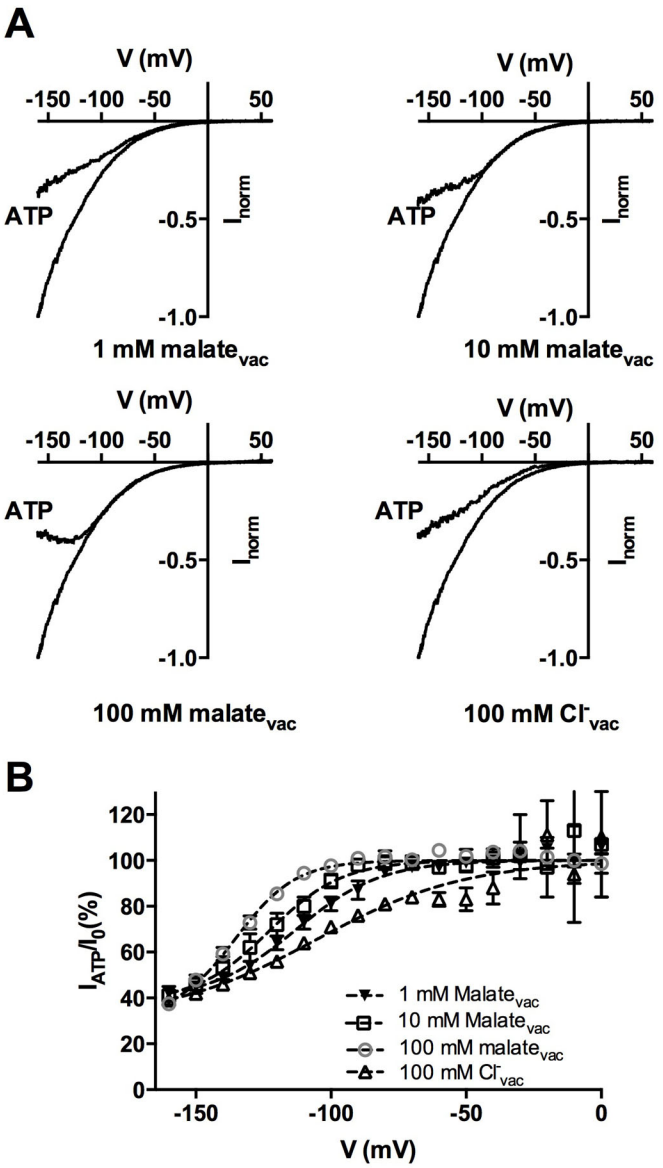

Figure 4. Intra-vacuolar malate removes the block of cytosolic ATP.

(A) Currents elicited by a voltage ramp (from +60 mV to -160 mV in 1.5 s, holding potential +60 mV) in malate based cytosolic solution with vacuolar solutions containing 100 mM Cl^- (100 mM $malate_{cyt}$ / 100 mM Cl^-_{vac}) or various concentration of malate: 1 mM malate (100 mM $malate_{cyt}$ / 1 mM malate + 99 mM MES_{vac}), 10 mM malate (100 mM $malate_{cyt}$ / 10 mM malate + 90 mM MES_{vac}), 100 mM malate (100 mM $malate_{cyt}$ / 100 mM $malate_{vac}$), in the absence or the presence (ATP) of 1 mM free ATP in cytosolic solution. (B) Ratios ($I_{ATP}/I_{0,}$ mean ± SEM, n=5-7) between currents recorded in the absence

(I_0) and presence of 1 mM ATP_{cyt} (I_{ATP}) in cytosolic solution that contains 100 mM malate with different solutions in the pipette. The solid lines represent the data fitted with a Boltzmann with an offset equation (Eq. 3; Table 1).

The Inhibition of *At*ALMT9 by Cytosolic Nucleotides does not Require ATP Hydrolysis

Our data show that *At*ALMT9 is inhibited by cytosolic ATP in a dose and voltage dependent way, suggesting that the nucleotide directly block the pore of *At*ALMT9. However, in order to definitively exclude the possibility that the effect of ATP is based on a phosphorylation/dephosphorylation, we used a non-hydrolysable analogue of ATP, AMPPNP. In the presence of 1 mM ATP or AMPPNP in the cytosolic solution (100 mM $malate_{cyt}$ + 1 mM ATP or $AMPPNP_{cyt}$ / 100 mM $malate_{vac}$), the amplitudes of the malate currents at -160 mV were reduced to 37.4 ± 2.2 % and 26.0 ± 3.0 %, respectively (Fig. 5A). The fact that AMPPNP showed an even stronger inhibitory effect compared to ATP demonstrates that no phosphorylation of *At*ALMT9 occurs. We further analyzed the relative importance of the polyphosphate and nucleoside moieties in the block of *At*ALMT9-mediated currents. We found that the progressive reduction of the number of phosphate groups, and thus of negative charges, strongly impacted the inhibitory effect of the nucleotides with ADP being less efficient than ATP (I_{ADP}/I_{ctrl} = 56 ± 2% at -160 mV) and AMP even less (I_{AMP}/I_{ctrl}=90 ± 1% at -160 mV) (Fig. 5A). Differently, the nucleoside part seems to have a marginal role since 1 mM free GTP showed an effect similar to ATP (I_{GTP}/I_{ctrl}=48 ± 2% at -160 mV; Fig. 5A). These data suggest that the number of charges carried by the nucleotide are fundamental for the block of *At*ALMT9-mediated currents. Previously, we found that Lysine 193 (K193) is part of the permeation pathway of *At*ALMT9 and its mutation (K193E) affects both anion permeation rectification and the efficacy of citrate to block the currents (Zhang et al., 2013). Thus, in an attempt to find a site of interaction of ATP with the channel, we tested whether the mutation of K193 impacted the ATP blockade. We found that the currents mediated by the $AtALMT9_{K193E}$ variants were completely insensitive to 1 mM free ATP in the cytosolic-side solution (100 mM malate + 1mM ATP_{cyt} / 100 mM $malate_{vac}$; Fig. 5B). These data suggest that cytosolic nucleotides interact with the residue K193 and that the blocking mechanism was similar to the one observed

previously for citrate. Therefore, ATP is likely to block *At*ALMT9 mediated currents by obstructing the pore of *At*ALMT9.

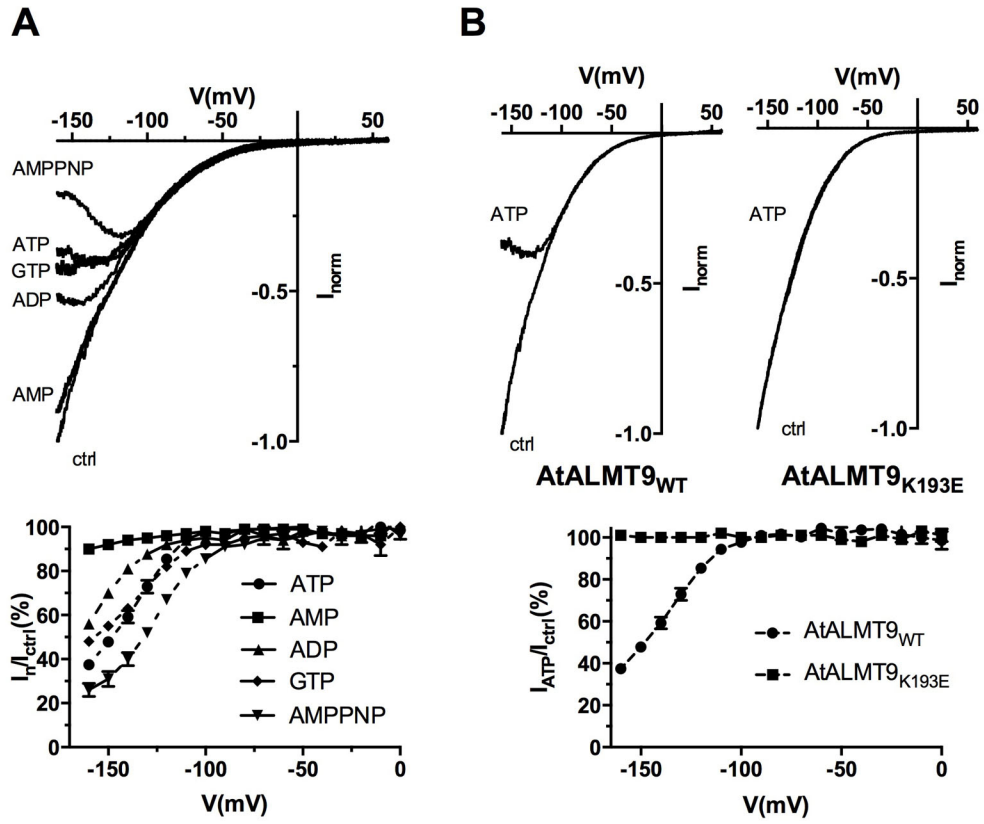

Figure 5. Effect of the non-hydrolysable nucleotide AMPPNP and of different cytosolic nucleotides on *At*ALMT9 mediated malate currents.

(A) Upper panel: Representative I-V curves obtained with a ramp (from +60 mV to -160 mV in 1.5 s, holding potential +60 mV) in control solution (ctrl: 100 mM $malate_{cyt}$ / 100 mM $malate_{vac}$) and in the presence of 1 mM different nucleotides (100 mM $malate_{cyt}$ + 1 mM ATP, ADP, AMP, GTP or $AMPPNP_{cyt}$ / 100 mM $malate_{vac}$). Lower panel: mean ratios between currents in presence of 1 mM different nucleotides (I_n) and control solution (I_{ctrl}) at different membrane potentials (n= 4~7). (B) I-V curves and mean ratios, as described in (A), are obtained with a voltage ramp (from +60 mV to -160 mV in 1.5 s) measured in excised cytosolic-side out patches from vacuoles overexpressing $AtALMT9_{WT}$ (n=7) and $AtALMT9_{K193E}$ (n=6) in the presence of 1 mM ATP in the control solution (100 mM $malate_{cyt}$ / 100 mM $malate_{vac}$). The dashed lines indicate the tendency but have no theoretical meaning. Error bars denote s.e.m.

5.4 Discussion

ALMTs form a family of anion channels that are important in different aspects of plant physiology. Among different ALMTs, *At*ALMT9 is the first member of the family which is localized to the vacuolar membrane (Kovermann et al., 2007). Recently, it was shown that *At*ALMT9 acts as a malate activated chloride channel in the tonoplast, playing an important role in stomatal opening (De Angeli et al., 2013). A further study provided evidence that *At*ALMT9 forms tetramers and a region possible forms the permeation pathway (Zhang et al., 2013). Since the I-V characteristic is a fundamental property of ion channels, in the present work we aimed to find a reason for the different I-V characteristic displayed by different members of the ALMT family. *At*ALMT1 and *At*ALMT9 display a monotonic and moderately voltage dependent inward rectifying I-V characteristics (Hoekenga et al., 2006; Kovermann et al., 2007). Differently, *At*ALMT12/QUAC1 displays an I-V characteristic that presents a strong voltage dependency at very negative membrane potentials and a bell shape (Meyer et al., 2010b). Earlier studies on *Arabidopsis* hypocotyl protoplasts showed that cytosolic ATP regulates the R-type currents (Thomine et al., 1997; Colcombet et al., 2001). Thus, a model of the R-type channel which is gated by the cytosolic nucleotides was proposed. The vacuolar localization of *At*ALMT9 appears to be very convenient since it allows the reversible application of nucleotides on the cytosolic side of the membrane, enabling to directly probe the effect of nucleotides on I-V characteristic of *At*ALMT9.

The main result we present in this work is that cytosolic nucleotides reversibly inhibit *At*ALMT9-mediated currents and that in presence of cytosolic nucleotides the I-V characteristic of *At*ALMT9 changes from monotonic to bell shaped (Fig. 1). In other terms the presence of ATP in the cytosolic solution is sufficient to make *At*ALMT9 display the same bell-shaped I-V characteristic as *At*ALMT12/QUAC1. This intriguing result suggests that the typical bell-shaped I-V characteristic is not a unique property of this clade of the ALMT family and that it does not result from an intrinsic voltage sensor in the ion channel protein. The understanding of the voltage dependency of *At*ALMT9 and *At*ALMT12 is relevant because of their roles in regulating stomatal movement (Meyer et al., 2010b; De Angeli et al., 2013). Our data indicate that the effect of ATP on *At*ALMT9 currents does not rely on a

phosphorylation mechanism but directly by blocking the permeation pathway of the channel. Indeed, the non-hydrolysable ATP analogue AMPPNP is able to block *At*ALMT9 mediated currents. Moreover, several lines of evidence point at an "open-channel block" mechanism. i) The effect is voltage dependent and more pronounced at negative voltages at which the channels' open probability is higher; ii) the dissociation constant (K_d^{ATP}) is voltage dependent, indicating that ATP enters the transmembrane electrical field; iii) the current is more noisy at membrane potentials at which ATP is effective (Fig. 1A); iv) ATP and the permeating anion compete since the K_d^{ATP} becomes lower when malate concentrations decrease (Fig. 2C). It is interesting to note that this is in line with the nucleotide-dependent gating mechanism of the R-type/QUAC channel in the plasma membrane proposed by Colcombet et al. (2001). Moreover, our results provide a strong molecular basis to interpret these findings by the identification of K193 as possible interaction site of ATP with *At*ALMT9 (Fig. 5B). Notably, in a previous study we found K193 to be part of a putative pore forming region (Zhang et al., 2013), further supporting the idea that ATP interacts with the pore region of *At*ALMT9.

Since the inhibition of *At*ALMT9 by ATP in malate based solutions transform the I-V curve of this channel from monotonic to bell shaped, similar to the one of R-type channels, our data support the idea that *At*ALMT12/QUAC1 is gated by cytosolic nucleotides and that the typical I-V characteristic of this channel comes from this voltage dependent block. It has to be noted that in all the situations in which the *At*ALMT12/QUAC1 has been measured ATP was present in significant amounts in the cytosolic solution (Meyer et al., 2010b). Moreover, the only attempt to remove ATP from the cytosolic solution revealed a change of the bell-shaped I-V characteristic to monotonic one (Colcombet et al., 2001). As a corollary our data also provide a simple and straightforward interpretation of a phenomenon that R-type currents are activated by extracellular malate (Hedrich and Marten, 1993; Raschke, 2003; Mumm et al., 2013). In this work we found that vacuolar malate (which correspond in our configuration to extracellular malate) is able to release the ATP block (Fig. 3, Fig. 4), consequently inducing an activation of the *At*ALMT9 currents. Thus, the malate activation of *At*ALMT12/QUAC1 would result from a release of ATP induced by the presence of extracellular malate.

It is interesting to address the question whether the ATP block of *At*ALMT9 currents can be relevant in a physiological context. Even if presently our data do not directly answer this question we can try to insert them in a physiological framework. Recently, we have shown that *At*ALMT9 is important in guard cells function for stomatal opening (De Angeli et al., 2013). Indeed, during stomatal opening *At*ALMT9 drives the influx of anions into the vacuole. The influx of anion via *At*ALMT9 is driven by hyperpolarized vacuolar membrane potentials which are maintained through H^+-ATPases (Gaxiola et al., 2007; Duby and Boutry, 2009; Palmgren and Nissen, 2011). During stomatal opening the high hydrolytic activity of the proton pump consumes ATP, decreasing its concentration in the cytosol. Subsequently, ATP is converted into AMP (Gout et al., 1992; Xia et al., 1995) which is nearly inactive in blocking *At*ALMT9 meditated anion currents. Thus, a drop of cytosolic ATP levels could induce a release of the *At*ALMT9 blockage and consequently facilitate anion accumulation in the vacuole. In addition, the accumulation of malate in the vacuolar lumen, which is known to occur in parallel to chloride accumulation, is also able to remove the ATP blockade (Fig. 3, Fig. 4). This blockade release consequently facilitate anion uptake into the vacuole. Therefore, both cytosolic and vacuolar malate can regulate *At*ALMT9 activity with a direct activation (De Angeli et al., 2013) and a release of ATP block, respectively. It is interesting to note that *At*ALMT9 is the second vacuolar anion transporter after *At*CLCa (De Angeli et al., 2009b) whose activity is inhibited by cytosolic ATP. This further suggests that regulation of vacuolar anion transporters and channels activity by cytosolic ATP has a physiological relevance.

5.4 Methods

Electrophysiology

Mesophyll protoplasts from *At*ALMT9-GFP overexpressing tobacco leaves were isolated by enzymatic digestion. The enzyme solution contained 0.3 % (w/v) cellulase R-10, 0.03 % (w/v) pectolyase Y-23, 1 mM $CaCl_2$, 500 mM sorbitol and 10 mM MES, pH 5.3, 550 mOsm. Protoplasts were washed twice and resuspended in the same solution without enzymes. Vacuoles were released from mesophyll protoplast by the

addition of 5 mM EDTA and a slight osmotic shock (500 mOsm, see medium below). Transformed vacuoles exhibiting an *At*ALMT9-GFP signal were selected using an epifluorescence microscope. Membrane currents from tonoplast patches were recorded in the excised cytosolic-side out configuration with the patch-clamp technique as described elsewhere (De Angeli et al., 2013). The procedure to perform patch clamp experiments is the same as described in the former work (Zhang et al., 2013).

The cytosolic solution contained (i) 100 mM malic acid, adjusted to pH 7.5 with BTP (Bis-Tris-Propane), ii) 30, 50, 100 mM malic acid, supplemented with nucleotides as indicated, adjusted to pH 7.5 with BTP and iii) 100 mM Cl^-, supplemented with nucleotides as indicated, adjusted to pH 7.5 with BTP. The osmolarity was adjusted to 500 mOsm using sorbitol. The pipette solution contained i) 112 mM malic acid, 5 mM HCl and was adjusted with BTP to pH 6. ii) 10 mM malic acid, 90 mM MES, 5 mM HCl and was adjusted with BTP. iiI) 1 mM malic acid, 99 mM MES, 5 mM HCl and was adjusted with BTP. iv) 100 mM HCl and was adjusted with BTP to pH 6. The osmolarity was adjusted to 550 mOsm using sorbitol. The ionic condition of (i) of cytosolic solution and (i) of the pipette solution is defined as control solution (ctrl). All chemicals were purchased from Sigma-Aldrich. Liquid junction potentials were measured according to Neher (1992) and corrected when higher than ±2 mV.

To estimate the fraction of the electrical field that ATP traverses to reach its binding site in Fig. 1B, the voltage-dependent dissociation constant relationship was fitted with the equation described by Woodhull (1973):

$$K_d^{ATP}(V_m) = K_d^{ATP}(0) \cdot e^{\frac{z\delta FV}{RT}} \quad (1)$$

in which $K_d^{ATP}(\mathrm{V_m})$ is the voltage-dependent dissociation constant of ATP, $K_d^{ATP}(0)$ the dissociation constant of ATP at 0 mV, V_m the transmembrane potential, z the valence of the blocker (-4 for ATP at pH=7.5), δ the fraction of the electrical membrane field traversed by the blocker, and F, R, and T the Faraday constant, gas constant and absolute temperature, respectively.

To estimate whether ATP inhibits *At*ALMT9 mediated current in the physiological range concentration, the dissociation constant in different malate concentrations (Fig. 2C) were fitted with an Exponential equation in the form of:

$$K_d^{ATP}([\mathrm{MA}])=K_d^{ATP}(0)e^{[MA]} \quad (2)$$

where $K_d^{ATP}([MA])$ is the malate concentration dependent dissociation constant of ATP, $K_d^{ATP}(0)$ is the dissociation constant of ATP at 0 mM malate. *[MA]* is the cytosolic malate concentration.

The fraction of current not blocked by a non-permeable blocker ATP in Fig. 1B, Fig. 2B, Fig. 3B and Fig. 4B is fitted by a Boltzmann function with an offset:

$$\frac{I}{I_0}=I_{unh}+\frac{100-I_{unh}}{1+e^{\frac{V_{1/2}-Vm}{RT/zF}}} \quad (3)$$

Where *I* is the current amplitude in the presence of ATP, I_0 is the current amplitude in a solution without ATP, I_{unh} is the minimum fraction of unblocked current by ATP, $V_{1/2}$ is the potential at which current is half blocked, *Vm* is the membrane potential, *z* is the valence of the blocker, *F*, *R*, and *T* the Faraday constant, gas constant and absolute temperature, respectively. Experiments were performed at room temperature (22-25 °C).

Nucleotides

Adenosine-5'-triphosphate (ATP) was tested either as a Mg^{2+} chelate or as a Tris salt (free ATP as indicated). The Adenosine-5'-phosphate (AMP) and Adenosine-5'-diphosphate (ADP) were tested as sodium salt. 5'-adenylylimidodiphosphate (AMPPNP) was Li^{3+} salt. Guanosine-5'-triphosphate (GTP) was tris salt. All the nucleotide were purchased from Sigma-Aldrich.

6. Result Chapter IV

Preliminary Results of *At*ALMT4

6.1 Introduction

Most fully developed plant cells contain a large central vacuole that can occupy more than 90% of the total cell volume. Such a large vacuole has a large storage capacity and plays a central role in cell homeostasis and metabolism. However, to fulfill these tasks, it needs the involvement of transporters that allow the exchange of nutrients and solutes across the vacuolar membrane. Among them, members of ALMT family have been identified and well characterized (Sasaki et al., 2004; Hoekenga et al., 2006; Kovermann et al., 2007; Pineros et al., 2008; Meyer et al., 2010b; Meyer et al., 2011).

The ALMT family of membrane proteins is exclusive to plants and no homologues exist in other eukarya, bacteria and archea. ALMTs have been found to exhibit different important physiological roles in plants, varying from detoxifying aluminum through extrusion of organic acids into the soil, to mediating anion fluxes through the plasma and vacuolar membrane of guard cells to regulate stomatal movements (Sasaki et al., 2004; Hoekenga et al., 2006; Meyer et al., 2010b; De Angeli et al., 2013). In *Arabidopsis thaliana*, the ALMT family consists of 14 members which can be grouped into three clades (Kovermann et al., 2007). The ALMT members that belong to clade II are thought to be localized in the vacuolar membrane. *At*ALMT9 was the first vacuolar ALMT identified and characterized in *Arabidopsis thaliana* (Kovermann et al., 2007). Studies with T-DNA insertion lines and electrophysiological characterization indicated that *At*ALMT9 is a vacuolar anion channel mediating the load of malate and fumarate into *Arabidopsis thaliana* mesophyll cells (Kovermann et al., 2007). In the first result chapter of this thesis, *At*ALMT9 was shown to also play a crucial role in guard cells in which the protein functions as a malate-activated chloride channel involved in stomata opening. Further studies in the second result chapter of this thesis unveiled structural details of *At*ALMT9 and a region involved in forming the pore. Moreover, *At*ALMT9 was shown to be a multimeric channel composed of probably four subunits. In this multimer, each monomer participates in forming the pore.

The second vacuolar membrane-targeted ALMT of clade II that was characterized is *At*ALMT6 (Meyer et al., 2011). *At*ALMT6 is expressed in guard cells and flower tissue and displays inward-rectifying malate current when overexpressed in guard cell

vacuoles. Interestingly, micromolar concentration of cytosolic calcium were required to activate *At*ALMT6-mediated malate currents. The threshold of this activation is regulated by the vacuolar pH and cytosolic malate. The co-modulation of these two parameters determines the functions of *At*ALMT6 as a malate influx or efflux channel. Although *At*ALMT6 has been identified as the first vacuolar malate channel of *Arabidopsis* guard cells, no stomatal phenotype had been observed in *At*ALMT6 knock-out mutants.

In this chapter, another vacuolar targeted *At*ALMT was identified and characterized. The *At*ALMT4 protein is targeted to the vacuolar membrane and *AtALMT4* is highly expressed in the leaves and roots. Electrophysiological analysis demonstrated that *At*ALMT4 is permeable to malate. The *Arabidopsis thaliana atalmt4* knock-out mutants exhibited an impairment of drought tolerance compared to wild-type plants. Together, these findings suggest that *At*ALMT4 may potentially play a role in regulation stomata movement.

6.2 Results

*At*ALMT4 is Localized in the Tonoplast

A phylogenetic analysis revealed that *At*ALMT4 (At1g25480) belongs to clade II, in which *At*ALMT9 and *At*ALMT6 have been identified to be vacuolar anion channels in *Arabidopsis* (Kovermann et al., 2007; Meyer et al., 2011; De Angeli et al., 2013). Based on these reports, *At*ALMT4 was hypothesized to have the same subcellular localization. In order to test this hypothesis, a construct was generated, in which the green fluorescence protein (GFP) was fused to the C-terminus of *At*ALMT4 protein in the pART27 vector (Gleave, 1992). Transient expression of this fusion protein in *N. benthamiana* under the control of the 35S promoter was achieved using Agrobacterium-mediated leaf transformation. Confocal laser scanning microscopy analysis of vacuoles extracted from transiently transformed tobacco mesophyll protoplasts revealed that *At*ALMT4 is targeted to the vacuolar membrane (Fig. 1a) as *At*ALMT6 and *At*ALMT9 in *Arabidopsis*.

Tissue specific Expression Analysis of *At*ALMT4

To investigate the detailed tissue expression pattern of *AtALMT4*, we made use of the Genevestigator database (https://www.genevestigator.com/gv/). These data indicated that *AtALMT4* is expressed in seeds, leaves and flower tissues in *Arabidopsis*. However, no data are available on roots. In order to verify these data, *Arabidopsis* plants were transformed with the *β-glucuronidase* (GUS) gene under the control of a 1836bp genomic region of the *At*ALMT4 promoter upstream of the start codon. Microscopic analysis of the transgenic plants showed that strong GUS activity was detected in root tissues 3 and 4 days after germination. No appreciable signal could be detected in leaves until 5 days after germination (Fig. 1b). Taken together, these observations not only confirm the microarray gene expression data, but also suggest that *AtALMT4* expression is strong in roots.

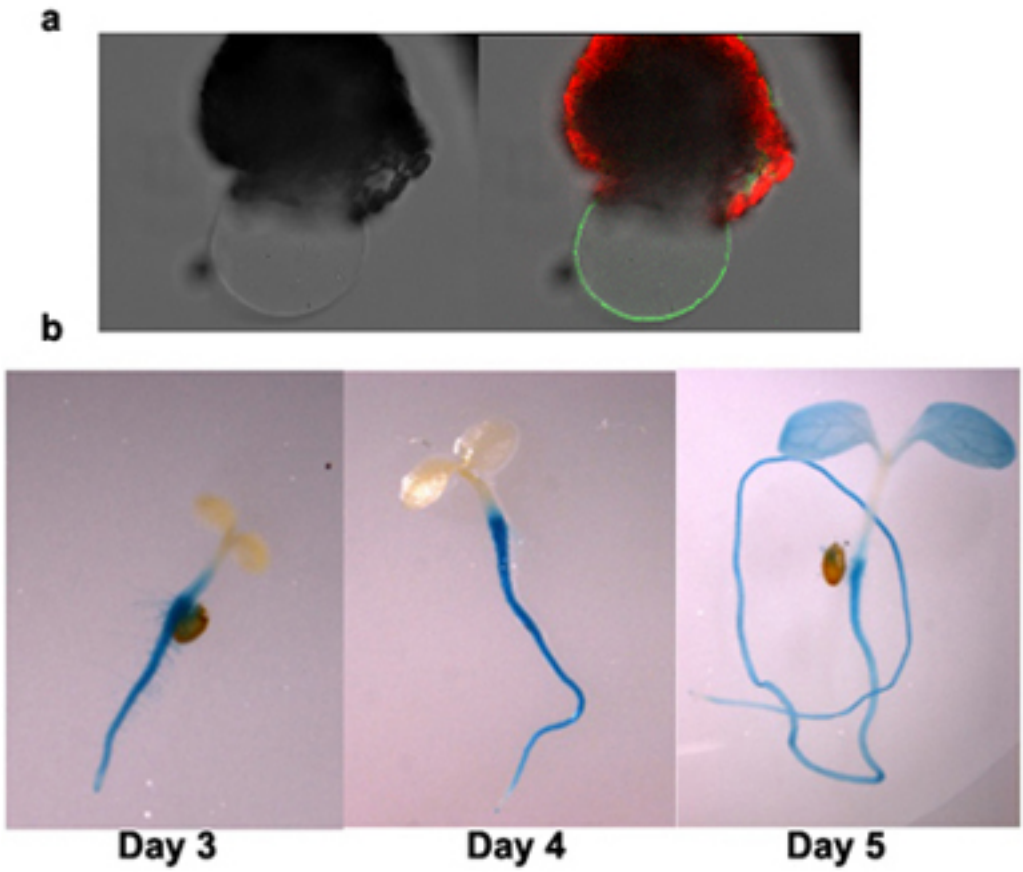

Figure 1. Intracellular localization and tissue specific expression of *At*ALMT4.

(a) Fluorescence (right) and transmission (left) images of vacuoles released from lysed tobacco mesophyll protoplasts transiently overexpressing *At*ALMT4-GFP. The GFP fluorescence (green) and

chlorophyll autofluoresence (red) demonstrated that *At*ALMT4-GFP was localized in the vacuolar membrane. (b) Seedlings of *Arabidopsis* expressing GUS under the control of *At*ALMT4 promoter were subjected to GUS staining and subsequent EtOH destaining 3, 4 and 5 days after germination. The blue color indicates the expression of *AtALMT4-promoter::GUS*.

*At*ALMT4 is Permeable to Malate

The fact that *At*ALMT4-GFP is localized in the vacuolar membrane allowed the application of the patch-clamp technique to characterize its channel properties. In order to verify whether *At*ALMT4 is permeable to malate, the electrophysiological experiments were performed on isolated vacuoles from transiently transformed tobacco (*Nicotiana benthamiana*) protoplasts that overexpressed *At*ALMT4-GFP. In symmetric ionic conditions (100 mM $malate_{cyt}$ / 100 mM $malate_{vac}$), patches in the cytosolic-side-out excised configuration displayed malate currents with time-dependent relaxation kinetics (Fig. 2a) similar to those observed for *At*ALMT9 (Kovermann et al., 2007; result chapter I of this thesis) and *At*ALMT6 (Meyer et al., 2011). The mean amplitude of *At*ALMT4 mediated malate currents under these ionic conditions was -501 ± 94 pA at a membrane potential of -120 mV, while the mean amplitude from untransformed vacuoles was -66 ± 36 pA at -120 mV (Fig. 2b). These results suggest that *At*ALMT4 may be capable of mediating the fluxes of malate across the vacuolar membrane.

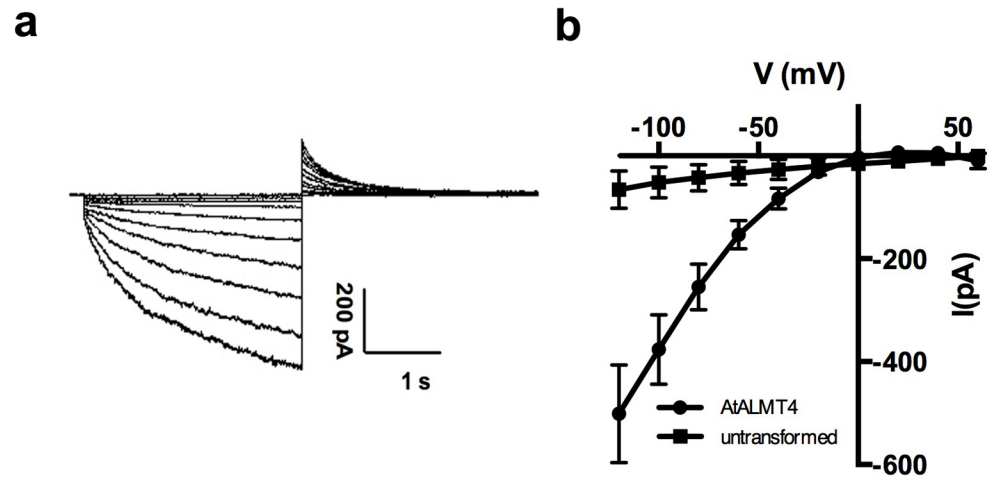

Figure 2. *At*ALMT4 mediates malate currents across the tonoplast.

(a) A current trace from excised cytosolic-side-out patches obtained from *At*ALMT4-GFP overexpressing tobacco vacuoles in symmetric malate conditions (100 mM $malate_{cyt}$ / 100 mM $malate_{vac}$). Currents were elicited with 3 s voltage pulses ranging from + 60 mV to -120 mV in -20 mV steps, followed by a 4 s tail pulse at +60 mV, the holding potential was set to + 60 mV. (b) Mean current-voltage curves of malate currents obtained from *At*ALMT4-GFP overexpressing (n=10) and untransformed tobacco vacuoles (n=3) (Error bars represent SD).

Analysis of *At*ALMT4 Knock-out Lines

In order to investigate the physiological functions of *At*ALMT4, two independent knock-out lines of *At*ALMT4, *atalmt4-1* and *atalmt4-2*, were obtained. By sequencing, the insertion was verified to reside in the first and third exon of *At*ALMT4 in *atalmt4-1* and *atalmt4-2*, respectively (Fig. 3a). Homozygous plants were identified by genotyping through PCR with different combination of appropriate primers and the absence of *At*ALMT4 transcript in the homozygous plants were verified by RT-PCR (Fig. 3b).

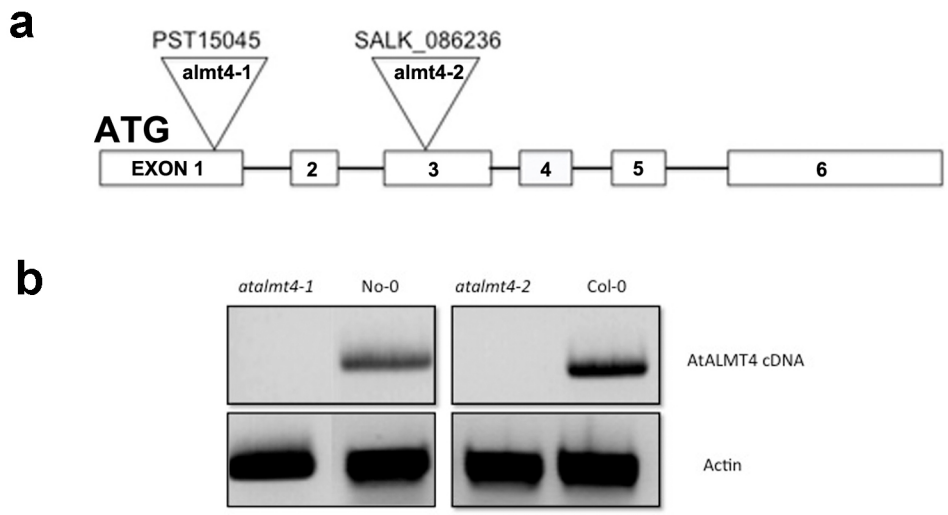

Figure 3. Two knock-out lines of *At*ALMT4.

(a) The position of insertion of two knock-out line in *At*ALMT4 genomic DNA. The insertion site is located in the first and third exon in *atalmt4-1* and *atalmt4-2*, respectively. (b) Semi quantitative RT-PCR analysis of *At*ALMT4 transcript in *At*ALMT4 knock-out lines and corresponding wild-type plants. The transcript of actin is shown as a control.

Since *At*ALMT6, 9 and 12 were identified to be expressed in guard cells and two of them (*At*ALMT9 and *At*ALMT12) are involved in stomatal movement, stomata opening assays were performed subsequently on epidermal strips from these two independent *atalmt4* knock-out lines. Epidermal strips were incubated in the light in 30 mM KCl solution (10 mM MES-KOH, 30 mM KCl, pH=5.7) for 2 hours and the stomatal aperture of *atalmt4* knock-out lines and wild-type plant was measured. Fig. 4a shows that the stomatal aperture values for *atalmt4* knock-out lines and their corresponding wild-types. Stomatal apertures of *atalmt4-1* and *atalmt4-2* were 30 ± 8% and 16 ± 10% larger than those of the corresponding wild-type plants (Fig. 4a). Interestingly, the *atalmt4-1* knock-out line also exhibited decreased drought tolerance compared to the corresponding wild-type plants (Fig. 4b), while in *atalmt4-2* mutant lines this phenotype was also visible but not statistically significant (data not shown). 20 days after the last watering, plants of the *atalmt4-1* knock-out line had 39 ± 5% less relative water content than the corresponding wild-type plants, while *atalmt4-2* plants displayed a decrease of 8 ± 4%, however this difference was not statistically significant (Fig. 4c). The difference in severity of drought stress response between the two knock-out lines may be due to their different ecotype background, namely Nossen-0 and Columbia-0 for *atalmt4-1* and *atalmt4-2*, respectively. Taken together, these results suggest that *At*ALMT4 may function in regulation of stomatal movement and may impact on the plant's water use efficiency.

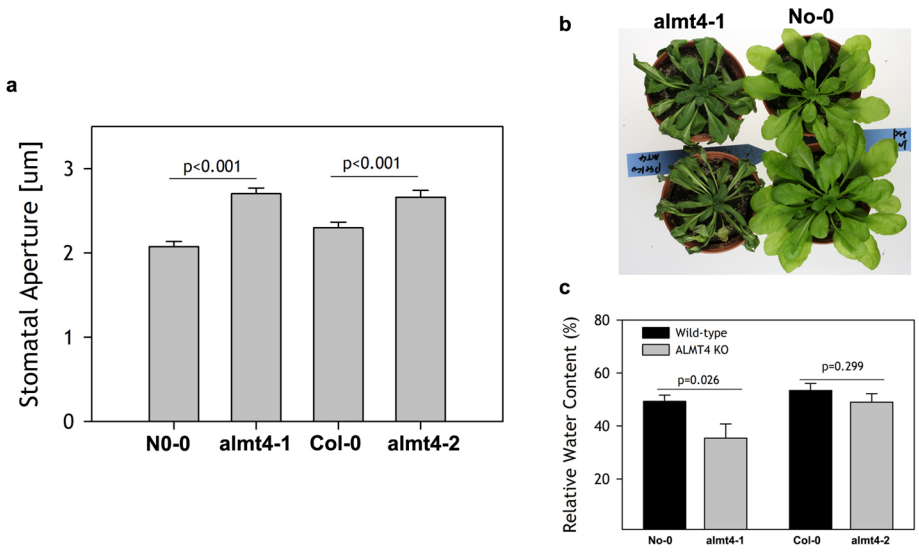

Figure 4. *At*ALMT4 is involved in stomatal movement in *Arabidopsis*.

(a) Stomatal aperture of *atalmt4-1* and *atalmt4-2* mutants and the corresponding wild-type plants measured using stripped epidermis layers. Measurements from three independent plants were performed after 2 hours of incubation in 30 mM KCl buffer in white light (n=100 stomata). *At*ALMT4 knock-out plants displayed an increased aperture compared to the corresponding wild-type plants, a difference that is statistically significant at the p<0.001 level (Student's *t-test*). (b) *atalmt4-1* mutants are more sensitive to drought stress. 20 days after watering, the wild-type plants were still turgescent, while *atalmt4-1* mutants were wilted. (c) Relative water content (RWC was calculated with the following equation: RWC=(FW-DW)/FW, whereby FW is fresh weight and DW is dry weight) in wild-type and *atalmt4* mutant plants. The bar chart shows the relative water content of *atalmt4-1, atalmt4-2* and the corresponding wild-type plants 20 days after stopping watering. (p values present Student's *t-test*).

6.3 Discussion

In *Arabidopsis*, the ALMT family consists of 14 members that can be grouped into three clads (Kovermann et al., 2007). Clade II consists of 5 members (*At*ALMT3, 4, 5, 6, 9), two of which have been well characterized and found to being localized in the vacuolar membrane (Kovermann et al., 2007, Meyer et al., 2011; result chapter I of this thesis). In this chapter, a further member of clade II, *At*ALMT4, was preliminarily characterized. The analysis of the GFP fusion protein showed that *At*ALMT4 is localized in the vacuolar membrane (Fig. 1a), which was reminiscent of the vacuolar membrane localization of *At*ALMT6 and *At*ALMT9. The expression pattern of *AtALMT4* that showed an expression in both shoots and roots (Fig. 1b), was similar to

that of *AtALMT9* but different to that of *AtALMT6*, which is not expressed in roots (Meyer et al., 2011). Moreover, the observation that *AtALMT4* was exclusively expressed in roots in the first three days after seeds germination implies that *At*ALMT4 may have a defined physiological role in this developmental stage of the root. However, in order to verify this hypothesis, further studies need to be conducted.

As in previous studies on *At*ALMT6 and *At*ALMT9, excised cytosolic-side-out patches on *At*ALMT4 overexpressing tobacco vacuoles also showed malate inward currents into the vacuole, in a fashion similar to *At*ALMT6 and *At*ALMT9 (Fig. 2). However, the mean amplitude of malate currents mediated by *At*ALMT4 was only one third of that observed for *At*ALMT9. This indicates that *At*ALMT4 transports malate less efficiently than *At*ALMT9. This may be due either to the fact that *At*ALMT4 has a lower open probability or has a less conductive single channel. Another possibility for that difference might be that due to the vacuole isolation procedure, putative regulators of *At*ALMT4 in the cytosol are missing. Interestingly, *At*ALMT4 exhibited a large time constant of the tail currents relaxation kinetics that was almost 10 times larger than that of *At*ALMT9 (Cornelia Eisenach, personal communication). This indicates that once activated, *At*ALMT4 channels closed much more slowly than *At*ALMT9. Alternatively, *At*ALMT4 may have the potential function to transport malate out of vacuole. Moreover, by contrast to *At*ALMT9, *At*ALMT4 does not transport inorganic anions like Cl^-, NO_3^-, phosphates (HPO_4^{3-} and $H_2PO_4^{2-}$) and SO_4^{2-} (Cornelia Eisenach, personal communication). This difference in substrate selectivity between *At*ALMT4 and *At*ALMT9 suggest that *At*ALMT4 may play an important role in cytosolic malate homeostasis. To investigate different properties of gating and selectivity between *At*ALMT9 and *At*ALMT4, further structural studies need to be conducted on *At*ALMT4.

The dicarboxylic acid malate is an important plant metabolite. The transport of malate by tonoplast-intrinsic anion channels and transporters facilitates the vacuolar malate uptake and release, which is crucial for the regulation of stomatal movement. Functional deletion of *At*ALMT4 caused an increased stomatal aperture and sensitivity to drought stress (Fig. 4). These phenotypes might be attribute to the reduced release of malate from the vacuole during the stomatal closure process. This, in turn, would cause increased osmotic potentials hampering stomatal closure. Furthermore, functional deletion of *At*ALMT4 in Nossen-0 background knock-out

lines caused decreased drought tolerance, while that in Columbia-0 background was not significantly different (Fig. 4). The different observations between the two ecotype background mutants indicate that *At*ALMT4 may function in the malate release from vacuoles and be further involved in drought stress tolerance probably under certain environmental conditions.

In conclusion, the studies on *At*ALMT4 suggest that *At*ALMT4 is a malate anion channel in the vacuolar membrane involved in drought stress tolerance. Although the expression of *AtALMT4* in guard cells was shown recently (Obulareddy et al., 2013), its expression pattern and detailed channel properties are still superficially studied. Further experiments are required to clarify its contribution to stomatal movement and drought stress tolerance.

6.4 Methods

Plant material and growth conditions

All wild-type (Columbia-0 and Nossen-0) and *atalmt4* mutant plants of *Arabidopsis thaliana* were grown in a growth chamber (8h light 22°C / 16h dark 18°C, 55% relative humidity) in potting soil. For drought stress experiments, plants were grown in a defined amount of sieved soil in round pots (6 cm diameter) with regular irrigation for 8 weeks. Watering was stopped for drought stress treatment.

Selection of atalmt4 knockout lines

Two independent T-DNA insertion lines, *atalmt4-1* (PST15045) and *atalmt4-2* (SALK_086236), were obtained from the RIKEN bio-resource center and the Salk Institute Genomic Analysis Laboratory *Arabidopsis* T-DNA insertion collection, respectively. Genomic DNA was extracted from wild-type plants and mutant plants, and the T-DNA insertion locus were verified by PCR genotyping using *AtALMT4* specific primers. To select homozygous lines we used the *AtALMT4* specific primer pst15045-For (5'-TGTGATATGCCTAATATTGG -3') and pst15045-Rev (5'-CATATTCATACGACTTCATCG -3') and T-DNA specific primer Ds5-2a (5'-TCCGTTCCGTTTTCGTTTTTTAC -3') for *atalmt4-1*. The *AtALMT4* specific primer SALK_086236-For (5'-TTCGATCAAATCTTCCGGATTT -3') and SALK_086236-Rev (5'-CTTCAAGTGAATTGGCCACAC -3') and T-DNA specific primer LBb1.3

(5'-ATTTTGCCGATTTCGGAAC-3') for *atalmt4-2*. The abundance of the *AtALMT4* transcript in homozygous knock-out lines and wild-type plants (see below) was assayed by RT-PCR using the *At*ALMT4 specific primers ALMT4 forward (5'-ACGCgtcgacATGGCTGACCAAACT AGAGAAG-3') and ALMT4 reverse (5'-ACATgcatgcTATCCGTGTCTCGCTAACTTGT-3'). As loading control actin transcript was amplified with the primers 5'-TGGAATCCACGAGACAACCT-3' and 5'-TTCTGTGAACGATTCCTGGAC-3'.

Stomatal aperture measurements

The stomatal aperture measurements of *At*ALMT4 wild-type and knock-out plants were conducted as described in Result Chapter I.

Tissue-specific expression of AtALMT4 in Arabidopsis

A 1836bp promoter fragment up stream of *AtALMT4* was cloned into the pGreen0229 vector with the GUS gene. The vector construct was transformed into *Arabidopsis* using the Agrobacterium-mediated floral-dipping method (Clough and Bent, 1998). Transgenic plants were selected by BASTA resistance and plants of the T_2 generation were selected. Different days after germination, these transgenic plants were incubated in GUS staining buffer (50mM $NaHPO_4$ pH=7.2, 0.5% Triton X-100, 1mM X-Gluc) at 37°C for 12 h, which was subsequently replaced with 70% ethanol to remove pigments. The samples were examined using a light microscope.

Overexpression of AtALMT4-GFP in Nicotiana benthamiana

For transient overexpression of *AtALMT4,* the cDNA was cloned into the vector pART27 (Gleave, 1992). The Agrobacterium-mediated infiltration of *N. benthamiana* leaves was performed as described by Yang et al. (2001), with slight modifications. After infiltration, the tobacco plants were grown in the greenhouse (16h light/8h dark, 25°C). 2-3days after infiltration, vacuoles were isolated for patch-clamp experiments.

Patch-clamp

Mesophyll protoplasts from *At*ALMT4-GFP overexpressing tobacco leaves were isolated by enzymatic digestion. The enzyme solution contained 0.3 % (w/v) cellulase R-10, 0.03 % (w/v) pectolyase Y-23, 1 mM $CaCl_2$, 500 mM sorbitol and 10 mM MES, pH 5.3, 550 mOsm. Protoplasts were washed twice and resuspended in the same

solution without enzymes. Vacuoles were released from mesophyll protoplast by the addition of 5 mM EDTA and applying a slight osmotic shock (500 mOsm, see medium below). Transformed vacuoles exhibiting an *At*ALMT4-GFP signal were selected using an epifluorescence microscope. Membrane currents from patches of the tonoplast were recorded using the excised cytosolic-side out patch-clamp technique as described in Result Chapter I.

The pipette solution contained 112 mM malic acid, 5 mM HCl and was adjusted with BisTrisPropane (BTP) to pH 6. The osmolarity was adjusted with sorbitol to 550 mOsm. The bath solution contained 100 mM malic acid, 3 mM $MgCl_2$, 0.1 mM $CaCl_2$, adjusted to pH 7.5 with BTP. The osmolarity was adjusted to 500 mOsm using sorbitol. All chemicals were purchased from Sigma-Aldrich. Liquid junction potentials were measured and corrected when higher than ± 2 mV (Neher, 1992). Current-voltage characteristics were obtained by subtracting the current at t=0 from the quasi-stationary currents (averaging the last 50 ms of the current trace) elicited by main voltage pulses.

Microscopy

Intracellular localization of *At*ALMT4-GFP was determined by performing an osmotic shocked based lysis to release vacuoles of tobacco protoplasts overexpressing the *At*ALMT4-GFP construct. Microscopy was conducted using a Leica DMIRE2 (www.http://www.leica-microsystems.com) laser scanning microscope which was equipped with a x63 glycerol objective. GFP fluorescence signals were imaged at an excitation wavelength of 488 nm, the emission was detected between 500 and 530 nm. The appropriate Leica confocal software has been used for image acquisition.

7. Result Chapter V

The Vacuolar Channel *Vv*ALMT9 Mediates Malate and Tartrate Accumulation in Berries of *Vitis vinifera*

Alexis De Angeli, Ulrike Baetz, Rita Francisco, Jingbo Zhang, Maria Manuela Chaves and Ana Regalado

Published in *Planta* 2013 Aug;238 (2):283-91.

Planta (2013) 238:283–291
DOI 10.1007/s00425-013-1888-y

ORIGINAL ARTICLE

The vacuolar channel VvALMT9 mediates malate and tartrate accumulation in berries of *Vitis vinifera*

Alexis De Angeli · Ulrike Baetz · Rita Francisco · Jingbo Zhang · Maria Manuela Chaves · Ana Regalado

Received: 22 January 2013 / Accepted: 21 April 2013 / Published online: 5 May 2013

Abstract *Vitis vinifera* L. represents an economically important fruit species. Grape and wine flavour is made from a complex set of compounds. The acidity of berries is a major parameter in determining grape berry quality for wine making and fruit consumption. Despite the importance of malic and tartaric acid (TA) storage and transport for grape berry acidity, no vacuolar transporter for malate or tartrate has been identified so far. Some members of the aluminium-activated malate transporter (ALMT) anion channel family from *Arabidopsis thaliana* have been shown to be involved in mediating malate fluxes across the tonoplast. Therefore, we hypothesised that a homologue of these channels could have a similar role in *V. vinifera* grape berries. We identified homologues of the Arabidopsis vacuolar anion channel AtALMT9 through a TBLASTX search on the *V. vinifera* genome database. We cloned the closest homologue of AtALMT9 from grape berry cDNA and designated it VvALMT9. The expression profile revealed that VvALMT9 is constitutively expressed in berry mesocarp tissue and that its transcription level increases during fruit maturation. Moreover, we found that VvALMT9 is targeted to the vacuolar membrane. Using patch-clamp analysis, we could show that, besides malate, VvALMT9 mediates tartrate currents which are higher than in its Arabidopsis homologue. In summary, in the present study we provide evidence that VvALMT9 is a vacuolar malate channel expressed in grape berries. Interestingly, in *V. vinifera*, a tartrate-producing plant, the permeability of the channel is apparently adjusted to TA.

Keywords Anion transport · Grape berry ripening · Ion channel · Malic acid · Tartaric acid · Vacuole

Abbreviations

ALMT	Aluminium-activated malate transporter
MA	Malic acid
TA	Tartaric acid
SUC	Succinic acid
AA	L-Ascorbic acid
PEPC	Phosphoenolpyruvate carboxylase
MDH	Malate dehydrogenase
ME	Malic enzyme
AttDT	*Arabidopsis thaliana* tonoplast dicarboxylate transporter
DAF	Days after flowering

Introduction

Grape berries (*Vitis vinifera* L.) exhibit a double-sigmoid growth pattern that results from two successive periods of vacuolar swelling during which the nature of accumulated solutes changes significantly (Coombe 1992). During the first period, called green or herbaceous stage, berries accumulate mainly organic acids in the vacuole [predominantly malic acid (MA) and tartaric acid (TA)] and have a constant vacuolar pH of 2.5 (Terrier et al. 2001). At the onset of ripening (*véraison*), berries often become coloured

A. De Angeli and U. Baetz contributed equally to the work.

A. De Angeli (✉) · U. Baetz · R. Francisco · J. Zhang
Institute of Plant Biology, University of Zurich, Zollikerstr. 107, 8008 Zurich, Switzerland
e-mail: alexis.deangeli@botinst.uzh.ch; deangeli.alexis@gmail.com

R. Francisco · M. M. Chaves · A. Regalado
Instituto de Tecnologia Química e Biológica, Universidade Nova de Lisboa, Av. da República, 2780-157 Oeiras, Portugal

and start to accumulate sugars. At maturity, the concentrations of glucose and fructose may be higher than 1 M (Coombe 1976; Terrier et al. 2001). In parallel, their organic acid content decreases, whereby the vacuolar pH increases to about 3.5 (Terrier et al. 2001). Tartaric and malic acid generally account for 69–92 % of all organic acids in grape berries, and both of them reach maximal concentrations at the end of the green stage (Conde et al. 2007). However during ripening, the content of MA in berries continuously decreases, while that of TA remains constant. The acidity of berries is a major parameter determining their quality. The overall consumer appreciation is more related to the titratable acidity/sugar content than to the soluble sugars alone. Besides flavour and colour, the pH of grapes at harvest is a critical parameter for vinification. Wine pH depends on three major factors: the total amount of acids, the ratio of MA to TA and the concentration of potassium (Conde et al. 2007).

Despite their similar chemical nature, MA and TA synthesis follow different pathways. The biosynthesis of TA starts with L-ascorbic acid (AA) and is still not fully understood (Saito and Kasai 1969). The accumulation of TA resulting in high levels in mature berries suggests a strongly active metabolic pathway that may compete for AA with redox-associated functions more commonly linked to in vivo AA pools (Melino et al. 2009). In contrast, the precursor of MA is sucrose which is translocated from the leaves to the green berries. The main enzymes involved in malate synthesis (phosphoenolpyruvate carboxylase, PEPC and malate dehydrogenase, MDH) have been identified and shown to be active in grape berries (Taureilles-Saurel et al. 1995a, b; Fernie and Martinoia 2009; Sweetman et al. 2009). Instead, the decrease in acid content during grape berry ripening has been mainly associated with mitochondrial malate oxidation, most likely by malic enzyme (ME) (Kanellis and Roubelakis-Angelakis 1993).

Tonoplast transporters of MA and dicarboxylic acids have long been sought given the imperative vacuolar storage of these compounds. Emmerlich et al. (2003) identified the *Arabidopsis thaliana* tonoplast dicarboxylate transporter (*At*tDT) in mesophyll cells at the molecular level. Subsequently, members of the aluminium-activated malate transporter (ALMT) gene family (*A. thaliana* ALMT9 and 6) were identified to encode vacuolar malate channels in mesophyll and guard cells (Kovermann et al. 2007; Meyer et al. 2011).

The amount of MA and TA has a fundamental impact on grape berry quality for the wine-making industry (Conde et al. 2007). Despite the importance of MA and TA transport processes in grape berries, no vacuolar transporter for malate has been identified in *V. vinifera* until now and to the best of our knowledge no tartrate transporter/channel has been reported in plants. Therefore, in the present work we tried to fill this lack of information aiming at identifying a malate/tartrate transporter in *V. vinifera*. We hypothesised that an *At*ALMT9 homologue could code for a vacuolar malate/tartrate channel in grape berries. Here, we describe the cloning and characterisation of a grape berry ALMT (*V. vinifera* ALMT). We identify VvALMT9 and show that it is able to mediate malate and tartrate accumulation in the vacuole of grape berries.

Materials and methods

Plant material

Berry samples (*V. vinifera* cv. Aragonez) were collected from an experimental plot at the commercial vineyard Monte dos Seis Reis (South of Portugal, Estremoz, Portugal). Berries were collected during the summer season of 2007 in pre-*véraison* (49DAF), *véraison* (68DAF), maturation (81 DAF) and full maturation stage (97 DAF). Collected berries were immediately frozen in liquid nitrogen and stored at −80 °C before usage.

Molecular cloning of VvALMT9

Total RNA was extracted from mature mesocarp (pulp) tissues using the method of Reid et al. (2006). Mesocarp tissue was ground in liquid nitrogen to a fine powder and immediately added to pre-warmed RNA extraction buffer. RNA was purified using the RNeasy kit (Qiagen) in the presence of DNaseI according to manufacturer's instructions (RNase-Free DNase Set; Qiagen). Full-length cDNAs were synthesised using RT included in the LongRange 2Step RT-PCR kit (Qiagen) according to the manufacturer's instructions. VvALMT9 full-length cDNA was amplified using the high fidelity DNA polymerase Phusion™ (Finnzymes). The resulting PCR product was cloned into pDONR™ 221 as entry vector and pH7FWG2™ as destination vector (Gateway® Technology, Invitrogen).

Phylogenetic analysis

The *V.vinifera* genome (http://www.cns.fr/spip/Vitis-vinifera-e.html), phytozome (http://www.phytozome.net) and the National Center for Biotechnology Information (NCBI; http://www.ncbi.nlm.nih.gov/) databases were screened using *At*ALMT9 (At3g18440) as query to find homologous grapevine sequences. Multiple sequence alignments were performed with the ClustalW algorithm (http://align.genome.jp/) using default parameters (Thompson et al. 1994). The phylogenetic analysis was performed with the phylogeny software (http://www.phylogeny.fr).

Overexpression of VvALMT9-GFP and AtALMT9-GFP in *Nicotiana benthamiana*

For transient overexpression (Kovermann et al. 2007) of VvALMT9-GFP and AtALMT9-GFP, the cDNA was cloned into pH7FWG2™ or the pART27 vector, respectively. The *Agrobacterium*-mediated infiltration of *N. benthamiana* leaves was performed as described with slight modifications (Holsters et al. 1980). After *Agrobacterium*-mediated infiltration, tobacco plants were grown in the greenhouse (16 h light/8 h dark, 25 °C). 2–3 days after the *Agrobacterium*-mediated infiltration, the transformed leaves were used to extract protoplasts and vacuoles for confocal microscopy and patch-clamp experiments. *N. benthamiana* seeds were derived from own stocks.

Intracellular localisation of VvALMT9-GFP

Protoplasts and vacuoles of *N. benthamiana* leaves overexpressing VvALMT9-GFP were isolated as described for patch-clamp experiments. Microscopy was conducted using a Leica DMIRE2 (http://www.leica-microsystems.com) laser scanning microscope. The microscope was equipped with a 63× glycerol objective. For image acquisition, the appropriate Leica confocal software was used. GFP fluorescence was imaged at an excitation wavelength of 488 nm, and the emission signal was detected between 500 and 530 nm.

Gene expression of VvALMTs

Total RNA was extracted from 150 mg grape berry pulp (mesocarp) using the RNeasy Plant Mini Kit (Qiagen) following the manufacturer's instructions. An on-column DNase I digestion step was included. Total RNA (1 µg) was reverse transcribed using M-MLV reverse transcriptase (Promega) and oligo (dT) priming. Transcript levels were determined by quantitative real-time PCR using the 7500 Fast Real-Time PCR System (Applied Biosystems) with the 7500 Software version 2.0.4. Reactions were performed in a final volume of 20 µL with 5 µL cDNA (diluted 1:10), 0.25 µM gene-specific primers and 10 µL SYBR Green PCR Master Mix (Applied Biosystems). Reaction conditions for the thermal cycling were as follows: after enzyme activation at 95 °C for 10 min, amplification was carried out in a two-step PCR procedure with 40 cycles of 15 s at 95 °C for denaturation and 1 min at 60 °C for annealing/extension. All reactions were performed in technical triplicates of three biological replicates. Gene primer sequences used in the qRT-PCR analyses were as follows: VvALMT5 forward 5′-GAGTGCCAGCTCCTTGTCTT-3′, VvALMT5 reverse 5′-TTTTGGAGCTGGAAGGTCCG-3′; VvALMT6 forward 5′-GAAACAATCCCCTTGGCCCT-3‘, VvALMT6 reverse 5′-ACATTTTGGAGCCTGGCAAC-3‘; VvALMT9 forward 5′-TGAATTTGTTGCGAGGCTTCA-3′, VvALMT9 reverse 5′-CACCTGCGCAATCTTGTTCC-3′; VvALMT13 forward 5′-CCTTGCCACCTTCACTTCCT-3′, VvALMT13 reverse 5′-CACTGCAAGCTGGTCAACTG-3′. Dissociation curves were analysed to verify the specificity of each amplification reaction; the dissociation curve was obtained by heating the amplicon from 60 to 95 °C. Transcript levels were calculated using the standard curve method and normalised against the VvActin gene (GU585869) as described by (Pfaffl 2001).

Protoplast preparation and patch-clamp recordings on isolated vacuoles

Tobacco leaves were gently scratched on the abaxial side and floated in the enzymatic solution for 30–45 min at 30 °C. The enzyme solution contained 0.3 % (w/v) cellulase R-10, 0.03 % (w/v) pectolyase Y-23, 1 mM $CaCl_2$, 500 mM sorbitol and 10 mM Mes, pH 5.3. Protoplasts were washed twice and resuspended in solution without enzymes. Vacuoles were isolated by calcium and osmotic shock. Membrane currents were recorded using the patch-clamp technique as described elsewhere (Meyer et al. 2011). Briefly, currents were recorded with an EPC10 patch-clamp amplifier (HEKA electronics) using the Patchmaster software (HEKA Electronics, Lambrecht/Pfalz, Germany). Data were analysed with the FitMaster software (HEKA electronics). Following the formation of giga seals between the patch pipette and the vacuolar membrane, the excised vacuole-side-out patches were obtained after having established the whole-vacuole configuration by pulling the pipette away from the vacuole. Pipette solutions contained 112 mM MA, 5 mM HCl and 3 mM $MgCl_2$ adjusted to pH 6.0 with 100 mM 1,3-bis[tris(hydroxymethyl)methylamino]propane (BTP). The standard bath solution contained 100 mM MA, 160 mM BTP, 3 mM $MgCl_2$ and 0.1 mM $CaCl_2$, pH 7.5. For selectivity studies, MA in the standard bath solution was replaced by equimolar amounts of TA. The osmotic pressure of all solutions was 550 mOsm adjusted with D-sorbitol. Ionic solutions bathing the vacuole were exchanged by a gravity-driven perfusion system coupled to a peristaltic pump. Current–voltage characteristics were either obtained by subtracting the current at $t = 0$ from the quasi-stationary currents (averaging the last 50 ms of the current trace) elicited by main pulses; or from the value of the tail currents (at $t = 0$) fitted by a monoexponential function. Error bars represent standard error throughout the article.

Results

Cloning VvALMT9, a homologue of the Arabidopsis vacuolar channel AtALMT9 from *Vitis vinifera*

Since two members of the ALMT family from *A. thaliana* (AtALMT9 and 6; Kovermann et al. 2007; Meyer et al. 2011) have been demonstrated to mediate malate fluxes across the tonoplast, we hypothesised that ALMTs could have a similar role in *V. vinifera* berries. To identify a homologue of the Arabidopsis vacuolar anion channel AtALMT9 (At3g18440; Kovermann et al. 2007), we performed a TBLASTX search on the genome database of *V. vinifera* (http://www.phytozome.net) using the cDNA of this channel as a query. The search identified five sequences displaying a significant similarity to *AtALMT9* (e value $\leq 10^{-30}$). We found that the genomic sequence GSVIVG01008270001 exhibited the highest degree of similarity (e value $= 10^{-161}$). We cloned the grape berry cDNA of the closest homologue of *AtALMT9* from mRNA extracted from the mesocarp of grape berries and designated it *VvALMT9* (Fig. 1). The alignment of the cloned cDNA sequence with the Vitis genome revealed that the *VvALMT9* gene consisted of six exons coding for a protein of 588 amino acids. VvALMT9 displays a high degree of identity with AtALMT9 (64 %). To further analyse the ALMT family in *V. vinifera* we performed additionally a BLAST search on the Vitis proteome (http://www.phytozome.net) using the AtALMT9 amino acid sequence. A dendrogram based on the amino acid similarity indicates that the 13 members of the ALMT family in *V. vinifera* are grouped in three clades as in Arabidopsis (Fig. 1). Notably, even if the total number of ALMTs is similar in Arabidopsis (14 members) and Vitis (13 members), the number of members per clade is different between the two species. Clade I, to which AtALMT1 (Hoekenga et al. 2006) belongs, contains in *V. vinifera* eight members, while it includes five members in *A. thaliana*. Clade II is represented in *V. vinifera* by four members. In contrast, in *A. thaliana* clade II contains five members including AtALMT9 and 6 (Kovermann et al. 2007; Meyer et al. 2011). Interestingly, clade III incorporates only one member in *V. vinifera*, whereas in Arabidopsis there are four members, amongst them AtALMT12 (Meyer et al. 2010).

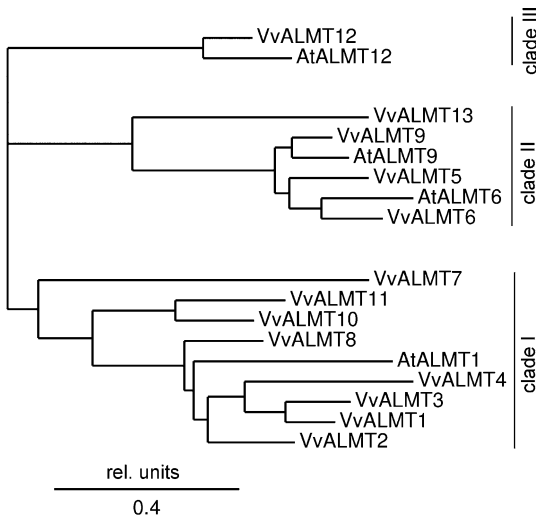

Fig. 1 Dendrogram of the ALMT protein family in *V. vinifera*. Based on multiple amino acid sequence alignments using ClustalW (Thompson et al. 1994) the 13 members of the VvALMT protein family were classified into three main clades as in *A. thaliana*. Clade I members: VvALMT1, VvALMT2, VvALMT3, VvALMT4, VvALMT7, VvALMT8, VvALMT10 and VvALMT11 (GSVIVT01036162001, GSVIVT01037570001, GSVIVT01037569001, GSVIVT01036157001, GSVIVT01011122001, GSVIVT01011148001, GSVIVT01019627001, GSVIVT01027186001). Clade II members: VvALMT5, VvALMT6, VvALMT9 and VvALMT13 (GSVIVT01011922001, GSVIVT01011922001b, GSVIVT01008270001, GSVIVT01019447001). Clade III: VvALMT12 (GSVIVT01013184001). The ALMTs from *A. thaliana* that have been already characterised are inserted in the dendrogram. Branch lengths are given in relative units illustrating the level of occurred evolutionary change

VvALMT9 expression levels increase during grape berry development

To elucidate whether the members of VvALMT clade II including VvALMT9 could feature physiological relevance during fruit development and maturation, we conducted expression profile analysis using quantitative real-time PCR. On that purpose, grape berry mesocarp tissue was used to extract RNA at different developmental stages of the fruit. Despite not detecting significant expression levels for VvALMT6 and marginal transcription of VvALMT13 in this tissue, the other clade members VvALMT9 and VvALMT5 were substantially transcribed in berries at all examined stages (Fig. 2). In the green phase (49 days after flowering, DAF) and at the onset of ripening (68 DAF) transcript levels of VvALMT9 were lower relative to the fully developed fruit. After induction of the ripening process (81 and 97 DAF), expression levels rose approximately four times. VvALMT13 showed generally a less pronounced expression magnitude than VvALMT9, but a similar tendency of transcriptional up-regulation during fruit development. In contrast, VvALMT5 was constantly highly expressed throughout maturation, therefore representing the prevalent member of clade II VvALMTs in grape berries. Thus, with the expression profile we demonstrate that VvALMTs are constitutively transcribed in grape mesocarp tissue. Further, VvALMT9 transcript levels experience a marked increase throughout the ripening process. Altogether, these results suggest that clade II VvALMTs might be involved in grape berry maturation.

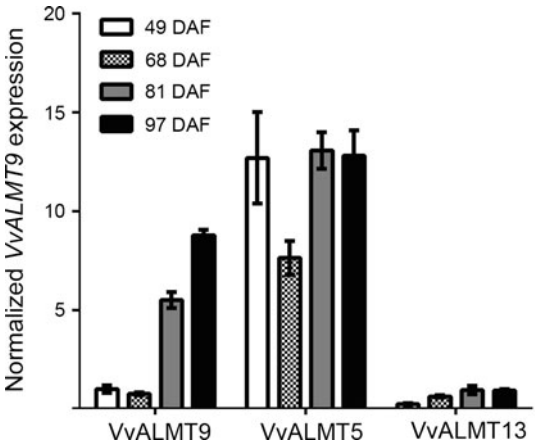

Fig. 2 Quantitative real-time PCR expression profile of VvALMTs in grape berry mesocarp. Displayed are expression profiles of VvALMT9, VvALMT5 and VvALMT13 in mesocarp tissue during fruit development and ripening (49–97 days after flowering, DAF). VvActin (GU585869) served as a reference gene. Relative expression levels of VvALMTs were normalised to VvALMT9 at 49 DAF. Results represent the mean ± standard deviation (SD) of three biological replicates

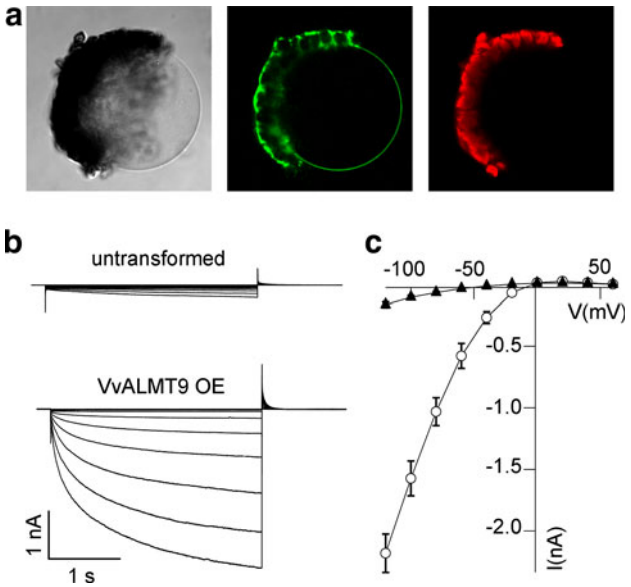

Fig. 3 Intracellular localisation and anion conductivity of VvALMT9-GFP. **a** Transmission, GFP fluorescence and chlorophyll autofluorescence images showing the tonoplastic localisation of VvALMT9-GFP in an isolated vacuole after lysis of *N. benthamiana* protoplasts which transiently overexpressed VvALMT9-GFP. **b** Representative malate current recordings of non-transformed and VvALMT9-GFP overexpressing vacuoles obtained from patches in excised cytosolic-side-out configuration. Currents were elicited with 3 s voltage pulses ranging from +60 to −120 mV in −20 mV steps followed by a 1.5 s tail pulse at +60 mV. The holding potential was +60 mV. **c** Mean current–voltage relationships of vacuolar patches of non-transformed (*filled triangles*; $n = 4$) and VvALMT9-GFP overexpressing (*open circles*; $n = 7$) protoplasts in symmetrical malate conditions $\left(100\,\text{mM malate}^{2-}_{cyt}/100\,\text{mM malate}^{2-}_{vac}\right)$. *Error bars* represent ±SE

VvALMT9 is localised in the tonoplast

To investigate the subcellular localisation of VvALMT9, we generated a construct encoding the VvALMT9 protein with a C-terminal GFP fusion in pH7FWG2 (Gateway® Technology, Invitrogen). Subsequently, we transiently expressed VvALMT9 in *N. benthamiana* leaves by agro-infiltration (Holsters et al. 1980). Confocal laser scanning microscopy analysis of vacuoles extracted from lysed protoplasts of transiently transformed tobacco leaves allowed localising VvALMT9-GFP in the tonoplast (Fig. 3a). These data indicate that VvALMT9 is targeted to the vacuolar membrane as its counterpart in Arabidopsis.

VvALMT9 is an ionic channel mediating malate currents

The localisation of VvALMT9 in the tonoplast allowed using the patch-clamp technique to characterise the properties of the putative ion channel. Electrophysiological experiments were conducted on vacuoles obtained from *N. benthamiana* protoplasts transiently transformed with the VvALMT9-GFP construct. Vacuoles expressing VvALMT9-GFP were selected by their fluorescence signal under the microscope and chosen for patch-clamp experiments in excised cytosolic-side-out configuration (i.e. with the cytosolic side of the membrane exposed to the bath solution). As a first step we compared the currents that could be measured in vacuoles from excised patches from non-transformed and transformed cells (Fig. 3b). We found that in symmetric malate concentrations (100 mM malate^{2-}_{cyt} and 100 mM malate^{2-}_{vac}), patches from fluorescent vacuoles displayed a voltage-dependent inward current with a time of half activation of $t_{1/2} = 290 \pm 20$ ms reminiscent of the currents observed in AtALMT9 and AtALMT6 overexpressing vacuoles (Kovermann et al. 2007; Meyer et al. 2011). In patches of transformed vacuoles, we measured current amplitudes of -1.6 ± 0.2 nA, while in patches from non-transformed vacuoles the detected amplitudes were -0.10 ± 0.01 nA at −100 mV (Fig. 3c). The ten times higher currents found in patches from transiently transformed vacuoles indicate that VvALMT9 is able to mediate ionic currents across the tonoplast. To verify whether the currents observed in VvALMT9 transformed vacuoles are mediated by malate, we switched the cytosolic side solution from 100 mM malate^{2-}_{cyt} to 10 mM malate^{2-}_{cyt} and followed the reversal potential and the change in current amplitude (Fig. 4). During the exchange of the cytosolic side solution, the currents mediated by VvALMT9 decreased from -1.6 ± 0.2 nA in 100 mM malate^{2-}_{cyt} to -0.19 ± 0.09 nA in 10 mM malate^{2-}_{cyt} at −100 mV (Fig. 4b). In 100 mM malate^{2-}_{cyt} and

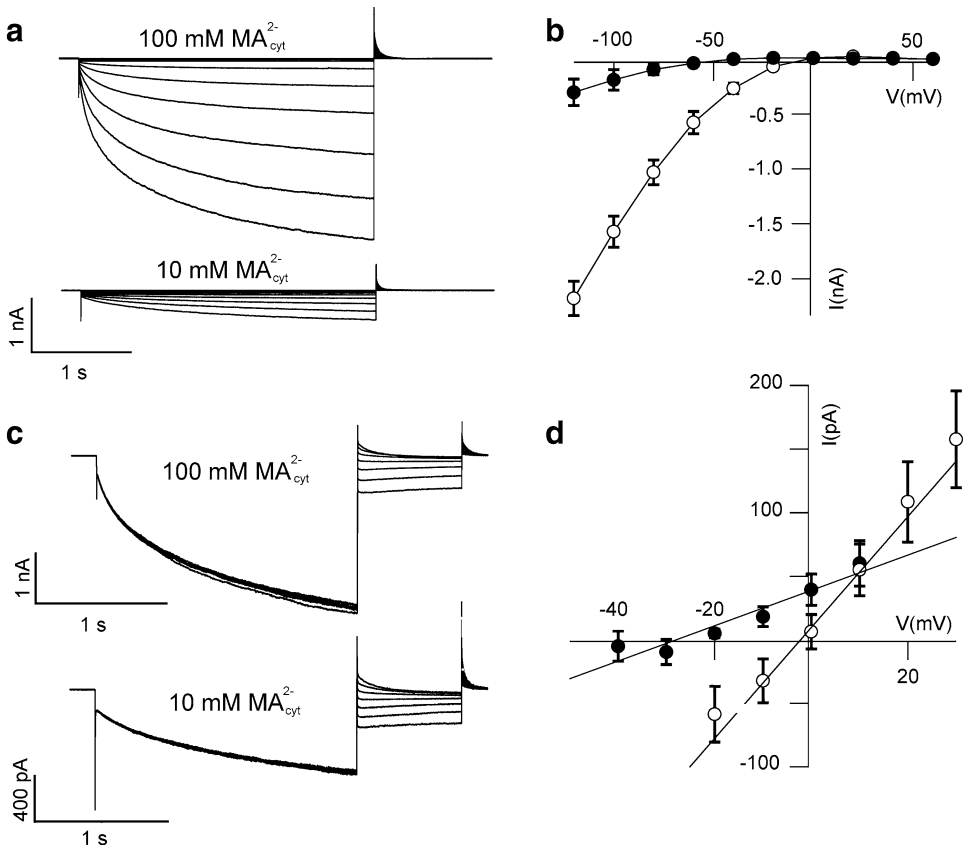

Fig. 4 Analysis of malate inward fluxes across the tonoplast mediated by VvALMT9. **a** Representative current traces measured in excised cytosolic-side-out patches of VvALMT9-overexpressing vacuoles in the presence of 100 mM cytosolic malate and after the exchange to a 10 mM cytosolic malate solution at different applied membrane potentials. Currents were elicited with 3 s voltage pulses ranging from +60 to −120 mV in −20 mV steps followed by a 1.5 s tail pulse at +60 mV. The holding potential was +60 mV. **b** I–V curves comparing the voltage-dependent inward current of VvALMT9 between 100 mM (*open circles*; $n = 7$) and 10 mM (*filled circles*; $n = 7$) cytosolic malate concentrations. **c** Current traces representing the tail current of patches in 100 and 10 mM malate at the cytosolic side. Currents were elicited by an activating pre-pulse at −100 mV (2 s), followed by a series of test pulses ranging from +30 to −20 mV (100 mM MA^{2-}_{cyt}) and +10 to −40 mV (10 mM MA^{2-}_{cyt}) in −10 mV steps (1 s). The holding potential was at +60 mV. **d** Corresponding reversal potentials obtained from a linear fit of the mean current–voltage relations of instantaneous tail currents from patches of vacuoles overexpressing VvALMT9 in 100 mM (*open circles*; $n = 4$) and 10 mM malate (*filled circles*; $n = 4$) in the cytosolic bath solution. The values of the instantaneous tail currents derived from a monoexponential fit of the tail current responses. The theoretical Nernst potential of $malate^{2-}$ in 100 mM symmetrical malate conditions is $E_{Nernst}(100\,mM\,MA^{2-}_{cyt}) = 0\,mV$ and in 10 mM cytosolic $malate^{2-}$ concentrations it is $E_{Nernst}(100\,mM\,MA^{2-}_{cyt}) = -28\,mV$. *Error bars* are ±SE

10 mM $malate^{2-}_{cyt}$, the measured reversal potential was +1±1 mV and −29 ± 1 mV, respectively (Fig. 4d). In both cases, these reversal potentials approximate the Nernst potential of $malate^{2-}$ in the investigated conditions ($E_{Nernst}(100\,mM\ malate^{2-}_{cyt} = 0\,mV$ and $E_{Nernst}(100\,mM\ malate^{2-}_{cyt} = -28\,mV$). Therefore, these data show that the current observed in VvALMT9 expressing vacuoles is carried by malate.

VvALMT9 can transport tartrate better than AtALMT9

During the green stage, grape berries accumulate large amounts of MA and TA in the vacuole. Therefore, we were interested in whether VvALMT9 is able to mediate tartrate currents beside malate currents. We conducted a parallel study of TA permeation in AtALMT9 and VvALMT9 (Fig. 5). By exchanging 100 mM $malate^{2-}_{cyt}$ with 100 mM $tartrate^{2-}_{cyt}$, we observed that both VvALMT9 and AtALMT9 expressing vacuoles could mediate tartrate currents. Referring to the malate currents, the tartrate currents had 61 ± 6 % and 48 ± 4 % of the amplitude at −100 mV in VvALMT9 and AtALMT9, respectively (Fig. 5c). Interestingly, the ratio between the currents of tartrate and malate (I_{TA}/I_{MA}) indicates that VvALMT9 is more conductive for tartrate than AtALMT9 (Fig. 5d). Moreover, the current ratio increases with the applied membrane potential (Fig. 5d). This slight voltage

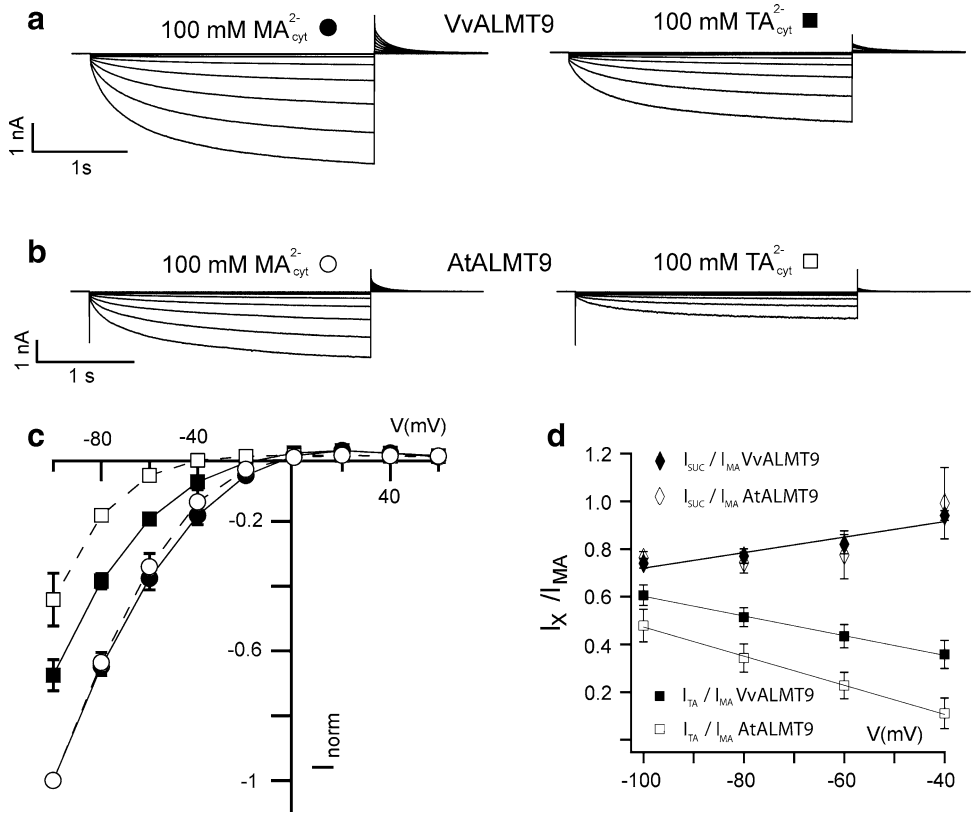

Fig. 5 Comparison between the ion selectivity of VvALMT9 and AtALMT9 for malate and tartrate. **a, b** Representative currents recorded in the presence of 100 mM malate$^{2-}_{cyt}$ (*left traces*) and 100 mM tartrate$^{2-}_{cyt}$ (*right traces*). The cytosolic malate solution was exchanged with a tartrate solution while keeping the same patches from vacuoles overexpressing VvALMT9 (**a**) and AtALMT9 (**b**). Currents were elicited with 3 s voltage pulses ranging from +60 to −120 mV in −20 mV steps followed by a 1.5 s tail pulse at +60 mV The holding potential was +60 mV. **c** Corresponding current amplitude plots derived from excised cytosolic-side-out patches from VvALMT9 overexpressing vacuoles exposed to 100 mM malate (filled circles) and 100 mM tartrate (*filled squares*, $n = 4$), as well as from AtALMT9 overexpressing vacuoles exposed to 100 mM malate (*open circles*; $n = 4$) and 100 mM tartrate (*open squares*; $n = 4$). **d** Ratio between succinate and malate currents mediated by ALMT9 of *V. vinifera* (*filled diamonds*) and *A. thaliana* (*open diamonds*) and ratio between tartrate and malate currents mediated by ALMT9 of *V. vinifera* (*filled squares*) and *A. thaliana* (*open squares*) plotted as a function of the applied membrane potential. *Error bars* denote ±SE

dependency of the I_{TA}/I_{MA} ratio is more pronounced in AtALMT9 than in VvALMT9 (in Fig. 5d the slope of the fitted line is 0.004 mV^{-1} for VvALMT9 and 0.006 mV^{-1} for AtALMT9). Notably, we illustrate in an equally conducted set of experiments that when exchanging from 100 mM malate$^{2-}_{cyt}$ to 100 mM succinate$^{2-}_{cyt}$ that this dicarboxylic acid is likewise transported by VvALMT9 and AtALMT9 (Fig. 5d). The succinate currents were 76 ± 2 and 74 ± 3 % of the currents in malate in VvALMT9 and AtALMT9 at −100 mV, respectively. This indicates that the permeability of succinic acid is identical between the homologous channels of Arabidopsis and *V. vinifera*. In summary, the data show that both VvALMT9 as well as AtALMT9 are slightly less permeable for tartrate than for malate and succinate. Nonetheless, the ratio I_{TA}/I_{MA} provides evidence that VvALMT9 conducts tartrate ions better than AtALMT9. Taken together, these results indicate that both, MA and TA, can be transported in the vacuoles of *V. vinifera* berries through VvALMT9. Hence, VvAtLMT9 is the first malate and tartrate channel identified so far in grape berries.

Discussion

In *V. vinifera*, the accumulation of organic acids in the vacuole is involved in berry development and has a great impact on the final quality of grapes from an agronomical point of view. In this species, the data on the vacuolar transporters involved in the accumulation of MA and TA in berry vacuoles are scarce and no information is available concerning their molecular identity. Based on previous studies in *A. thaliana* (Kovermann et al. 2007; Meyer et al. 2011), we hypothesised that members of the ALMT family

could be involved in the vacuolar accumulation of MA and TA in *V. vinifera* berries. In a preliminary phylogenetic analysis, we found that 13 members of the ALMT family can be identified in the *V. vinifera* genome (Fig. 1). The 13 VvALMTs cluster in three clades that correspond to the clades previously described in Arabidopsis (Kovermann et al. 2007). However, the number of members per clade is different between the two species with clade I being overrepresented and clade III harbouring a single member in *V. vinifera* (Fig. 1). Instead, clade II to which VvALMT9 belongs is represented by a similar number of members in grapevine (Kovermann et al. 2007). We found that when transiently expressed in tobacco leaves, VvALMT9-GFP is localised in the tonoplast as AtALMT9-GFP (Fig. 3a). Further electrophysiological analysis on excised cytosolic-side-out patches of vacuoles obtained from transiently transformed tobacco protoplasts allowed us to demonstrate that VvALMT9 was able to mediate an inward rectifying malate and tartrate current facilitating the accumulation of these dicarboxylic acids in the vacuoles of grape berries (Figs. 4, 5). The comparison between the substrate selectivity properties of VvALMT9 and AtALMT9 reveals that VvALMT9, like AtALMT9, transports malate and succinate better than tartrate (Fig. 5). Nonetheless, VvALMT9 is able to catalyse the transport of TA more efficiently than AtALMT9, which is in contrast to the transport of succinic acid, a metabolic intermediate which is not accumulated substantially in grape berries. This functional difference between the two homologous proteins is intriguing since grape berries are one of the few fruits accumulating significant amounts of TA (Saito and Kasai 1968).

The extremely acidic pH values found in grape vacuoles in the green stage (~2.5) allow the accumulation of MA and TA via a passive transport system like an anion channel. Indeed, at this pH 99 % of MA and TA are in the fully protonated or monovalent form ($pK_A^{1,MA} = 3.40$, $pK_A^{2,MA} = 5.11$, $pK_A^{1,TA} = 2.98$, $pK_A^{2,TA} = 4.34$; Weast and Astle 1982–1983). The ALMTs are known to mediate only the transport of the divalent form of dicarboxylic acids (Meyer et al. 2011). Hence, in grape berries TA and MA can be taken up from the neutral cytosol across the tonoplast as divalent anions (MA^{2-} and TA^{2-}). Once in the vacuole at pH 2.5, these acids become neutral or monovalent which prevents the conduction by anion channels back to the cytosol. This mechanism, known as ion trapping (Briggs et al. 1987), facilitates loading of grape berry vacuoles with MA and TA (Fig. 6). The unidirectional acid flux might explain the requirement of less anion channels during the green stage compared to the mature grape berry as represented by lower expression levels of VvALMT9 (Fig. 2). The decline in vacuolar acidity observed

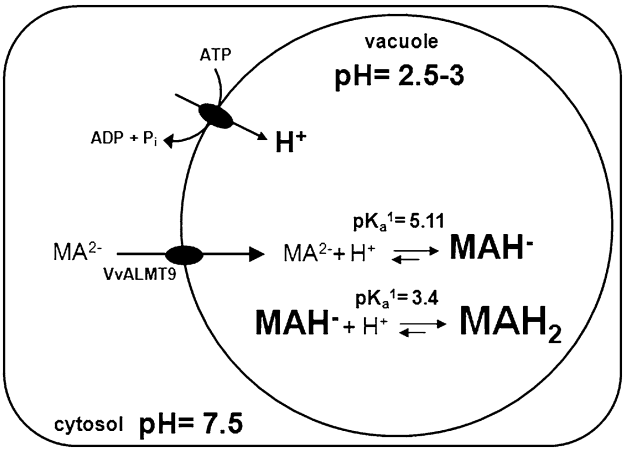

Fig. 6 The ion-trapping mechanism results in vacuolar malate accumulation in grape berries. In the cytosol at pH 7.5, MA is present in its fully deprotonated divalent form malate^{2-} (MA^{2-}). MA^{2-} can be transported by the inward rectifier VvALMT9 into the vacuole. Once in the extremely acidic vacuole of grape berries (pH = 2.5–3), MA^{2-} becomes protonated and accumulates mainly as MAH_2 or in the monovalent form, MAH^-. Both forms of MA are not permeable through ALMTs and thus they are trapped in the vacuolar lumen. The unidirectional flux of malate forms the basic principle of its vacuolar accumulation to high levels. Tartaric acid can be accumulated in the vacuole by the same ion-trapping mechanism since the acidity constants are $pK_A^{1,TA} = 2.98$ and $pK_A^{2,TA} = 4.34$

systematically during grape berry ripening was shown to be accompanied by an increase in tonoplast passive diffusion (Terrier et al. 2001). The up-regulation of global VvALMT expression could consequently be a counteraction for excessive MA and TA decompartementation through anion leakage. Similarly, the rise of mRNA and protein abundance of both vacuolar proton pumps in grape berries during maturation was suggested to partly compensate for passive permeability of the tonoplast (Terrier et al. 2001). A second explanation for the transcriptional up-regulation of VvALMT9 could be an involvement in releasing organic acids from the vacuole during maturation. In late stages of ripening, the vacuolar pH rises to 3.5–4. Under these conditions, a minor proportion of the vacuolar MA would dissociate into the divalent form (MA^{2-}) and be a substrate of VvALMT9. It is therefore possible that the channel catalyses the release of MA^{2-} from the vacuole to the cytosol at this particular phase of development. However, although we cannot exclude this second hypothesis per se, our data demonstrate that anion fluxes mediated by VvALMT9 are directed into the vacuole, thus supporting a role of VvALMT9 in counteracting excessive organic acid decompartementation during maturation.

In conclusion, in the present work we provide evidence that malate and tartrate can be accumulated in the vacuoles of *V. vinifera* berries by VvALMT9. Hence, the present findings represent a step towards understanding

carboxylate metabolism and storage in grapes which are crucial factors impacting wine quality and production.

Acknowledgments We would like to thank Prof. Enrico Martinoia (University of Zurich, Switzerland) for his scientific support and helpful discussions, Dr. Stefan Meyer (University of Zurich, Switzerland) for discussions, Dr. Nelson Saibo (Genomics of Plant Stress Laboratory–ITQB, Universidade Nova de Lisboa, Portugal) for kindly providing the cloning vectors and Duarte Figueiredo (Genomics of Plant Stress Laboratory–ITQB, Universidade Nova de Lisboa), Tânia Serra (Genomics of Plant Stress Laboratory–ITQB, Universidade Nova de Lisboa) and André Cordeiro (Genomics of Plant Stress Laboratory–ITQB, Universidade Nova de Lisboa) for technical support with the preliminary *Nicotiana* agroinfiltration experiments. AR and RF acknowledge FCT for the financial support through fellow FRH/BPD/34986/2007 and SFRH/BPD/74210/2010, respectively. AD was supported by a long-term EMBO fellowship (ALTF 87-2009), JZ by the Chinese Scholarship Council and UB by the Swiss National Foundation (31003A_141090/1).

References

Briggs GG, Rigitano RLO, Bromilow RH (1987) Physico-chemical factors affecting uptake by roots and translocation to shoots of weak acids in barley. Pestic Sci 19:101–112

Conde C, Silva P, Fontes N, Dias ACP, Tavares RM, Sousa MJ, Agasse A, Delrot S, Geros H (2007) Biochemical changes throughout grape berry development and fruit and wine quality. Food 1:1–22

Coombe BG (1976) The development of fleshy fruits. Annu Rev Plant Physiol 27:207–228

Coombe BG (1992) Research on development and ripening on the grape berry. Am J Enol Vitic 43:101–110

Emmerlich V, Linka N, Reinhold T, Hurth MA, Traub M, Martinoia E, Neuhaus HE (2003) The plant homolog to the human sodium/dicarboxylic cotransporter is the vacuolar malate carrier. Proc Natl Acad Sci USA 100:11122–11126

Fernie AR, Martinoia E (2009) Malate: Jack of all trades or master of a few? Phytochemistry 70:828–832

Hoekenga OAL, Maron G, Piñeros MA, Cançado GM, Shaff J, Kobayashi Y, Ryan PR, Dong B, Delhaize E, Sasaki T, Matsumoto H, Yamamoto Y, Koyama H, Kochian LV (2006) *AtALMT1*, which encodes a malate transporter, is identified as one of several genes critical for aluminum tolerance in *Arabidopsis*. Proc Natl Acad Sci USA 103:9738–9743

Holsters M, Silva B, Van Vliet F, Genetello C, De Block M, Dhaese P, Depicker A, Inzé D, Engler G, Villarroel R (1980) The functional organization of the nopaline *A. tumefaciens* plasmid pTiC58. Plasmid 3:212–230

Kanellis AK, Roubelakis-Angelakis KA (1993) Grapes. In: Seymour GI, Taylor J, Tucker GA (eds) Biochemistry of fruit ripening. Chapman & Hall, London, pp 189–234

Kovermann P, Meyer S, Hörtensteiner S, Picco C, Scholz-Starke J, Ravera S, Lee Y, Martinoia E (2007) The Arabidopsis vacuolar malate channel is a member of the ALMT family. Plant J 52:1169–1180

Melino VJ, Soole KL, Ford CM (2009) Ascorbate metabolism and the developmental demand for tartaric and oxalic acids in ripening grape berries. BMC Plant Biol 9:145

Meyer S, Mumm P, Imes D, Endler A, Weder B, Al-Rasheid KA, Geiger D, Marten I, Martinoia E, Hedrich R (2010) *At*ALMT12 represents an R-type anion channel required for stomatal movement in Arabidopsis guard cells. Plant J 63:1054–1062

Meyer S, Scholz-Starke J, De Angeli A, Kovermann P, Burla B, Gambale F, Martinoia E (2011) Malate transport by the vacuolar AtALMT6 channel in guard cells is subject to multiple regulation. Plant J 67:247–257

Pfaffl MW (2001) A new mathematical model for relative quantification in real-time RT-PCR. Nucleic Acids Res 29(9):e45

Reid KE, Olsson N, Schlosser J, Peng F, Lund ST (2006) An optimized grapevine RNA isolation procedure and statistical determination of reference genes for real-time RT-PCR during berry development. BMC Plant Biol 6:27

Saito K, Kasai Z (1968) Accumulation of tartaric acid in the ripening process of grapes. Plant Cell Physiol 9:529–537

Saito K, Kasai Z (1969) Tartaric acid synthesis from l-ascorbic acid-1-^{14}C in grape berries. Phytochemistry 8:2177–2182

Sweetman C, Deluc G, Cramer GR, Ford CM, Soole KL (2009) Regulation of malate metabolism in grape berry and other developing fruits. Phytochemistry 70:1329–1344

Taureilles-Saurel C, Romieu CG, Robin JP, Flanzy C (1995a) Grape (*Vitis vinifera* L.) malate dehydrogenase. I. Intracellular compartmentationof the isoforms. Am J Enol Vitic 46:22–28

Taureilles-Saurel C, Romieu CG, Robin JP, Flanzy C (1995b) Grape (*Vitis vinifera* L.) malate dehydrogenase. II. Characterization of the major mitochondrial and cytosolic isoforms and their role in ripening. Am J Enol Vitic 46:29–36

Terrier N, Sauvage FX, Ageorges A, Romieu C (2001) Changes in acidity and in proton transport at the tonoplast of grape berries during development. Planta 213:20–28

Thompson JD, Higgins DG, Gibson TJ (1994) CLUSTAL W: improving the sensitivity of progressive multiple sequence alignment through sequence weighting, position-specific gap penalties and weight matrix choice. Nucleic Acids Res 22:4673–4680

Weast RC, Astle MJ (1982–1983) CRC Handbook of chemistry and physics. CRC Press. Boca Raton

8. General Conclusions and Outlook

The aim of this thesis was to further characterize *At*ALMT9 based on the work of Kovermann et al. (2007). In this study, *At*ALMT9 has been found to transport not only malate and fumarate but also slightly chloride from the cytosol to the vacuole. Besides CLCs, electrophysiological studies indicated that the influx of chloride ions into the vacuole is also catalyzed by chloride channels, but so far their molecular identity was not determined. The research presented in this thesis provides the first evidence that *At*ALMT9 acts as a vacuolar chloride channel *in vivo*.

In this thesis, electrophysiological studies revealed that *At*ALMT9 is permeable to chloride, confirming the findings of Kovermann et al (2007). Interestingly, the chloride currents mediated by *At*ALMT9 are modulated by cytosolic malate. In the presence of malate, the chloride transport activity of *At*ALMT9 is activated via an increase of the channel open probability rather than the single channel conductance. This observation is a further confirmation that ALMTs are channels and not transporters. Furthermore, *AtALMT9* is also expressed in guard cells and the *At*ALMT9 protein mediating influx of chloride ions into vacuoles is essential for stomatal opening. *At*ALMT9-loss-of-function plants exhibited impaired stomatal opening and drought stress sensitivity. In summary, the discovery that *At*ALMT9 constitutes a vacuolar chloride channel, which has been sought for over 20 years, assigns a completely novel function to this anion channel. Additionally, the chloride currents activation by malate also reveals a so far unknown signaling function of malate in the stomatal opening process. In contrast to the well characterized *At*ALMT9, the results on *At*ALMT4 presented in this thesis are a first step towards its characterization. Even though more research is needed to understand the function and regulation of *At*ALMT4, the phenotypic difference between mutants of *AtALMT4* and *AtALMT9*, which show that *atalmt4* plants are more drought sensitive, implies that *At*ALMT4 may transport malate across the vacuolar membrane into the cytosol under certain environmental conditions and hence be involved in the stomatal closure processes. These findings on *At*ALMT9 and *At*ALMT4 may pave the way to further elucidate the regulation of guard cell anion channels and the modulation of stomatal aperture, allowing to produce plants that are more drought tolerant and more

productive under certain environmental conditions.

However, in this thesis, the functional characterization of *At*ALMT9 and *At*ALMT4 mainly focused on their physiological role in guard cells. Considering that *AtALMT9* and *AtALMT4* are also expressed in roots, the potential physiological role of *At*ALMT9 and *At*ALMT4 in this tissue needs to be investigated. As known, under salt stress condition, Na^+ that enters the cytosol may be sequestered into the vacuole to reduce its toxicity in the cytosol. In parallel, the corresponding anion, in most case Cl^- may also be transported into the vacuole as a charge balance and to detoxify the cytosol from harmful effects. Considering this, *At*ALMT9 may exhibit a potential physiological function in salt tolerance. Hence, the further functional characterization of *At*ALMT9 and the expression patterns of *At*ALMTs (determined by real-time PCR) responding to the salt stress would be of great value.

In addition to the modulation by cytosolic malate, the regulation of *At*ALMT9 anion channel activity by nucleotides was also elucidated in this thesis. The studies in the third result chapter suggest that cytosolic free nucleotides regulate the activity of the vacuolar anion channel *At*ALMT9 by altering the voltage-dependency. This occurs by an open channel block mechanism. Combining these results with the malate activation, we can conclude that during the stomatal opening process, the activation of the V-type H^+-ATPase presumably activates the influx of anions (chloride by *At*ALMT9) and cations into the vacuole. The stimulation of this proton pump could consume and decrease the concentration of cytosolic ATP and thus also reduce free ATP, resulting in a reduced inhibition of *At*ALMT9. In the meantime, the malate in the cytosol activates the chloride transport activity of *At*ALMT9. Thus, the chloride anion flux across the vacuolar membrane via *At*ALMT9 is regulated by the combination of malate activation and nucleotide inhibition to facilitate stomatal movement. Beside these two regulators, *At*ALMT9 activity may be also regulated by other factors, such as protein phosphorylation. (De-) phosphorylation has been identified to be crucial in the regulation of ion channels and transporters activity (Lee et al., 2007; Geiger et al., 2009; Geiger et al., 2010; Imes et al., 2013). Therefore, it may be of interest to identify potential phosphorylation sites in *At*ALMT9 and other ALMT members and further study their functional significance. How phosphorylation processes modulate the activity of these ALMTs channels in response to growth condition and whether some interaction partners (e.g. kinase and phosphatase) participate in this process remains to be explored in future.

In this thesis, the investigation of the structural elements implicated in ALMT function was also conducted, which is a prerequisite to understand the functional and physiological differences between ALMTs and their impact on anion transport in plants. We used *At*ALMT9 as a model and expressed a large number of site-directed *At*ALMT9 mutants in *Nicotiana bethamiana* to identify important amino acids. Firstly, citrate was identified to be an open channel blocker of *At*ALMT9, which competitively enters the pore and occludes the conduction pathway of *At*ALMT9. Secondly, charged, highly conserved amino acids in the vacuolar ALMT proteins were identified and were shown to be essential for *At*ALMT9 functionality. Among these, two residues (K93 and E130) form a salt bridge connecting the first and second putative transmembrane α-helices (TMα1 and TMα2). Three positively charged residues (K193, R200 and R215) in TMα5 fundamentally contribute to the functionality of the conduction pathway of *At*ALMT9 and, thus, this transmembrane domain was identified to be a probable pore-forming domain. Moreover, similarly to other ion channel families, *At*ALMT9 functions as a homo-oligomer in which probably four subunits contribute to form one functional channel. The structural investigation of *At*ALMT9 in this thesis provides new molecular, biochemical and biophysical details about the ALMT structure-function relationship. Although this thesis reveals that *At*ALMT9 is able to form functional channels facilitating the anion flux independently by forming homo-oligomers, it is still unknown whether *At*ALMT9 may form hetero-oligomers with other ALMTs. In *Arabidopsis*, the ALMTs in clade II (*At*ALMT9, *At*ALMT6 and *At*ALMT3, *At*ALMT4, *At*ALMT5, unpublished data) have been found to localize in the tonoplast. Therefore, if these ALMTs form hetero-oligomers, how do these protein-protein interactions change the channel transport activity and properties? To address these questions, bimolecular fluorescence complementation (BiFC) assay should be conducted between these ALMTs in the future and if an interaction between different vacuolar ALMTs can be observed, a detailed electrophysiological characterization should be carried out.

Furthermore, the phenotype of *atalmt4* plants indicates that this ALMT could serve as vacuolar malate exporter. However, preliminary studies showed only malate inward rectifying (vacuole uptake) currents. Is this phenotype related to another, yet unknown mechanism or can for example phosphorylation induce the export of malate? Only *At*ALMT6, whose expression is predominantly restricted to guard cells and flower

tissues, was shown to mediate, under certain conditions, malate efflux from the vacuole. In case none of other ALMTs are able to export malate from the vacuole, which channels are responsible for this important step?

In conclusion, in this thesis, the vacuolar anion channel *At*ALMT9, which is relevant for plant function and is a main model for ALMT investigations in our laboratory, was intensively characterized in respect to its physiological functions, its electrophysiological properties including the structural organization and its mode of regulation. Although much progress has been made in the functional and biophysical characterization of vacuolar ALMTs, many questions remain to be answered. The data published and yet not published from this thesis indicate that vacuolar ALMTs exhibit common features, but fulfill different physiological roles. Future research will focus on understanding the function of different the vacuolar ALMTs in plants.

9. References

Accardi A, Miller C (2004) Secondary active transport mediated by a prokaryotic homologue of ClC Cl- channels. Nature **427:** 803-807

Accardi A, Walden M, Nguitragool W, Jayaram H, Williams C, Miller C (2005) Separate ion pathways in a Cl-/H+ exchanger. J Gen Physiol **126:** 563-570

Acharya BR, Assmann SM (2009) Hormone interactions in stomatal function. Plant Mol Biol **69:** 451-462

Ache P, Becker D, Ivashikina N, Dietrich P, Roelfsema MRG, Hedrich R (2000) GORK, a delayed outward rectifier expressed in guard cells of Arabidopsis thaliana, is a K+-selective, K+-sensing ion channel. Febs Letters **486:** 93-98

Alberts B, Johnson A, Lewis J, Raff M, Roberts K, Walter P (2002) Molecular Biology of the Cell. 4th edition. New York: Garland Science.

Badri DV, Vivanco JM (2009) Regulation and function of root exudates. Plant Cell and Environment **32:** 666-681

Bais HP, Weir TL, Perry LG, Gilroy S, Vivanco JM (2006) The role of root exudates in rhizosphere interactions with plants and other organisms. Annu Rev Plant Biol **57:** 233-266

Barbier-Brygoo H, De Angeli A, Filleur S, Frachisse JM, Gambale F, Thomine S, Wege S (2011) Anion channels/transporters in plants: from molecular bases to regulatory networks. Annu Rev Plant Biol **62:** 25-51

Bergsdorf EY, Zdebik AA, Jentsch TJ (2009) Residues important for nitrate/proton coupling in plant and mammalian CLC transporters. J Biol Chem **284:** 11184-11193

Blatt MR (2000) Cellular signaling and volume control in stomatal movements in plants. Annu Rev Cell Dev Biol **16:** 221-241

Brandt B, Brodsky DE, Xue S, Negi J, Iba K, Kangasjarvi J, Ghassemian M, Stephan AB, Hu H, Schroeder JI (2012) Reconstitution of abscisic acid activation of SLAC1 anion channel by CPK6 and OST1 kinases and branched ABI1 PP2C phosphatase action. Proc Natl Acad Sci U S A **109:** 10593-10598

Buchner P, Takahashi H, Hawkesford MJ (2004) Plant sulphate transporters: co-ordination of uptake, intracellular and long-distance transport. J Exp Bot **55:** 1765-1773

Cheffings CM, Pantoja O, Ashcroft FM, Smith JA (1997) Malate transport and vacuolar ion channels in CAM plants. J Exp Bot **48 Spec No:** 623-631

Chen T, Cai X, Wu X, Karahara I, Schreiber L, Lin J (2011) Casparian strip development and its potential function in salt tolerance. Plant Signal Behav **6:** 1499-1502

Chen YH, Hu L, Punta M, Bruni R, Hillerich B, Kloss B, Rost B, Love J, Siegelbaum SA, Hendrickson WA (2010) Homologue structure of the SLAC1 anion channel for closing stomata in leaves. Nature **467:** 1074-U1157

Clough SJ, Bent AF (1998) Floral dip: a simplified method for Agrobacterium-mediated transformation of Arabidopsis thaliana. Plant J **16:** 735-743

Colcombet J, Thomine S, Guern J, Frachisse JM, Barbier-Brygoo H (2001) Nucleotides provide a voltage-sensitive gate for the rapid anion channel of arabidopsis hypocotyl cells. J Biol Chem **276:** 36139-36145

De Angeli A, Monachello D, Ephritikhine G, Frachisse JM, Thomine S, Gambale F, Barbier-Brygoo H (2006) The nitrate/proton antiporter AtCLCa mediates nitrate accumulation in plant vacuoles. Nature **442:** 939-942

De Angeli A, Monachello D, Ephritikhine G, Frachisse JM, Thomine S, Gambale F, Barbier-Brygoo H (2009a) Review. CLC-mediated anion transport in plant cells. Philos Trans R Soc Lond B Biol Sci **364:** 195-201

De Angeli A, Moran O, Wege S, Filleur S, Ephritikhine G, Thomine S, Barbier-Brygoo H, Gambale F (2009b) ATP Binding to the C Terminus of the Arabidopsis thaliana Nitrate/Proton Antiporter, AtCLCa, Regulates Nitrate Transport into Plant Vacuoles. J Biol Chem **284:** 26526-26532

De Angeli A, Zhang J, Meyer S, Martinoia E (2013) AtALMT9 is a malate-activated vacuolar chloride channel required for stomatal opening in Arabidopsis. Nat Commun **4:** 1804

Delhaize E, Craig S, Beaton CD, Bennet RJ, Jagadish VC, Randall PJ (1993) Aluminum Tolerance in Wheat (Triticum aestivum L.) (I. Uptake and Distribution of Aluminum in Root Apices). Plant Physiol **103:** 685-693

Delhaize E, Ryan PR, Hebb DM, Yamamoto Y, Sasaki T, Matsumoto H (2004) Engineering high-level aluminum tolerance in barley with the ALMT1 gene. Proc Natl Acad Sci U S A **101:** 15249-15254

Delhaize E, Ryan PR, Randall PJ (1993) Aluminum Tolerance in Wheat (Triticum aestivum L.) (II. Aluminum-Stimulated Excretion of Malic Acid from Root Apices). Plant Physiol **103:** 695-702

Demir F, Horntrich C, Blachutzik JO, Scherzer S, Reinders Y, Kierszniowska S, Schulze WX, Harms GS, Hedrich R, Geiger D, Kreuzer I (2013) Arabidopsis nanodomain-delimited ABA signaling pathway regulates the anion channel SLAH3. Proc Natl Acad Sci U S A **110:** 8296-8301

Di Leva F, Domi T, Fedrizzi L, Lim D, Carafoli E (2008) The plasma membrane Ca2+ ATPase of animal cells: structure, function and regulation. Arch Biochem Biophys **476:** 65-74

Dietrich P, Hedrich R (1994) Interconversion of Fast and Slow Gating Modes of Gcac1, a Guard-Cell Anion Channel. Planta **195:** 301-304

Dreyer I, Gomez-Porras JL, Riano-Pachon DM, Hedrich R, Geiger D (2012) Molecular Evolution of Slow and Quick Anion Channels (SLACs and QUACs/ALMTs). Front Plant Sci **3:** 263

Duby G, Boutry M (2009) The plant plasma membrane proton pump ATPase: a highly regulated P-type ATPase with multiple physiological roles. Pflugers Archiv-European Journal of Physiology **457:** 645-655

Durrett TP, Gassmann W, Rogers EE (2007) The FRD3-mediated efflux of citrate into the root vasculature is necessary for efficient iron translocation. Plant Physiol **144:** 197-205

Dutzler R, Campbell EB, Cadene M, Chait BT, MacKinnon R (2002) X-ray structure of a ClC chloride channel at 3.0 A reveals the molecular basis of anion selectivity. Nature **415:** 287-294

Dutzler R, Campbell EB, MacKinnon R (2003) Gating the selectivity filter in ClC chloride channels. Science **300:** 108-112

Emmerlich V, Linka N, Reinhold T, Hurth MA, Traub M, Martinoia E, Neuhaus HE (2003) The plant homolog to the human sodium/dicarboxylic cotransporter is the vacuolar malate carrier. Proc Natl Acad Sci U S A **100:** 11122-11126

Farre EM, Tiessen A, Roessner U, Geigenberger P, Trethewey RN, Willmitzer L (2001) Analysis of the compartmentation of glycolytic intermediates, nucleotides, sugars, organic acids, amino acids, and sugar alcohols in potato tubers using a nonaqueous fractionation method. Plant Physiol **127:** 685-700

Fernie AR, Carrari F, Sweetlove LJ (2004) Respiratory metabolism: glycolysis, the TCA cycle and mitochondrial electron transport. Curr Opin Plant Biol **7:** 254-261

Fernie AR, Martinoia E (2009) Malate. Jack of all trades or master of a few? Phytochemistry **70:** 828-832

Fischer RA (1968) Stomatal opening: role of potassium uptake by guard cells. Science **160:** 784-785

Furuichi T, Sasaki T, Tsuchiya Y, Ryan PR, Delhaize E, Yamamoto Y (2010) An extracellular hydrophilic carboxy-terminal domain regulates the activity of TaALMT1, the aluminum-activated malate transport protein of wheat. Plant J **64:** 47-55

Furukawa J, Yamaji N, Wang H, Mitani N, Murata Y, Sato K, Katsuhara M, Takeda K, Ma JF (2007) An aluminum-activated citrate transporter in barley. Plant Cell Physiol **48:** 1081-1091

Gadsby DC (2009) Ion channels versus ion pumps: the principal difference, in principle. Nat Rev Mol Cell Biol **10:** 344-352

Gao XQ, Li CG, Wei PC, Zhang XY, Chen J, Wang XC (2005) The dynamic changes of tonoplasts in guard cells are important for stomatal movement in Vicia faba. Plant Physiol **139:** 1207-1216

Gao XQ, Wang XL, Ren F, Chen J, Wang XC (2009) Dynamics of vacuoles and actin filaments in guard cells and their roles in stomatal movement. Plant Cell and Environment **32:** 1108-1116

Gaxiola RA, Palmgren MG, Schumacher K (2007) Plant proton pumps. FEBS Lett **581:** 2204-2214

Gaxiola RA, Yuan DS, Klausner RD, Fink GR (1998) The yeast CLC chloride channel functions in cation homeostasis. Proc Natl Acad Sci U S A **95:** 4046-4050

Geelen D, Lurin C, Bouchez D, Frachisse JM, Lelievre F, Courtial B, Barbier-Brygoo H, Maurel C (2000) Disruption of putative anion channel gene AtCLC-a in Arabidopsis suggests a role in the regulation of nitrate content. Plant J **21:** 259-267

Geiger D, Maierhofer T, AL-Rasheid KAS, Scherzer S, Mumm P, Liese A, Ache P, Wellmann C, Marten I, Grill E, Romeis T, Hedrich R (2011) Stomatal Closure by Fast Abscisic Acid Signaling Is Mediated by the Guard Cell Anion Channel SLAH3 and the Receptor RCAR1. Science Signaling **4**

Geiger D, Scherzer S, Mumm P, Marten I, Ache P, Matschi S, Liese A, Wellmann C, Al-Rasheid KAS, Grill E, Romeis T, Hedrich R (2010) Guard cell anion channel SLAC1 is regulated by CDPK protein kinases with distinct Ca2+ affinities. Proc Natl Acad Sci U S A **107:** 8023-8028

Geiger D, Scherzer S, Mumm P, Stange A, Marten I, Bauer H, Ache P, Matschi S, Liese A, Al-Rasheid KAS, Romeis T, Hedrich R (2009) Activity of guard cell anion channel SLAC1 is controlled by drought-stress signaling kinase-phosphatase pair. Proc Natl Acad Sci U S A **106:** 21425-21430

Gerhardt R, Heldt HW (1984) Measurement of Subcellular Metabolite Levels in Leaves by Fractionation of Freeze-Stopped Material in Nonaqueous Media. Plant Physiol **75:** 542-547

Gleave AP (1992) A Versatile Binary Vector System with a T-DNA Organizational-Structure Conducive to Efficient Integration of Cloned DNA into the Plant Genome. Plant Molecular Biology **20:** 1203-1207

Gouaux E, MacKinnon R (2005) Principles of selective ion transport in channels and pumps. Science **310:** 1461-1465

Gout E, Bligny R, Douce R (1992) Regulation of intracellular pH values in higher plant cells. Carbon-13 and phosphorus-31 nuclear magnetic resonance studies. J Biol Chem **267:** 13903-13909

Graves AR, Curran PK, Smith CL, Mindell JA (2008) The Cl(-)/H(+) antiporter ClC-7 is the primary chloride permeation pathway in lysosomes. Nature **453:** 788-792

Green LS, Rogers EE (2004) FRD3 controls iron localization in Arabidopsis. Plant Physiol **136:** 2523-2531

Gudesblat GE, Torres PS, Vojnov AA (2009) Stomata and pathogens: Warfare at the gates. Plant Signal Behav **4:** 1114-1116

Guo FQ, Young J, Crawford NM (2003) The nitrate transporter AtNRT1.1 (CHL1) functions in stomatal opening and contributes to drought susceptibility in Arabidopsis. Plant Cell **15:** 107-117

Hafke JB, Hafke Y, Smith JA, Luttge U, Thiel G (2003) Vacuolar malate uptake is mediated by an anion-selective inward rectifier. Plant J **35:** 116-128

Harada H, Kuromori T, Hirayama T, Shinozaki K, Leigh RA (2004) Quantitative trait loci analysis of nitrate storage in Arabidopsis leading to an investigation of the contribution of the anion channel gene, AtCLC-c, to variation in nitrate levels. J Exp Bot **55:** 2005-2014

Hedrich R (2012) Ion channels in plants. Physiol Rev **92:** 1777-1811

Hedrich R, Busch H, Raschke K (1990) Ca2+ and nucleotide dependent regulation of voltage dependent anion channels in the plasma membrane of guard cells. EMBO J **9:** 3889-3892

Hedrich R, Kurkdjian A, Guern J, Flugge UI (1989) Comparative studies on the electrical properties of the H+ translocating ATPase and pyrophosphatase of the vacuolar-lysosomal compartment. EMBO J **8:** 2835-2841

Hedrich R, Marten I (1993) Malate-Induced Feedback-Regulation of Plasma-Membrane Anion Channels Could Provide a Co2 Sensor to Guard-Cells. Embo Journal **12:** 897-901

Hetherington AM (2001) Guard cell signaling. Cell **107:** 711-714

Hille B. (2001) Ion Channels of Excitable Memranes. (Sinauer, Sunderland, MA, ed. 3)

Ho CH, Lin SH, Hu HC, Tsay YF (2009) CHL1 Functions as a Nitrate Sensor in Plants. Cell **138:** 1184-1194

Hoekenga OA, Maron LG, Pineros MA, Cancado GMA, Shaff J, Kobayashi Y, Ryan PR, Dong B, Delhaize E, Sasaki T, Matsumoto H, Yamamoto Y, Koyama H, Kochian LV (2006) AtALMT1, which encodes a malate transporter, is identified as one of several genes critical for aluminum tolerance in Arabidopsis. Proc Natl Acad Sci U S A **103:** 9738-9743

Hosy E, Vavasseur A, Mouline K, Dreyer I, Gaymard F, Poree F, Boucherez J, Lebaudy A, Bouchez D, Very AA, Simonneau T, Thibaud JB, Sentenac H (2003) The Arabidopsis outward K+ channel GORK is involved in regulation of stomatal movements and plant transpiration (vol 100, pg 5549, 2003). Proc Natl Acad Sci U S A **100:** 7418-7418

Hurth MA, Suh SJ, Kretzschmar T, Geis T, Bregante M, Gambale F, Martinoia E, Neuhaus HE (2005) Impaired pH homeostasis in Arabidopsis lacking the vacuolar dicarboxylate transporter and analysis of carboxylic acid transport across the tonoplast. Plant Physiol **137:** 901-910

Imes D, Mumm P, Bohm J, Al-Rasheid KAS, Marten I, Geiger D, Hedrich R (2013) Open stomata 1 (OST1) kinase controls R-type anion channel QUAC1 in Arabidopsis guard cells. Plant J **74:** 372-382

Jentsch TJ (2008) CLC chloride channels and transporters: from genes to protein structure, pathology and physiology. Crit Rev Biochem Mol Biol **43:** 3-36

Jorgensen PL, Hakansson KO, Karlish SJD (2003) Structure and mechanism of Na,K-ATPase: Functional sites and their interactions. Annual Review of Physiology **65:** 817-849

Jossier M, Kroniewicz L, Dalmas F, Le Thiec D, Ephritikhine G, Thomine S, Barbier-Brygoo H, Vavasseur A, Filleur S, Leonhardt N (2010) The Arabidopsis vacuolar anion transporter, AtCLCc, is involved in the regulation of stomatal movements and contributes to salt tolerance. Plant J **64:** 563-576

Kang J, Park J, Choi H, Burla B, Kretzschmar T, Lee Y, Martinoia E (2011) Plant ABC Transporters. Arabidopsis Book **9:** e0153

Kim TH, Bohmer M, Hu H, Nishimura N, Schroeder JI (2010) Guard cell signal transduction network: advances in understanding abscisic acid, CO2, and Ca2+ signaling. Annu Rev Plant Biol **61:** 561-591

Kinoshita T, Shimazaki K (1999) Blue light activates the plasma membrane H(+)-ATPase by phosphorylation of the C-terminus in stomatal guard cells. EMBO J **18:** 5548-5558

Kobayashi Y, Hoekenga OA, Itoh H, Nakashima M, Saito S, Shaff JE, Maron LG, Pineros MA, Kochian LV, Koyama H (2007) Characterization of

AtALMT1 expression in aluminum-inducible malate release and its role for rhizotoxic stress tolerance in Arabidopsis. Plant Physiol **145:** 843-852

Kolb HA, Marten I, Hedrich R (1995) Hodgkin-Huxley analysis of a GCAC1 anion channel in the plasma membrane of guard cells. J Membr Biol **146:** 273-282

Kollmeier M, Dietrich P, Bauer CS, Horst WJ, Hedrich R (2001) Aluminum activates a citrate-permeable anion channel in the aluminum-sensitive zone of the maize root apex. A comparison between an aluminum-sensitive and an aluminum-resistant cultivar. Plant Physiol **126:** 397-410

Kovermann P, Meyer S, Hortensteiner S, Picco C, Scholz-Starke J, Ravera S, Lee Y, Martinoia E (2007) The Arabidopsis vacuolar malate channel is a member of the ALMT family. Plant J **52:** 1169-1180

Laanemets K, Wang YF, Lindgren O, Wu J, Nishimura N, Lee S, Caddell D, Merilo E, Brosche M, Kilk K, Soomets U, Kangasjarvi J, Schroeder JI, Kollist H (2013) Mutations in the SLAC1 anion channel slow stomatal opening and severely reduce K+ uptake channel activity via enhanced cytosolic [Ca2+] and increased Ca2+ sensitivity of K+ uptake channels. New Phytol **197:** 88-98

Lebaudy A, Very AA, Sentenac H (2007) K+ channel activity in plants: Genes, regulations and functions. Febs Letters **581:** 2357-2366

Lee M, Choi Y, Burla B, Kim YY, Jeon B, Maeshima M, Yoo JY, Martinoia E, Lee Y (2008) The ABC transporter AtABCB14 is a malate importer and modulates stomatal response to CO2. Nat Cell Biol **10:** 1217-1223

Lee SC, Lan W, Buchanan BB, Luan S (2009) A protein kinase-phosphatase pair interacts with an ion channel to regulate ABA signaling in plant guard cells. Proc Natl Acad Sci U S A **106:** 21419-21424

Li W, Wang Y, Okamoto M, Crawford NM, Siddiqi MY, Glass AD (2007) Dissection of the AtNRT2.1:AtNRT2.2 inducible high-affinity nitrate transporter gene cluster. Plant Physiol **143:** 425-433

Ligaba A, Katsuhara M, Ryan PR, Shibasaka M, Matsumoto H (2006) The BnALMT1 and BnALMT2 genes from rape encode aluminum-activated malate transporters that enhance the aluminum resistance of plant cells. Plant Physiol **142:** 1294-1303

Ligaba A, Kochian L, Pineros M (2009) Phosphorylation at S384 regulates the activity of the TaALMT1 malate transporter that underlies aluminum resistance in wheat. Plant J **60:** 411-423

Linder B, Raschke K (1992) A slow anion channel in guard cells, activating at large hyperpolarization, may be principal for stomatal closing. FEBS Lett **313:** 27-30

Liu J, Magalhaes JV, Shaff J, Kochian LV (2009) Aluminum-activated citrate and malate transporters from the MATE and ALMT families function independently to confer Arabidopsis aluminum tolerance. Plant J **57:** 389-399

Liu KH, Tsay YF (2003) Switching between the two action modes of the dual-affinity nitrate transporter CHL1 by phosphorylation. EMBO J **22:** 1005-1013

Lopatin AN, Makhina EN, Nichols CG (1994) Potassium Channel Block by Cytoplasmic Polyamines as the Mechanism of Intrinsic Rectification. Nature **372:** 366-369

Lozier RH, Bogomolni RA, Stoeckenius W (1975) Bacteriorhodopsin: a light-driven proton pump in Halobacterium Halobium. Biophys J **15:** 955-962

Lu Z (2004) Mechanism of rectification in inward-rectifier K+ channels. Annu Rev Physiol **66:** 103-129

Lv QD, Tang RJ, Liu H, Gao XS, Li YZ, Zheng HQ, Zhang HX (2009) Cloning and molecular analyses of the Arabidopsis thaliana chloride channel gene family. Plant Science **176:** 650-661

Ma JF (2000) Role of organic acids in detoxification of aluminum in higher plants. Plant Cell Physiol **41:** 383-390

Ma Y (2009) Regulators of PP2C phosphatase activity function as abscisic acid sensors (vol 324, pg 1064, 2009). Science **324:** 1266-1266

MacRobbie EA (1998) Signal transduction and ion channels in guard cells. Philos Trans R Soc Lond B Biol Sci **353:** 1475-1488

Magalhaes JV, Liu J, Guimaraes CT, Lana UG, Alves VM, Wang YH, Schaffert RE, Hoekenga OA, Pineros MA, Shaff JE, Klein PE, Carneiro NP, Coelho CM, Trick HN, Kochian LV (2007) A gene in the multidrug and toxic compound extrusion (MATE) family confers aluminum tolerance in sorghum. Nat Genet **39:** 1156-1161

Markovich D, Murer H (2004) The SLC13 gene family of sodium sulphate/carboxylate cotransporters. Pflugers Arch **447:** 594-602

Marmagne A, Vinauger-Douard M, Monachello D, de Longevialle AF, Charon C, Allot M, Rappaport F, Wollman FA, Barbier-Brygoo H, Ephritikhine G (2007) Two members of the Arabidopsis CLC (chloride channel) family, AtCLCe and AtCLCf, are associated with thylakoid and Golgi membranes, respectively. J Exp Bot **58:** 3385-3393

Martinoia E, Flugge UI, Kaiser G, Heber U, Heldt HW (1985) Energy-Dependent Uptake of Malate into Vacuoles Isolated from Barley Mesophyll Protoplasts. Biochimica Et Biophysica Acta **806:** 311-319

Martinoia E, Meyer S, De Angeli A, Nagy R (2012) Vacuolar Transporters in Their Physiological Context. Annu Rev Plant Biol **63:** 183-213

Martinoia E, Rentsch D (1994) Malate Compartmentation - Responses to a Complex Metabolism. Annu Rev Plant Physiol Plant Mol Biol **45:** 447-467

Mathieu Y, Guern J, Pean M, Pasquier C, Beloeil JC, Lallemand JY (1986) Cytoplasmic pH Regulation in Acer pseudoplatanus Cells: II. Possible Mechanisms Involved in pH Regulation during Acid-Load. Plant Physiol **82:** 846-852

Meyer S, De Angeli A, Fernie AR, Martinoia E (2010a) Intra- and extra-cellular excretion of carboxylates. Trends Plant Sci **15:** 40-47

Meyer S, Mumm P, Imes D, Endler A, Weder B, Al-Rasheid KAS, Geiger D, Marten I, Martinoia E, Hedrich R (2010b) AtALMT12 represents an R-type anion channel required for stomatal movement in Arabidopsis guard cells. Plant J **63:** 1054-1062

Meyer S, Scholz-Starke J, De Angeli A, Kovermann P, Burla B, Gambale F, Martinoia E (2011) Malate transport by the vacuolar AtALMT6 channel in guard cells is subject to multiple regulation. Plant J **67:** 247-257

Miller AJ, Fan X, Orsel M, Smith SJ, Wells DM (2007) Nitrate transport and signalling. J Exp Bot **58:** 2297-2306

Miyazono K, Miyakawa T, Sawano Y, Kubota K, Kang HJ, Asano A, Miyauchi Y, Takahashi M, Zhi Y, Fujita Y, Yoshida T, Kodaira KS, Yamaguchi-Shinozaki K, Tanokura M (2009) Structural basis of abscisic acid signalling. Nature **462:** 609-614

Monachello D, Allot M, Oliva S, Krapp A, Daniel-Vedele F, Barbier-Brygoo H, Ephritikhine G (2009) Two anion transporters AtClCa and AtClCe fulfil interconnecting but not redundant roles in nitrate assimilation pathways. New Phytol **183:** 88-94

Moon GJ, Clough BF, Peterson CA, Allaway WG (1986) Apoplastic and Symplastic Pathways in Avicennia-Marina (Forsk) Vierh Roots Revealed by Fluorescent Tracer Dyes. Australian Journal of Plant Physiology **13:** 637-648

Motoda H, Sasaki T, Kano Y, Ryan PR, Delhaize E, Matsumoto H, Yamamoto Y (2007) The Membrane Topology of ALMT1, an Aluminum-Activated Malate Transport Protein in Wheat (Triticum aestivum). Plant Signal Behav **2:** 467-472

Mueckler M (1994) Facilitative glucose transporters. Eur J Biochem **219:** 713-725

Mustilli AC, Merlot S, Vavasseur A, Fenzi F, Giraudat J (2002) Arabidopsis OST1 protein kinase mediates the regulation of stomatal aperture by abscisic

acid and acts upstream of reactive oxygen species production. Plant Cell **14:** 3089-3099

Mumm P, Imes D, Martinoia E, Al-Rasheid KA, Geiger D, Marten I, Hedrich R (2013) C-terminus mediated voltage gating of Arabidopsis guard cell anion channel QUAC1. Mol Plant

Nagahashi G, Thomson WW, Leonard RT (1974) The casparian strip as a barrier to the movement of lanthanum in corn roots. Science **183:** 670-671

Neher E (1992) Correction for liquid junction potentials in patch clamp experiments. Methods Enzymol **207:** 123-131

Negi J, Matsuda O, Nagasawa T, Oba Y, Takahashi H, Kawai-Yamada M, Uchimiya H, Hashimoto M, Iba K (2008) CO2 regulator SLAC1 and its homologues are essential for anion homeostasis in plant cells. Nature **452:** 483-U413

Nilson SE, Assmann SM (2007) The control of transpiration. Insights from Arabidopsis. Plant Physiol **143:** 19-27

Nishimura N, Hitomi K, Arvai AS, Rambo RP, Hitomi C, Cutler SR, Schroeder JI, Getzoff ED (2009) Structural mechanism of abscisic acid binding and signaling by dimeric PYR1. Science **326:** 1373-1379

Obulareddy N, Panchal S, Melotto M (2013) Guard cell purification and RNA isolation suitable for high-throughput transcriptional analysis of cell-type responses to biotic stresses. Mol Plant Microbe Interact **26:** 844-849

Okamoto M, Kumar A, Li W, Wang Y, Siddiqi MY, Crawford NM, Glass AD (2006) High-affinity nitrate transport in roots of Arabidopsis depends on expression of the NAR2-like gene AtNRT3.1. Plant Physiol **140:** 1036-1046

Orsel M, Chopin F, Leleu O, Smith SJ, Krapp A, Daniel-Vedele F, Miller AJ (2006) Characterization of a two-component high-affinity nitrate uptake system in Arabidopsis. Physiology and protein-protein interaction. Plant Physiol **142:** 1304-1317

Palmgren MG (2001) Plant plasma membrane H+-ATPases: Powerhouses for nutrient uptake. Annu Rev Plant Physiol Plant Mol Biol **52:** 817-845

Palmgren MG, Nissen P (2011) P-Type ATPases. Annual Review of Biophysics, Vol 40 **40:** 243-266

Pandey S, Zhang W, Assmann SM (2007) Roles of ion channels and transporters in guard cell signal transduction. Febs Letters **581:** 2325-2336

Park SY, Fung P, Nishimura N, Jensen DR, Fujii H, Zhao Y, Lumba S, Santiago J, Rodrigues A, Chow TFF, Alfred SE, Bonetta D, Finkelstein R, Provart NJ, Desveaux D, Rodriguez PL, McCourt P, Zhu JK, Schroeder JI, Volkman BF, Cutler SR (2009) Abscisic Acid Inhibits Type 2C Protein

Phosphatases via the PYR/PYL Family of START Proteins. Science **324:** 1068-1071

Peterson CA (1987) The Exodermal Casparian Band of Onion Roots Blocks the Apoplastic Movement of Sulfate-Ions. J Exp Bot **38:** 2068-2081

Picollo A, Pusch M (2005) Chloride/proton antiporter activity of mammalian CLC proteins ClC-4 and ClC-5. Nature **436:** 420-423

Pilot G, Lacombe B, Gaymard F, Cherel I, Boucherez J, Thibaud JB, Sentenac H (2001) Guard cell inward K+ channel activity in Arabidopsis involves expression of the twin channel subunits KAT1 and KAT2. J Biol Chem **276:** 3215-3221

Pineros MA, Cancado GM, Maron LG, Lyi SM, Menossi M, Kochian LV (2008) Not all ALMT1-type transporters mediate aluminum-activated organic acid responses: the case of ZmALMT1 - an anion-selective transporter. Plant J **53:** 352-367

Pineros MA, Cancado GMA, Kochian LV (2008) Novel properties of the wheat aluminum tolerance organic acid transporter (TaALMT1) revealed by electrophysiological characterization in Xenopus oocytes: Functional and structural implications. Plant Physiol **147:** 2131-2146

Pineros MA, Kochian LV (2001) A patch-clamp study on the physiology of aluminum toxicity and aluminum tolerance in maize. Identification and characterization of Al(3+)-induced anion channels. Plant Physiol **125:** 292-305

Pineros MA, Magalhaes JV, Carvalho Alves VM, Kochian LV (2002) The physiology and biophysics of an aluminum tolerance mechanism based on root citrate exudation in maize. Plant Physiol **129:** 1194-1206

Poffenroth M, Green DB, Tallman G (1992) Sugar Concentrations in Guard Cells of Vicia faba Illuminated with Red or Blue Light : Analysis by High Performance Liquid Chromatography. Plant Physiol **98:** 1460-1471

Post RL, Hegyvary C, Kume S (1972) Activation by adenosine triphosphate in the phosphorylation kinetics of sodium and potassium ion transport adenosine triphosphatase. J Biol Chem **247:** 6530-6540

Raschke K (2003) Alternation of the slow with the quick anion conductance in whole guard cells effected by external malate. Planta **217:** 651-657

Rausch C, Bucher M (2002) Molecular mechanisms of phosphate transport in plants. Planta **216:** 23-37

Roelfsema MR, Hedrich R, Geiger D (2012) Anion channels: master switches of stress responses. Trends Plant Sci **17:** 221-229

Roelfsema MRG, Hedrich R (2005) In the light of stomatal opening: new insights into 'the Watergate'. New Phytologist **167:** 665-691

Roelfsema MRG, Levchenko V, Hedrich R (2004) ABA depolarizes guard cells in intact plants, through a transient activation of R- and S-type anion channels. Plant J **37:** 578-588

Rogers EE, Guerinot ML (2002) FRD3, a member of the multidrug and toxin efflux family, controls iron deficiency responses in Arabidopsis. Plant Cell **14:** 1787-1799

Roschzttardtz H, Seguela-Arnaud M, Briat JF, Vert G, Curie C (2011) The FRD3 Citrate Effluxer Promotes Iron Nutrition between Symplastically Disconnected Tissues throughout Arabidopsis Development. Plant Cell **23:** 2725-2737

Ryan P, Delhaize E, Jones D (2001) Function and Mechanism of Organic Anion Exudation from Plant Roots. Annu Rev Plant Physiol Plant Mol Biol **52:** 527-560

Ryan PR, Skerrett M, Findlay GP, Delhaize E, Tyerman SD (1997) Aluminum activates an anion channel in the apical cells of wheat roots. Proc Natl Acad Sci U S A **94:** 6547-6552

Santiago J, Dupeux F, Round A, Antoni R, Park SY, Jamin M, Cutler SR, Rodriguez PL, Marquez JA (2009) The abscisic acid receptor PYR1 in complex with abscisic acid. Nature **462:** 665-U143

Sasaki T, Mori IC, Furuichi T, Munemasa S, Toyooka K, Matsuoka K, Murata Y, Yamamoto Y (2010) Closing plant stomata requires a homolog of an aluminum-activated malate transporter. Plant Cell Physiol **51:** 354-365

Sasaki T, Yamamoto Y, Ezaki B, Katsuhara M, Ahn SJ, Ryan PR, Delhaize E, Matsumoto H (2004) A wheat gene encoding an aluminum-activated malate transporter. Plant J **37:** 645-653

Scheel O, Zdebik AA, Lourdel S, Jentsch TJ (2005) Voltage-dependent electrogenic chloride/proton exchange by endosomal CLC proteins. Nature **436:** 424-427

Schroeder JI, Allen GJ, Hugouvieux V, Kwak JM, Waner D (2001) Guard Cell Signal Transduction. Annu Rev Plant Physiol Plant Mol Biol **52:** 627-658

Schroeder JI, Hagiwara S (1989) Cytosolic Calcium Regulates Ion Channels in the Plasma-Membrane of Vicia-Faba Guard-Cells. Nature **338:** 427-430

Schroeder JI, Keller BU (1992) Two types of anion channel currents in guard cells with distinct voltage regulation. Proc Natl Acad Sci U S A **89:** 5025-5029

SchulzLessdorf B, Lohse G, Hedrich R (1996) GCAC1 recognizes the pH gradient across the plasma membrane: A pH-sensitive and ATP-dependent anion channel links guard cell membrane potential to acid and energy metabolism. Plant J **10:** 993-1004

Shimazaki K, Doi M, Assmann SM, Kinoshita T (2007) Light regulation of stomatal movement. Annu Rev Plant Biol **58:** 219-247

Skou JC, Esmann M (1992) The Na,K-ATPase. J Bioenerg Biomembr **24:** 249-261

Smith FW, Rae AL, Hawkesford MJ (2000) Molecular mechanisms of phosphate and sulphate transport in plants. Biochimica Et Biophysica Acta-Biomembranes **1465:** 236-245

Solomon E, Berg L, Martin D (2004) Biology. 7th edition. Brooks Cole.

Steudle E (2000) Water uptake by roots: effects of water deficit. J Exp Bot **51:** 1531-1542

Sze H, Li X, Palmgren MG (1999) Energization of plant cell membranes by H+-pumping ATPases. Regulation and biosynthesis. Plant Cell **11:** 677-690

Talbott LD, Zeiger E (1998) The role of sucrose in guard cell osmoregulation. J Exp Bot **49:** 329-337

Thomine S, Guern J, Barbier-Brygoo H (1997) Voltage-Dependent Anion Channel of Arabidopsis Hypocotyls: Nucleotide Regulation and Pharmacological Properties. The Journal of Membrane Biology **159:** 71-82

Tomasi N, Kretzschmar T, Espen L, Weisskopf L, Fuglsang AT, Palmgren MG, Neumann G, Varanini Z, Pinton R, Martinoia E, Cesco S (2009) Plasma membrane H-ATPase-dependent citrate exudation from cluster roots of phosphate-deficient white lupin. Plant Cell and Environment **32:** 465-475

Tsay YF, Chiu CC, Tsai CB, Ho CH, Hsu PK (2007) Nitrate transporters and peptide transporters. FEBS Lett **581:** 2290-2300

Tsay YF, Schroeder JI, Feldmann KA, Crawford NM (1993) The herbicide sensitivity gene CHL1 of Arabidopsis encodes a nitrate-inducible nitrate transporter. Cell **72:** 705-713

Vahisalu T, Kollist H, Wang YF, Nishimura N, Chan WY, Valerio G, Lamminmaki A, Brosche M, Moldau H, Desikan R, Schroeder JI, Kangasjarvi J (2008) SLAC1 is required for plant guard cell S-type anion channel function in stomatal signalling. Nature **452:** 487-U415

Van Kirk CA, Raschke K (1978) Presence of Chloride Reduces Malate Production in Epidermis during Stomatal Opening. Plant Physiol **61:** 361-364

Vance CP, Uhde-Stone C, Allan DL (2003) Phosphorus acquisition and use: critical adaptations by plants for securing a nonrenewable resource. New Phytol **157:** 423-447

Vavasseur A, Raghavendra AS (2005) Guard cell metabolism and CO2 sensing. New Phytol **165:** 665-682

von der Fecht-Bartenbach J, Bogner M, Dynowski M, Ludewig U (2010) CLC-b-mediated NO-3/H+ exchange across the tonoplast of Arabidopsis vacuoles. Plant Cell Physiol **51:** 960-968

von der Fecht-Bartenbach J, Bogner M, Krebs M, Stierhof YD, Schumacher K, Ludewig U (2007) Function of the anion transporter AtCLC-d in the trans-Golgi network. Plant J **50:** 466-474

Wang Y, Papanatsiou M, Eisenach C, Karnik R, Williams M, Hills A, Lew VL, Blatt MR (2012) Systems dynamic modeling of a guard cell Cl- channel mutant uncovers an emergent homeostatic network regulating stomatal transpiration. Plant Physiol **160:** 1956-1967

Wang Y, Wu WH (2013) Potassium transport and signaling in higher plants. Annu Rev Plant Biol **64:** 451-476

Ward JM, Maser P, Schroeder JI (2009) Plant ion channels: gene families, physiology, and functional genomics analyses. Annu Rev Physiol **71:** 59-82

Ward JM, Pei ZM, Schroeder JI (1995) Roles of Ion Channels in Initiation of Signal Transduction in Higher Plants. Plant Cell **7:** 833-844

Wege S, Jossier M, Filleur S, Thomine S, Barbier-Brygoo H, Gambale F, De Angeli A (2010) The proline 160 in the selectivity filter of the Arabidopsis NO(3)(-)/H(+) exchanger AtCLCa is essential for nitrate accumulation in planta. Plant J **63:** 861-869

Wikstrom M (2004) Cytochrome c oxidase: 25 years of the elusive proton pump. Biochim Biophys Acta **1655:** 241-247

Winter H, Robinson DG, Heldt HW (1994) Subcellular Volumes and Metabolite Concentrations in Spinach Leaves. Planta **193:** 530-535

Woodhull AM (1973) Ionic blockage of sodium channels in nerve. J Gen Physiol **61:** 687-708

Xia JH, Saglio P, Roberts JKM (1995) Nucleotide Levels Do Not Critically Determine Survival of Maize Root-Tips Acclimated to a Low-Oxygen Environment. Plant Physiol **108:** 589-595

Yamaguchi M, Sasaki T, Sivaguru M, Yamamoto Y, Osawa H, Ahn SJ, Matsumoto H (2005) Evidence for the plasma membrane localization of Al-activated malate transporter (ALMT1). Plant and Cell Physiology **46:** 812-816

Yamashita A, Singh SK, Kawate T, Jin Y, Gouaux E (2005) Crystal structure of a bacterial homologue of Na+/Cl--dependent neurotransmitter transporters. Nature **437:** 215-223

Yang KY, Liu YD, Zhang SQ (2001) Activation of a mitogen-activated protein kinase pathway is involved in disease resistance in tobacco. Proc Natl Acad Sci U S A **98:** 741-746

Yazaki Y, Asukagawa N, Ishikawa Y, Ohta E, Sakata M (1988) Estimation of Cytoplasmic Free Mg2+ Levels and Phosphorylation Potentials in Mung Bean Root Tips by In Vivo 31P NMR Spectroscopy. Plant and Cell Physiology **29:** 919-924

Yin P, Fan H, Hao Q, Yuan XQ, Wu D, Pang YX, Yan CY, Li WQ, Wang JW, Yan N (2009) Structural insights into the mechanism of abscisic acid signaling by PYL proteins. Nature Structural & Molecular Biology **16:** 1230-U1242

Yoshida R, Umezawa T, Mizoguchi T, Takahashi S, Takahashi F, Shinozaki K (2006) The regulatory domain of SRK2E/OST1/SnRK2.6 interacts with ABI1 and integrates abscisic acid (ABA) and osmotic stress signals controlling stomatal closure in Arabidopsis. J Biol Chem **281:** 5310-5318

Zdebik AA, Zifarelli G, Bergsdorf EY, Soliani P, Scheel O, Jentsch TJ, Pusch M (2008) Determinants of anion-proton coupling in mammalian endosomal CLC proteins. J Biol Chem **283:** 4219-4227

Zhang J, Baetz U, Krugel U, Martinoia E, De Angeli A (2013) Identification of a probable pore forming domain in the multimeric vacuolar anion channel AtALMT9. Plant Physiol **163**: 830-843

Zhang WH, Ryan PR, Tyerman SD (2001) Malate-permeable channels and cation channels activated by aluminum in the apical cells of wheat roots. Plant Physiol **125:** 1459-1472

Zhou M, Morais-Cabral JH, Mann S, MacKinnon R (2001) Potassium channel receptor site for the inactivation gate and quaternary amine inhibitors. Nature **411:** 657-661

Zifarelli G, Pusch M (2009) Conversion of the 2 Cl(-)/1 H+ antiporter ClC-5 in a NO3(-)/H+ antiporter by a single point mutation. EMBO J **28:** 175-182

10. Acknowledgements

Ph.D study and writing this thesis was a long journey. But one of the joys of completion is to look over this doctoral journey and remember all the peoples who have helped and supported me along this long road over the past four years.

First of all, I would like to express my heartfelt gratitude to Prof. Enrico Martinoia, who gave me the opportunity to come to Switzerland and make my thesis in such a good laboratory. Thanks very much for his wisdom, support and great guidance, without which this thesis would never have existed. Also my sincere gratitude for his kind "father" smiles and encouragement, which will always inspire me. Furthermore, I would like to thank Dr. Alexis De Angeli. Thank him very much for his support whenever I felt frustrated, especially during the first year. His knowledge and advice helped me to stay on track and his guidance let me improve my theoretical and practical skills, especially on electrophysiology. I also would like to thank Prof. Stefan Hörtensteiner and Prof. Leo Ebert for being members of my thesis committee.

I am very grateful to the "ALMT family": Dr. Stefan Meyer, Ulrike Bätz and Dr. Cornelia Eisenach, who are always open for discussion, sharing ideas and encouraging me to overcome many difficulties. Thank them for critically reading this manuscript and the manuscripts of my publications.

Other members of the lab also deserve my sincerest thanks. Their friendship and assistance allow me to complete my work. Special thanks go to Rita Francisco, Miyoung Lee, Santiago Alejandro Martinez, Bo Burla, Undine Krügel, Daniel Horrer, Maja Schellenberg, Barbara Bassin, Lorenzo Borghi, Rita Saraiva and Bastien Christ. I am really happy to share the wonderful time in Zurich.

Many thanks to Karl Huwiler, Daniel Bollier, Daniel Stutz, Reto Schild, Italia Sacco and secretary office for particular assistance.

Last but not the least, I would like to thank my parents and my girlfriend Jing Tian for the always supporting in those years. Their love provided the inspiration and encouragement to allow me to finish this journey.

Publications

De Angeli, A., *Zhang, J., Meyer, S. and Martinoia E. AtALMT9 is a malate-activated vacuolar chloride channel required for stomatal opening in Arabidopsis. Nat Commun. 2013; 4:1804. doi: 10.1038/ncomms2815. (*Co-first author)

Zhang, J., Bätz, U., Krügel, U., Martinoia, E. and De Angeli A. Identification of a probable pore forming domain in the multimeric vacuolar anion channel AtALMT9. Plant Physiol. 2013 Oct;163 (2):830-843.

De Angeli A, Baetz U, Francisco R, Zhang J, Chaves MM, Regalado A. The vacuolar channel VvALMT9 mediates malate and tartrate accumulation in berries of Vitis vinifera. Planta. 2013 Aug;238 (2):283-91.

Zhang, J., Martinoia, E. and De Angeli A. (2013) The intercellular nucleotides dependent regulation on the vacuolar anion channel AtALMT9 in Arabidopsis. (Submission in preparation)